

# **Multifunctional MAP-based Structures in Organo- and Metal-Catalysed Reactions**

A thesis submitted in partial fulfilment of the requirements for the degree of

**Doctor of Philosophy**

by

**Sviatoslav Sergeevich Eliseenko**

Master of Research (Chemistry)

Department of Molecular Sciences

Macquarie University

Sydney, Australia

March 2020



## TABLE OF CONTENT

ABSTRACT.....	iii
STATEMENT OF ORIGINALITY .....	iv
PUBLICATION LIST.....	v
ACKNOWLEDGEMENTS .....	vi
DEDICATION .....	ix
ABBREVIATIONS.....	x
LIST OF FIGURES.....	xiii
LIST OF SCHEMES.....	xiv
LIST OF TABLES .....	xvi
<b>CHAPTER 1. The MAP Scaffold as a Versatile Platform for Hybrid Catalysis.....</b>	<b>2</b>
<b>1.1. Background.....</b>	<b>2</b>
<b>1.2. 1,1'-Binaphthyl Scaffold as a Candidate for "Hybrid" System Design.....</b>	<b>3</b>
<b>1.3. MAP-based Structures in Metal- and Organocatalysed Asymmetric Processes .....</b>	<b>4</b>
1.3.1. MAP-metal coordination.....	4
1.3.2. MAP and its derivatives in metal-catalysed processes.....	7
1.3.3. MAP and its derivatives in organocatalysed processes .....	13
1.3.3.1. MAP-based bifunctional organocatalysts .....	14
1.3.3.2. Trifunctional MAP-based organocatalysts with an amino bridge and external acid activation	17
1.3.4. Synthesis of MAP-based trifunctional catalysts .....	20
<b>1.4. Metal- and Organocatalytic Hybrid Catalysis.....</b>	<b>22</b>
1.4.1. Structures exhibiting catalytic dualism .....	22
1.4.2. Aminophosphine ligands as organocatalysts .....	24
<b>1.5. Aim and Project Outline.....</b>	<b>26</b>
<b>1.6. References .....</b>	<b>28</b>
<b>CHAPTER 2. New MAP-based Multifunctional Organocatalysts with Improved Cooperativity ....</b>	<b>34</b>
<b>2.1. Introduction .....</b>	<b>34</b>
2.1.1 Catalysts efficient in both aza-MBH and MBH reactions .....	34
2.1.2 MAP-based trifunctional systems in the MBH reaction .....	36
2.1.3 Pyrrole as a candidate for improved cooperative catalysis design.....	37
<b>2.2 Results and Discussion.....</b>	<b>37</b>
<b>2.3 Cross Reference of Compounds in Tetrahedron paper and Thesis.....</b>	<b>83</b>
<b>2.4 References .....</b>	<b>85</b>
<b>CHAPTER 3. Multifunctional MAP-based Systems as Ligands in Enantiodivergent Catalysis.....</b>	<b>88</b>
<b>3.1 Introduction.....</b>	<b>88</b>
3.1.1 Catalytic dualism: organocatalysts as ligands.....	88
3.1.2 MAP-based ligands in Pd-catalysed asymmetric allylic substitution .....	88
3.1.3 H-bonding ligands for enantiodivergency in asymmetric allylic substitution.....	92

3.1.4	<i>Chapter 3 goals and plan</i> .....	95
<b>3.2</b>	<b>Results and Discussion</b> .....	96
3.2.1	<i>MAP-based structures 1.46a,d,h,i and 1.48a in Pd-catalysed allylic substitution</i> .....	96
3.2.2	<i>MAP-based structures 1.46a,i, 1.48a, and 2.4c in other metal-catalysed reactions</i> .....	121
<b>3.3</b>	<b>Experimental</b> .....	123
3.3.1	<i>General information</i> .....	123
3.3.2	<i>Experimental part</i> .....	123
<b>3.4</b>	<b>Cross Reference of Compounds in Manuscript and Thesis</b> .....	125
<b>3.5</b>	<b>References</b> .....	126
<b>CHAPTER 4. MAP-based Catalytic Systems for Cascade Chirality Transfer in Model Reactions</b>		<b>130</b>
<b>4.1</b>	<b>Introduction</b> .....	130
4.1.1	<i>Chirality induction from non-racemic substrates</i> .....	130
4.1.2	<i>Design of processes with complex catalytic organisation</i> .....	132
4.1.3	<i>MAP-based structures as catalysts in cascade or sequential processes</i> .....	133
4.1.4	<i>Chapter 4 goals and plan</i> .....	135
<b>4.2</b>	<b>Results and Discussion</b> .....	137
4.2.1	<i>Trifunctional system in an aza-MBH / nucleophilic addition cascade</i> .....	137
4.2.2	<i>Trifunctional system in an aza-MBH / epoxidation sequential process</i> .....	141
4.2.3	<i>Trifunctional system in an aza-MBH / diethylzinc addition sequence</i> .....	146
<b>4.3</b>	<b>Conclusions</b> .....	152
<b>4.4</b>	<b>Experimental Section</b> .....	153
4.4.1	<i>General information</i> .....	153
4.4.2	<i>aza-MBH / nucleophilic cyclization cascade</i> .....	154
4.4.3	<i>aza-MBH / epoxidation sequential process</i> .....	156
4.4.4	<i>aza-MBH / diethylzinc addition sequential process</i> .....	165
<b>4.5</b>	<b>References</b> .....	168
<b>CHAPTER 5. Conclusions and Future Directions</b> .....		<b>172</b>
<b>5.1</b>	<b>Conclusions</b> .....	172
<b>5.2</b>	<b>Future directions</b> .....	173
<b>APPENDICES</b> .....		<b>I</b>

## ABSTRACT

Asymmetric catalysis is essential to meeting increasing demands of chiral molecules and substances for pharmaceutical and material industries. Combination of major catalytic approaches to achieve efficient asymmetric catalysis is of current interest but often limited by the design of compatible and cooperative catalytic systems. MAP-based trifunctional systems, containing phosphine as a Lewis base, amine as a Brønsted base, and an aromatic Brønsted acid group, are proficient in cooperative organocatalytic *aza*-MBH processes and can potentially also serve as multidentate ligands in metal-catalysed reactions for developing hybrid catalysts in sequential organo- and metal-catalysed processes. The application of a single structure as an organocatalyst and ligand in a complex process may present new opportunities for addressing the compatibility issue of hybrid catalysis.

In this thesis, we report the design, synthesis, and catalytic investigations of new MAP-based trifunctional catalysts for organo- and metal-based catalysis, in single or cascade reactions. First, a new series of trifunctional organocatalysts with various pyrrole-type Brønsted acids were investigated in the *aza*-MBH reaction to improve catalytic cooperativity and reaction scope. The main representatives of trifunctional MAP-based systems were then tested as ligands in asymmetric allylic substitution and demonstrated the potential to enantiodivergent catalysis, based on the additional ligand-induced H-bonding interactions. A model trifunctional system possessing a phenolic Brønsted acid was also investigated on its organizational ability to translate chirality in cascade or sequential processes. The findings on the organisational properties of MAP-based trifunctional catalytic systems should lead to new design principles in the development of cascade and hybrid catalysis for efficient asymmetric synthesis.

## STATEMENT OF ORIGINALITY

*This work has not previously been submitted for a degree or diploma in any university. To the best of my knowledge and belief, the thesis contains no material previously published or written by another person except where due reference is made in the thesis itself.*

\_\_\_\_\_  
Sviatoslav S. Eliseenko

Date: 1<sup>st</sup> March 2020

## PUBLICATION LIST

[1] Eliseenko, S. S.; Liu, F., Switchable pyrrole-based hydrogen bonding motif in enantioselective trifunctional organocatalysis. *Tetrahedron* **2019**, 75 (4), 518-526.

The candidate Sviatoslav S. Eliseenko synthesized all compounds for this study and acquired all data. The manuscript was prepared by Sviatoslav S. Eliseenko and Fei Liu together.

[2] Eliseenko, S. S.; M. Bhadbhade, Liu, F. Multifunctional chiral aminophosphines for enantiodivergent catalysis in a palladium-catalyzed allylic alkylation reaction.

*The manuscript is submitted for review in Chirality journal.*

The candidate Sviatoslav S. Eliseenko synthesized all compounds for this study and acquired all data except X-Ray analysis of the described palladium complexes. The X-Ray and the corresponding crystallographic analysis were performed by Mohan Bhadbhade. The crystallographic data and ORTEP pictograms for Supplementary information were provided by Mohan Bhadbhade. The manuscript was prepared by Sviatoslav S. Eliseenko and Fei Liu together.

## ACKNOWLEDGEMENTS

I would like to thank the following people, without whom this thesis would not have been possible:

My supervisor, Dr. **Fei Liu**, for support during my PhD project. You have always been nearby to provide support and, at the same time, give me the freedom to test my ideas and carry out research independently. I am grateful a lot for your guidance. A special thank you for your scientific philosophy that always motivated and kept me excited about the project.

My co-supervisor, Assoc. Prof. **Koushik Venkatesan**, for help and recommendations. Thank you for the opportunity to work in your laboratory and for your efforts to keep the lab operational and comfortable for us. A special thank you for lunch conversations that extended my understanding of the world.

My research group:

**Alexander Moore**, who inspired me by the unprecedented balancing between research and the life outside of the uni. You gave me a lot of motivation. It was a pleasure to work in the same lab with so responsible, resistant to failures, technically and professionally knowledgeable person.

**Bilqees Sameem (Lubna)** for your support in times when nobody is available. I was happy to have you ready to save my life during the weekend and after-hours labwork.

**Dr. Ivan Salazar Estrada** for your kind heart. You always felt when I needed a friend's support and you were giving it to me. A separate thank you for all the philosophical discussions we have had.

**Harold Spedding** for amazing diving into Australian English. You gave me extremely bright and colourful emotions and, I believe, shaped my informal English-speaking skills. You were always ready to support conversations and I was always getting something new from it.

**Payal Barua** for opportunities to extend my knowledge in biological sciences and Bengali culture.

**Dr. Ryan Kenny** for your inestimable professional recommendations, unbelievable reviving of LUCY-HPLC whenever she was sick, and for synthesized chemicals, you shared with me in my rough times. I admire your level of standards and will always keep it in my mind as a reference point.

2WW Laboratory mates:

**Dominik Suter** for all the adventures and traditions we have had during our candidatures, for all our conversations. You were always ready to go somewhere and share time with me.

**Robert Malmberg** for your unquenchable drive and positive that energized me during my project. I still cannot believe that a human can have such health, especially when you ran a marathon after a party.

**Sandhya Verma** for the introduction in Indian culture and for desserts you made for us.

**Teja Maganti** for the sharing with me of your knowledge in so diverse fields.

**Dr. Tobias von Arx** for your sharp jokes and creation of positive ambience in the lab and office.

**Neil Anderson** for your friendship and interesting stories about Australian life.

**Dr. Aleksei N. Marianov** who was always ready to share a cup of coffee in tough situations and give friendly recommendations. It was important for me to have a Russian-speaking friend here and I am happy that we have met.

CBMS staff and fellow students for help in research method training: Erika Davies and Nicole Cordina (NMR), Kavita Ragini and Remi Rouquette (LCMS), Mark Tran and Tony Wang (FT-IR), Anthony Gurlica (Safety and general lab management), Atul Bhatnagar and Matthew McKay (HRMS), Nancy Li, Shin Yoong Lim and Mark Rego (Financials), Michelle Kang and Koko Numata (Administrators)

The K. Venkatesan, J. Jamie, C. McRae, I. Jamie, P. Karuso, A. Try, A. Piggot, B. Messerle, and Y. Jiang research groups for material supply and general assistance. People from CRC project for general support.

Macquarie University for the iMQRES scholarship (2015071) and PGRF grant.

My mother, **Galina Tikhonovna Eliseenko**, for moral support, invaluable recommendations, and your boundless love.

**Ita Meltser** who supported me during the whole project. It was, probably, hard to have a boyfriend - PhD student, but you have always shown full understanding, love, and desire to help.

Thank you all for your faith in me.

## DEDICATION

I dedicate this thesis to my mother,

Galina Tikhonovna Eliseenko

I believe you are proud of me, but you should first of all be proud of yourself. Everything that I achieved and will achieve further takes roots from the moral principles you have laid in me, and endless love that you generously share with me from the first my day.

Посвящается моей маме,

Галине Тихоновне Елисеенко

Я уверен, ты гордишься мной, но тебе, в первую очередь, стоит гордиться собой. Всё, что я достиг и ещё достигну в будущем, берёт своё начало в тех моральных принципах, что ты заложила в меня, а также в безграничной любви, которую ты щедро даришь мне с моего самого первого дня.

## ABBREVIATIONS

°	degrees
°C	degrees Celsius
Å	angstrom
μ	micro
AAA	asymmetric allylic alkylation
Ac	acetyl
acac	acetylacetonate
Ac	acetatyl
Alk	alkyl
Ar	aryl
atm	atmosphere
ATR	attenuated total reflectance
<i>aza</i> -MBH	<i>aza</i> -Morita–Baylis–Hillman
AZOP	2-( <i>N'</i> -arylozo)-2'-diphenylphosphino-1,1'-binaphthyl
BINAP	2,2'-bis(diphenylphosphino)-1,1'-binaphthyl
BINOL	1,1'-bi-2-naphthol
Bn	benzyl
Boc	<i>t</i> -butyl dicarbonate
Bu	butyl
BSA	<i>N,O</i> -bis(trimethylsilyl)acetate
Bz	benzoyl
BzOH	benzoic acid
cod	1,5-cyclooctadiene
Cy	cyclohexyl
dba	dibenzylidenacetone
DCE	dichloroethane
DCM	dichloromethane
DEAD	diethyl azodicarboxylate
DMSO	dimethylsulfoxide
dr	diastereomeric ratio
EDG	electron-donating group
<i>ee</i>	enantiomeric excess
Et	ethyl

eq.	equivalent
EWG	electron-withdrawing group
h	hour
H <sub>8</sub> -MAP	2-(dimethylamino)-2'-(diphenylphosphino)-5,5',6,6',7,7',8,8'-octahydro-1,1'-binaphthyl
HAM	hydroaminomethylation
HAROL	1,4-hydroxyarylalcohol
HPLC	high-performance liquid chromatography
HRMS	high resolution mass spectrometry
<i>i</i>	iso
IR	infrared
ICD	isocupreidine
<i>m</i>	meta
MAP	2-(dimethylamino)-2'-(diphenylphosphino)-1,1'-binaphthyl
MAPO	2-amino-2'-diphenylphosphinoyl-1,1'-binaphthyl
MBH	Morita–Baylis–Hillman
Me	methyl
mg	milligram
min	minute
mL	millilitre
MOC	memory of chirality
MOM	methoxymethyl
MOP	2-(diphenylphosphino)-2'-methoxy-1,1'-binaphthyl
MS	molecular sieve
MVK	methyl vinyl ketone
NBE	norbornene
NCS	<i>N</i> -chlorosuccinimide
NMP	<i>N</i> -methyl-2-pyrrolidone
NMR	Nuclear magnetic resonance
NOBIN	2-amino-2'-hydroxy-1,1'-binaphthyl
Nu	nucleophile
<i>o</i>	ortho
<i>p</i>	para
PCC	pyridinium chlorochromate
Ph	phenyl

Pr	propyl
pro	prochiral
PTE	proton transfer elimination
<i>rac</i>	racemic
QUINAP	1-(2-diphenylphosphin-1-naphthyl)isoquinoline
R	any functional group
<i>re</i>	stereochemical descriptor (as in the <i>re</i> face)
rt	room temperature
<i>si</i>	stereochemical descriptor (as in the <i>si</i> face)
<i>t, tert</i>	tertiary
TBHP	<i>tert</i> -butyl hydroperoxide
Tf	trifluoromethane sulfonyl
TFA	trifluoroacetate
THF	tetrahydrofuran
TLC	thin-layer chromatography
TPP	triphenylphosphine
TS	transition state
Ts	toluene sulfonyl
UV	ultraviolet

## LIST OF FIGURES

Figure 1	a) Privileged 1,1'-binaphthyl scaffold representatives; b) MAP-based multifunctional prototype.	3
Figure 2	a) P,C $\sigma$ allyl complexes of MAP; b) P,N allyl complex of H <sub>8</sub> -MAP.	5
Figure 3	Shi's P,N complex <b>1.7</b> .	6
Figure 4	P,N,N <sub>pyr</sub> MAP-based complexes <b>1.8–1.10</b> .	6
Figure 5	P,C <sub>carbene</sub> MAP-based complexes <b>1.11</b> and <b>1.12</b> .	7
Figure 6	General mechanism of an MBH reaction.	14
Figure 7	Proposed favoured TS with benzoic acid promoted PTE.	18
Figure 8	Potential of <i>aza</i> -MBH adducts as intermediates and ligands/auxiliaries in multistep processes.	133
Figure 9	<sup>1</sup> H NMR spectra of <b>4.11</b> in CDCl <sub>3</sub> indicating key proton patterns for anti/syn diastereomers assignment.	139
Figure 10	HPLC traces of product <b>4.11</b> , obtained from the <b>1.46a</b> -catalysed cascade.	141
Figure 11	<sup>1</sup> H NMR spectra of <b>4.12b</b> in CDCl <sub>3</sub> indicating key proton patterns for diastereomers assignment.	142
Figure 12	HPLC traces of product <b>4.14</b> obtained from <b>1.46a</b> -catalysed diethylzinc addition to racemic <i>aza</i> -MBH adduct <b>1.37b</b> (top) and from the <b>1.46a</b> -catalysed <i>aza</i> -MBH / diethylzinc addition sequence (bottom).	150
Figure 13	<sup>1</sup> H NMR spectra of <b>4.14</b> in CDCl <sub>3</sub> indicating key proton patterns for diastereomers assignment.	151

## LIST OF SCHEMES

Scheme 1	Palladium complexation modes on MAP.	5
Scheme 2	a) Cu/ <b>1.16</b> -catalyzed diethylzinc addition to chalcones and aldehydes; b) Cu/ <b>1.17</b> -catalysed diethylzinc addition to benzylideneacetones.	8
Scheme 3	a) MAP-based ligands <b>1.19</b> and <b>1.20a</b> in Cu-catalysed asymmetric Henry reaction; b) MAP-based ligands <b>1.19</b> in Cu-catalysed asymmetric chlorination and hydroxylation.	9
Scheme 4	a) Rh-catalysed acetophenone <b>1.25a</b> hydrogenation; b) Ir-catalysed olefins <b>1.27</b> hydrogenation.	10
Scheme 5	a) Ru-catalyzed ketones <b>1.25</b> hydrogenation; b) H-bond fixation of DMSO additive for the chiral pocket formation.	12
Scheme 6	a) $\alpha$ -Methylstyrenes <b>1.33</b> Rh-catalyzed hydroformylation; b) Silicon-oriented Rh-catalyzed $\beta$ -hydroformylation of alkenes <b>1.35</b> .	13
Scheme 7	a) MAP-based amides in <i>aza</i> -MBH reactions; b) MAP-based amides in allylic substitution of MBH acetates <b>1.39</b> .	15
Scheme 8	a) Catalyst <b>1.42a</b> in <i>aza</i> -MBH reaction; b) Catalyst <b>1.43a</b> in allylic substitution of MBH carbonates <b>1.44</b> with oxazolones.	16
Scheme 9	Tests of functional motif roles in MAP-based trifunctional system.	18
Scheme 10	a) Phenol acidity influence on multifunctional catalysis; b) Efficiency improvement in aniline-derived MAP-based multifunctional catalysts <b>1.48</b> .	20
Scheme 11	Synthesis of a MAP-based multifunctional prototype.	21
Scheme 12	$\beta$ -ICD in selected <i>aza</i> -MBH (a) and MBH (b) reaction tests.	35
Scheme 13	Catalysts <b>2.2</b> and <b>2.3</b> in selected <i>aza</i> -MBH (a) and MBH (b) reaction tests.	35
Scheme 14	MAP-based trifunctional catalysts <b>1.46</b> and <b>1.48</b> in MBH reaction tests.	36
Scheme 15	a) Kocovsky's work; b) and c) Ding's works; d) Kudo's work.	89
Scheme 16	MAP-based imine ligands <b>1.19</b> with phenol moieties in AAA.	91
Scheme 17	a) Enantiodivergency of AAA by bis(oxazole) H-bonding ligand <b>3.7a</b> ; b) The proposed origin of the enantiodivergency.	93
Scheme 18	a) H-bonding ligands <b>3.8a</b> , <b>b</b> and control ligands <b>3.8c–e</b> in asymmetric allylic amination; b) Stabilization of the “W”-isomer	94

	by the remote hydroxy the group.	
Scheme 19	Planned a) Pd-catalyzed AAA; b) Cu-catalysed diethylzinc addition; c) Rh-catalysed hydrogenation.	95
Scheme 20	Ligand <b>1.46a</b> in Rh-catalysed hydrogenation of methyl 2-acetamidoacrylate <b>3.9</b> .	74
Scheme 21	Example of MOC approach with the transformation of the initial chirality element.	131
Scheme 22	Example of the chelation model with maintained nature of the initial chiral center.	131
Scheme 23	Cascade of hydroaminomethylation interrupted by oxidation and reduction.	134
Scheme 24	Pd-catalyzed three-component cross-coupling cascade.	134
Scheme 25	Asymmetric tandem double Michael reactions catalyzed by ( <i>R</i> )- <b>1.16b</b> .	135
Scheme 26	Proposed <i>aza</i> -MBH / nucleophilic cyclization cascade.	136
Scheme 27	a) Proposed chiral <i>aza</i> -MBH / epoxidation sequential process; b) Racemic epoxidation of MBH adducts <b>2.1</b> .	136
Scheme 28	Proposed chiral <i>aza</i> -MBH / diethylzinc addition dual catalytic sequential process.	137
Scheme 29	<i>aza</i> -MBH adduct <b>1.37b</b> decomposition investigation in epoxidation conditions.	142
Scheme 30	Model racemic conditions for the MBH / epoxidation sequential process.	143
Scheme 31	a) <i>aza</i> -MBH adduct <b>1.37b</b> for Fe-catalysed epoxidation; b) Active in Sharpless epoxidation conditions MBH adducts <b>2.1</b> .	145
Scheme 32	a) Proposed stabilization of organozinc reagent by <i>aza</i> -MBH adduct <b>1.37b</b> ; b) Six-membered N,O-stabilisation of Zn in Reformatsky reaction; c) N,O-Zn complex for polymerization processes; d) N,O-ligand for conjugate addition of organozinc reagents.	147
Scheme 33	A control experiment with substrate <b>4.17</b> .	148
Scheme 34	a) Chiral tests of diethylzinc addition to <i>aza</i> -MBH adduct <b>1.37b</b> ; b) A tandem chiral <i>aza</i> -MBH / diethylzinc addition sequence.	149

## LIST OF TABLES

Table 1	Application of structures exhibiting dual catalytic properties.	23
Table 2	Application of structures exhibiting dual catalytic properties.	25
Table 3	Ligands <b>1.46a,i</b> , <b>1.48a</b> , and <b>2.4c</b> in Cu-catalysed diethylzinc addition to chalcone <b>1.13a</b> .	121
Table 4	Conditions investigation for <i>aza</i> -MBH / nucleophilic addition cascade	138
Table 5	Test of trifunctional organocatalyst <b>1.46a</b> in <i>aza</i> -MBH / nucleophilic addition cascade.	140
Table 6	Test of trifunctional organocatalyst <b>1.46a</b> in an <i>aza</i> -MBH / epoxidation sequence.	144
Table 7	Investigation of diethylzinc addition to racemic <i>aza</i> -MBH adduct <b>1.37b</b> .	146

# **CHAPTER 1**

## **The MAP Scaffold as a Versatile Platform for Hybrid Catalysis**

## CHAPTER 1. The MAP Scaffold as a Versatile Platform for Hybrid Catalysis

### 1.1. Background

Pharmaceutical and material industry needs in asymmetric catalysis are growing rapidly over the last decades and require intense investigations in this field.<sup>1-3</sup> Designing asymmetric catalytic systems de novo, however, remains a difficult task.<sup>4</sup> We have coined the “REAP” factor to describe the challenges for finding and developing high-performance catalysts: Rationale, Efficiency, Adaptability, and Proficiency.<sup>5</sup> Rational design of catalysts requires well-defined mechanistic understanding. Efficiency relies on finding the optimal cost-benefit ratio. Adaptability characterizes the necessary modular nature to catalyst syntheses for easier customization and, as a consequence, a reaction scope expansion. Proficiency is primarily defined as a concurrent enantioselectivity and reaction rate enhancement. Very few designed catalysts can fulfil the requirements of the “REAP” factor, however, many catalytic systems can satisfy the requirements partially.

All catalytic asymmetric processes can be broadly divided into three main domains: enzymatic systems, metal-based systems, and organic catalysts.<sup>6-10</sup> Enzymes provide the highest catalytic proficiency out of the three. However, enzymes often have very limited substrate scope.<sup>11</sup> Metal-catalytic processes can demonstrate high reaction rates and enantioselectivity, however, scalability and purification can present issues in terms of efficiency and sustainability.<sup>12, 13</sup> Organocatalysts are readily available, easily modifiable, and less toxic than metal catalysts. However, lower proficiency and high loadings limit the application of organocatalysts in many scenarios.<sup>5, 14, 15</sup>

In order to improve catalytic proficiency, novel generations of organo- and metal-catalysts, mimicking the enzymatic types of activation, have been developed.<sup>16-19</sup> Various combinations of four major catalytic motifs such as Brønsted and Lewis bases and acids became a dominant strategy in enzyme-mimicking design.<sup>20</sup> These catalytic motifs can be tuned and organized to

deliver precise chains of weak interactions between substrate and catalyst, similar to those formed between enzymes and substrates. “Hybrid catalysis”, defined as a combination of organocatalytic and metal activations supported by weak interactions, can increase the potential of higher catalytic proficiency, however, catalytic generality of this approach is challenging due to the complexity required in the design process. Nonetheless, hybrid catalysis is one starting point of developing complex catalysis that may in the long-term reveal new catalytic concepts and lead to novel catalytic systems with high performance potentials.

## 1.2. 1,1'-Binaphthyl Scaffold as a Candidate for “Hybrid” System Design

The 1,1'-binaphthyl scaffold (Figure 1a) is considered a privileged structure for developing catalytic systems<sup>21</sup> due to its high resistance to racemization in various reaction conditions, opportunities for the modular installation of functional groups, and extensive investigations in both organo- and metal-catalysed processes. The activity of main representatives of symmetrical binaphthyls, BINAP and BINOL, has been thoroughly investigated in cyclization, aldol, Strecker, Morita–Baylis–Hillman, reduction, Reissert, Diels–Alder, Friedel–Crafts, Nazarov, Ugi, Henry, ene-type, Mannich, Michael, cross-metathesis, ring-expansion, Bayer–Villiger, pericyclic, and coupling reactions.<sup>22-30</sup>

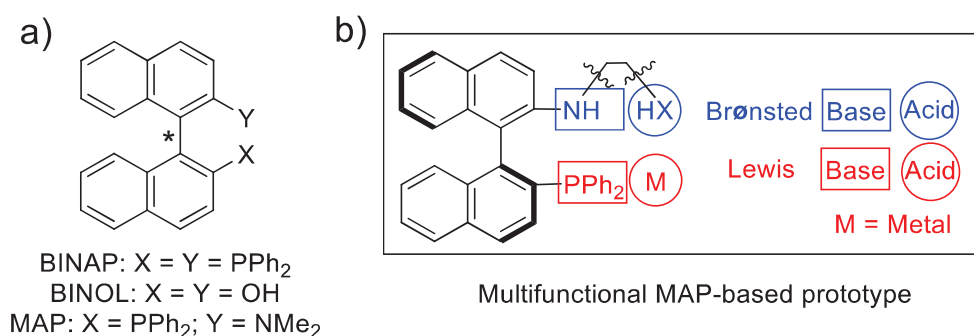


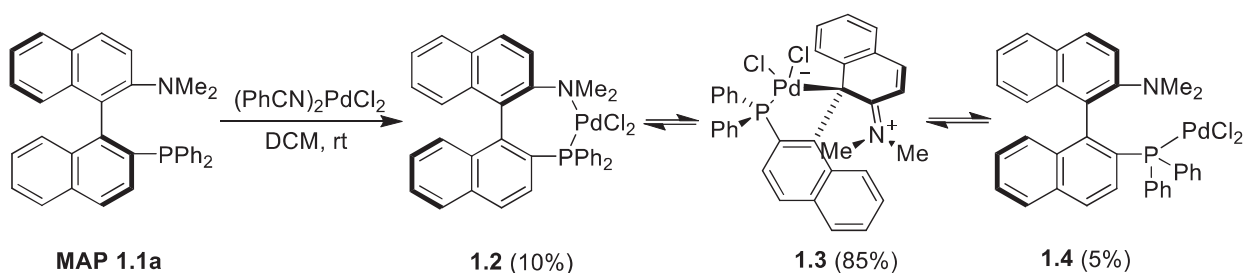
Figure 1 a) Privileged 1,1'-binaphthyl scaffold representatives; b) MAP-based multifunctional prototype.

The 2-amino-2'-phosphino-representatives of 1,1'-binaphthyls, also known as MAP-based derivatives, are a focus here due to several unique structural features (Figure 1b). The phosphine fragment can serve as a strong metal-chelating motif in metal-catalysed reactions or as a Lewis base catalytic function for initiation of organocatalytic processes. The second fragment, a protic secondary amine, can also serve as a mild metal-chelating fragment or a donor or acceptor of hydrogen bonds for an improved catalytic organization. Moreover, the amino group is easily modifiable, and additional catalytic functions such as Brønsted acids can be introduced as substituents. Clearly, the MAP-based multifunctional prototype, possessing diverse catalytic motifs for organocatalysis activation, metal-chelating centers for metal-catalysed processes promotion, and protic Brønsted acid and base fragments for H-bonding network formation, can be an excellent candidate for hybrid catalysis. The following literature survey will first highlight the main aspects of MAP-based structures application in metal- and organocatalysed asymmetric processes, followed by catalytic structures that are known to act as both ligands and organocatalysts.

### 1.3. MAP-based Structures in Metal- and Organocatalysed Asymmetric Processes

#### 1.3.1. MAP-metal coordination

Seminal investigations of palladium coordination modes on MAP **1.1a** were performed by the Kočovský's group. Initially, the P,N coordination mode **1.2** was postulated (Scheme 1).<sup>31-33</sup> However, the isolation and X-ray characterization of the MAP-PdCl<sub>2</sub> complex, prepared from bis(benzonitrile)palladium(II) dichloride and (*S*)-MAP, demonstrated a P,C<sub>σ</sub> coordination mode **1.3** rather than monodentate P **1.4** or bidentate P,N **1.2** modes.<sup>34</sup> The additional NMR investigations of the MAP-PdCl<sub>2</sub> complex in solvent showed that all possible P,N- **1.2**, P,C<sub>σ</sub>- **1.3**, and P-species **1.4** were present as a 10 : 85 : 5 mixture, respectively, in a dynamic equilibrium.



Scheme 1 Palladium complexation modes on MAP.

The initial studies of MAP as ligand were carried out in Pd-catalysed allylic alkylation reactions,<sup>31, 34-39</sup> and the  $\eta^3$ -allyl complexes of MAP with palladium were synthesized to investigate the possible catalytic species that may form in the reaction conditions (Figure 2a). The X-ray crystallography data of complexes **1.5** confirmed the unusual P,C $\sigma$ -ligation character of palladium on MAP.<sup>34, 39</sup> The P,C $\sigma$ -coordination is proposed to be driven by the lower distortion in the formed complex **1.3** than in P,N-mode **1.2**.<sup>34</sup> The similar P,C $\sigma$ -coordination of palladium is also common for biaryl ligands that have been successfully applied in Suzuki-Miyaura coupling processes.<sup>40, 41</sup>

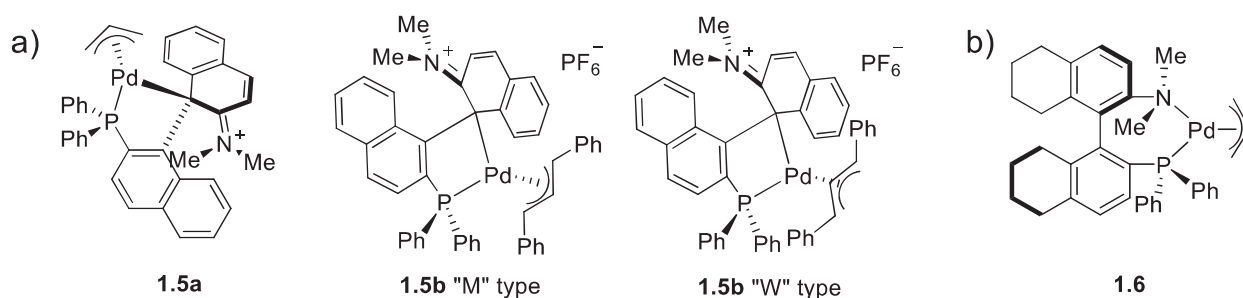
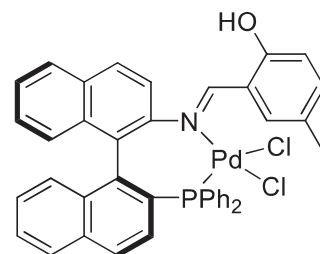


Figure 2 a) P,C $\sigma$  allyl complexes of MAP; b) P,N allyl complex of H<sub>8</sub>-MAP.

The NMR investigations of complex **1.5b** in deuterated chloroform solution revealed the presence of two diastereomeric rotamers, “M” and “W” (by the positioning of the allylic unit), along with the presence of minor P,N-chelated Pd species. However, the change of the bite angle between two palladium donors in these MAP-type ligands may switch the chelating mode from P,C $\sigma$  to P,N due to the increased energy of P,C $\sigma$ -mode in the system with the partially reduced

binaphthyl core.<sup>39</sup> Thus, the X-ray data collected from complex **1.6** (Figure 2b), formed from the partially reduced ligand H<sub>8</sub>-MAP (bite angle 98.9°, compared to 85.02° for MAP), unambiguously showed the P,N-coordination mode of palladium.<sup>39</sup>

The presence of additional strong chelation centers can also induce the change in the MAP ligand's coordination mode. As such, the replacement of the amine fragment with an imine changes the coordination pattern from P,C<sub>σ</sub> to P,N mode, furnishing the seven-membered chelate **1.7** (Figure 3).<sup>42</sup> Remarkably, the phenolic fragment in complex **1.7** does not participate in the coordination of palladium and can further be used as a Brønsted acid functionality for organized catalysis.



**1.7**

Figure 3 Shi's P,N complex **1.7**.

The inclusion in the MAP structure of another strongly chelating center, such as a pyridine ring, changes the chelation pattern further to tridentate P,N,N<sub>pyr</sub> mode for the first-row transition metals and Ru-complexes.<sup>43</sup> X-ray analysis demonstrates that copper(I) forms an uncommon trigonal monopyramidal (Figure 4 left) complex **1.8** while iron(II), cobalt(II), and nickel(II) provide similar square monopyramidal complexes **1.9** (Figure 4 middle). Ruthenium(II) furnished the classic octahedral sp<sup>3</sup>P, sp<sup>3</sup>N, sp<sup>2</sup>N complex **1.10** with a DMSO-S/Cl *trans* arrangement (Figure 4 right).

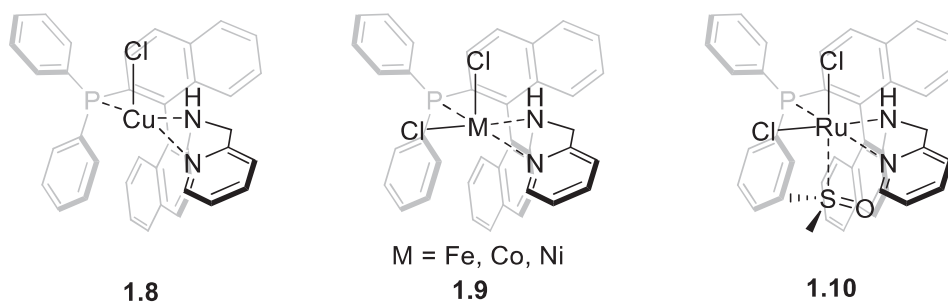


Figure 4 P,N,N<sub>pyr</sub> MAP-based complexes **1.8–1.10**.

The coordinating behaviour of *N*-heterocyclic carbene-containing MAP analogous was studied on the examples of Ir, Rh, and Pd complexes **1.11** and **1.12** (Figure 5).<sup>44, 45</sup> Based on the X-ray

data, all complexes demonstrated the expected P,C<sub>carbene</sub> *cis*-chelation mode between the metal and the ligand.

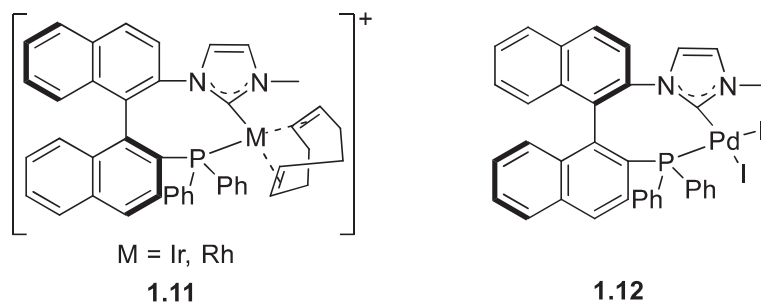


Figure 5 P,C<sub>carbene</sub> MAP-based complexes **1.11** and **1.12**.

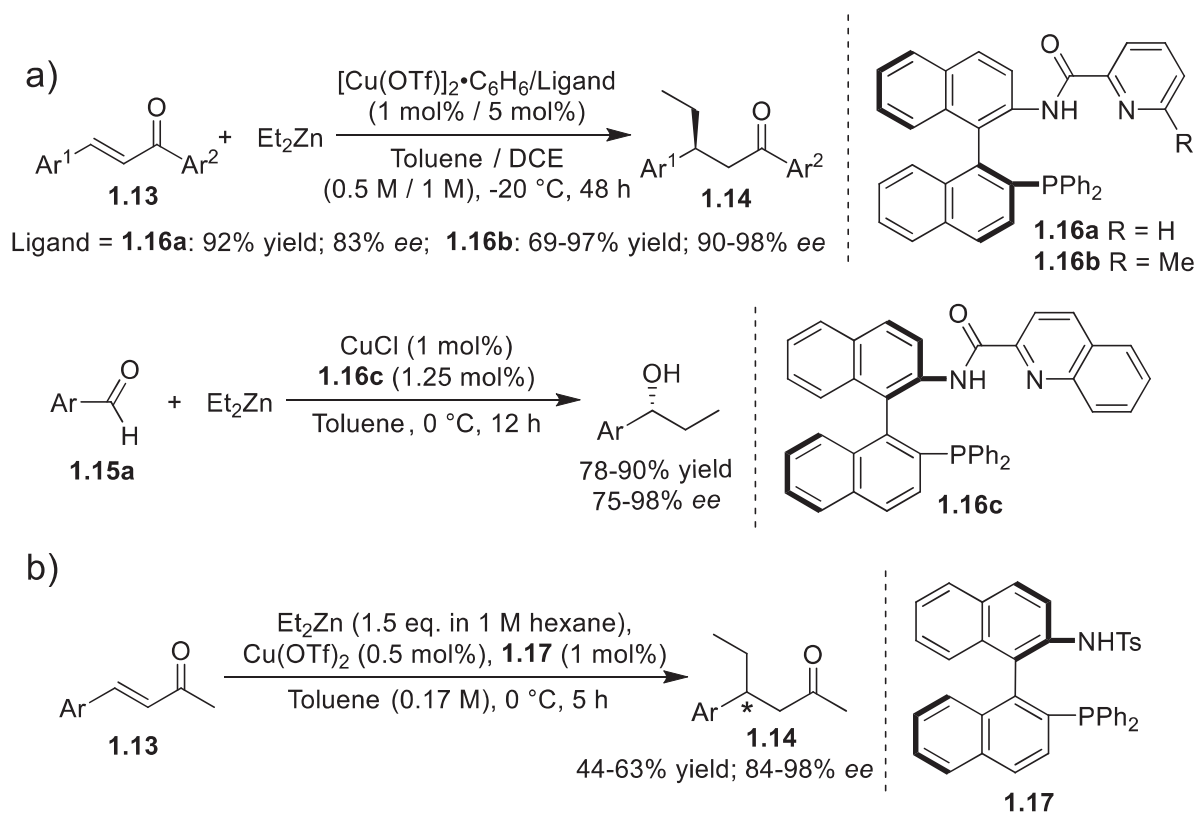
In summary, there is limited consistency of the data on the coordinational behaviour of MAP-based ligands. The complexation of these ligands directly depends on the additional functional motifs and structural features of the binaphthyl core. Classic MAP as a ligand tends to form unusual P,C<sub>σ</sub> complex. However, the insertion of additional strongly coordinating motifs or the alteration of the bite angle of metal donors may redirect the complexation to a P,N-mode.

### 1.3.2. MAP and its derivatives in metal-catalysed processes

Metal-catalysed processes where MAP-based structures have been applied as ligands can be broadly classified by the metal used. At the early stages of MAP investigation, most reactions have been carried out with palladium or copper. However, in the later decades, the attention turned to hydrogenation and hydrofunctionalisation reactions, catalysed predominantly by rhodium and ruthenium (see Appendices A1 for the full list of MAP-based ligands and applications).

Historically, MAP **1.1a** was developed as a ligand and extensively studied in complexes with palladium. The range of asymmetric reactions, catalysed by Pd/MAP varies from common allylic substitution,<sup>31, 36, 42, 46, 47</sup> coupling reactions,<sup>44, 48-51</sup> and  $\alpha$ -arylation or vinylation<sup>52-55</sup> of enolates to exotic dearomatization processes<sup>56, 57</sup> (further details in Chapter 3). In addition to in-depth

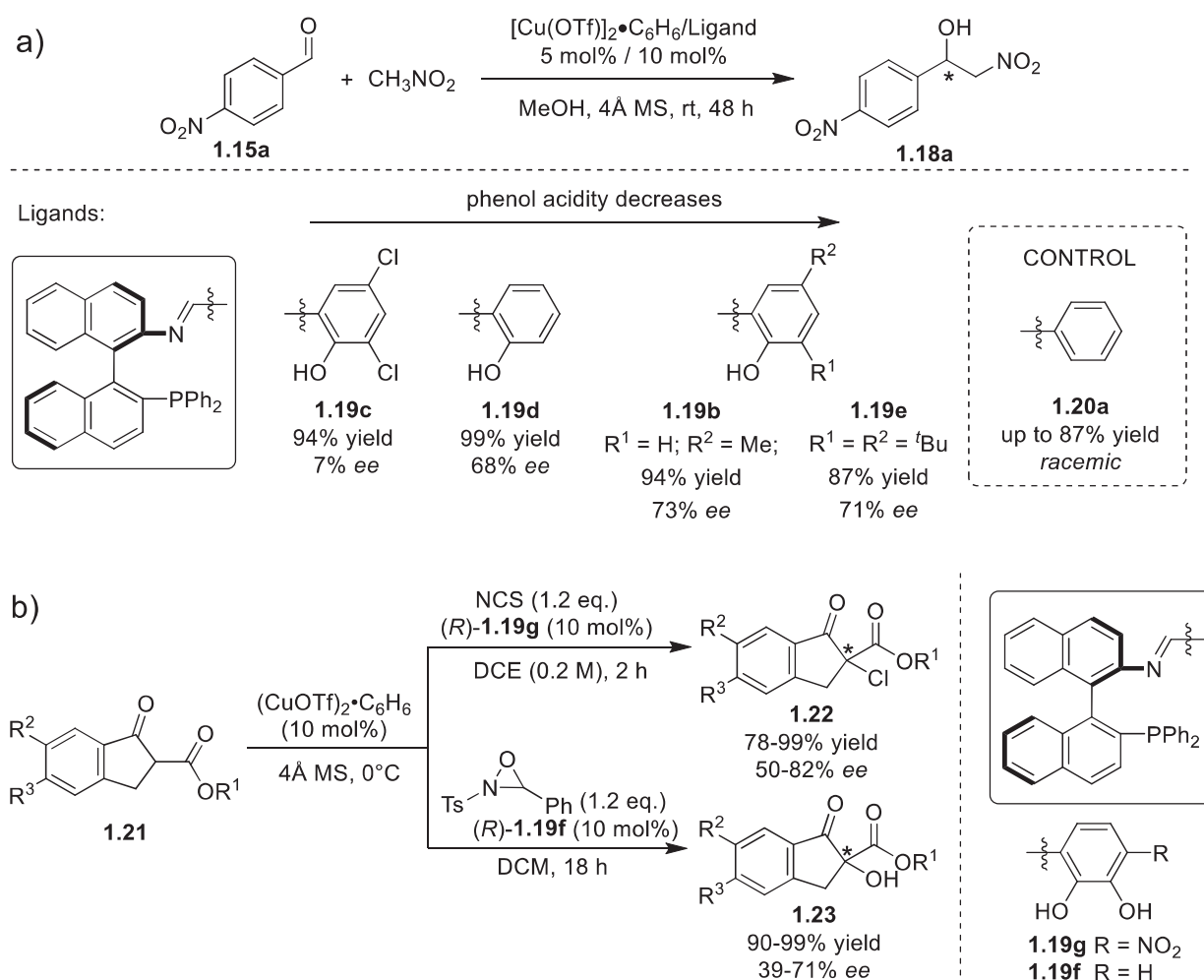
studies of Pd/MAP-catalysed reactions, the next first-row transition metal/MAP complexes that have received significant attention come from copper. The weaker binding of the metal to the ligand donors can provide a wider opportunity to introduce functional fragments in organocatalytic pathway together with metal-catalysed cycles.



Scheme 2 a) Cu/**1.16**-catalysed diethylzinc addition to chalcones and aldehydes; b) Cu/**1.17**-catalysed diethylzinc addition to benzylideneacetones.

An early investigation of Cu/MAP catalysis was carried out on the asymmetric diethylzinc addition to enones **1.13** and later to aromatic aldehydes **1.15** where reactions most probably proceed through the formation of cuprates. Pyridineamide MAP-derived ligands **1.16** were developed by Zhang *et al.* and demonstrated high selectivity in Cu-catalysed diethylzinc addition to acyclic chalcones **1.13** (83–98% ee)<sup>58</sup> or aromatic aldehydes **1.15** (75–98% ee)<sup>59</sup> (Scheme 2a). The more rigid amide bridge in the ligand structure may support the conformational rigidity of the binaphthyl backbone providing better asymmetry transfer. The pyridineamide ligands (*R*)-**1.16b** have been recently applied in Cu-catalysed tandem double Michael process.<sup>60</sup> Another

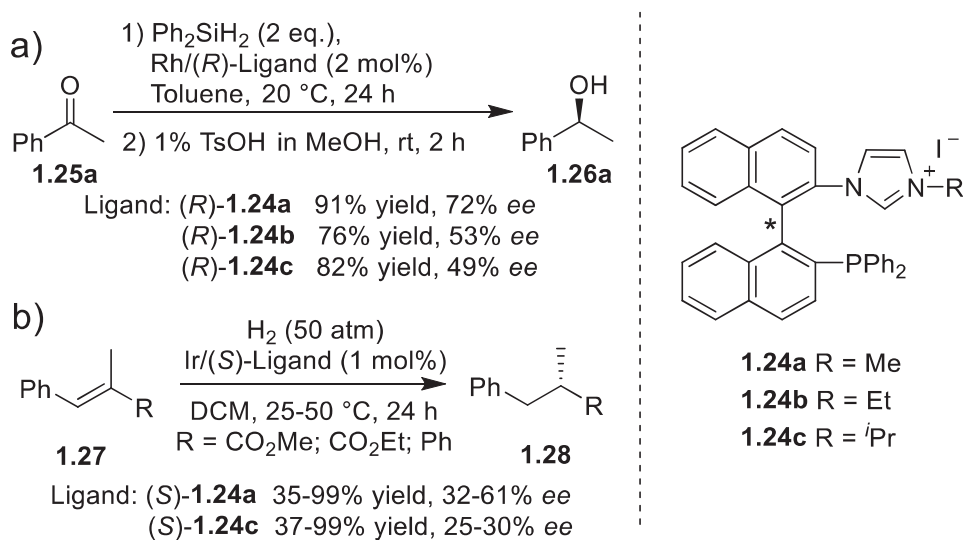
ligand that was successfully used in Cu-catalysed asymmetric diethylzinc addition to acyclic substrates such as benzylideneacetones **1.13** is a sulfonyl-substituted MAP-ligand **1.17** which provided the corresponding products **1.14** in >90% *ee* (Scheme 2b).<sup>61</sup> Both ligands **1.16** and **1.17** contain carbonyl or sulfonyl oxygen fragments in their structures that may improve the asymmetric induction of diethylzinc addition via an additional ligation of zinc to these fragments.



Scheme 3 a) MAP-based ligands **1.19** and **1.20a** in Cu-catalysed asymmetric Henry reaction; b) MAP-based ligands **1.19** in Cu-catalysed asymmetric chlorination and hydroxylation.

Phosphine–Schiff ligands **1.19** or **1.20a**, containing a phenolic fragment<sup>62</sup> were tested in asymmetric Henry reaction (Scheme 3a) where copper participates as a Lewis acid for aldehydes activation. The enantioselectivity of the reaction clearly responds to the alteration of the phenolic

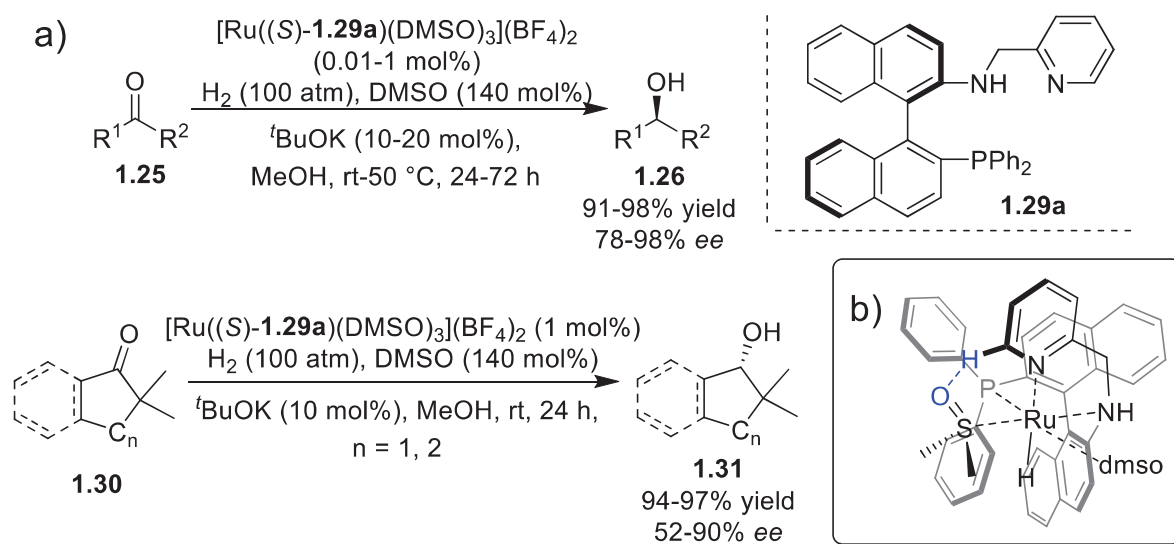
hydroxyl acidity that may indicate supporting H-bonding interactions in the catalytic process. Phenol-containing ligand **1.19c** with a more acidic phenol provides almost racemic outcome when the ligand **1.19d** with the unsubstituted phenol affords a substantial rise of the product's **1.18a** *ee* level to 68% in comparable reaction conditions. Further introduction of electron-donating moieties in the *para*-position to the phenolic hydroxyl in ligands **1.19b** and **1.19e** increased the *ee* level further up to 73% (Scheme 3a). While the control ligand **1.20a** without the Brønsted acid gave the racemic product **1.18a**. The <sup>1</sup>H NMR investigations of the Cu/**1.19b** complex demonstrated a downfield shift of the imine signal and disappearance of the phenolic hydrogen signal as compared to the free ligand spectra. The phosphorus signal revealed a downfield shift and was thought to indicate that Cu(I) can be potentially *N,O,P*-coordinated on the ligand **1.19b**. Later, Schiff base ligands **1.19** were also tested in Cu-catalysed asymmetric hydroxylation<sup>63</sup> or chlorination<sup>64</sup> of  $\beta$ -keto esters **1.21** and provided products **1.22** and **1.23** in up to 82% *ee* (Scheme 3b). For both reactions, ligands **1.19f, g** containing catechol-like fragments were found to be more enantioselective than their monophenol containing analogue **1.19b-e**. However, the enhancement of the complex's Lewis acidity by insertion of electron-withdrawing substituents may also influence the starting aldehyde recruitment and cannot be excluded.



Scheme 4 a) Rh-catalysed acetophenone **1.25a** hydrogenation; b) Ir-catalysed olefins **1.27** hydrogenation.

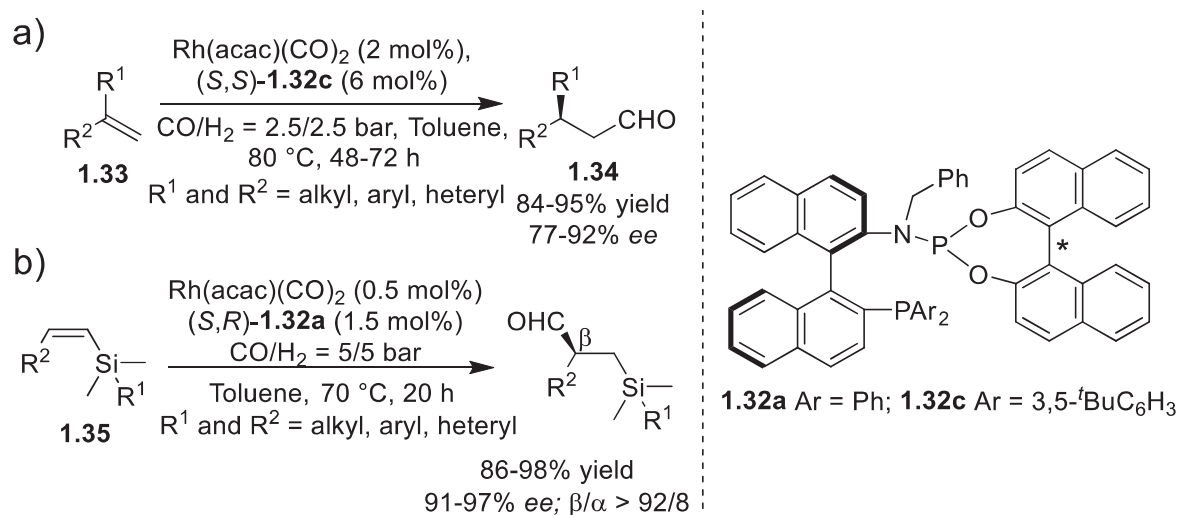
The modern MAP-based catalysis demonstrated a significant shift from palladium- or copper-catalysed processes to hydrogenation and hydrofunctionalisation reactions, catalysed by rhodium, iridium, and ruthenium where metals serve as hydride carriers. The early works in hydrogenation have been performed using carbene-derived MAP ligands **1.24** (Scheme 4).<sup>44, 45</sup> All complexes demonstrated moderate enantioselectivity in Rh-catalysed acetophenones **1.25a** hydrogenation (Scheme 4a)<sup>44</sup> and Ir-catalysed olefins **1.27** hydrogenation (Scheme 4b).<sup>45</sup> Enantioselectivity erosion was observed with the introduction of bulky substituents into the carbene core. For example, *iso*-propyl-substituted ligand **1.24c** provides the hydrogenation product **1.26a** in 49% *ee*, when its methyl-substituted analog **1.24a** gives 72% *ee* (Scheme 4a). Based on the analysis of experimental and crystallographic data, authors proposed that the extrusion of metal from the chiral backbone is higher than it is necessary for the enantioselective reaction that negatively affects efficient chirality transfer.

The pyridine-containing complex of **1.29a** with ruthenium, described previously in complexation section (Figure 4, complex **1.10**), demonstrated good to excellent enantioselectivity (in most cases >96% *ee*) in ketone **1.25** hydrogenation (Scheme 5a).<sup>43, 65, 66</sup> The DMSO additive was found crucial for the enantioselective catalysis. The chiral transfer occurs in the pocket formed by the ligand and a DMSO molecule ligated *trans* to the *sp*<sup>3</sup> N ligand site (Scheme 5b).<sup>66</sup> The DMSO molecule is additionally fixed by an H-bond between an  $\alpha$ -hydrogen of the ligand's pyridine moiety and the DMSO oxygen that allows the formation of a chiral pocket.



Scheme 5 a) Ru-catalysed ketones **1.25** hydrogenation; b) H-bond fixation of DMSO additive for the chiral pocket formation.

Recently Zhang *et al.* developed regio- and enantioselective protocols of Rh/**1.32**-catalysed asymmetric hydroformylation of vinyl heteroarenes (>90% *ee*)<sup>67</sup>,  $\alpha$ -methylstyrenes (77-92% *ee*)<sup>68</sup>, allylic alcohols and amines (80-92% *ee*)<sup>69</sup>, 1,1'-dialkyl olefins (90-99% *ee*)<sup>70</sup>, acrylic acid derivatives (up to 96% *ee*)<sup>71</sup> and hydrocyanation of alkenes.<sup>72</sup> For the Rh-catalysed  $\alpha$ -methylstyrenes **1.33** hydroformylation, (*S,R*)-**1.32** ligands were inefficient, providing little conversion while (*S,S*)-**1.32**, especially (*S,S*)-**1.32c**, provided the products with excellent regio- and enantioselectivity (Scheme 6a).<sup>68</sup> P,P-mode of Rh complexation was proposed, based on the previous investigations of **1.32** analogs<sup>73, 74</sup> and the importance of hindered phosphine centers in the (*S,S*)-configuration. As a further development of hydroformylation protocols, silicon-oriented (*S,R*)-**1.32a**/Rh-catalysed  $\beta$ -hydroformylation of alkenes **1.35** has been recently published (Scheme 6b).<sup>75</sup> High regio- and enantioselectivity of hydroformylation was achieved for aromatic and aliphatic substrates. The importance of silicone substituent for regioselectivity was proved experimentally by using control substrates without the silicon moiety.



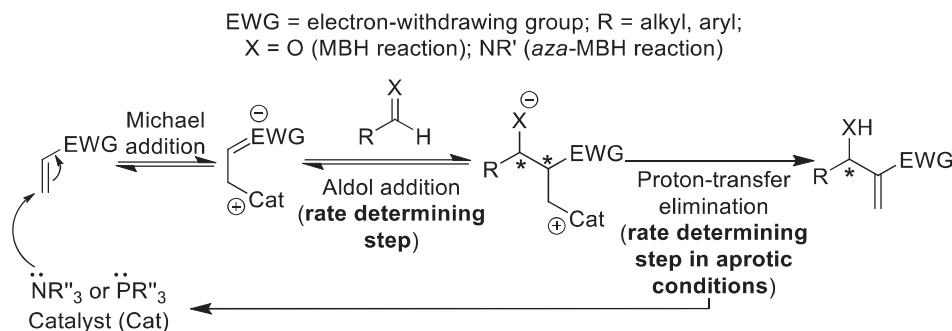
Scheme 6 a)  $\alpha$ -Methylstyrenes **1.33** Rh-catalysed hydroformylation; b) Silicon-oriented Rh-catalysed  $\beta$ -hydroformylation of alkenes **1.35**.

### 1.3.3. MAP and its derivatives in organocatalysed processes

MAP-based structures, bearing a phosphine Lewis base and a protic amine, have the potential to initiate reactions by the nucleophilic phosphine fragment and additionally organize reactions by weak interactions with the participation of the amino group. Almost all tests of MAP-based structures as organocatalysts were performed in two processes, namely Morita–Baylis–Hillman (MBH) reactions and allylic substitution of MBH adducts. This section reviews how different protic fragments of MAP-based organocatalysts can help organize reactions by H-bonding interactions (see Appendices A2 for the full list of MAP-based organocatalysts and applications).

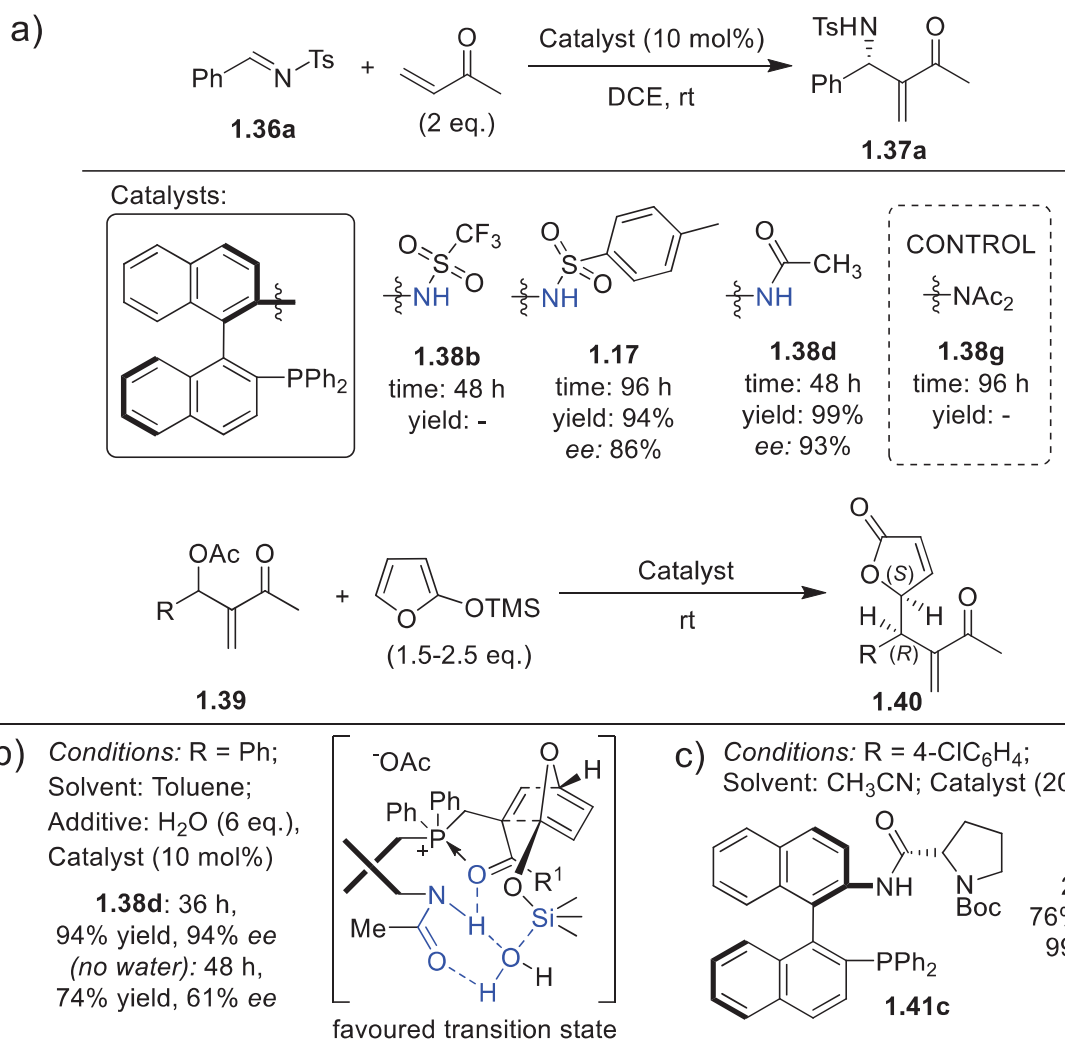
The general MBH mechanism (Figure 6)<sup>76</sup> starts with a reversible Michael addition of a catalyst to an activated alkene that forms a zwitterionic intermediate, which is exposed to an aldehyde/imine for the aldol addition (rate-limiting step). The adduct undergoes the proton transfer elimination (PTE) that gives the final MBH product and regenerates the catalyst, and this step may be rate-limiting in aprotic solvents. The reversibility of the first two steps, the shift of rate-determining step from PTE to aldol addition upon the product accumulation, and the

presence of the aldol intermediate as four diastereomers complicates the reaction mechanism making it very challenging for catalyst design that can control selectivity throughout the reaction process.



### 1.3.3.1. MAP-based bifunctional organocatalysts

All bifunctional amide-containing MAP-based organocatalysts have been investigated in detail in *aza*-MBH reactions<sup>77, 78</sup> and allylic amination (Scheme 7).<sup>79, 80</sup> *N*-acyl substituted catalyst **1.38d** (Scheme 7a) was able to proficiently catalyze the *aza*-MBH reaction providing the product **1.37a** in 99% yield and 93% *ee*.<sup>77</sup> Moreover, model tests demonstrate a clear dependence of proficiency on the presence and acidity of the organocatalyst's amide proton. Thus, the reaction does not occur with catalyst **1.38b**, bearing the most acidic amide proton, or with **1.38g** in the absence of an amide proton. The *N*-tosyl substituted catalyst **1.17**, which was described as an efficient ligand in asymmetric diethylzinc addition (Scheme 2b), demonstrated high activity in the organocatalysed asymmetric *aza*-MBH processes (Scheme 7a).

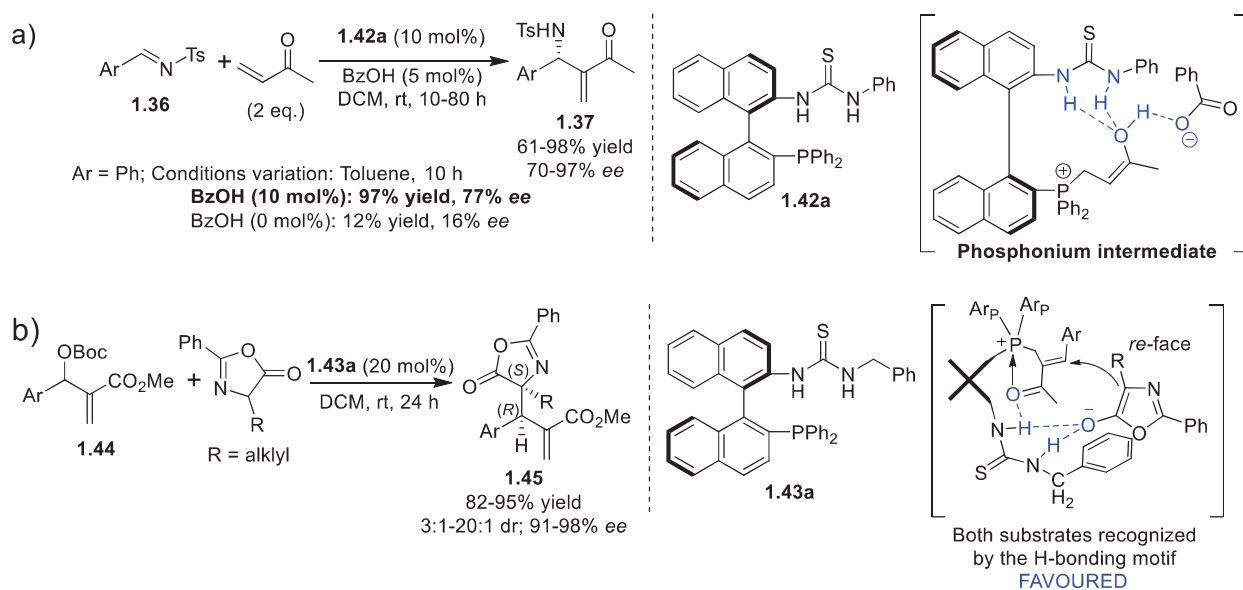


Scheme 7 a) MAP-based amides **1.38b,d,g** and **1.17** in *aza*-MBH reactions; b) MAP-based amides **1.38d** and **1.41c** in allylic substitution of MBH acetates **1.39**.

The amide catalysts were further tested in the asymmetric substitution of MBH acetates **1.39**<sup>79, 81</sup>,<sup>82</sup> and carbonates.<sup>80</sup> In these reports, the amide proton again plays a pivotal role in asymmetric induction.<sup>82</sup> Catalyst **1.38d** provides the alkylation product **1.40a** in 94% yield and 94% *ee* (Scheme 7b).<sup>82</sup> The enantioselective protocol requires water as an additive, and a proposed transition state illustrates how the amide moiety fixes both substrates through a water molecule via a network of H-bonding interactions (Scheme 7b). Later new pyrrolidine-containing MAP-based amides **1.41** were reported, bearing an additional source of chirality in the amide sidearm.<sup>80, 81</sup> The catalyst **1.41c**, containing an *N*-Boc protected pyrrolidine fragment, was the most proficient among the series, providing the product **1.40** in 76% yield and 99% *ee* over 24 h

(Scheme 7b right).<sup>81</sup> A set of control experiments with pyrrolidine unsubstituted catalysts indicated that the pyrrolidinic nitrogen may not play a significant role in chirality transfer.<sup>81</sup>

Thiourea-containing MAP-based catalysts **1.42** and **1.43** constitute another type of bifunctional organocatalysts, bearing a phosphine as the Lewis base and a thiourea fragment as a multidentate Brønsted acid motif. A set of diverse MAP-based urea and thiourea organocatalysts were designed and tested in the *aza*-MBH reaction,<sup>83</sup> allylic substitution,<sup>80, 84-86</sup> and annulations.<sup>87-90</sup> The model thiourea catalyst **1.42a** demonstrated the ability to implement enantioselective *aza*-MBH reactions in excellent yields and up to 91% *ee* (Scheme 8a).<sup>83</sup> The catalysis requires an external Brønsted acid additive to switch on the proficient pathway providing faster and more enantioselective formation of the product **1.37** (Scheme 8a). It was proposed that benzoic acid may help stabilize the phosphonium enolate intermediate cooperatively with the thiourea moiety via H-bonding (Scheme 8a right).



Scheme 8 a) Catalyst **1.42a** in *aza*-MBH reaction; b) Catalyst **1.43a** in allylic substitution of MBH carbonates **1.44** with oxazolones.

Diphenyl phosphite and phosphane,<sup>84</sup> oxindols and benzofuranones,<sup>80, 85</sup> oxazolones, and phthalimide<sup>86</sup> have been used as nucleophiles in allylic substitution reactions catalysed by thiourea-derived MAP catalysts. The first generation of *N*-aryl substituted thiourea catalysts **1.42**

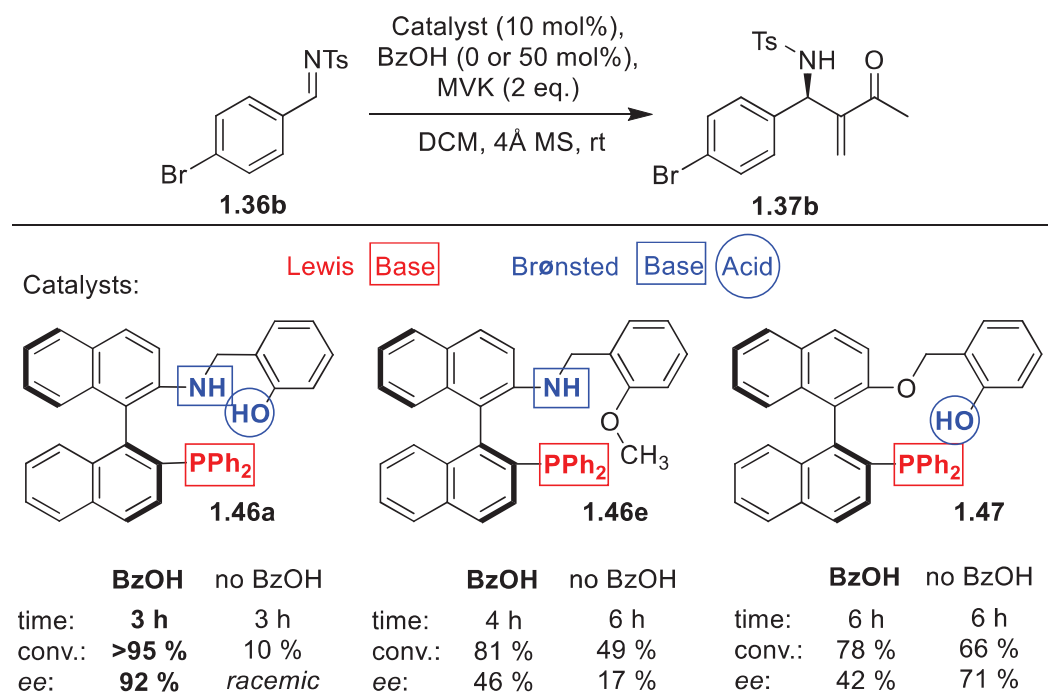
was inefficient in allylic substitution reactions,<sup>84, 86</sup> and the next generation of more structurally flexible thioureas **1.43** was developed. Catalysts **1.43** bear a methylene bridge between thiourea and the aromatic ring that allows the positioning of this ring to sterically restrict one of the nucleophile approaches.<sup>86</sup> In allylic substitution of MBH carbonates **1.44** with oxazolones, the thiourea catalyst **1.43a** provided highly diastereo- and enantioselective catalysis (Scheme 8b). Adequate phosphine nucleophilicity and acidity of the thiourea Brønsted acid motif were found crucial for enantioselective catalysis. In the suggested mechanism, the oxazolone anion, generated by <sup>t</sup>BuO<sup>-</sup> (formed after BocO<sup>-</sup> decomposition), can be recognized by the thiourea moiety (Scheme 8b right) to set up a selective attack of the oxazolone nucleophile to the allylic substrate.

#### *1.3.3.2. Trifunctional MAP-based organocatalysts with an amino bridge and external acid activation*

Acid activated, trifunctional MAP-based catalysts, containing a phosphine Lewis base, amino Brønsted base, and phenol Brønsted acid, were designed and applied in *aza*-MBH reactions.<sup>91-93</sup> The extension from bifunctional to trifunctional mode was achieved by the insertion of a Brønsted base motif that can interact with an external Brønsted acid additive. The polar or ionic nature of this interaction may help stabilize the zwitterionic intermediate increasing the reaction rate in non-polar aprotic solvents without enantioselectivity erosion.<sup>93</sup> The interaction between the external acid and the Brønsted base function could additionally favour a proficient proton transfer elimination pathway.<sup>93</sup> The trifunctional mode requires the external acid activation for enhancing reaction rate and enantioselectivity at ambient temperature, while the bifunctional mode requires low temperatures (low reaction rates) to achieve high enantioselectivity.

The model catalyst **1.46a** with an unsubstituted phenol ring is able to proficiently catalyze the *aza*-MBH reaction between *N*-tosylsubstituted benzaldimine **1.36b** and MVK, providing product

**1.37b** in >95% conversion over 3 h and up to 92% *ee* (Scheme 9).<sup>93</sup> The catalytic system is switchable and requires an external Brønsted acid additive for the proficient pathway activation (Scheme 9, **1.46a** example).<sup>93</sup> The role of every catalytic motif in cooperative catalysis has been investigated by a series of control experiments (Scheme 9).



Scheme 9 Tests of functional motif roles in MAP-based trifunctional system.

Bifunctional control catalysts **1.46e** (Brønsted acid control) and **1.47** (Brønsted base control) were tested in reactions with or without the benzoic acid additive. Catalyst **1.46e**, containing only the Lewis base and Brønsted base, demonstrated lower proficiency but retained its catalytic response to acid activation, while the catalyst **1.47**, bearing only the Lewis base and Brønsted acid, was deactivated by the external acid additive.

In the trifunctional mechanism of catalysis, an acid additive is able to regulate mechanistic complications mentioned on page 14, activating the reaction by H-bonding interactions. The acid additive facilitates a

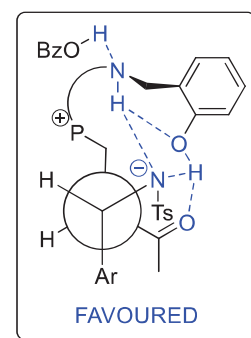
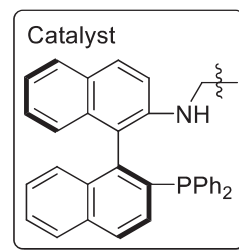
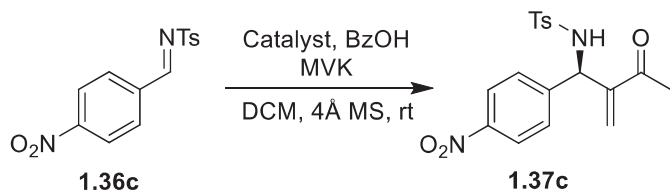


Figure 7 Proposed favoured TS with benzoic acid promoted PTE.

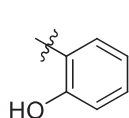
transition state with lower activation energy that favours one particular enantioselective PTE pathway (Figure 7).<sup>91-93</sup>

The acidity of the phenol Brønsted acid function plays a significant role in the formation of efficient H-bonding interactions. The tests of trifunctional MAP-based systems **1.46**, bearing electron-withdrawing and electron-donating substituents on the phenolic ring, showed that increased acidity of the Brønsted acid function can improve the proficiency of catalysis up to a certain limit (Scheme 10a).<sup>92</sup> The introduction of electron-withdrawing fluorine and bromine atoms in catalyst **1.46h** decreased the reaction time from 3 h to 15 minutes without the loss of enantioselectivity, providing one of the fastest *aza*-MBH processes at ambient temperature (Scheme 10a, catalyst **1.46h** vs. **1.46a**). However, the insertion of the nitro group into the catalyst structure (**1.46j** example) reduced the reaction rate, highlighting the importance of adequate acidity of the Brønsted acid motif for proficient catalysis. The negative influence of highly acidic Brønsted acid motif presence has been demonstrated earlier showing the possible quenching of the zwitterionic intermediate or phosphine Lewis base motif.<sup>94</sup> The influence of the bulky *ortho-tert*-butyl group is not so prominent on the reaction rate as the acidity influence that has been demonstrated by control experiments.<sup>92</sup> Altering of the phenol Brønsted acid to *N*-tosylaniline allowed a lower catalyst loading from 10 mol% for **1.46a** to 2 mol% for **1.48a** (Scheme 10).<sup>95, 96</sup> This is significantly lower than for most organocatalysts where loadings are typically 10–50 mol%. The ability of trifunctional catalyst **1.48a** to provide proficient organocatalysis also depends on an adequate acidity of the Brønsted acid function.<sup>95</sup> All catalysts presented in Scheme 10 are acid-switchable and required external acid activation for catalytic proficiency.<sup>92, 93, 95, 96</sup> The phenol and aniline Brønsted acid motif position was found particularly important for enantioselectivity as well.<sup>93</sup>



a) Conditions: Catalyst/BzOH (10/10 mol%), MVK (2 eq.)

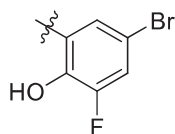
b) Conditions: Catalyst/BzOH 1/1, MVK (3 eq.)



**1.46a**

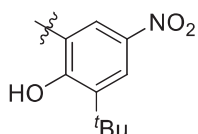
3 h  
>95% conv  
80% ee

15 min  
15% conv  
80% ee



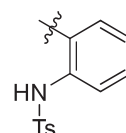
**1.46h**

15 min  
87% conv  
88% ee



**1.46j**

15 min  
57% conv  
87% ee



**1.48a**

10 mol%	5 mol%	2 mol%
30 min	30 min	30 min
>95% conv	>95% conv	89% conv
82% ee	88% ee	90% ee

Scheme 10 a) Phenol acidity influence on multifunctional catalysis; b) Efficiency improvement in aniline-derived MAP-based multifunctional catalysts **1.48**.

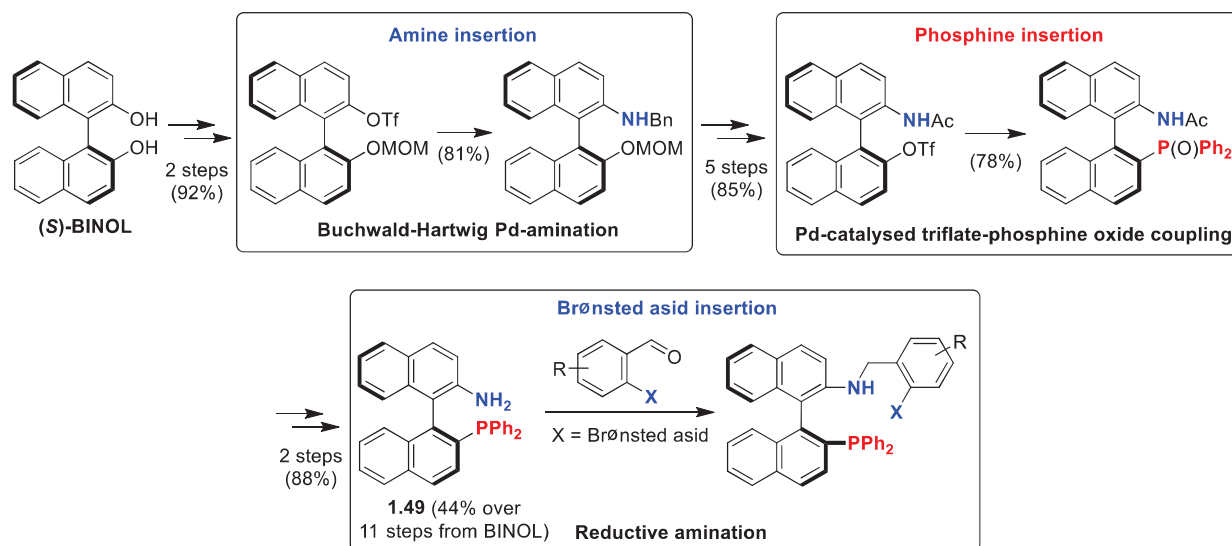
Despite the proficient catalysis provided by the trifunctional catalysts **1.46** and **1.48**, the reaction scope remains limited. The trifunctional prototype catalysts show significantly lower activities in the MBH reaction between 4-nitrobenzaldehyde **1.15a** and MVK, compared to the *aza*-MBH system (further details in Chapter 2, Scheme 14).<sup>92, 93, 96</sup>

Therefore, MAP-based structures were extensively studied in both metal- and organocatalyzed processes. The H-bonding activation was widely applied in organocatalytic processes but not prominent in the hybrid approach. So far, only *N*-tosyl substituted MAP-based structure **1.17** has been tested for a dual role of ligand and organocatalyst.

#### 1.3.4. Synthesis of MAP-based trifunctional catalysts

Currently, there are three main strategies for MAP core formation. The first is the lithiation strategy was reported by Buchwald *et al.*<sup>33, 53</sup> and includes initial Pd-amination of 2,2'-dibromo-1,1'-binaphthyl followed by a lithiation step for the phosphine insertion. This protocol affords

MAP-derivatives in 22% yield over four steps. The second approach was described by Maarseveen *et al.*<sup>97</sup> and it is based on the initial triflate coupling of BINOL derivative for phosphine insertion, followed by a Staudinger ligation step for amino group installation. The Staudinger pathway affords a MAP core in 41 h with 88% yield over five steps.



Scheme 11 Synthesis of a MAP-based multifunctional prototype.

The third and more reliable pathway was used in this project and includes a sequential modification of BINOL to *N*-benzyl-*O*-MOM-protected NOBIN (2-amino-2'-hydroxy-1,1'-binaphthyl) in 74.5% yield over three steps by combined Maruoka's<sup>98</sup> and Brückner's<sup>99</sup> procedures (Scheme 11). The key step, amino group installation, occurs via a Buchwald–Hartwig amination protocol. The further modification of *N*-benzyl-*O*-MOM-protected NOBIN to MAP-derivative can be performed in 58% yield over eight steps by Kočovský's<sup>31</sup> procedure with the key insertion of phosphine fragment via Pd-catalysed triflate coupling. This protocol results in the aminophosphine **1.49** which further has been used to reductively aminate an aldehyde, bearing an additional Brønsted acid function. This approach is modular to improve the “adaptability” characteristic of this catalytic system by readily incorporating different catalytic motifs in a convergent way.

## 1.4. Metal- and Organocatalytic Hybrid Catalysis

### 1.4.1. Structures exhibiting catalytic dualism

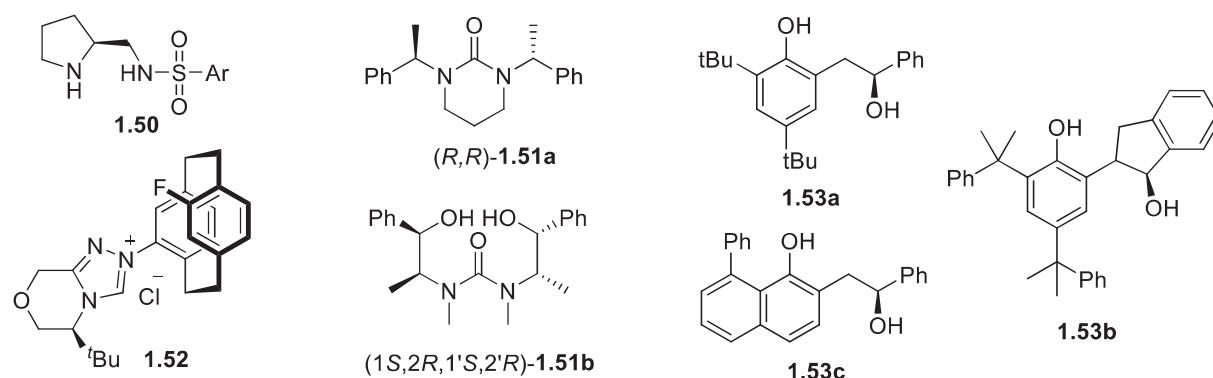
The combination of metal catalysis and organocatalysis is a modern and extensively developing field.<sup>100-102</sup> The application of metal- and organocatalytic cycles in one-pot or sequential processes afforded reactions that were not accessible by metal- or organocatalysis separately. However, the main issue remains the compatibility of catalysts applied in combination.<sup>103</sup> The use of one structure as the ligand and the organocatalyst may address the compatibility issue. Despite the simplicity of the idea, an efficient combination of organocatalytic and metal-ligating properties in a structure is challenging with only limited examples known (Table 1) such as carbene- **1.52**,<sup>104, 105</sup> urea- **1.51**,<sup>106</sup> pyrrolidine-containing structures **1.50**,<sup>107</sup> and 1,4-hydroxyarylalcohols **1.53** (HAROLs).<sup>108</sup>

Pyrrolidine-containing diamines **1.50** have been tested as organocatalysts in asymmetric  $\alpha$ -amination of aldehydes and as ligands in ruthenium-catalysed hydrogenation of prochiral ketones (Table 1, Entry 1).<sup>107</sup> The organocatalytic tests of **1.50** demonstrated the formation of the final *N*-aminooxazolidinones in modest yields, however in >80% *ee*. The efficiency of these structures as ligands is lower than as organocatalysts. Ruthenium-catalysed ketone hydrogenation tests demonstrated poor conversions and enantioselectivity. Attempts to prolong the reaction time did not lead to increased conversion that may indicate the decomposition of catalysts in reaction conditions.

Other structures **1.51** reported as organocatalyst and ligand, includes an *N*-substituted urea moiety as a core Lewis base fragment (Table 1, Entry 2).<sup>106</sup> Structures **1.51a** and **1.51b** were tested in aldolic condensations as organocatalysts and in copper-catalysed diethylzinc addition as ligands. Compound **1.51a** was found more efficient as organocatalyst providing high regio- and enantioselectivity, however, it demonstrated poor activity in the metal-catalysed process providing the racemic adduct in 16% yield. The structure **1.51b**, in turn, is able to provide both

organo- and metal-catalysed processes albeit at a modest level. As a ligand in diethylzinc addition, **1.51b** furnishes the adduct in 50% yield and 46% *ee* level. The further optimization of the diethylzinc addition process reached 62% *ee* using butyllithium as an additive.

Table 1 Application of structures exhibiting dual catalytic properties.



Entry	Structure	Ligand role		Organocatalyst role	
		Reaction	<i>ee</i> , [%]	Reaction	<i>ee</i> , [%]
1	<b>1.50</b> <sup>107</sup>	Ru-catalysed hydrogenation of prochiral ketones	31-61	$\alpha$ -Amination of aldehydes by DEAD	61-86
2	<b>1.51a,b</b> <sup>106</sup>	Diethylzinc addition to aldehydes	<b>1.51a</b> : -2 <b>1.51b</b> : 62	Aldol condensation	<b>1.51a</b> : 89 <b>1.51b</b> : 10
3	<b>1.52</b>	Cu-catalysed $\alpha$ -silylation of <i>N</i> -tosylimines <sup>104</sup>	80-98	$\alpha$ -Silylation of <i>N</i> -tosylimines <sup>104</sup>	68-92
		Cu-catalysed $\beta$ -borylation of enones <sup>105</sup>	58-99	$\beta$ -Borylation of enones <sup>105</sup>	65-84
4	<b>1.53a-c</b> <sup>108</sup>	Ti-promoted diethylzinc addition to benzaldehyde	<b>1.53a</b> : 58 <b>1.53b</b> : 83 <b>1.53c</b> : 80	MBH	<b>1.53a</b> : <i>rac</i> <b>1.53b</b> : 14 <b>1.53c</b> : 40

The next example is [2.2]paracyclophane-derived *N*-heterocyclic carbene **1.52** that was applied in organocatalytic and copper-catalysed asymmetric  $\alpha$ -silylation of *N*-tosylimines or  $\beta$ -borylation of enones (Table 1, Entry 3).<sup>104, 105</sup> The enantioselectivity of organocatalytic processes are slightly lower than for copper-catalysed counterparts, however, it still reaches 92% and 84% *ee* for silylation and borylation processes, respectively. Structure **1.52** as a ligand exhibited high proficiency in copper-catalysed processes providing excellent yields and enantioselectivities. These impressive results highlight the catalytic dualism of carbenecyclophane **1.52**.

HAROL-type structures **1.53** have been tested as organocatalysts in the MBH reaction and as ligands in diethylzinc addition (Table 1, Entry 4).<sup>108</sup> Exhibiting a modest organocatalytic activity in the MBH reaction, HAROLs provided the MBH adduct in up to 52% yield over 48 h. The best results from catalyst **1.53c** furnished the product in 40% *ee*. All HAROLs **1.53** served better as ligands in diethylzinc addition, allowing product formation in up to 83% *ee*.

All presented structures exhibiting catalytic dualism mostly tend to provide proficient catalysis as either an organocatalyst or a ligand for metal-catalysis but not in both. The next section reviews the latest cases of aminophosphine-containing organocatalysts<sup>109-115</sup> and ligands.<sup>115-124</sup>

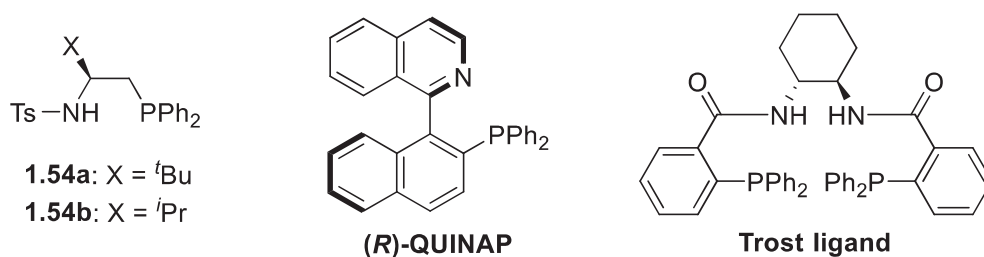
#### 1.4.2. Aminophosphine ligands as organocatalysts

While diverse aminophosphines have been thoroughly investigated as catalytic structures, only a few have been successfully tested in both metal- and organocatalysis. The data on the application of aminophosphines as dual catalysts are compiled in Table 2.

Aminophosphine **1.54a** was able to proficiently catalyse a formal [4+4] annulation as organocatalyst, providing product in 83% yield and 92% *ee*.<sup>125</sup> Notably, the same **1.54a** structure as a ligand demonstrated efficient asymmetric induction in copper-catalysed diethylzinc addition to cyclic enones, furnishing a wide row of products in 84-97% *ee*.<sup>126</sup> This activity makes aminophosphine **1.54a** one of the most efficient hybrid catalytic systems providing metal- and

organocatalysis. Analogous to aminophosphine **1.54a**, structure **1.54b** exhibited high enantioselectivity in a vast range of organocatalytic processes such as Rauhurt-Currier,<sup>127-130</sup> MBH,<sup>131, 132</sup> Michael domino,<sup>133</sup> and annulations.<sup>125, 134, 135</sup> However, the activity of **1.54b** in copper-catalysed diethylzinc addition test was limited with the product formation in only 50% *ee*.<sup>126</sup>

Table 2 Application of structures exhibiting dual catalytic properties.



Entry	Structure	Ligand role		Organocatalyst role	
		Reaction	<i>ee</i> , [%]	Reaction	<i>ee</i> , [%]
1	<b>1.54a, b</b>	Cu-catalysed diethylzinc addition to cyclic enones <sup>126</sup>	<b>1.54a</b> : 84-97 <b>1.54b</b> : 50%	Formal [4+4] annulation <sup>125</sup>	<b>1.54a</b> : 92
				Rauhurt-Currier, <sup>127-130</sup> MBH, <sup>131, 132</sup> Michael domino, <sup>133</sup> Annulations <sup>125, 134, 135</sup>	<b>1.54b</b> : up to 98 <b>1.54b</b> : 40-57 <b>1.54b</b> : 84 <b>1.54b</b> : up to 99
2	<b>(R)-QUINAP, Trost ligand</b>	Recognised privileged ligands <sup>116, 136, 137</sup>	up to 99	[3+2] annulation <sup>138</sup>	19-28

An opposite approach, where privileged phosphine ligands were screened in organocatalytic [3+2] annulation process was applied by Marinetti *et al.*<sup>138</sup> Among other phosphines, well-known aminophosphine ligands QUINAP<sup>116</sup> and the Trost ligand<sup>136, 137</sup> have been tested. Unfortunately, while highly efficient in metal-catalysed processes, (*R*)-QUINAP and Trost ligand as organocatalysts provided the product in only 28% and 19% *ee*, respectively.

## 1.5. Aim and Project Outline

This project is focused on the investigation and further development of the MAP-based trifunctional prototype and its organisational abilities. MAP-based trifunctional systems, such as **1.46** and **1.48**, can be investigated as organocatalysts as well as ligands for metal-catalysed processes in hybrid cascades or multistep reactions.

Three specific goals are listed below:

1. Investigate new Brønsted acid motifs that may maintain or improve the organocatalytic scope while potentially providing metal chelation capabilities.
2. Test MAP-based multifunctional systems as ligands in metal-catalysed processes for a deeper understanding of their dualistic nature.
3. Investigate MAP-based multifunctional systems for their ability to organize chirality transfer through hybrid multistep and cascade processes to complex molecules with several stereocenters.

In Chapter 2, a pyrrole-type Brønsted acid was tested in the trifunctional system to potentially improve catalytic cooperativity and reaction scope. Chapter 3 is focused on the application of MAP-based organocatalysts as ligands in metal-catalysed processes and highlights the influence of Brønsted acid functionalities on the degree and sense of asymmetric induction. Chapter 4 provides the preliminary investigations of MAP-based systems in multistep/cascade processes

with potentially dual catalytic properties. The last chapter summarises the main findings and provides potential avenues for future investigations.

## 1.6. References

1. I. Ojima, *Catalytic Asymmetric Synthesis*, John Wiley, Hoboken, N.J., 3rd edn., 2010.
2. J. R. Cossy, in *Comprehensive Chirality*, eds. E. M. Carreira and H. Yamamoto, Elsevier, Amsterdam, 2012, pp. 1-7.
3. D. Krištofiková, V. Modrocká, M. Mečiarová and R. Šebesta, *ChemSusChem*, 2020, **13**, 2828-2858.
4. T. P. Yoon, *Beilstein J. Org. Chem.*, 2017, **13**, 63-64.
5. F. Liu, *Chirality*, 2013, **25**, 675-683.
6. P. I. Dalko, *Enantioselective Organocatalysis*, WILEY-VCH, Weinheim, 2007.
7. V. Gotor, I. Alfonso and E. García-Urdiales, *Asymmetric Organic Synthesis with Enzymes*, Wiley-VCH, Weinheim, 2008.
8. K. Drauz, H. Gröger and O. May, *Enzyme Catalysis in Organic Synthesis*, Wiley-VCH, Weinheim, Germany, 3rd, completely rev. and enl. edn., 2012.
9. H. Pellissier, *Chem. Rev.*, 2013, **113**, 442-524.
10. K. Maruoka, *Asian J. Org. Chem.*, 2014, **3**, 319-319.
11. M. T. Reetz, *Chem. Rec.*, 2016, **16**, 2449-2459.
12. J. R. Ludwig and C. S. Schindler, *Chem*, 2017, **2**, 313-316.
13. P. Howard, G. Morris and G. Sunley, in *Metal-catalysis in Industrial Organic Processes*, eds. G. P. Chiusoli and P. M. Maitlis, The Royal Society of Chemistry, 2006, pp. 1-22.
14. V. Lykourinou, A. I. Hanafy, G. F. Z. da Silva, K. S. Bisht, R. W. Larsen, B. T. Livingston, A. Angerhofer and L.-J. Ming, *Eur. J. Inorg. Chem.*, 2008, 2584-2592.
15. R. Kenny and F. Liu, *Eur. J. Org. Chem.*, 2015, 5304-5319.
16. D. A. Nicewicz and D. W. C. MacMillan, *Science*, 2008, **322**, 77-80.
17. J. Ma, X. Ding, Y. Hu, Y. Huang, L. Gong and E. Meggers, *Nat. Commun.*, 2014, **5**.
18. F. Held, D. Grau and S. Tsogoeva, *Molecules*, 2015, **20**, 16103.
19. O. V. Serdyuk, A. Zamfir, F. Hampel and S. B. Tsogoeva, *Adv. Synth. Catal.*, 2012, **354**, 3115-3121.
20. J. Seayad and B. List, *Org. Biomol. Chem.*, 2005, **3**, 719-724.
21. Q.-L. Zhou, *Privileged Chiral Ligands and Catalysts*, Wiley-VCH, Weinheim, 2011.
22. B. List and S. Arseniyadis, *Asymmetric Organocatalysis*, Springer, Heidelberg ; New York, 2010.
23. M. Hatano and K. Ishihara, *Asian J. Org. Chem.*, 2014, **3**, 352-365.
24. G. Ma and M. P. Sibi, *Chem. Eur. J.*, 2015, **21**, 11644-11657.
25. C. M. Che and J. Huang, *Coord. Chem. Rev.*, 2003, **242**, 97-113.
26. P. Kočovský, Š. Vyskočil and M. Smrčina, *Chem. Rev.*, 2003, **103**, 3213-3246.
27. J. Hannedouche, J. Collin, A. Trifonov and E. Schulz, *J. Organomet. Chem.*, 2011, **696**, 255-262.
28. M. Turlington and L. Pu, *Synlett*, 2012, **23**, 649-684.
29. M. Kitamura, T. Ohkuma, S. Inoue, N. Sayo, H. Kumobayashi, S. Akutagawa, T. Ohta, H. Takaya and R. Noyori, *J. Am. Chem. Soc.*, 1988, **110**, 629-631.
30. A. de Meijere and F. Diederich, *Metal-Catalyzed Cross-Coupling Reactions*, Wiley-VCH, Weinheim, 2 edn., 2004.
31. Š. Vyskočil, M. Smrčina, V. Hanuš, M. Polášek and P. Kočovský, *J. Org. Chem.*, 1998, **63**, 7738-7748.
32. D. W. Old, J. P. Wolfe and S. L. Buchwald, *J. Am. Chem. Soc.*, 1998, **120**, 9722-9723.
33. A. Aranyos, D. W. Old, A. Kiyomori, J. P. Wolfe, J. P. Sadighi and S. L. Buchwald, *J. Am. Chem. Soc.*, 1999, **121**, 4369-4378.
34. P. Kočovský, Š. Vyskočil, I. Čisarová, J. Sejbal, I. Tišlerová, M. Smrčina, G. C. Lloyd-Jones, S. C. Stephen, C. P. Butts, M. Murray and V. Langer, *J. Am. Chem. Soc.*, 1999, **121**, 7714-7715.

35. G. C. Lloyd-Jones, S. C. Stephen, M. Murray, C. P. Butts, Š. Vyskočil and P. Kočovský, *Chem. Eur. J.*, 2000, **6**, 4348-4357.
36. Y. Wang, H. Guo and K. Ding, *Tetrahedron: Asymmetry*, 2000, **11**, 4153-4162.
37. I. J. S. Fairlamb, G. C. Lloyd-Jones, Š. Vyskočil and P. Kočovský, *Chem. Eur. J.*, 2002, **8**, 4443-4453.
38. L. Gouriou, G. C. Lloyd-Jones, Š. Vyskočil and P. Kočovský, *J. Organomet. Chem.*, 2003, **687**, 525-537.
39. Y. Wang, X. Li, J. Sun and K. Ding, *Organometallics*, 2003, **22**, 1856-1862.
40. R. Martin and S. L. Buchwald, *Acc. Chem. Res.*, 2008, **41**, 1461-1473.
41. T. E. Barder, S. D. Walker, J. R. Martinelli and S. L. Buchwald, *J. Am. Chem. Soc.*, 2005, **127**, 4685-4696.
42. Y.-W. Sun, J.-J. Jiang, M.-X. Zhao, F.-J. Wang and M. Shi, *J. Organomet. Chem.*, 2011, **696**, 2850-2856.
43. T. Yamamura, S. Nakane, Y. Nomura, S. Tanaka and M. Kitamura, *Tetrahedron*, 2016, **72**, 3781-3789.
44. P. Gu, Q. Xu and M. Shi, *Tetrahedron*, 2014, **70**, 7886-7892.
45. P. Gu, J. Zhang, Q. Xu and M. Shi, *Dalton Trans.*, 2013, **42**, 13599-13606.
46. Y. Wang, X. Li and K. Ding, *Tetrahedron Lett.*, 2002, **43**, 159-161.
47. M. Kawamura, R. Kiyotake and K. Kudo, *Chirality*, 2002, **14**, 724-726.
48. X. Shen, G. O. Jones, D. A. Watson, B. Bhayana and S. L. Buchwald, *J. Am. Chem. Soc.*, 2010, **132**, 11278-11287.
49. A. Herrbach, A. Marinetti, O. Baudoin, D. Guénard and F. Guéritte, *J. Org. Chem.*, 2003, **68**, 4897-4905.
50. S.-i. Kuwabe, K. E. Torraca and S. L. Buchwald, *J. Am. Chem. Soc.*, 2001, **123**, 12202-12206.
51. J. Yin and S. L. Buchwald, *J. Am. Chem. Soc.*, 2000, **122**, 12051-12052.
52. A. M. Taylor, R. A. Altman and S. L. Buchwald, *J. Am. Chem. Soc.*, 2009, **131**, 9900-9901.
53. T. Hamada and S. L. Buchwald, *Org. Lett.*, 2002, **4**, 999-1001.
54. T. Hamada, A. Chieffi, J. Åhman and S. L. Buchwald, *J. Am. Chem. Soc.*, 2002, **124**, 1261-1268.
55. A. Chieffi, K. Kamikawa, J. Åhman, J. M. Fox and S. L. Buchwald, *Org. Lett.*, 2001, **3**, 1897-1900.
56. J. García-Fortanet, F. Kessler and S. L. Buchwald, *J. Am. Chem. Soc.*, 2009, **131**, 6676-6677.
57. S. Rousseaux, J. García-Fortanet, M. A. Del Aguila Sanchez and S. L. Buchwald, *J. Am. Chem. Soc.*, 2011, **133**, 9282-9285.
58. X. Hu, H. Chen and X. Zhang, *Angew. Chem., Int. Ed.*, 1999, **38**, 3518-3521.
59. Q. Wang, S. Li, C.-J. Hou, T.-T. Chu and X.-P. Hu, *Appl. Organomet. Chem.*, 2019, **33**, e5108.
60. Q. Wang, S. Li, C.-J. Hou, T.-T. Chu and X.-P. Hu, *Tetrahedron*, 2019, **75**, 3943-3950.
61. T. Morimoto, N. Mochizuki and M. Suzuki, *Tetrahedron Lett.*, 2004, **45**, 5717-5722.
62. J.-J. Jiang and M. Shi, *Tetrahedron: Asymmetry*, 2007, **18**, 1376-1382.
63. J.-J. Jiang, J. Huang, D. Wang, M.-X. Zhao, F.-J. Wang and M. Shi, *Tetrahedron: Asymmetry*, 2010, **21**, 794-799.
64. J.-J. Jiang, J. Huang, D. Wang, Z.-L. Yuan, M.-X. Zhao, F.-J. Wang and M. Shi, *Chirality*, 2011, **23**, 272-276.
65. T. Yamamura, H. Nakatsuka, S. Tanaka and M. Kitamura, *Angew. Chem., Int. Ed.*, 2013, **52**, 9313-9315.
66. S. Nakane, T. Yamamura, S. K. Manna, S. Tanaka and M. Kitamura, *ASC Catal.*, 2018, **8**, 11059-11075.
67. B. Wei, C. Chen, C. You, H. Lv and X. Zhang, *Org. Chem. Front.*, 2017, **4**, 288-291.

68. C. You, S. Li, X. Li, J. Lan, Y. Yang, L. W. Chung, H. Lv and X. Zhang, *J. Am. Chem. Soc.*, 2018, **140**, 4977-4981.
69. C. You, S. Li, X. Li, H. Lv and X. Zhang, *ASC Catal.*, 2019, **9**, 8529-8533.
70. D. Zhang, C. You, X. Li, J. Wen and X. Zhang, *Org. Lett.*, 2020, **22**, 4523-4526.
71. S. Li, Z. Li, C. You, X. Li, J. Yang, H. Lv and X. Zhang, *Org. Lett.*, 2020, **22**, 1108-1112.
72. X. Li, C. You, J. Yang, S. Li, D. Zhang, H. Lv and X. Zhang, *Angew. Chem., Int. Ed.*, 2019, **58**, 10928-10931.
73. Y. Deng, H. Wang, Y. Sun and X. Wang, *ASC Catal.*, 2015, **5**, 6828-6837.
74. M. Lei, Z. Wang, X. Du, X. Zhang and Y. Tang, *J. Phys. Chem. A*, 2014, **118**, 8960-8970.
75. C. You, X. Li, Y. Yang, Y.-S. Yang, X. Tan, S. Li, B. Wei, H. Lv, L.-W. Chung and X. Zhang, *Nat. Commun.*, 2018, **9**, 2045.
76. H. Sasai and S. Takizawa, in *Comprehensive Chirality*, eds. E. M. Carreira and H. Yamamoto, Elsevier, Amsterdam, 2012, pp. 234-263.
77. M.-J. Qi, T. Ai, M. Shi and G. Li, *Tetrahedron*, 2008, **64**, 1181-1186.
78. X.-Y. Guan, Y.-Q. Jiang and M. Shi, *Eur. J. Org. Chem.*, 2008, 2150-2155.
79. G.-N. Ma, S.-H. Cao and M. Shi, *Tetrahedron: Asymmetry*, 2009, **20**, 1086-1092.
80. D. Wang, Y.-L. Yang, J.-J. Jiang and M. Shi, *Org. Biomol. Chem.*, 2012, **10**, 7158-7166.
81. Y. Wei, G.-N. Ma and M. Shi, *Eur. J. Org. Chem.*, 2011, 5146-5155.
82. Y.-Q. Jiang, Y.-L. Shi and M. Shi, *J. Am. Chem. Soc.*, 2008, **130**, 7202-7203.
83. Y.-L. Shi and M. Shi, *Adv. Synth. Catal.*, 2007, **349**, 2129-2135.
84. H.-P. Deng and M. Shi, *Eur. J. Org. Chem.*, 2012, 183-187.
85. Y.-L. Yang, C.-K. Pei and M. Shi, *Org. Biomol. Chem.*, 2011, **9**, 3349-3358.
86. H.-P. Deng, Y. Wei and M. Shi, *Eur. J. Org. Chem.*, 2011, 1956-1960.
87. R.-Q. Xu, Q. Gu, W.-T. Wu, Z.-A. Zhao and S.-L. You, *J. Am. Chem. Soc.*, 2014, **136**, 15469-15472.
88. X.-N. Zhang, H.-P. Deng, L. Huang, Y. Wei and M. Shi, *Chem. Commun.*, 2012, **48**, 8664-8666.
89. H.-P. Deng, Y. Wei and M. Shi, *Org. Lett.*, 2011, **13**, 3348-3351.
90. X.-N. Zhang and M. Shi, *ASC Catal.*, 2013, **3**, 507-512.
91. C. Anstiss, J.-M. Garnier and F. Liu, *Org. Biomol. Chem.*, 2010, **8**, 4400-4407.
92. J.-M. Garnier and F. Liu, *Org. Biomol. Chem.*, 2009, **7**, 1272-1275.
93. J.-M. Garnier, C. Anstiss and F. Liu, *Adv. Synth. Catal.*, 2009, **351**, 331-338.
94. P. Buskens, J. Klankermayer and W. Leitner, *J. Am. Chem. Soc.*, 2005, **127**, 16762-16763.
95. C. Anstiss, PhD, Macquarie University, 2011.
96. C. Anstiss and F. Liu, *Tetrahedron*, 2010, **66**, 5486-5491.
97. P. N. M. Botman, O. David, A. Amore, J. Dinkelaar, M. T. Vlaar, K. Goubitz, J. Fraanje, H. Schenk, H. Hiemstra and J. H. van Maarseveen, *Angew. Chem., Int. Ed.*, 2004, **43**, 3471-3473.
98. T. Ooi, K. Ohmatsu and K. Maruoka, *J. Am. Chem. Soc.*, 2007, **129**, 2410-2411.
99. D. Sälinger and R. Brückner, *Synlett*, 2009, **2009**, 109-111.
100. S. Afewerki and A. Córdova, *Top. Curr. Chem.*, 2019, **377**, 38.
101. Z. Shao and H. Zhang, in *Comprehensive Inorganic Chemistry II*, eds. J. Reedijk and K. Poepelmeier, Elsevier, Amsterdam, 2 edn., 2013, pp. 155-175.
102. D.-F. Chen, Z.-Y. Han, X.-L. Zhou and L.-Z. Gong, *Acc. Chem. Res.*, 2014, **47**, 2365-2377.
103. Q.-L. Zhou, *Angew. Chem., Int. Ed.*, 2016, **55**, 5352-5353.
104. Z. Chen, Y. Huo, P. An, X. Wang, C. Song and Y. Ma, *Org. Chem. Front.*, 2016, **3**, 1725-1737.

105. L. Wang, Z. Chen, M. Ma, W. Duan, C. Song and Y. Ma, *Org. Biomol. Chem.*, 2015, **13**, 10691-10698.
106. M. Hernández-Rodríguez, C. G. Avila-Ortiz, J. M. del Campo, D. Hernández-Romero, M. J. Rosales-Hoz and E. Juaristi, *Aust. J. Chem.*, 2008, **61**, 364-375.
107. N. Dahlin, A. Bøgevig and H. Adolfsson, *Adv. Synth. Catal.*, 2004, **346**, 1101-1105.
108. Ö. Dilek, M. A. Tezeren, T. Tilki and E. Ertürk, *Tetrahedron*, 2018, **74**, 268-286.
109. H. Ni, W.-L. Chan and Y. Lu, *Chem. Rev.*, 2018, **118**, 9344-9411.
110. H. Guo, Y. C. Fan, Z. Sun, Y. Wu and O. Kwon, *Chem. Rev.*, 2018, **118**, 10049-10293.
111. H. Y. Su and M. S. Taylor, *J. Org. Chem.*, 2017, **82**, 3173-3182.
112. Y. Xiao, Z. Sun, H. Guo and O. Kwon, *Beilstein J. Org. Chem.*, 2014, **10**, 2089-2121.
113. Y. Wei and M. Shi, *Chem. - Asian J.*, 2014, **9**, 2720-2734.
114. L.-W. Xu, *ChemCatChem*, 2013, **5**, 2775-2784.
115. W. Li and J. Zhang, *Chem. Soc. Rev.*, 2016, **45**, 1657-1677.
116. B. V. Rokade and P. J. Guiry, *ASC Catal.*, 2018, **8**, 624-643.
117. T. Zell and D. Milstein, *Acc. Chem. Res.*, 2015, **48**, 1979-1994.
118. R. H. Morris, *Acc. Chem. Res.*, 2015, **48**, 1494-1502.
119. Y.-Y. Li, S.-L. Yu, W.-Y. Shen and J.-X. Gao, *Acc. Chem. Res.*, 2015, **48**, 2587-2598.
120. J. R. Khusnutdinova and D. Milstein, *Angew. Chem., Int. Ed.*, 2015, **54**, 12236-12273.
121. M. Asay and D. Morales-Morales, *Dalton Trans.*, 2015, **44**, 17432-17447.
122. M. P. Carroll and P. J. Guiry, *Chem. Soc. Rev.*, 2014, **43**, 819-833.
123. A. S. Valeria and P. S. Irina, *Curr. Org. Chem.*, 2012, **16**, 2893-2920.
124. J. Wassenaar and J. N. H. Reek, *Org. Biomol. Chem.*, 2011, **9**, 1704-1713.
125. H. Ni, X. Tang, W. Zheng, W. Yao, N. Ullah and Y. Lu, *Angew. Chem., Int. Ed.*, 2017, **56**, 14222-14226.
126. I. J. Krauss and J. L. Leighton, *Org. Lett.*, 2003, **5**, 3201-3203.
127. A. Albrecht, A. Skrzyńska, A. Przydacz and Ł. Albrecht, *Synlett*, 2015, **26**, 2679-2684.
128. S. Takizawa, T. M.-N. Nguyen, A. Grossmann, M. Suzuki, D. Enders and H. Sasai, *Tetrahedron*, 2013, **69**, 1202-1209.
129. S. Takizawa, T. M.-N. Nguyen, A. Grossmann, D. Enders and H. Sasai, *Angew. Chem., Int. Ed.*, 2012, **51**, 5423-5426.
130. J.-J. Gong, T.-Z. Li, K. Pan and X.-Y. Wu, *Chem. Commun.*, 2011, **47**, 1491-1493.
131. F. Zhong, Y. Wang, X. Han, K.-W. Huang and Y. Lu, *Org. Lett.*, 2011, **13**, 1310-1313.
132. X. Han, Y. Wang, F. Zhong and Y. Lu, *Org. Biomol. Chem.*, 2011, **9**, 6734-6740.
133. S. Takizawa, K. Kishi, M. Kusaba, B. Jianfei, T. Suzuki and H. Sasai, *Heterocycles*, 2017, **95**, 761-767.
134. E. Li and Y. Huang, *Chem. Eur. J.*, 2014, **20**, 3520-3527.
135. Z. Jin, R. Yang, Y. Du, B. Tiwari, R. Ganguly and Y. R. Chi, *Org. Lett.*, 2012, **14**, 3226-3229.
136. B. M. Trost, M. R. Machacek and A. Aponick, *Acc. Chem. Res.*, 2006, **39**, 747-760.
137. I. C. Lennon and M. Jackson, in *e-EROS Encycl. Reagents Org. Synth.*, 2012.
138. N. Fleury-Brégeot, L. Jean, P. Retailleau and A. Marinetti, *Tetrahedron*, 2007, **63**, 11920-11927.



## **CHAPTER 2**

# **New MAP-based Multifunctional Organocatalysts with Improved Cooperativity**

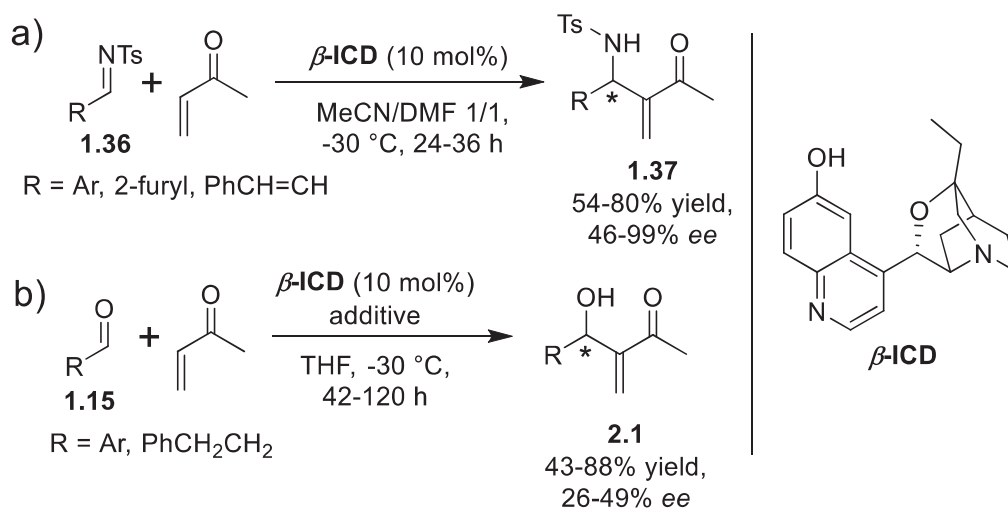
## CHAPTER 2. New MAP-based Multifunctional Organocatalysts with Improved Cooperativity

### 2.1. Introduction

Multifunctional catalytic systems are able to organize a reaction environment providing proficient catalysis in most cases via the creation of a subtle H-bonding network.<sup>1, 2</sup> To build such an efficient network, catalytic motifs work in cooperation to provide a synergistic outcome.<sup>1, 3</sup> The following chapter is devoted to the development of MAP-based catalytic systems with new Brønsted acid motifs to potentially enhance cooperation between the activator and the catalytic system in order to extend the reaction scope of the trifunctional MAP-based organocatalysts.

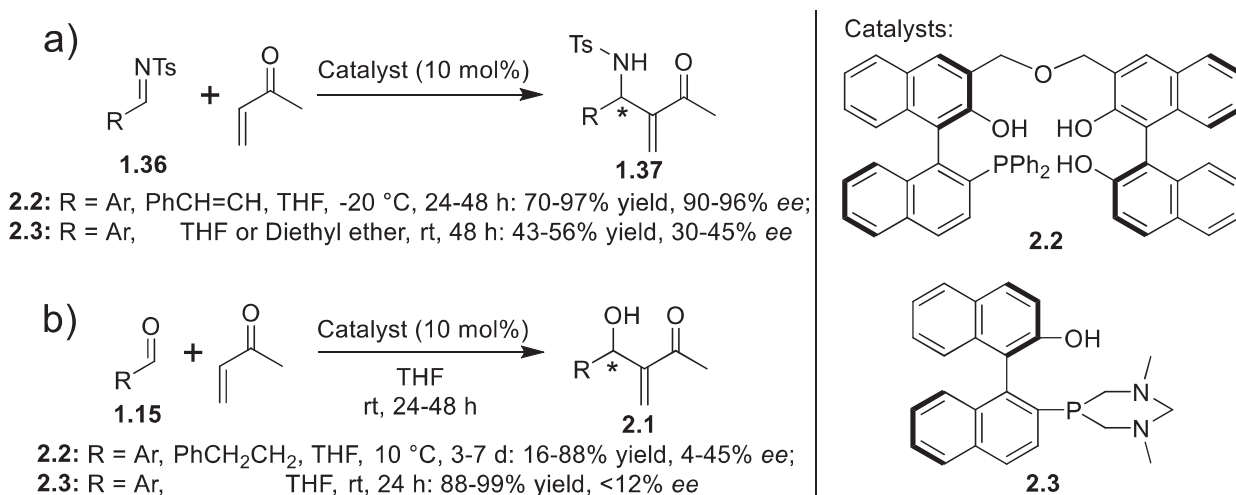
#### 2.1.1 Catalysts efficient in both *aza*-MBH and MBH reactions

Many efficient catalysts were developed for *aza*-MBH or MBH processes over the last decades. However, only a few of them were able to proficiently catalyse both reactions.<sup>4-19</sup> This issue of catalytic generality could be explained by the complex, condition-dependent mechanisms of the MBH processes.<sup>1</sup> For example, bifunctional catalyst  $\beta$ -isocupreidine ( $\beta$ -ICD) demonstrated the ability to furnish *aza*-MBH adducts **1.37** in excellent enantioselectivity and up to 80% yields (Scheme 12a).<sup>9, 17</sup> However, the activity of  $\beta$ -ICD was poor in the MBH tests with only up to 49% *ee* and 43-88% yields (Scheme 12b), except for very reactive substrates such as 1,1,1,3,3,3-hexafluoroisopropyl acrylate<sup>12, 19</sup> or isatins.<sup>4, 7</sup>



Scheme 12  $\beta$ -ICD in selected *aza*-MBH (a) and MBH (b) reaction tests.

Other MOP-based bifunctional catalysts **2.2** and **2.3** have been tested in both *aza*-MBH and MBH reactions.<sup>20-22</sup> However, in spite of their good activities in *aza*-MBH processes (Scheme 13a), these catalysts demonstrated low levels of efficiency in MBH reactions (Scheme 13b).



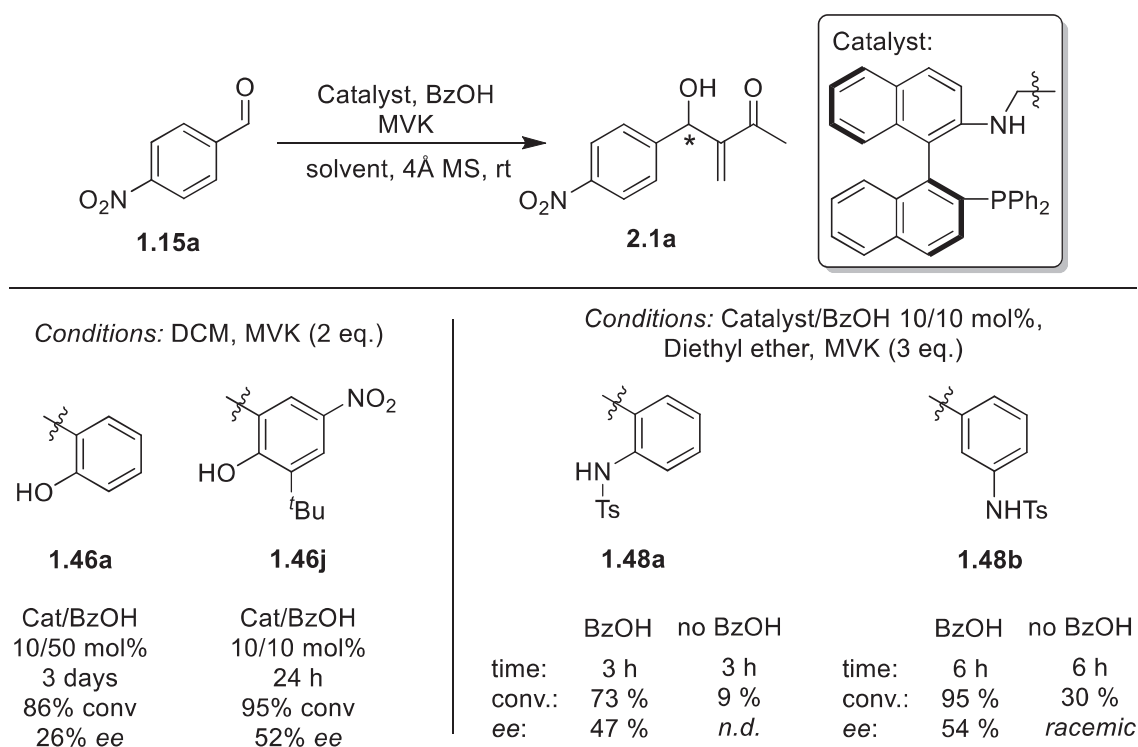
Scheme 13 Catalysts **2.2** and **2.3** in selected *aza*-MBH (a) and MBH (b) reaction tests.

An *L*-proline/imidazole co-catalytic system was able to provide proficient catalysis of *aza*-MBH<sup>11</sup> and MBH<sup>14</sup> processes. Nevertheless, this system was not tested in reactions with aromatic electrophiles and MVK.

In conclusion, general asymmetric catalysis for the *aza*-MBH and MBH reactions is a long-standing issue for this class of reactions.

### 2.1.2 MAP-based trifunctional systems in the MBH reaction

The trifunctional MAP-based organocatalytic systems **1.46** and **1.48** were developed using *aza*-Morita–Baylis–Hillman reactions.<sup>23-25</sup> The complex mechanism of MBH reaction (Paper,<sup>26</sup> Scheme 1a) also limited the generality of this system.<sup>27-32</sup> The attempts to apply the trifunctional prototypes in MBH reaction between 4-nitrobenzaldehyde **1.15a** and MVK demonstrated a dramatic loss of activity, compared to *aza*-MBH reactions (Scheme 14).<sup>23-25</sup> The reaction rate of **1.46a** and **1.46j** was 8–25 times slower with up to only 52% *ee* value.<sup>23, 24</sup> Catalysts **1.48a** and **1.48b** exhibited higher catalytic rates (73–95% conversion in 3–6 h) with little improvements in enantioselectivity (up to 54% *ee*).<sup>25</sup> These observations raised new questions on possible new catalytic motifs for investigation in order to improve the generality of the catalysis.



Scheme 14 MAP-based trifunctional catalysts **1.46** and **1.48** in MBH reaction tests.

### 2.1.3 *Pyrrole as a candidate for improved cooperative catalysis design*

The pyrrolyl fragment may serve as a good candidate for the catalytical functionality and cooperativity improvement. Firstly, a pyrrole ring can be used as a metal ligating fragment. The application of pyrrolyl compounds as ligands<sup>33-36</sup> indicates the efficiency of this fragment for metal ligation. Another property of the pyrrole ring is its ability to form H-bonding interactions. The recent examples demonstrated pyrrole substances as H-bonding catalysts in Mannich-type<sup>37</sup> and Michael addition reactions.<sup>38</sup> Electron-rich pyrrole rings can also provide CH/ $\pi$  bonding as indicated by crystallographic investigations.<sup>39, 40</sup> Pyrrole-containing MAP-based multifunctional organocatalysts are novel and have not been investigated before. The initial synthesis and several tests of two pyrrolyl-containing catalysts (**1a**, **b** in Paper) were performed prior to this PhD thesis in the master of research training program. All other data in the publication was performed during this thesis work.

## 2.2 Results and Discussion

The synthesis of new catalysts, their catalytic activity investigation, and major findings in terms of their catalytic generality in the MBH reaction class are discussed in the following publication.<sup>26</sup>



# Switchable pyrrole-based hydrogen bonding motif in enantioselective trifunctional organocatalysis



Sviatoslav S. Eliseenko, Fei Liu<sup>\*,\*</sup>

Department of Molecular Sciences, Macquarie University, Sydney, NSW 2109, Australia

## ARTICLE INFO

### Article history:

Received 11 October 2018

Received in revised form

10 December 2018

Accepted 11 December 2018

Available online 19 December 2018

### Keywords:

Switchable catalysis

Cooperativity

Trifunctional organocatalysis

Enantioselectivity

Pyrroles

Morita–Baylis–Hillman reaction

## ABSTRACT

Pyrroles are versatile chemical motifs for molecular recognition or ligand design but their utility as catalytic components are underexplored. We incorporated a pyrrole motif into our acid-switchable, MAP-based trifunctional organocatalytic system. The switching-on of this system by an external Brønsted acid, 3-methyl benzoic acid, presented proficient catalysis in both *aza*-Morita–Baylis–Hillman (MBH, up to >95% conversion and 88% *ee* over 3 h) and MBH (up to 81% conversion and 77% *ee* over 6 h) reactions. The enhanced catalytic generality and proficiency may be due to the new cooperativity via CH/ $\pi$  interactions between pyrrole and the acid switch.

© 2018 Elsevier Ltd. All rights reserved.

## 1. Introduction

Pyrroles are chemical motifs prevalent in bioactive compounds [1], ligands [2], sensors [3], and molecular assemblies [4]. The versatile chemistry of pyrroles in part derives from the multifunctional pyrrolyl NH group that is weakly acidic and basic, in addition to the electron-rich  $\pi$  system primed for electrophilic substitution reactions and also hydrogen-bonding interactions [5]. The role of pyrroles as catalytic components, however were mainly explored within the context of calix[4]pyrrole systems and remain under developed [6]. More recently, pyrrole NH motifs have been used in hydrogen bonding catalysis as part of a tunable H-bonding catalyst [6a,c], expanding significantly from its normal coordination role as a ligand. Questions now can be raised on new roles of pyrrole in switchable catalysis [7] given pyrrole's multifunctional nature. Here we report a novel example of a pyrrole-containing, acid-switchable, enantioselective trifunctional organocatalytic system with enhanced generality and enantioselectivity, likely due to the multifunctional aspect of the pyrrole motif involving not only the NH hydrogen-bond donor but also the  $\pi$  electron system through CH/ $\pi$  hydrogen bonding [8]. This catalysis extends beyond the

typical role of pyrrole as a coordination or pH switching site.

We have, in our prior work, originated a switchable, enantioselective trifunctional organocatalytic prototype for activating enones in carbon-carbon bond forming reactions such as the Morita–Baylis–Hillman (MBH) reaction (Fig. 1a) [9]. The prototype trifunctional system is built on a very versatile MAP-based chemical system [10]. The MAP-based catalysts typically contain three catalytic motifs: a phosphine nucleophile for reaction initiation, an amine Brønsted base for responding to the external acid switch, and a phenol Brønsted acid for H-bonding interactions that help stabilize the formation of zwitterionic intermediates [9,11]. An external, strong Brønsted acid additive, such as benzoic acid, switches the catalysis from slow and racemic to fast and enantioselective, particularly for the *aza*-MBH reactions that are often slow in rate with capricious catalytic scope [12]. We have also investigated multiple generations of this system by tuning the acidity of the internal Brønsted acid motif [12f,13a,11,13b,c,9], and in all cases, benzoic acid has been the best additive to switch on the fast and enantioselective catalysis. One persistent issue for this switchable system however is to extend the generality to cover not just the *aza*-MBH but also the MBH reactions. One potential solution is to find more synergistic noncovalent interactions between the acid-activator and the catalyst. This may also address a long-standing challenge of engineering compact molecular assemblies with tunable catalytic properties that require a more synergistic

\* Corresponding author.

E-mail address: [fei.liu@mq.edu.au](mailto:fei.liu@mq.edu.au) (F. Liu).

## How can we improve the synergic interactions between external and internal Brønsted acids?

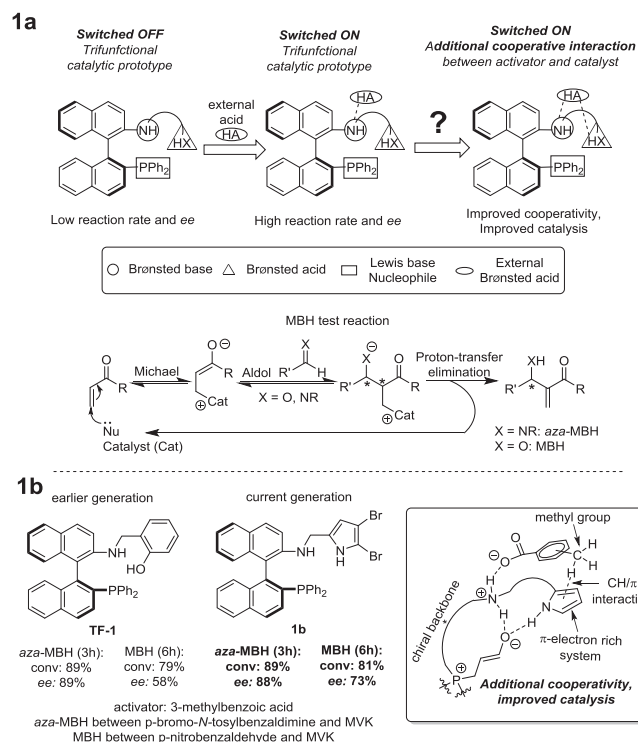


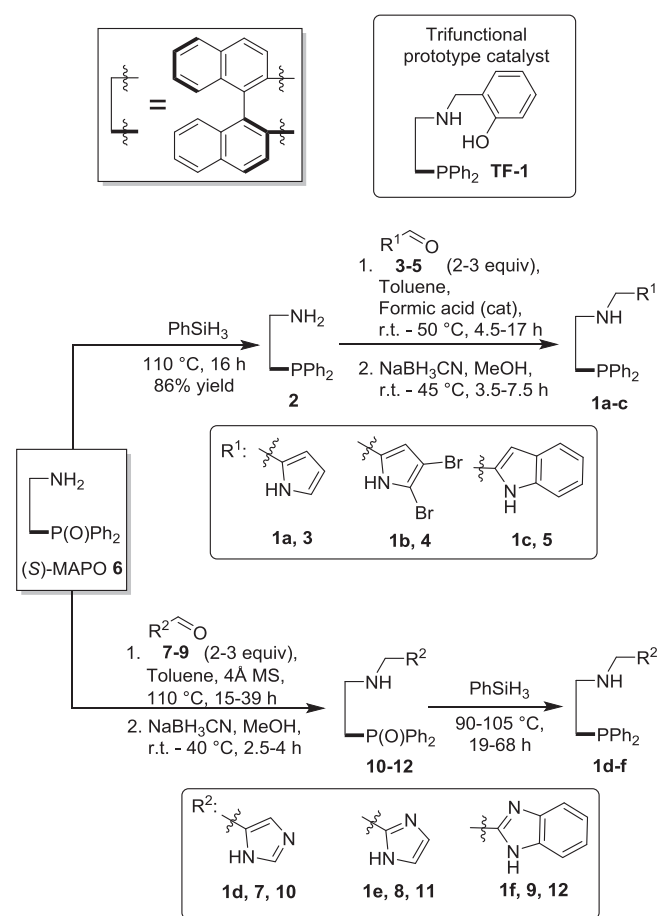
**Fig. 1.** a) Switchable and enantioselective trifunctional organocatalytic prototype given a general mechanism of a test MBH reaction; b) Enhancing switchable catalysis with multifunctional recognition motifs such as pyrroles.

network of molecular recognition arrangements.

To test this hypothesis, we investigated the potential of the multifunctional pyrrole motif that contains weakly acidic NH group for H-bonding interactions and the electron-rich  $\pi$  system that could act, in close spatial proximity, as an H bond acceptor that may enhance the interaction with the external acid activator (Fig. 1b). We found that a pyrrole-based catalyst, activated by 3-methyl benzoic acid, provided catalytic improvement in MBH catalysis with an increase in *ee* by 15% (approx. 1.5 fold by *e.r.*, up to 73%), in comparison to our earlier generations of catalysts such as trifunctional catalyst **TF-1**. Pyrrole phosphines were previously used as *N*-phosphinepyrrole ligands in complexes with Rh in hydroformylations [14], Pd in CO-ethene co-polymerization [15], Pt in benzene vinylation [16], and Ir in enantioselective hydrogenation [17]. The complexation patterns of *N*-pyrrole-phosphine ligands with Cr, Ru, Mo, W, and Se were also reported [18]. The 2-phosphino-*N*-aryl or alkyl substituted pyrroles were investigated as ligands for Pd [19] and Ru [20]. The ligands where both pyrrole and phosphine fragments bind Ni [21] or Cu [22] were also described. Pyrrole-containing phosphines are also known as bioactive molecules [23]. However, phosphine pyrroles have not been used previously as organocatalysts and our chiral phosphine-pyrrole system here represents the first set of such examples.

## 2. Results and discussion

A series of pyrrole-containing catalysts were designed and synthesized (Scheme 1). The unsubstituted pyrrole catalyst **1a** was synthesized as the base model, and other catalysts, **1b–f**, were developed to vary the acidity of the pyrrole NH motif and its steric



**Scheme 1.** Synthesis of catalysts **1a–f**.

factor. Considering that changing the Brønsted acid motif acidity can improve the catalytic proficiency [13c], catalysts **1d–f** containing more acidic imidazole motifs were also investigated for comparison. The additional steric variation may influence the enantioselectivity by biasing the substrate approach. To investigate the steric influence around the pyrrolic NH center, catalysts **1b, c, f** containing sterically bulky and electron withdrawing bromine atoms or fused benzene ring were synthesized. Catalysts **1c** and **1f** contain benzimidazolyl and benzopyrrolyl fragments with a more extended  $\pi$  system that may also influence the catalytic proficiency via  $\pi$  interactions with the substrate or external acid activator. Tuning of the phosphine Lewis base was not attempted, as our prior investigations (unpublished data) indicated that adding substituents onto the aryl phosphine to increase the Lewis base nucleophilicity actually resulted in loss of catalysis, likely due to unexpected interference with the acid switch.

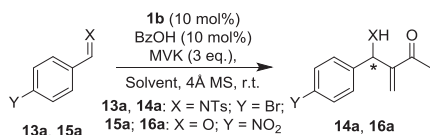
The synthesis of new catalysts **1a–f** was performed by modified reported procedures [9] from the key intermediate (S)-MAPO **6** [10a-c,24,9] in 2 steps (Scheme 1). For the synthesis of pyrrolyl- and indolyl-containing catalysts **1a–c**, the aminophosphine **2** was initially synthesized from **6** by chemoselective phosphine oxide reduction. Further reductive amination of the corresponding aldehydes **3–5** by aminophosphine **2** furnished catalysts **1a–c** (Scheme 1). Attempts to synthesize imidazolyl- and benzimidazolyl-containing catalysts **1d–f** were met with significant difficulties as phosphine oxidation occurred during the reductive amination step. Therefore, the reductive amination of aldehydes **7–9** was performed with (S)-MAPO **6**, followed by a subsequent phosphine oxide reduction to afford catalysts **1d–f**

(Scheme 1).

The synthesis of **11** and **1e** required up to 70 h of reactions whereas all other catalysts and their phosphine oxide precursors can be synthesized in much less time (~20 h). The purification of catalysts **1a–f** and precursors **10–12** were challenging due to the low stability of these compounds [25]. Catalyst **1b** was chosen for solvent screening due to its easier purification process (Table 1). Consistent with earlier hallmark profiles of our trifunctional organocatalysts, dichloromethane and diethyl ether were the best solvents for the *aza*-MBH and MBH model reactions, respectively (Table 1, entries 1 and 10) [11,13c,9]. More polar solvents such as acetonitrile resulted in poor yields and low enantioselectivity (Table 1, entries 6 and 13). No product formation occurred in polar protic solvents such as methanol (Table 1, entries 7 and 14). This confirms our working hypothesis that this enantioselective trifunctional catalysis relies on ion pairing upon activation by an acid additive.

After the identification of the best solvent for the *aza*-MBH and MBH test reactions, the external acid additives were screened (Table 2). For comparison, model **TF-1** (Scheme 1) was also tested (Table 2, entries 24, 25). The response of switching on catalytic proficiency (coupled rate and *ee* enhancement) to the acid activation is one of the main criteria of a trifunctional catalysis mode [9], in which the activation by an external acid likely occurs via the participation of its counterion in the irreversible, final proton-transfer step [9,11]. Benzoic acid ( $pK_a$  4.20) was found to be the best activator for previous generations of catalysts [11,13c,9]. Therefore, a set of aromatic acids with comparable  $pK_a$  values was tested along with other types of organic acids such as phenylphosphinic and acetic acids (Table 2). Interestingly, 3-methyl benzoic acid ( $pK_a$  4.24) was found to be the best acid additive for both the *aza*-MBH and MBH test reactions, providing the corresponding products in the good *ee* (88% for *aza*-MBH; 73% for MBH) and good yields (Table 2, entries 6 and 13). Notably, benzoic acid, which was the best activator for previous generations of catalysts, demonstrated lower proficiency than 3-methyl benzoic acid, providing *aza*-MBH and MBH products in 84% and 70% *ee*, respectively (Table 2, entries 1 and 11). The 3-chloro- and 4-cyanobenzoic acid additive with lower  $pK_a$  values (3.83 and 3.55 correspondingly)

**Table 1**  
Solvent screening of **1b**-catalyzed *aza*-MBH and MBH reactions.



Entry	X (Y)	Solvent	Time [h]	Conv <sup>a</sup> ( <i>ee</i> <sup>b</sup> ) [%]
1	NTs (Br)	DCM	3	77 (84)
2	NTs (Br)	Chloroform	3	73 (79)
3	NTs (Br)	Ether	3	95 <sup>c</sup> (59)
4	NTs (Br)	THF	3	89 (76)
5	NTs (Br)	Toluene	3	>95 <sup>c</sup> (73)
6	NTs (Br)	Acetonitrile	3	50 <sup>c</sup> (18)
7	NTs (Br)	Methanol	24	No reaction (n.d.)
8	O (NO <sub>2</sub> )	DCM	6	17 (69)
9	O (NO <sub>2</sub> )	Chloroform	6	18 (64)
10	O (NO <sub>2</sub> )	Ether	6	75 (70)
11	O (NO <sub>2</sub> )	THF	6	29 (69)
12	O (NO <sub>2</sub> )	Toluene	6	53 (73)
13	O (NO <sub>2</sub> )	Acetonitrile	6	8 (39)
14	O (NO <sub>2</sub> )	Methanol	24	No reaction (n.d.)

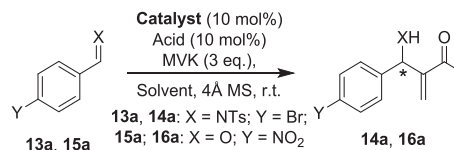
<sup>a</sup> Calculated by <sup>1</sup>H NMR spectroscopy.

<sup>b</sup> Determined by chiral HPLC analysis.

<sup>c</sup> 27 mol% loading of **1b**.

**Table 2**

Acid additive and loading screening of *aza*-MBH and MBH reactions.



Entry	Catalyst	X (Y)	Acid additive	Solvent	Time [h]	Conv <sup>a</sup> ( <i>ee</i> <sup>b</sup> ) [%]
1	<b>1b</b>	NTs (Br)	BzOH	DCM	3	77 (84)
2	<b>1b</b>	NTs (Br)	4-F-BzOH	DCM	3	62 (85)
3	<b>1b</b>	NTs (Br)	2-Naphthoic	DCM	3	60 (81)
4	<b>1b</b>	NTs (Br)	Acetic	DCM	3	>95 (80)
5	<b>1b</b>	NTs (Br)	Phenylphosphinic	DCM	24	8 (-2)
6	<b>1b</b>	NTs (Br)	<b>3-Me-BzOH</b>	<b>DCM</b>	<b>3</b>	<b>89 (88)</b>
7	<b>1b</b>	NTs (Br)	2-Me-BzOH	DCM	3	>95 (86)
8	<b>1d</b>	NTs (Br)	BzOH	DCM	3	29 (56)
9	<b>1d</b>	NTs (Br)	4-F-BzOH	DCM	3	25 (54)
10	<b>1d</b>	NTs (Br)	3-Me-BzOH	DCM	3	27 (60)
11	<b>1b</b>	O (NO <sub>2</sub> )	BzOH	Ether	6	75 (70)
12	<b>1b</b>	O (NO <sub>2</sub> )	4-F-BzOH	Ether	6	70 (69)
13	<b>1b</b>	O (NO <sub>2</sub> )	<b>3-Me-BzOH</b>	<b>Ether</b>	<b>6</b>	<b>81 (73)</b>
14	<b>1b</b>	O (NO <sub>2</sub> )	2-Me-BzOH	Ether	6	85 (74)
15	<b>1b</b>	O (NO <sub>2</sub> )	3-Cl-BzOH	Ether	6	11 (69) <sup>c</sup>
16	<b>1b</b>	O (NO <sub>2</sub> )	4-CN-BzOH	Ether	6	>5 (61) <sup>c</sup>
17	<b>1b</b>	O (NO <sub>2</sub> )	Acetic	Ether	6	81 (51)
18	<b>1b</b>	O (NO <sub>2</sub> )	Phenylphosphinic	Ether	24	7 (34)
19	<b>1b</b>	O (NO <sub>2</sub> )	1-Naphthoic	Ether	6	35 (69)
20	<b>1b</b>	O (NO <sub>2</sub> )	2-Naphthoic	Ether	6	62 (73)
21	<b>1d</b>	O (NO <sub>2</sub> )	BzOH	Ether	24	70 (39)
22	<b>1d</b>	O (NO <sub>2</sub> )	3-Me-BzOH	Ether	24	93 (39)
23	<b>1d</b>	O (NO <sub>2</sub> )	2-Naphthoic	Ether	24	70 (37)
24	<b>TF-1</b>	NTs (Br)	3-Me-BzOH	DCM	3	89 (89)
25	<b>TF-1</b>	O (NO <sub>2</sub> )	3-Me-BzOH	Ether	6	79 (58)

<sup>a</sup> Calculated by <sup>1</sup>H NMR spectroscopy.

<sup>b</sup> Determined by chiral HPLC analysis.

<sup>c</sup> *ee* level determined for conversion after 24 h.

provided significant rate loss in the MBH reaction (Table 2, entries 15, 16), suggesting likely quenching of the zwitterionic intermediate via protonation [12d].

Benzoic acid and 3-methyl benzoic acid both have comparable  $pK_a$  values, but 3-methyl benzoic acid provided better results with little observable steric interference. A further test of 2-methylbenzoic acid with a significantly lower  $pK_a$  than 3-methylbenzoic acid (3.91 vs. 4.24 correspondingly) demonstrated a comparable proficiency in both *aza*-MBH and MBH reactions (Table 2, entries 6 and 13 vs. 7 and 14). These results suggest an important role of the methyl substituent in the acid additive for the proficient catalysis that is independent of the  $pK_a$ . Such an improvement with a bulkier acid activator is unexpected and may be explained by the additional CH/ $\pi$  hydrogen bonding stabilization possibly between the electron rich pyrrole fragment of the catalyst and methyl group of the external acid additive (Scheme 1b).

The screening of the acid additive influence on the imidazolyl-containing catalyst **1d** provided a comparable trend albeit at

lower proficiency (Table 2, entries 8–10 and 21–23). We have shown [13c] that the acidity and the spatial position of the Brønsted acid motif on the catalyst will impact on the proficiency of the catalysis. The lower proficiency (e.g. slower rate and lower enantioselectivity) of the imidazole-containing catalysts, compare to the pyrrole series, may be due to the higher acidity of the imidazole NH and also the position of the NH proton. The activity of **1b**, activated by 3-methyl benzoic acid, is comparable to the control, phenol-containing catalyst **TF-1** in the test *aza*-MBH reaction, but noticeably higher in the MBH reaction (Table 2, entries 1, 11 vs 24, 25). Thus, catalyst **1b** provided the highest enantioselectivity in MBH test reactions among other generations of MAP-base trifunctional catalysts, likely due to the aforementioned additional CH/ $\pi$  cooperation in the switchable catalytic system [11,13c,9].

For catalyst **1b**, the acid additive loading effect was next investigated and found to be consistent for both *aza*-MBH and MBH reactions (Table 3). The use of an acid loading more than the equimolar loading to catalyst **1b** showed significant erosion of both reaction rate and enantioselectivity in the *aza*-MBH reaction (Table 3, entries 5, 6 vs 4), but only erosion of the reaction rate in the MBH test reaction (Table 3, entries 14, 13 vs 12). Less than equimolar acid additive loading to that of the catalyst demonstrated slight reduction in proficiency for *aza*-MBH test reactions (Table 3, entry 3 vs 4) and slightly higher reaction rates in MBH test reactions albeit in lower enantioselectivity (Table 3, entry 11 vs 12). The catalytic profile of the pyrrole catalysts is different from that of phenol-containing catalyst **TF-1** as this catalyst demonstrated the highest proficiency at 5 equivalent loading of an acid additive to the catalyst [9]. The catalyst loading, as expected, influenced mostly the reaction rate, providing a higher rate at a higher loading (Table 3). The enantioselectivity of test reactions did not vary as significantly with different catalyst loadings (Table 3, entry 1 vs 2, 4, 7 and 8 vs 9, 10, 15). Therefore, a loading at 5 mol% of the catalyst with the acid additive could also be used in *aza*-MBH and MBH reactions.

With the conditions optimized, new catalysts **1a–f** were tested in *aza*-MBH and MBH reactions in the presence and absence of the 3-methyl benzoic acid additive (Fig. 2). All catalysts require the acid

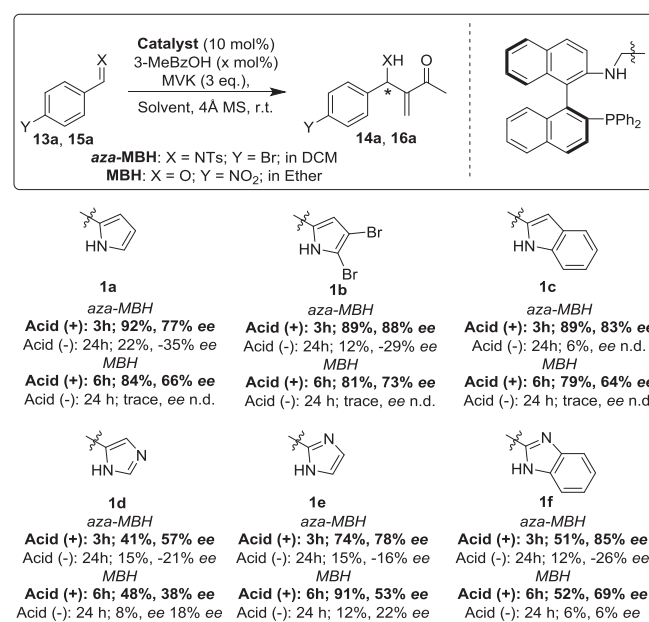


Fig. 2. Activity profile of acid-switchable catalysts **1a–f** in *aza*-MBH and MBH test reactions.

activation to switch on the catalysis. The control reactions without the acid additive demonstrated a sharp reduction in both the reaction rate and the level of enantioselectivity (Fig. 2). Again this concurrent rise of both the enantioselectivity and the reaction rate with acid activation, which is performed at room temperature to maintain the catalytic rate (i.e. no enantioselectivity improvement at lower temperatures), is consistent with our switchable trifunctional catalytic mode as noted before for trifunctional MAP-based catalysts [9,11]. The *aza*-MBH product **14a** of opposite enantioselectivity (up to -35% ee) were observed in *aza*-MBH reactions without the acid additive (Fig. 2, **1a, b, d–f**).

The substituted pyrrole-containing catalysts **1b** and **1c** (fused benzene ring), compared to the unsubstituted catalyst **1a**, provided higher enantioselectivity in both *aza*-MBH and MBH reactions, albeit in lower reaction rates due to likely higher steric congestion (Fig. 2). The imidazolyl-containing catalysts **1d–f** were less active than pyrrolyl-containing analogs with lower reaction rates. The 4-imidazolyl-containing catalyst **1d** showed the lowest activity, resulting in the formation of *aza*-MBH product **14a** in only 41% conversion and 57% ee over 3 hours and the MBH product in 48% conversion and 38% ee over 6 hours (Fig. 2). As discussed earlier, this may be explained by possible imidazole ring tautomerization that makes the position of the Brønsted acid function less optimal for hydrogen bonding interactions between all catalytic motifs. The imidazole ring tautomerization in catalysts **1e** or **1f** does not seem to influence significantly the catalytic proficiency, as both of the nitrogen centers are in equal  $\alpha$ -positions to the methylene bridge. Therefore 2-imidazolyl-containing catalysts **1e** or **1f** provided products in comparable enantioselectivity to that of pyrrolyl-containing catalysts **1a** or **1c**, albeit in lower conversion. This is consistent with our prior observations that increasing the internal Brønsted acid acidity can improve the catalytic activity to a certain point [13c]. Catalyst **1b** was found to be the most active in both *aza*-MBH and MBH test reactions providing products up to 88% ee at 89% conversion over 3 hours in the *aza*-MBH case and 73% ee at 81% conversion over 6 hours in the MBH case (Fig. 2).

Taking into account the promising activity of new catalysts, the substrate scope of the best catalyst **1b** was investigated in the *aza*-

Table 3  
Acid activator loading screening of **1b**-catalyzed *aza*-MBH and MBH reactions.

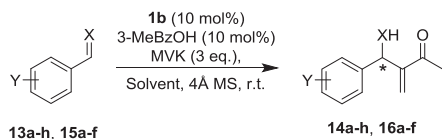
Entry	<b>1b</b> loading [mol %]	3-MeBzOH loading [mol %]	X (Y)	Solvent	Time [h]	Conv <sup>a</sup> (ee <sup>b</sup> ) [%]
1	1	1	NTs (Br)	DCM	3	19 (88)
2	5	5	NTs (Br)	DCM	3	57 (86)
3	10	5	NTs (Br)	DCM	3	76 (84)
4	10	10	NTs (Br)	DCM	3	89 (88)
5	10	25	NTs (Br)	DCM	3	49 (78)
6	10	50	NTs (Br)	DCM	3	24 (75)
7	20	20	NTs (Br)	DCM	3	>95 (84)
8	1	1	O (NO <sub>2</sub> )	Ether	24	14 (67)
9	5	5	O (NO <sub>2</sub> )	Ether	6	70 (69)
10	10	10	O (NO <sub>2</sub> )	Ether	6	81 (73)
11	10	5 <sup>c</sup>	O (NO <sub>2</sub> )	Ether	6	66 (63)
12	10	10 <sup>c</sup>	O (NO <sub>2</sub> )	Ether	6	62 (73)
13	10	25 <sup>c</sup>	O (NO <sub>2</sub> )	Ether	6	46 (74)
14	10	50 <sup>c</sup>	O (NO <sub>2</sub> )	Ether	6	35 (74)
15	20	20	O (NO <sub>2</sub> )	Ether	3	>95 (72)

<sup>a</sup> Calculated by <sup>1</sup>H NMR spectroscopy.

<sup>b</sup> Determined by chiral HPLC analysis.

<sup>c</sup> 2-Naphthoic acid was used instead of 3-methyl benzoic acid.

**Table 4**  
Substrate scope investigation with **1b**.



Entry	X (Y)	Solvent	Time [h]	Conv <sup>a</sup> [%]	ee <sup>b</sup> [%]
1	NTs (4-Br) <b>14a</b>	DCM	3	89 (>95 <sup>c</sup> )	88
2	NTs (3-NO <sub>2</sub> ) <b>14b</b>	DCM	3	>95	77
3	NTs (2-Cl) <b>14c</b>	DCM	3	40 (>95 <sup>c</sup> )	76
4	NTs (4-Me) <b>14d</b>	DCM	3	18 (86 <sup>c</sup> )	86 <sup>d</sup>
5	NTs (2-NO <sub>2</sub> ) <b>14e</b>	DCM	3	53 (>95 <sup>c</sup> )	58
6	NTs (4-Cl) <b>14f</b>	DCM	3	59 (>95 <sup>c</sup> )	82
7	NTs (4-F) <b>14g</b>	DCM	3	21 (>95 <sup>c</sup> )	79
8	NTs (4-CN) <b>14h</b>	DCM	3	55 (>95 <sup>c</sup> )	57
9	O (4-NO <sub>2</sub> ) <b>16a</b>	Ether	6	81 (>95 <sup>c</sup> )	73
10	O (3-NO <sub>2</sub> ) <b>16b</b>	Ether	6	68 (>95 <sup>c</sup> )	73
11	O (4-CN) <b>16c</b>	Ether	6	64 (95 <sup>c</sup> )	73
12	O (4-Br) <b>16d</b>	Ether	6	16 (56 <sup>c</sup> )	75 <sup>d</sup>
13	O (2-NO <sub>2</sub> ) <b>16e</b>	Ether	6	14 (58 <sup>c</sup> )	59 <sup>d</sup>
14	O (3-Br) <b>16f</b>	Ether	6	10 (48 <sup>c</sup> )	77 <sup>d</sup>

<sup>a</sup> Calculated by <sup>1</sup>H NMR spectroscopy.

<sup>b</sup> Determined by chiral HPLC analysis.

<sup>c</sup> Conversion in 24 h.

<sup>d</sup> ee level determined for conversion after 24 h.

MBH and MBH reaction (Table 4). Substituted *N*-tosyl benzaldimines with *ortho*-, *meta*-, and *para*-substituents and aromatic aldehydes bearing electron-withdrawing groups were investigated under the optimized conditions.

Catalyst **1b** catalyzed both *aza*-MBH and MBH reactions and demonstrated the widest scope in all of our generations of trifunctional organocatalysts. Most of the *aza*-MBH substrates, containing *para*-substituents, provided the corresponding adducts in comparable enantioselectivity (79–88% *ee*) although with lower conversion for deactivated imine **13d** as expected (Table 4, entries 4 vs. 1). The *aza*-MBH reactions with substrates containing *meta*- and *ortho*-substituents (Table 4, entries 2, 3, 5) showed some loss in enantioselectivity or rate, again consistent with prior observations for substrates that are more sterically congested.

For the MBH reactions, aromatic substrates bearing electron-withdrawing groups provided adducts with consistent *ee* around 73–77% (Table 4, Entries 9–11). Less active 4-bromo- or 3-bromo-substituted aldehydes (**15d** or **15f**) demonstrated only 10–16% conversion in 6 h but longer reaction time to 24 h improved conversion significantly without *ee* erosion (Table 4, entries 12, 14). Substrates with larger *ortho*-substitution, such as imine **14e** and aldehyde **15e**, provided reduced reaction rate and enantioselectivity, suggesting unfavorable steric interactions at that position (Table 4, entries 5 and 13). To date there have been many proficient catalysts reported for the *aza*-MBH or MBH reactions [12f], however, only a few can demonstrate good proficiency in both reactions, due to the very complex mechanisms behind this reaction class [12f]. Bifunctional catalyst  $\beta$ -isocupreidine ( $\beta$ -ICD) provided *aza*-MBH [26] products in up to 99% *ee* and 54–80% yield over 24–36 h at  $-30^\circ\text{C}$ , but demonstrated significantly lower proficiency in MBH [27] product formation (up to 49% *ee* and 43–88% yield over 72 h at  $-30^\circ\text{C}$ ), except for very reactive isatins [28] or 1,1,1,3,3,3-hexafluoroisopropyl acrylate (HFIPA) [29] as an activated alkene. Other examples of bifunctional catalytic systems, active in both *aza*-MBH and MBH reactions between MVK and aromatic electrophiles are MOP-based Shi's [30] and He's [31] catalysts that demonstrated low proficiency in MBH despite the promising activity in the *aza*-MBH analogs. The chiral proline/imidazole

catalytic system was also used for proficient catalysis of both *aza*-MBH [32] and MBH [33] reactions, however, substrates such as MVK and aromatic electrophiles were not tested with this catalytic system. The ability of pyrrolyl-containing catalyst **1b** to catalyze both *aza*-MBH and MBH reactions with expanded substrate scope is suggestive of an enhanced molecular recognition network provided by the pyrrole motif in the presence of 3-methyl benzoic acid and encouraging for future work of catalyst design that may help find additional solutions to the generality limitation of this type of reactions.

### 3. Conclusions

In conclusion, new catalytic roles of a pyrrole motif have been established in a switchable and enantioselective trifunctional organocatalytic cycle that improved the generality of the catalytic systems. Such improvement may be attributed to additional, favourable CH/ $\pi$  hydrogen bonding interactions between the electron rich pyrrolyl moiety and the external activator, 3-methyl benzoic acid to switch on the catalysis. While pyrrole phosphines have commonly been used as ligands before, we show here for the first time that they can be effective organocatalysts. This will facilitate future work in developing the pyrrole motif in catalysis beyond its common ligand role. Further work will involve additional investigation and characterization of substituted pyrroles and acid switches with compact molecular recognition network for new or enhanced catalysis. This may also, in general, contribute to the new use of pyrroles for building molecular assemblies in roles different from the established utility as a coordination or pH-switching site.

### 4. Experimental section

#### 4.1. General information

All reagents unless specified otherwise are commercially available and purified by standard procedures [34]. Chloroform-*d* was purchased from Cambridge Isotope Laboratories, USA and stored over anhydrous potassium carbonate before use. Bromomethyl methyl ether was distilled from anhydrous sodium sulfate and used immediately after distillation. Cesium carbonate was dried before reactions. Air and moisture sensitive reactions were performed under a nitrogen atmosphere. Reactions were magnetically stirred and monitored by thin-layer chromatography (TLC) using Merck silica gel 60 F<sub>254</sub> aluminium pre-coated plates (0.25 mm). Flash column chromatography was performed on Merck silica gel 60 (0.015–0.040 mm). <sup>1</sup>H, <sup>13</sup>C, and <sup>31</sup>P experiments were performed at 298 K on either a Bruker DPX 400 MHz spectrometer equipped with a 5 mm QNP probe. Chemical shifts were reported in ppm using the residual CHCl<sub>3</sub> peak as an internal reference ( $\delta_{\text{H}} = 7.26$  ppm,  $\delta_{\text{C}} = 77.16$  ppm). All <sup>31</sup>P NMR spectroscopy was performed on a Bruker DPX 400 MHz spectrometer at 298 K, and all spectra were referenced to external H<sub>3</sub>PO<sub>4</sub> (0 ppm). All spectra were processed using Bruker TOPSPIN software versions 3.5p17. Infrared spectra were taken on Thermo Scientific Nicolet iS5FT-IR Spectrometer with an attenuated total reflectance (ATR) accessory and maximum absorption peaks were reported in cm<sup>-1</sup>. High-resolution mass analysis was provided by Australian Proteome Analysis Facility (APAF), Macquarie University, Sydney, Australia. Chiral HPLC analysis was performed using a Shimadzu Prominence system with either a Daicel Chiral Columns CHIRALPAK<sup>®</sup> AD-H column or a Regis Chiral Technologies Whelk-O1 column. HPLC grade solvents were degassed before use. Specific rotation was measured at 23–24 °C on a P1010 digital polarimeter (Jasco, Japan). The commercially available aldehydes were used for catalysts synthesis

except for 4,5-dibromopyrrole-2-carboxaldehyde **4** that was obtained [35] via the bromination of pyrrole-2-carboxaldehyde **3**. (S)-MAPO **6** and aminophosphine **2** were synthesized by established procedures [9,24]

## 4.2. Experimental details

### 4.2.1. General procedure for MBH or aza-MBH reactions

Catalyst (10 mol%, 0.0025 mmol), imine or aldehyde (0.025 mmol) and acid additive (10 mol%, 0.0025 mmol) were combined under N<sub>2</sub> from dichloromethane stock solutions in a 1.5 mL teflon capped vial with 4 Å molecular sieves. Dichloromethane was evaporated by nitrogen flow. Then reaction solvent was added to the mixture (final concentration C = 0.2 M to imine or aldehyde after addition of MVK in the reaction solvent). A solution of MVK (0.075 mmol) was added to the mixture at stirring at room temperature. Aliquots (10 µL) of the reaction mixture were taken at 0.5, 3, 6, 24 h and dried immediately by nitrogen flow to remove the volatiles. The residue was re-dissolved in chloroform-*d* and filtered to determine the conversion of starting material to product by <sup>1</sup>H NMR and then analyzed by chiral HPLC (1:4 *i*-propanol:hexane) to determine *ee* ratios.

### 4.2.2. (S)-N-((1H-pyrrol-2-yl)methyl)-2'-(diphenylphosphaneyl)-[1,1'-binaphthalen]-2-amine (**1a**)

To a solution of (S)-(+)-2-(diphenylphosphine)-1,1'-binaphthyl-2'-amine **2** (100 mg, 0.221 mmol) and 2-pyrrolicarboxaldehyde (42 mg, 0.441 mmol) in dry toluene (4 mL) was added a drop of formic acid at room temperature and the reaction mixture was stirred for 15 h. The mixture was pre-cooled (ice/NaCl bath) and dry methanol (15 µL) was added followed by the addition of NaBH<sub>4</sub> (21 mg, 0.551 mmol) in one portion and stirred at room temperature for 10 min. The mixture was treated with water and the organic phase was extracted by dichloromethane 3 times. The combined organic phases were washed with brine, dried over anhydrous magnesium sulfate and concentrated under vacuum. The residue was purified by flash chromatography on silica gel (toluene; crude mixture/SiO<sub>2</sub> as 1/250 w/w) to furnish **1a** (28 mg, 24% yield) as a white solid. <sup>1</sup>H NMR (400 MHz, CDCl<sub>3</sub>) δ 3.72 (bs, 1H), 4.15–4.28 (m, 2H), 5.93–5.98 (m, 1H), 6.05–6.10 (m, 1H), 6.44–6.50 (m, 1H), 6.53 (d, *J* = 8.0 Hz, 1H), 6.87–6.94 (m, 1H), 6.97–7.03 (m, 2H), 7.05–7.20 (m, 5H), 7.24–7.38 (m, 7H), 7.44 (dd, *J* = 2.9, 8.6 Hz, 1H), 7.49–7.55 (m, 1H), 7.69 (d, *J* = 8.0 Hz, 1H), 7.81 (d, *J* = 8.9 Hz, 1H), 7.91 (d, *J* = 8.5 Hz, 1H), 7.92 (d, *J* = 8.2 Hz, 1H), 8.23 (bs, 1H); <sup>31</sup>P NMR (162 MHz, CDCl<sub>3</sub>) δ -13.06; <sup>13</sup>C NMR (100 MHz, CDCl<sub>3</sub>) δ 41.59, 104.80, 108.43, 113.59, 116.97, 121.88, 124.22, 125.44, 126.25, 126.33 (d, *J*<sub>C-P</sub> = 2.2 Hz), 127.09, 127.36, 127.90, 128.23, 128.30, 128.35, 128.37, 128.50, 128.64, 128.68, 128.78, 128.84, 129.18, 129.93 (d, *J*<sub>C-P</sub> = 2.9 Hz), 130.69 (d, *J*<sub>C-P</sub> = 1.5 Hz), 133.61 (d, *J*<sub>C-P</sub> = 8.07 Hz), 133.81 (d, *J*<sub>C-P</sub> = 8.5 Hz), 134.02 (d, *J*<sub>C-P</sub> = 2.2 Hz), 134.41, 137.75, 141.43, 141.78, 143.42 (d, *J*<sub>C-P</sub> = 2.2 Hz); IR (ATR, cm<sup>-1</sup>) ν 3427, 3051, 1618, 1596, 1511, 1492, 1430, 1332, 1298, 1255, 1214, 1151, 1089, 1024; HRMS Found [M+H]<sup>+</sup>, 533.21356. C<sub>37</sub>H<sub>30</sub>N<sub>2</sub>P requires [M+H]<sup>+</sup>, 533.21466; [α]<sub>D</sub><sup>23</sup> -15.94 (c 1.0, CHCl<sub>3</sub>).

### 4.2.3. (S)-N-((4,5-dibromo-1H-pyrrol-2-yl)methyl)-2'-(diphenylphosphaneyl)-[1,1'-binaphthalen]-2-amine (**1b**)

To a solution of (S)-(+)-2-(diphenylphosphine)-1,1'-binaphthyl-2'-amine **2** (56 mg, 0.124 mmol) and 4,5-dibromo-2-pyrrolicarboxaldehyde (63 mg, 0.248 mmol) in dry toluene (2.3 mL) was added a drop of formic acid at room temperature and the reaction mixture was stirred for 4.5 h. The mixture was pre-cooled (ice/acetone bath) and dry methanol (15 µL) was added followed by the addition of NaBH<sub>3</sub>CN (15.5 mg, 0.247 mmol) in one

portion and stirred at room temperature for 7.5 h. The mixture was treated with water and the organic phase was extracted by dichloromethane 3 times. The combined organic phases were washed with brine, dried over anhydrous magnesium sulfate and concentrated under vacuum. The residue was purified by flash chromatography on silica gel (hexane/dichloromethane gradient) to furnish **1b** (44 mg, 51% yield) as a white solid. <sup>1</sup>H NMR (400 MHz, CDCl<sub>3</sub>) δ 3.92 (bs, 1H), 4.18–4.34 (m, 2H), 5.96–6.12 (m, 1H), 6.36 (d, *J* = 8.5 Hz, 1H), 6.73–6.81 (m, 1H), 6.94–7.13 (m, 7H), 7.21–7.33 (m, 4H), 7.34–7.39 (m, 3H), 7.42 (dd, *J* = 3.3, 8.5 Hz, 1H), 7.49–7.55 (m, 1H), 7.62 (d, *J* = 8.0 Hz, 1H), 7.79 (d, *J* = 8.9 Hz, 1H), 7.92 (d, *J* = 8.6 Hz, 1H), 7.93 (d, *J* = 8.1 Hz, 1H), 9.74 (bs, 1H); <sup>31</sup>P NMR (162 MHz, CDCl<sub>3</sub>) δ -12.38; <sup>13</sup>C NMR (100 MHz, CDCl<sub>3</sub>) δ 41.08, 98.21, 108.20, 113.25, 121.99, 124.28, 126.09 (d, *J*<sub>C-P</sub> = 2.2 Hz), 126.20, 127.22, 127.36, 127.42, 127.71, 128.19, 128.27, 128.38, 128.73 (d, *J*<sub>C-P</sub> = 1.5 Hz), 128.85, 128.91 (d, *J*<sub>C-P</sub> = 2.2 Hz), 130.07, 130.19, 131.70, 133.20, 133.57, 133.76, 134.08, 134.29, 134.36, 136.47 (d, *J*<sub>C-P</sub> = 8.1 Hz), 136.99 (d, *J*<sub>C-P</sub> = 6.6 Hz), 141.69; IR (ATR, cm<sup>-1</sup>) ν 3416, 3051, 1617, 1596, 1512, 1492, 1431, 1293, 1254, 1152, 1092, 1024, 968; HRMS Found [M+H]<sup>+</sup>, 691.03129. C<sub>37</sub>H<sub>28</sub>Br<sub>2</sub>N<sub>2</sub>P requires [M+H]<sup>+</sup>, 691.03364; [α]<sub>D</sub><sup>23</sup> -41.98 (c 0.77, CHCl<sub>3</sub>).

### 4.2.4. (S)-N-((1H-indol-2-yl)methyl)-2'-(diphenylphosphaneyl)-[1,1'-binaphthalen]-2-amine (**1c**)

To a solution of (S)-(+)-2-(diphenylphosphine)-1,1'-binaphthyl-2'-amine **2** (50 mg, 0.11 mmol) and 2-indolecarboxaldehyde (48 mg, 0.331 mmol) in dry toluene (2 mL) was added a drop of formic acid at room temperature and the reaction mixture was stirred for 15 h. The mixture was pre-cooled (ice/acetone bath) and dry methanol (134 µL, 3.308 mmol) was added followed by the addition of NaBH<sub>3</sub>CN (69.3 mg, 1.103 mmol, 10 eq) in one portion and stirred 40 °C for 3.5 h. The mixture was treated with water and the organic phase was extracted by dichloromethane 3 times. The combined organic phases were washed with brine, dried over anhydrous magnesium sulfate and concentrated under vacuum. The residue was purified by flash chromatography on silica gel (hexane/dichloromethane gradient) to furnish **1c** (45 mg, 70% yield) as a white solid. <sup>1</sup>H NMR (400 MHz, CDCl<sub>3</sub>) δ 3.92 (bs, 1H), 4.34–4.51 (m, 2H), 6.28–6.35 (m, 1H), 6.50 (d, *J* = 8.5 Hz, 1H), 6.83–6.91 (m, 1H), 6.99–7.20 (m, 10H), 7.29–7.40 (m, 7H), 7.47 (dd, *J* = 3.0, 8.5 Hz, 1H), 7.50–7.57 (m, 2H), 7.66 (d, *J* = 8.0 Hz, 1H), 7.76 (d, *J* = 8.9 Hz, 1H), 7.93 (d, *J* = 8.5 Hz, 1H), 7.94 (d, *J* = 8.2 Hz, 1H), 8.82 (bs, 1H); <sup>31</sup>P NMR (162 MHz, CDCl<sub>3</sub>) δ -13.01; <sup>13</sup>C NMR (100 MHz, CDCl<sub>3</sub>) δ 41.82, 98.73, 111.02, 113.51, 119.67, 120.02, 121.19, 121.97, 124.26, 126.25, 127.14, 127.37, 127.43, 127.83, 128.25, 128.32, 128.41, 128.69, 128.75, 128.86, 128.92, 129.02, 130.06, 130.41, 133.16 (d, *J*<sub>C-P</sub> = 7.2 Hz), 133.52, 133.71, 133.88, 133.93 (d, *J*<sub>C-P</sub> = 2.2 Hz), 134.08, 134.41, 135.80, 135.87, 135.96, 137.26, 137.36 (d, *J*<sub>C-P</sub> = 2.9 Hz), 137.52, 141.10, 141.43, 142.80; IR (ATR, cm<sup>-1</sup>) ν 3416, 3050, 1886, 1618, 1596, 1512, 1490, 1455, 1430, 1339, 1292, 1216, 1152, 1091, 1023; HRMS Found [M+H]<sup>+</sup>, 583.22877. C<sub>41</sub>H<sub>32</sub>N<sub>2</sub>P requires [M+H]<sup>+</sup>, 583.23031; [α]<sub>D</sub><sup>23</sup> -122.07 (c 1.0, CHCl<sub>3</sub>).

### 4.2.5. (S)-2'-(((1H-imidazol-5-yl)methyl)amino)-[1,1'-binaphthalen]-2-yl)diphenylphosphine oxide (**10**)

A mixture of (S)-(+)-2-(diphenylphosphine oxide)-1,1'-binaphthyl-2'-amine **6** (150 mg, 0.320 mmol) and 4(5)-formylimidazole (61.4 mg, 0.640 mmol) in the presence of 4 Å molecular sieves (0.7 g) in dry toluene (5.8 mL) was stirred at 110 °C for 17 h in a pressure tube. The mixture was cooled down to room temperature and then pre-cooled (ice/NaCl bath). After cooling, dry methanol (0.5 mL) was added and then NaBH<sub>3</sub>CN (20 mg, 0.320 mmol) was added in one portion and stirred at room temperature for 2.5 h. The mixture was filtered through folded filter.

The reaction mixture was treated with water and the organic phase was extracted with ethyl acetate (3 times). The combined organic phases were washed with brine, dried over anhydrous magnesium sulfate and concentrated under vacuum. The residue was purified by flash chromatography on silica gel (1–10% ethanol in chloroform; gradient) to furnish **10** (119.1 mg, 68% yield) as yellow foam.  $^1\text{H}$  NMR (400 MHz,  $\text{CDCl}_3$ )  $\delta$  4.06 (bs, 1H), 4.33–4.43 (m, 1H), 4.52–4.62 (m, 1H), 6.32 (d,  $J = 8.3$  Hz, 1H), 6.61–6.70 (m, 2H), 6.78–6.88 (m, 2H), 6.91–6.98 (m, 1H), 6.96 (d,  $J = 9.0$  Hz, 1H), 7.00 (s, 1H), 7.02–7.11 (m, 2H), 7.22 (d,  $J = 8.3$  Hz, 1H), 7.26–7.33 (m, 1H), 7.36 (d,  $J = 7.9$  Hz, 1H), 7.48 (d,  $J = 8.9$  Hz, 1H), 7.50–7.65 (m, 5H), 7.70 (s, 1H), 7.87–8.00 (m, 4H).  $^{31}\text{P}$  NMR (162 MHz,  $\text{CDCl}_3$ )  $\delta$  28.16;  $^{13}\text{C}$  NMR (100 MHz,  $\text{CDCl}_3$ )  $\delta$  39.41, 113.23, 113.83 (d,  $J_{\text{C-P}} = 5$  Hz), 121.44, 124.23, 126.00, 126.65, 127.19, 127.25, 127.32, 127.83, 128.32, 128.55, 128.64, 128.67, 128.73, 128.85, 128.92, 129.10, 129.24, 129.62, 129.71, 129.72, 130.12 (d,  $J = 2.3$  Hz), 130.53, 130.59, 131.56, 132.01, 132.05, 132.10, 132.37, 133.41, 133.52, 135.68 (dd,  $J_{\text{C-P}} = 8.8, 2.2$  Hz), 141.8 (d,  $J_{\text{C-P}} = 9.5$  Hz), 144.42; IR (ATR,  $\text{cm}^{-1}$ )  $\nu$  3054, 1618, 1597, 1497, 1435, 1342, 1301, 1258, 1215, 1153, 1112; HRMS Found  $[\text{M}+\text{H}]^+$ , 550.20391.  $\text{C}_{36}\text{H}_{29}\text{N}_3\text{OP}$  requires  $[\text{M}+\text{H}]^+$ , 550.20483;  $[\alpha]_{\text{D}}^{25} +80.83$  (c 1.0,  $\text{CHCl}_3$ ).

#### 4.2.6. (S)-N-((1H-imidazol-5-yl)methyl)-2'-(diphenylphosphanyl)-[1,1'-binaphthalen]-2-amine (**1d**)

A solution of **10** (70.5 mg, 0.128 mmol) in neat phenylsilane (80  $\mu\text{L}$ ) was heated at 96 °C for 19 hours. The volatiles were removed via nitrogen blow down and the residue was purified by flash chromatography on silica gel (hexane/ethyl acetate to ethyl acetate/ethanol; gradient) to yield **1d** (36.3 mg, 53%) as a white foam.  $^1\text{H}$  NMR (400 MHz,  $\text{CDCl}_3$ )  $\delta$  3.76 (bs, 1H), 4.21 (s, 2H), 6.53 (d,  $J = 8.4$  Hz, 1H), 6.71–6.75 (m, 1H), 6.86–6.92 (m, 1H), 6.97–7.04 (m, 2H), 7.05–7.20 (m, 6H), 7.21–7.34 (m, 6H), 7.35–7.38 (m, 1H), 7.45 (dd,  $J = 2.8, 8.6$  Hz, 1H), 7.47–7.53 (m, 1H), 7.69 (d,  $J = 8.0$  Hz, 1H), 7.80 (d,  $J = 8.9$  Hz, 1H), 7.90 (d,  $J = 8.5$  Hz, 2H);  $^{31}\text{P}$  NMR (162 MHz,  $\text{CDCl}_3$ )  $\delta$  -13.61;  $^{13}\text{C}$  NMR (100 MHz,  $\text{CDCl}_3$ )  $\delta$  40.47, 113.44, 116.43 (d,  $J_{\text{C-P}} = 8.7$  Hz), 121.89, 124.22, 126.27, 126.40 (d,  $J_{\text{C-P}} = 2.9$  Hz), 127.06, 127.29, 127.37, 127.89, 128.25, 128.32, 128.55, 128.60, 128.66, 128.71, 128.77, 129.84, 130.69, 133.08 (d,  $J_{\text{C-P}} = 7.0$  Hz), 133.40, 133.59, 133.70, 133.90, 134.09 (d,  $J_{\text{C-P}} = 2.2$  Hz), 134.39, 134.54, 136.62 (d,  $J_{\text{C-P}} = 11.5$  Hz), 137.22 (d,  $J_{\text{C-P}} = 9.5$  Hz), 137.79 (d,  $J_{\text{C-P}} = 12.5$  Hz), 141.43, 141.76, 142.97 (d,  $J_{\text{C-P}} = 2.2$  Hz); IR (ATR,  $\text{cm}^{-1}$ )  $\nu$  3051, 1618, 1596, 1492, 1430, 1340, 1301, 1251, 1214, 1150, 1088; HRMS Found  $[\text{M}+\text{H}]^+$ , 534.20872.  $\text{C}_{36}\text{H}_{29}\text{N}_3\text{P}$  requires  $[\text{M}+\text{H}]^+$ , 534.20991;  $[\alpha]_{\text{D}}^{25} -2.68$  (c 1.0,  $\text{CH}_2\text{Cl}_2$ ).

#### 4.2.7. (S)-(2'-(((1H-imidazol-2-yl)methyl)amino)-[1,1'-binaphthalen]-2-yl)diphenylphosphine oxide (**11**)

The mixture of (S)-(+)-2-(diphenylphosphine oxide)-1,1'-binaphthyl-2'-amine **6** (200 mg, 0.426 mmol) and 2-formylimidazole (82 mg, 0.852 mmol) in the presence of 4 Å MS (0.85 g) in dry toluene (8 mL) was stirred at 110 °C for 70 h in a pressure tube. The mixture was cooled down to room temperature and then pre-cooled (ice/NaCl bath). After cooling, dry methanol (2 mL) was added and then  $\text{NaBH}_4$  (80 mg, 2.13 mmol) was added in one portion and stirred at room temperature for 3 h. The mixture was filtered through folded filter. The reaction mixture was treated with water and the organic phase was extracted with ethyl acetate (3 times). The combined organic phases were washed with brine, dried over anhydrous magnesium sulfate and concentrated under vacuum. The residue was purified by flash chromatography on silica gel (toluene/ethyl acetate to ethyl acetate; gradient) to furnish **11** (80.4 mg, 34.3% yield) as yellow foam.  $^1\text{H}$  NMR (400 MHz,  $\text{CDCl}_3$ )  $\delta$  4.23 (t,  $J = 6.5$  Hz, 1H), 4.46 (dd,  $J = 6.1, 17.5$  Hz, 1H), 5.20 (dd,  $J = 7.1, 17.5$  Hz, 1H), 6.23 (d,  $J = 8.4$  Hz, 1H), 6.69–6.77 (m, 3H),

6.85–6.95 (m, 3H), 7.05–7.14 (m, 4H), 7.25 (d,  $J = 8.5$  Hz, 1H), 7.28–7.34 (m, 1H), 7.37 (d,  $J = 8.0$  Hz, 1H), 7.48–7.63 (m, 6H), 7.84–8.00 (m, 4H), 13.40 (bs, 1H);  $^{31}\text{P}$  NMR (162 MHz,  $\text{CDCl}_3$ )  $\delta$  28.17;  $^{13}\text{C}$  NMR (100 MHz,  $\text{CDCl}_3$ )  $\delta$  41.48, 112.39, 113.95 (d,  $J_{\text{C-P}} = 5.1$  Hz), 121.49, 124.11, 126.00, 126.72, 127.12, 127.48, 127.60, 127.78, 128.02, 128.32, 128.47, 128.54, 128.67, 128.79, 128.91, 129.04, 129.09, 129.17, 129.53, 129.95, 130.05, 130.53 (d,  $J_{\text{C-P}} = 2.9$  Hz), 130.72, 132.07, 132.15, 132.33, 133.12, 133.41, 133.52 (d,  $J_{\text{C-P}} = 10.3$  Hz), 135.71 (d,  $J_{\text{C-P}} = 2.2$  Hz), 142.00 (d,  $J_{\text{C-P}} = 8.7$  Hz), 143.58, 147.54; IR (ATR,  $\text{cm}^{-1}$ )  $\nu$  3053, 1618, 1598, 1551, 1498, 1436, 1300, 1178, 1155, 1113, 1096, 1024, 998, 869, 810, 744, 722, 696, 633; HRMS Found  $[\text{M}+\text{H}]^+$ , 550.20362.  $\text{C}_{36}\text{H}_{29}\text{N}_3\text{OP}$  requires  $[\text{M}+\text{H}]^+$ , 550.20483;  $[\alpha]_{\text{D}}^{25} 33.25$  (c 1.0,  $\text{CHCl}_3$ ).

#### 4.2.8. (S)-N-((1H-imidazol-2-yl)methyl)-2'-(diphenylphosphanyl)-[1,1'-binaphthalen]-2-amine (**1e**)

A solution of **11** (18.1 mg, 0.033 mmol) in neat phenylsilane (200  $\mu\text{L}$ ) was heated at 90 °C for 68 hours. The volatiles were removed via nitrogen blow down and the residue was purified by flash chromatography on silica gel (hexane/ethyl acetate; gradient) to yield **1e** (8.1 mg, 46%) as a white foam.  $^1\text{H}$  NMR (400 MHz,  $\text{CDCl}_3$ )  $\delta$  4.02 (t,  $J = 5.8$  Hz, 1H), 4.34 (dd,  $J = 6.3, 17.5$  Hz, 1H), 4.59 (dd,  $J = 5.3, 17.5$  Hz, 1H), 6.41 (d,  $J = 8.5$  Hz, 1H), 6.79–6.90 (m, 3H), 6.92–7.00 (m, 3H), 7.02–7.10 (m, 3H), 7.11–7.17 (m, 1H), 7.23–7.38 (m, 7H), 7.40 (dd,  $J = 3.2, 8.5$  Hz, 1H), 7.50–7.57 (m, 1H), 7.65 (d,  $J = 8.1$  Hz, 1H), 7.78 (d,  $J = 9.0$  Hz, 1H), 7.93 (d,  $J = 8.4$  Hz, 2H);  $^{31}\text{P}$  NMR (162 MHz,  $\text{CDCl}_3$ )  $\delta$  -12.79;  $^{13}\text{C}$  NMR (100 MHz,  $\text{CDCl}_3$ )  $\delta$  42.01, 112.88, 116.38 (d,  $J_{\text{C-P}} = 8.6$  Hz), 122.14, 124.18, 126.16 (d,  $J_{\text{C-P}} = 2.2$  Hz), 127.37, 127.30, 127.48, 127.51, 127.82, 128.30, 128.38, 128.40, 128.85, 128.94, 128.96, 129.03, 130.26, 133.13 (d,  $J_{\text{C-P}} = 7.2$  Hz), 133.33, 133.52, 133.92 (d,  $J = 2.2$  Hz), 133.97, 134.18, 134.434, 135.00 (d,  $J_{\text{C-P}} = 7.3$  Hz), 136.68 (d,  $J_{\text{C-P}} = 6.7$  Hz), 136.88 (d,  $J_{\text{C-P}} = 9.4$  Hz), 140.87, 141.19, 141.84 (d,  $J_{\text{C-P}} = 2.2$  Hz), 147.00; IR (ATR,  $\text{cm}^{-1}$ )  $\nu$  3050, 1618, 1596, 1511, 1493, 1431, 1295, 1262, 1215, 1151, 1091, 1023, 996, 914, 852, 810, 773, 739, 694, 629; HRMS Found  $[\text{M}+\text{H}]^+$ , 534.20915.  $\text{C}_{36}\text{H}_{29}\text{N}_3\text{P}$  requires  $[\text{M}+\text{H}]^+$ , 534.20991;  $[\alpha]_{\text{D}}^{25} -55.16$  (c 1.0,  $\text{CH}_2\text{Cl}_2$ ).

#### 4.2.9. (S)-(2'-(((1H-benzod[*j*]imidazol-2-yl)methyl)amino)-[1,1'-binaphthalen]-2-yl)diphenylphosphine oxide (**12**)

A mixture of (S)-(+)-2-(diphenylphosphine oxide)-1,1'-binaphthyl-2'-amine **6** (200 mg, 0.426 mmol) and 2-formyl-1H-benzimidazole (187 mg, 1.278 mmol) in the presence of 4 Å MS (0.85 g) in dry toluene (8 mL) was stirred at 110 °C for 14 h in a pressure tube. The mixture was cooled down to room temperature and then pre-cooled (ice/NaCl bath). After cooling, dry methanol (3 mL) was added and then  $\text{NaBH}_4$  (54 mg, 1.43 mmol) was added in one portion and stirred at room temperature for 1 h. The mixture was filtered through folded filter. The reaction mixture was treated with water and the organic phase was extracted with ethyl acetate (3 times). The combined organic phases were washed with brine, dried over anhydrous magnesium sulfate and concentrated under vacuum. The residue was purified by flash chromatography on silica gel (20–50% of hexane in ethyl acetate; gradient) to furnish **12** (212 mg, 83% yield) as yellow foam. The sample for analysis was recrystallised from toluene/hexane.  $^1\text{H}$  NMR (400 MHz,  $\text{CDCl}_3$ )  $\delta$  4.38 (t,  $J = 6.6$  Hz, 1H), 4.63 (dd,  $J = 6.3, 18.0$  Hz, 1H), 4.88 (dd,  $J = 7.0, 18.0$  Hz, 1H), 6.30 (d,  $J = 8.4$  Hz, 1H), 6.62–6.70 (m, 2H), 6.74–6.80 (m, 1H), 6.82–6.95 (m, 3H), 7.08–7.38 (m, 7H), 7.44 (d,  $J = 9.0$  Hz, 1H), 7.50–7.67 (m, 6H), 7.76 (d,  $J = 7.9$  Hz, 1H), 7.93–8.06 (m, 4H), 13.99 (bs, 1H);  $^{31}\text{P}$  NMR (162 MHz,  $\text{CDCl}_3$ )  $\delta$  -27.87;  $^{13}\text{C}$  NMR (100 MHz,  $\text{CDCl}_3$ )  $\delta$  42.60, 111.75, 112.54, 113.89 (d,  $J_{\text{C-P}} = 5.1$  Hz), 118.72, 121.46, 121.89, 124.23, 125.44, 125.95, 126.65, 127.20, 127.43, 127.55, 127.80, 127.94, 128.35, 128.77, 128.89, 129.00,

129.09, 129.68, 129.78, 130.23 (d,  $J_{C-P}$  = 3.8 Hz), 130.72, 132.07 (d,  $J_{C-P}$  = 2.2 Hz), 132.11, 132.20, 133.25, 133.48, 133.52, 133.59, 135.75 (d,  $J_{C-P}$  = 2.2 Hz), 142.01, 143.86, 154.91; IR (ATR,  $\text{cm}^{-1}$ )  $\nu$  3052, 1619, 1597, 1507, 1434, 1300, 1269, 1220, 1175, 1154, 1113; HRMS Found  $[M+H]^+$ , 600.21910.  $\text{C}_{40}\text{H}_{31}\text{N}_3\text{OP}$  requires  $[M+H]^+$ , 600.22048;  $[\alpha]_D^{23}$  -117.44 (c 1.0,  $\text{CHCl}_3$ ).

#### 4.2.10. (S)-N-((1H-benzo[d]imidazol-2-yl)methyl)-2'-(diphenylphosphanyl)-[1,1'-binaphthalen]-2-amine (**1f**)

A solution of **12** (40 mg, 0.067 mmol) in neat phenylsilane (300  $\mu\text{L}$ ) was heated at 110 °C for 14 hours. The volatiles were removed by nitrogen flow and the residue was purified by flash chromatography on silica gel (20–40% of hexane in ethyl acetate; gradient) to yield **1f** (32.8 mg, 84% yield) as white foam.  $^1\text{H}$  NMR (400 MHz,  $\text{CDCl}_3$ )  $\delta$  4.18 (t,  $J$  = 5.9 Hz, 1H), 4.55 (dd,  $J$  = 6.5, 18.0 Hz, 1H), 4.77 (dd,  $J$  = 5.4, 18.0 Hz, 1H), 6.40 (d,  $J$  = 8.5 Hz, 1H), 6.76–6.84 (m, 1H), 6.96–7.08 (m, 6H), 7.10–7.20 (m, 3H), 7.28–7.40 (m, 9H), 7.45 (dd,  $J$  = 3.4, 8.5 Hz, 1H), 7.51–7.57 (m, 1H), 7.61 (d,  $J$  = 8.0 Hz, 1H), 7.73 (d,  $J$  = 9.0 Hz, 1H), 7.94 (d,  $J$  = 8.2 Hz, 1H), 7.95 (d,  $J$  = 8.6 Hz, 1H), 10.52 (bs, 1H);  $^{31}\text{P}$  NMR (162 MHz,  $\text{CDCl}_3$ )  $\delta$  -12.52;  $^{13}\text{C}$  NMR (100 MHz,  $\text{CDCl}_3$ )  $\delta$  42.02, 112.61, 116.54 (d,  $J_{C-P}$  = 8.2 Hz), 122.30, 122.95, 124.27, 126.08 (d,  $J_{C-P}$  = 2.2 Hz), 126.43, 127.40, 127.58, 127.62, 127.78, 128.34, 128.42, 128.99, 129.09, 129.15, 129.94, 130.52, 133.17, 133.26, 133.44, 133.87 (d,  $J_{C-P}$  = 1.5 Hz), 134.06, 134.12, 134.33, 134.44, 136.25 (d,  $J_{C-P}$  = 6.6 Hz), 136.67 (d,  $J_{C-P}$  = 5.1 Hz), 140.55, 140.86, 141.13 (d,  $J_{C-P}$  = 2.2 Hz), 153.71 (d,  $J_{C-P}$  = 1.5 Hz); IR (ATR,  $\text{cm}^{-1}$ )  $\nu$  3051, 1618, 1596, 1511, 1492, 1452, 1428, 1323, 1293, 1266, 1216, 1151, 1092, 1023, 998, 951, 917, 845, 809, 737, 694, 628. HRMS Found  $[M+H]^+$ , 584.22415.  $\text{C}_{40}\text{H}_{31}\text{N}_3\text{P}$  requires  $[M+H]^+$ , 584.22556;  $[\alpha]_D^{23}$  -126.95 (c 1.0,  $\text{CH}_2\text{Cl}_2$ ).

#### Acknowledgements

We are grateful to Macquarie University for an iMQRES scholarship to SE.

#### Appendix A. Supplementary data

Supplementary data to this article can be found online at <https://doi.org/10.1016/j.tet.2018.12.016>.

#### References

- [1] a) A. Domagala, T. Jarosz, M. Lapkowski, *Eur. J. Med. Chem.* 100 (2015) 176–187; b) S. Said Fatahala, S. Hasabelnaby, A. Goudah, G. Mahmoud, R. Helmy Abd-El Hameed, *Molecules* 22 (2017) 461; c) E. Yasui, M. Wada, N. Takamura, *Tetrahedron Lett.* 50 (2009) 4762–4765; d) A. Aiello, E. Fattorusso, A. Giordano, M. Menna, W.E.G. Müller, S. Perović-Ottstadt, H.C. Schröder, *Bioorg. Med. Chem.* 15 (2007) 5877–5887.
- [2] a) N. Grüger, H. Wadepohl, L.H. Gade, *Dalton Trans.* 41 (2012) 14028–14030; b) A. Gualandri, L. Cerisoli, H. Stoeckli-Evans, D. Savoia, *J. Org. Chem.* 76 (2011) 3399–3408; c) C.A. Caputo, N.D. Jones, *Dalton Trans.* (2007) 4627–4640; d) C. Mazet, L.H. Gade, *Chem. Eur. J.* 8 (2002) 4308–4318.
- [3] a) H. Maeda, Y. Kusunose, *Chem. Eur. J.* 11 (2005) 5661–5666; b) R. Yamakado, Y. Ashida, R. Sato, Y. Shigetani, N. Yasuda, H. Maeda, *Chem. Eur. J.* 23 (2017) 4160–4168; c) A. Kuno, N. Tohnai, N. Yasuda, H. Maeda, *Chem. Eur. J.* 23 (2017) 11357–11365; d) Y. Haketa, Y. Bando, K. Takaishi, M. Uchiyama, A. Muranaka, M. Naito, H. Shibaguchi, T. Kawai, H. Maeda, *Angew. Chem. Int. Ed.* 51 (2012) 7967–7971; e) H. Maeda, Y. Bando, K. Shimomura, I. Yamada, M. Naito, K. Nobusawa, H. Tsumatori, T. Kawai, *J. Am. Chem. Soc.* 133 (2011) 9266–9269; f) H. Maeda, Y. Kusunose, Y. Mihashi, T. Mizoguchi, *J. Org. Chem.* 72 (2007) 2612–2616; g) H. Maeda, T. Shirai, Y. Bando, K. Takaishi, M. Uchiyama, A. Muranaka, T. Kawai, *M. Naito, Org. Lett.* 15 (2013) 6006–6009; h) Y. Haketa, H. Maeda, *Chem. Eur. J.* 17 (2011) 1485–1492; i) H. Maeda, M. Terasaki, Y. Haketa, Y. Mihashi, Y. Kusunose, *Org. Biomol. Chem.* 6 (2008) 433–436; j) H. Maeda, Y. Haketa, T. Nakanishi, *J. Am. Chem. Soc.* 129 (2007) 13661–13674.
- [4] a) R. Yamakado, T. Sakurai, W. Matsuda, S. Seki, N. Yasuda, S. Akine, H. Maeda, *Chem. Eur. J.* 22 (2016) 626–638; b) B. Dong, T. Sakurai, Y. Honsho, S. Seki, H. Maeda, *J. Am. Chem. Soc.* 135 (2013) 1284–1287; c) B. Dong, T. Sakurai, Y. Bando, S. Seki, K. Takaishi, M. Uchiyama, A. Muranaka, H. Maeda, *J. Am. Chem. Soc.* 135 (2013) 14797–14805; d) Y. Haketa, Y. Honsho, S. Seki, H. Maeda, *Chem. Eur. J.* 18 (2012) 7016–7020; e) Y. Haketa, S. Sasaki, N. Ohta, H. Masunaga, H. Ogawa, N. Mizuno, F. Araoka, H. Takezoe, H. Maeda, *Angew. Chem. Int. Ed.* 49 (2010) 10079–10083.
- [5] M. Nishio, Y. Umezawa, K. Honda, S. Tsuboyama, H. Suezawa, *CrystEngComm* 11 (2009) 1757–1788.
- [6] a) M. Roucan, M. Kielmann, S.J. Connon, S.S.R. Bernhard, M.O. Senge, *Chem. Commun.* 54 (2018) 26–29; b) G. Cafeo, M. De Rosa, F.H. Kohnke, P. Neri, A. Soriente, L. Valenti, *Tetrahedron Lett.* 49 (2008) 153–155; c) G. Hirata, H. Maeda, *Org. Lett.* 20 (2018) 2853–2856; d) M. Kielmann, M.O. Senge, *Angew. Chem. Int. Ed.* 57 (2018) 2–26, in press; e) D.S. Kim, J.L. Sessler, *Chem. Soc. Rev.* 44 (2015) 532–546; f) G. Aragay, D. Hernández, B. Verdejo, E. Escudero-Adán, M. Martínez, P. Ballester, *Molecules* 20 (2015) 16672; g) L. Adriaenssens, C. Estarellas, A. Vargas Jentzsch, M. Martínez Belmonte, S. Matile, P. Ballester, *J. Am. Chem. Soc.* 135 (2013) 8324–8330; h) J.R. Blas, J.M. López-Bes, M. Márquez, J.L. Sessler, F.J. Luque, M. Orozco, *Chem. Eur. J.* 13 (2007) 1108–1116; i) J.S. Park, C. Bejger, K.R. Larsen, K.A. Nielsen, A. Jana, V.M. Lynch, J.O. Jeppesen, D. Kim, J.L. Sessler, *Chem. Sci.* 3 (2012) 2685–2689.
- [7] a) U. Lüning, *Angew. Chem. Int. Ed.* 51 (2012) 8163–8165; b) J. Choudhury, S. Semwal, *Synlett* 29 (2018) 141–147; c) E. Peris, *Chem. Rev.* 11 (8) (2018) 9988–10031; d) A.J.M. Miller, *Dalton Trans.* 46 (2017) 11987–12000; e) V. Blanco, D.A. Leigh, V. Marcos, *Chem. Soc. Rev.* 44 (2015) 5341–5370; f) D. Troegel, J. Stohrer, *Coord. Chem. Rev.* 255 (2011) 1440–1459.
- [8] a) N.J. Zondlo, *Acc. Chem. Res.* 46 (2013) 1039–1049; b) M. Nishio, *Tetrahedron* 61 (2005) 6923–6950.
- [9] J.-M. Garnier, C. Anstiss, F. Liu, *Adv. Synth. Catal.* 351 (2009) 331–338.
- [10] a) D. Sälinger, R. Brückner, *Synlett* 2009 (2009) 109–111; b) T. Ooi, K. Ohmatsu, K. Maruoka, *J. Am. Chem. Soc.* 129 (2007) 2410–2411; c) S. Vyskočil, M. Smrčina, V. Hanuš, M. Polásek, P. Kočovský, *J. Org. Chem.* 63 (1998) 7738–7748; d) Y.-L. Yang, C.-K. Pei, M. Shi, *Org. Biomol. Chem.* 9 (2011) 3349–3358; e) P.N.M. Botman, O. David, A. Amore, J. Dinkelaar, M.T. Vlaar, K. Goubitz, J. Fraanje, H. Schenk, H. Hiemstra, J.H. van Maarseveen, *Angew. Chem. Int. Ed.* 43 (2004) 3471–3473.
- [11] C. Anstiss, F. Liu, *Tetrahedron* 66 (2010) 5486–5491.
- [12] a) D. Cantillo, C.O. Kappe, *J. Org. Chem.* 75 (2010) 8615–8626; b) I.T. Raheem, E.N. Jacobsen, *Adv. Synth. Catal.* 347 (2005) 1701–1708; c) K.E. Price, S.J. Broadwater, B.J. Walker, D.T. McQuade, *J. Org. Chem.* 70 (2005) 3980–3987; d) P. Buskens, J. Klankermayer, W. Leitner, *J. Am. Chem. Soc.* 127 (2005) 16762–16763; e) V.K. Aggarwal, S.Y. Fulford, G.C. Lloyd-Jones, *Angew. Chem. Int. Ed.* 44 (2005) 1706–1708; f) R. Kenny, F. Liu, *Chem. Rec.* 17 (2017) 535–553.
- [13] a) R. Kenny, F. Liu, *Eur. J. Org. Chem.* (2015) 5304–5319; b) C. Anstiss, J.-M. Garnier, F. Liu, *Org. Biomol. Chem.* 8 (2010) 4400–4407; c) J.-M. Garnier, F. Liu, *Org. Biomol. Chem.* 7 (2009) 1272–1275.
- [14] K. Junge, G. Oehme, A. Monsees, T. Riermeier, U. Dingerdissen, M. Beller, *J. Organomet. Chem.* 675 (2003) 91–96.
- [15] a) A.D. Burrows, M.F. Mahon, M. Varrone, *Dalton Trans.* (2003) 4718–4730; b) X. Shu, H. Liang, Q. Wu, F. Zhou, X. Zheng, H. Fu, B. Xu, R. Li, C. Zhang, H. Chen, *RSC Adv.* 7 (2017) 14816–14823; c) X.-L. Zheng, C.-Y. Zheng, F.-D. Zhou, H.-Y. Fu, M.-L. Yuan, R.-X. Li, B. Xu, H. Chen, *Chin. Chem. Lett.* 27 (2016) 678–680; d) R. Luo, H.-r. Liang, X.-l. Zheng, H.-y. Fu, M.-l. Yuan, R.-x. Li, H. Chen, *Catal. Commun.* 50 (2014) 29–33.
- [16] A.M. Brosnahan, A. Talbot, B.A. McKeown, S.E. Kalman, T.B. Gunnoe, D.H. Ess, M. Sabat, *J. Organomet. Chem.* 793 (2015) 248–255.
- [17] H.-U. Blaser, H.-P. Buser, R. Häusel, H.-P. Jalett, F. Spindler, *J. Organomet. Chem.* 621 (2001) 34–38.
- [18] a) M.M. Siddiqui, L. Radhakrishna, J.T. Mague, M.S. Balakrishna, *J. Organomet. Chem.* 824 (2016) 15–24; b) M.F. Semmelhack, A. Chlenov, D.M. Ho, *J. Am. Chem. Soc.* 127 (2005) 7759–7773.
- [19] a) J. Liu, H. Li, R. Dühren, J. Liu, A. Spannenberg, R. Franke, R. Jackstell, M. Beller, *Angew. Chem. Int. Ed.* 56 (2017) 11976–11980; b) K. Dong, R. Sang, X. Fang, R. Franke, A. Spannenberg, H. Neumann, R. Jackstell, M. Beller, *Angew. Chem. Int. Ed.* 56 (2017) 5267–5271; c) H. Li, H. Neumann, M. Beller, *Chem. Eur. J.* 22 (2016) 10050–10056; d) R. Jennerjahn, I. Piras, R. Jackstell, R. Franke, K.-D. Wiese, M. Beller, *Chem. Eur. J.* 15 (2009) 6383–6388; e) C.M. So, Z. Zhou, C.P. Lau, F.Y. Kwong, *Angew. Chem. Int. Ed.* 47 (2008) 6402–6406;

- f) W.C. Fu, Z. Zhou, F.Y. Kwong, *Organometallics* 35 (2016) 1553–1558;  
g) O.Y. Yuen, M. Charoensak, C.M. So, C. Kuhakarn, F.Y. Kwong, *Chem. Asian J.* 10 (2015) 857–861;  
h) J.V. Suárez-Meneses, E. Bonilla-Reyes, E.A. Blé-González, M.C. Ortega-Alfaro, R.A. Toscano, A. Cordero-Vargas, J.G. López-Cortés, *Tetrahedron* 70 (2014) 1422–1430;  
i) A. Zapf, R. Jackstell, F. Rataboul, T. Riermeier, A. Monsees, C. Fuhrmann, N. Shaikh, U. Dingerdissen, M. Beller, *Chem. Commun.* (2004) 38–39.
- [20] D. Pingen, C. Müller, D. Vogt, *Angew. Chem. Int. Ed.* 49 (2010) 8130–8133.  
[21] G.T. Venkanna, H.D. Arman, Z.J. Tonzetich, *ASC Catal.* 4 (2014) 2941–2950.  
[22] X. Liu, H. Nan, W. Sun, Q. Zhang, M. Zhan, L. Zou, Z. Xie, X. Li, C. Lu, Y. Cheng, *Dalton Trans.* 41 (2012) 10199–10210.  
[23] K. Moonen, I. Laureyn, C.V. Stevens, *Chem. Rev.* 104 (2004) 6177–6216.  
[24] C. Anstiss, P. Karuso, M. Richardson, F. Liu, *Molecules* 18 (2013) 2788.  
[25] Catalysts **1a–f** bind to solvent molecules that cannot be removed without significant catalyst decomposition. All catalysts demonstrated partial decomposition over long-term high vacuum exposure. The attempts to replace solvent molecules with dichloromethane or deuterated chloroform via co-evaporation by nitrogen flow led to partial decomposition of catalysts as well.  
[26] a) M. Shi, M.-J. Qi, X.-G. Liu, *Chem. Commun.* (2008) 6025–6027;  
b) M. Shi, Y.-M. Xu, *Angew. Chem. Int. Ed.* 41 (2002) 4507–4510.  
[27] M. Shi, J.-K. Jiang, *Tetrahedron: Asymmetry* 13 (2002) 1941–1947.  
[28] a) F. Zhong, G.-Y. Chen, Y. Lu, *Org. Lett.* 13 (2011) 82–85;  
b) X.-Y. Guan, Y. Wei, M. Shi, *Chem. Eur. J.* 16 (2010) 13617–13621.  
[29] a) A. Nakano, S. Kawahara, S. Akamatsu, K. Morokuma, M. Nakatani, Y. Iwabuchi, K. Takahashi, J. Ishihara, S. Hatakeyama, *Tetrahedron* 62 (2006) 381–389;  
b) Y. Iwabuchi, M. Nakatani, N. Yokoyama, S. Hatakeyama, *J. Am. Chem. Soc.* 121 (1999) 10219–10220.  
[30] a) M. Shi, Y.-H. Liu, L.-H. Chen, *Chirality* 19 (2007) 124–128;  
b) Y.-H. Liu, L.-H. Chen, M. Shi, *Adv. Synth. Catal.* 348 (2006) 973–979.  
[31] C. Wang, L. Wang, S. Zeng, S. Xu, Z. He, *Phosphorus Sulfur Silicon Relat. Elem.* 188 (2013) 1548–1554.  
[32] N. Utsumi, H. Zhang, F. Tanaka, C.F. Barbas, *Angew. Chem. Int. Ed.* 46 (2007) 1878–1880.  
[33] S.-H. Chen, B.-C. Hong, C.-F. Su, S. Sarshar, *Tetrahedron Lett.* 46 (2005) 8899–8903.  
[34] W.L.F. Armarego, C.L.L. Chai, *Purification of Laboratory Chemicals*, sixth ed., Butterworth-Heinemann, 2009, 6 ed.  
[35] S.T. Handy, J.J. Sabatini, *Org. Lett.* 8 (2006) 1537–1539.

Supplementary Information

**Switchable Pyrrole-based Hydrogen Bonding Motif  
in Enantioselective Trifunctional Organocatalysis**

Sviatoslav S. Eliseenko and Fei Liu\*

*Department of Molecular Sciences, Macquarie University, Sydney, NSW 2109, Australia*

Corresponding Author – Fax: +61-2-9850-8313; e-mail: fei.liu@mq.edu.au

## Table of content

1. General information	4
2. NMR spectra of catalysts <b>1a–f</b> and precursors <b>10–12</b>	5
• Figure 1. <sup>1</sup> H NMR spectra of catalyst <b>1a</b> with the extended aromatic region	5
• Figure 2. <sup>31</sup> P NMR spectra of catalyst <b>1a</b>	6
• Figure 3. <sup>13</sup> C NMR spectra of catalyst <b>1a</b> with the extended aromatic region	7
• Figure 4. <sup>1</sup> H NMR spectra of catalyst <b>1b</b> with the extended aromatic region	8
• Figure 5. <sup>31</sup> P NMR spectra of catalyst <b>1b</b>	9
• Figure 6. <sup>13</sup> C NMR spectra of catalyst <b>1b</b> with the extended aromatic region	10
• Figure 7. <sup>1</sup> H NMR spectra of catalyst <b>1c</b> with the extended aromatic region	11
• Figure 8. <sup>31</sup> P NMR spectra of catalyst <b>1c</b>	12
• Figure 9. <sup>13</sup> C NMR spectra of catalyst <b>1c</b> with the extended aromatic region	13
• Figure 10. <sup>1</sup> H NMR spectra of catalyst precursor <b>10</b> with the extended aromatic region	14
• Figure 11. <sup>31</sup> P NMR spectra of catalyst precursor <b>10</b>	15
• Figure 12. <sup>13</sup> C NMR spectra of catalyst precursor <b>10</b> with the extended aromatic region	16
• Figure 13. <sup>1</sup> H NMR spectra of catalyst <b>1d</b> with the extended aromatic region	17
• Figure 14. <sup>31</sup> P NMR spectra of catalyst <b>1d</b>	18
• Figure 15. <sup>13</sup> C NMR spectra of catalyst <b>1d</b> with the extended aromatic region	19

• Figure 16. <sup>1</sup> H NMR spectra of catalyst precursor <b>11</b> with the extended aromatic region	20
• Figure 17. <sup>31</sup> P NMR spectra of catalyst precursor <b>11</b>	21
• Figure 18. <sup>13</sup> C NMR spectra of catalyst precursor <b>11</b> with the extended aromatic region	22
• Figure 19. <sup>1</sup> H NMR spectra of catalyst <b>1e</b> with the extended aromatic region	23
• Figure 20. <sup>31</sup> P NMR spectra of catalyst <b>1e</b>	24
• Figure 21. <sup>13</sup> C NMR spectra of catalyst <b>1e</b> with the extended aromatic region	25
• Figure 22. <sup>1</sup> H NMR spectra of catalyst precursor <b>12</b> with the extended aromatic region	26
• Figure 23. <sup>31</sup> P NMR spectra of catalyst precursor <b>12</b>	27
• Figure 24. <sup>13</sup> C NMR spectra of catalyst precursor <b>12</b> with the extended aromatic region	28
• Figure 25. <sup>1</sup> H NMR spectra of catalyst <b>1f</b> with the extended aromatic region	29
• Figure 26. <sup>31</sup> P NMR spectra of catalyst <b>1f</b>	30
• Figure 27. <sup>13</sup> C NMR spectra of catalyst <b>1f</b> with the extended aromatic region	31
3. Representatives of chiral HPLC traces of <i>aza</i> -MBH adducts <b>14a</b> , <b>c</b> and MBH adducts <b>16a</b> , <b>c</b>	
• Figure 28. HPLC trace of MBH adduct <b>14c</b>	32
• Figure 29. HPLC trace of MBH adduct <b>14c</b>	33
• Figure 30. HPLC trace of MBH adduct <b>16a</b>	34
• Figure 31. HPLC trace of MBH adduct <b>16c</b>	35
4. References	36

## 1. General information

All reagents unless specified otherwise are commercially available and purified by standard procedures.<sup>1</sup> Chloroform-*d* was purchased from Cambridge Isotope Laboratories, USA and stored over anhydrous potassium carbonate before use. Bromomethyl methyl ether was distilled from anhydrous sodium sulfate and used immediately after distillation. Cesium carbonate was dried before reactions. Air and moisture sensitive reactions were performed under a nitrogen atmosphere. Reactions were magnetically stirred and monitored by thin-layer chromatography (TLC) using Merck silica gel 60 F<sub>254</sub> aluminium pre-coated plates (0.25 mm). Flash column chromatography was performed on Merck silica gel 60 (0.015–0.040 mm). <sup>1</sup>H, <sup>13</sup>C, and <sup>31</sup>P experiments were performed at 298 K on either a Bruker DPX 400 MHz spectrometer equipped with a 5mm QNP probe. Chemical shifts were reported in ppm using the residual CHCl<sub>3</sub> peak as an internal reference ( $\delta_{\text{H}} = 7.26$  ppm,  $\delta_{\text{C}} = 77.16$  ppm). All <sup>31</sup>P NMR spectroscopy was performed on a Bruker DPX 400 MHz spectrometer at 298 K, and all spectra were referenced to external H<sub>3</sub>PO<sub>4</sub> (0 ppm). All spectra were processed using Bruker TOPSPIN software versions 3.5p17. Infrared spectra were taken on Thermo Scientific Nicolet iS5FT-IR Spectrometer with an attenuated total reflectance (ATR) accessory and maximum absorption peaks were reported in cm<sup>-1</sup>. Low-resolution mass analysis was acquired on an Agilent 6130 quadrupole LC/MS system with an electrospray ionization source (ESI) using the Phenomenex Gemini C18 column (2.0 x 150 mm, particle size 3  $\mu\text{m}$ ); the mobile phase consisted of a gradient of 5–95% acetonitrile in water with 0.5% formic acid over 10 or 25 minutes (flow rate 0.5 mL/min, column temperature 40°C) and spectra were acquired in positive mode, scanning over the *m/z* range of 100–1000. High resolution mass analysis was provided by Australian Proteome Analysis Facility (APAF), Macquarie University, Sydney, Australia. Chiral HPLC analysis was performed using a Shimadzu Prominence system with either a Daicel Chiral Columns CHIRALPAK<sup>®</sup> AD-H column or a Regis Chiral Technologies Whelk-O1 column. HPLC grade solvents were degassed before use. Specific rotation was measured at 23°C on a P1010 digital polarimeter (Jasco, Japan). The commercially available aldehydes were used for catalysts synthesis except for 4,5-dibromopyrrole-2-carboxaldehyde **4** that was obtained by the known procedure<sup>2</sup> via the bromination of pyrrole-2-carboxaldehyde **3**. (*S*)-MAPO **6** and aminophosphine **2** were synthesized by known procedures.<sup>3-4</sup> *N*-Tosyl-4-bromobenzaldimine **13a** was synthesized by a known procedure.<sup>5</sup> *N*-tosyl-substituted benzaldimines **13b–d** were synthesized by slightly modified procedure.<sup>6</sup> Catalysts **1a–f** bind to solvent molecules that cannot be removed without significant catalyst decomposition. All catalysts demonstrated partial decomposition over extended high vacuum exposure. The attempts to replace solvent molecules with dichloromethane or deuterated chloroform via co-evaporation by nitrogen flow led to partial decomposition of catalysts as well.

## 2. NMR spectra of catalysts 1a-f and precursors 10-12

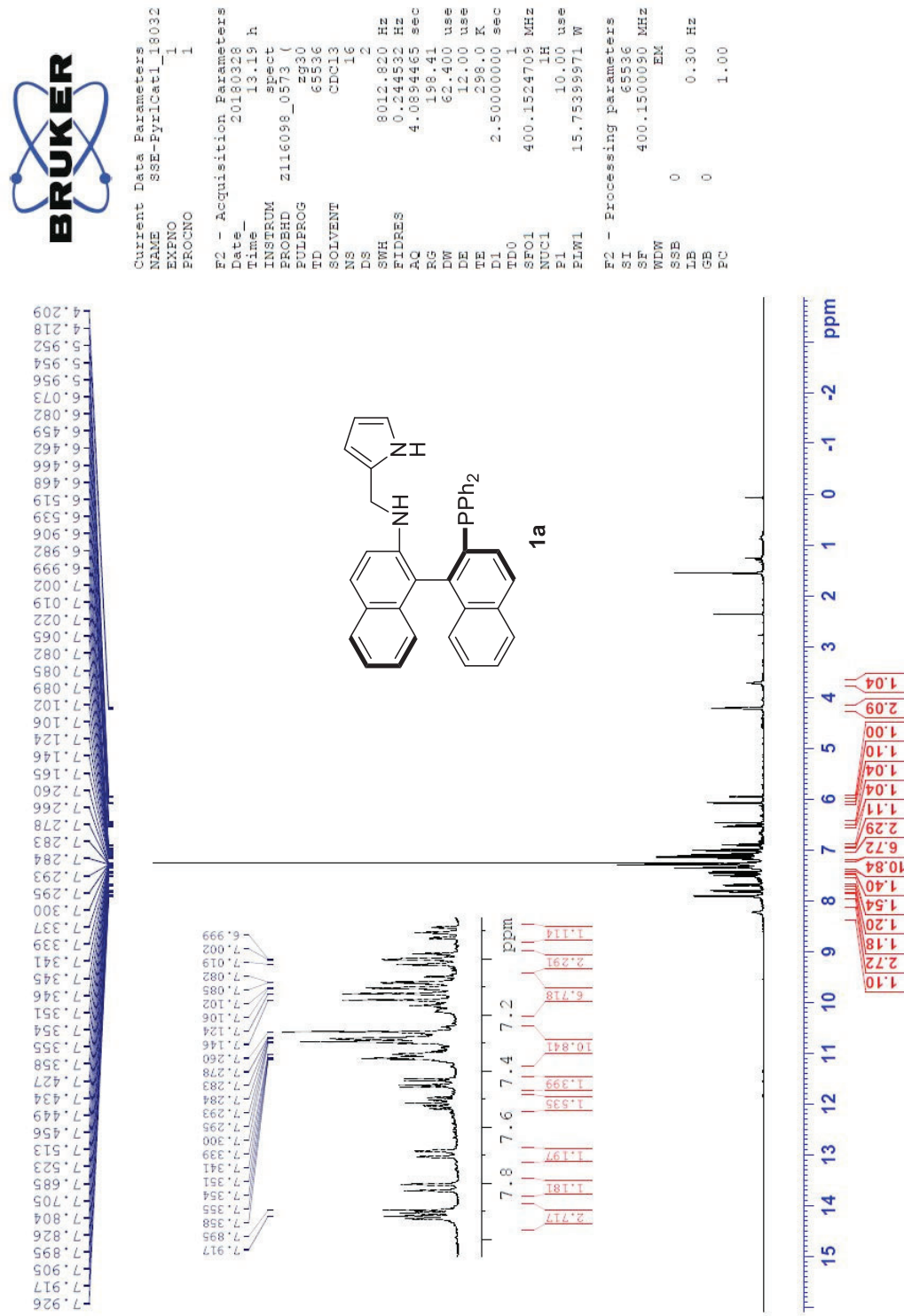


Figure 1. <sup>1</sup>H NMR spectra of catalyst **1a** with the extended aromatic region. The toluene and hexane peaks are observed after column purification. The catalyst is unstable under extended exposure of high vacuum.



Current Data Parameters  
NAME SSE-PyrCat1\_180328  
EXENO 2  
PROCNO 1

F2 - Acquisition Parameters  
Date\_ 20180328  
Time\_ 13.03 h  
INSTRUM spect  
PROBHD z116098\_0573 (zpgp30)  
PULPROG zgpg30  
TD 65536  
SOLVENT CDCl3  
NS 16  
DS 4  
SWH 64102.563 Hz  
FIDRES 1.956255 Hz  
AQ 0.5111808 sec  
RG 198.41  
DW 7.800 usec  
DE 6.50 usec  
TE 296.0 K  
D1 2.00000000 sec  
D11 0.03000000 sec  
TD0 1  
SFO1 161.9755899 MHz  
NUC1 31P  
P1 8.00 usec  
PLW1 55.60200119 W  
SFO2 400.1516006 MHz  
NUC2 1H  
CPDPRG2 waltz16  
PCPD2 90.00 usec  
PLW2 15.75399971 W  
PLW12 0.19449000 W  
PLW13 0.09782800 W

F2 - Processing parameters  
SI 32768  
SF 161.9836322 MHz  
WDW EM  
SSB 0  
LB 1.00 Hz  
GB 0  
PC 1.40

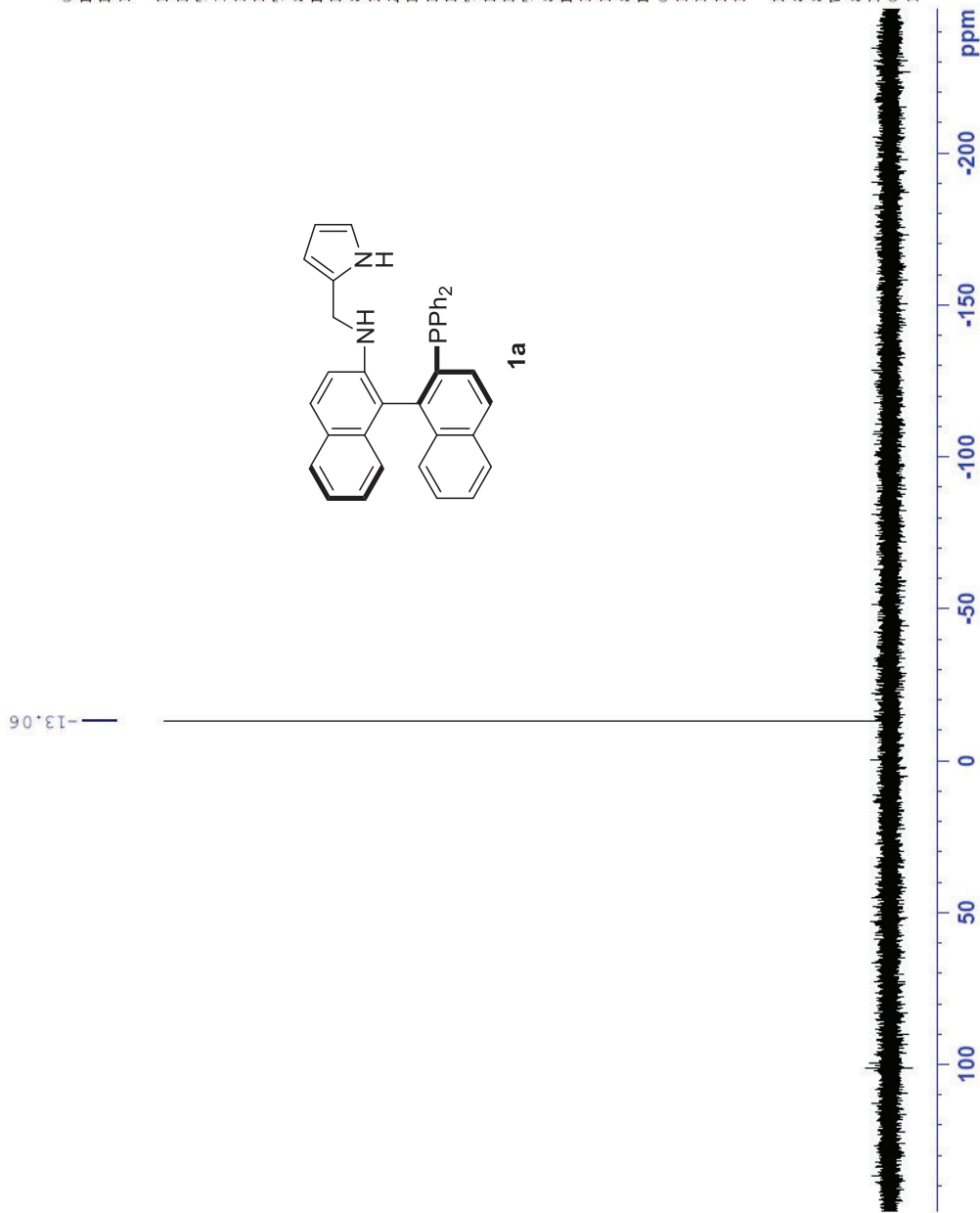
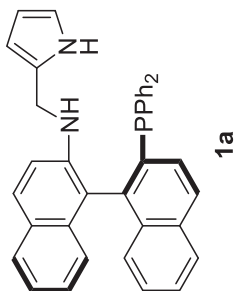


Figure 2. <sup>31</sup>P NMR spectra of catalyst **1a**.





7.933  
7.917  
7.912  
7.797  
7.774  
7.744  
7.632  
7.612  
7.539  
7.536  
7.522  
7.519  
7.515  
7.502  
7.498  
7.433  
7.425  
7.412  
7.403  
7.370  
7.367  
7.364  
7.362  
7.354  
7.350  
7.345  
7.307  
7.291  
7.288  
7.283  
7.275  
7.272  
7.267  
7.264  
7.260  
7.250  
7.230  
7.228  
7.098  
7.095  
7.084  
7.078  
7.052  
7.036  
7.033  
7.030  
7.016  
7.014  
7.007  
6.997  
6.993  
6.773  
6.769  
6.755  
6.368  
6.346  
6.050

Current Data Parameters  
 NAME SSE-PyrCat2\_4\_170  
 EXFNO 2  
 PROCNO 1

F2 - Acquisition Parameters  
 Date\_ 20170918  
 Time 11.56 h

INSTRUM spect  
 PROBHD Z116098\_0573 (zg30)  
 PULPROG zg30  
 TD 65536  
 SOLVENT CDCl3  
 NS 16  
 DS 2

SWH 8012.820 Hz  
 FIDRES 0.244532 Hz  
 AQ 4.0894465 sec  
 RG 198.41  
 DW 62.400 use  
 DE 12.00 use  
 TE 298.0 K  
 DI 2.50000000 sec

TD0 1  
 SF01 400.1524709 MHz  
 NUC1 1H  
 P1 10.00 use  
 PLW1 15.75399971 W

F2 - Processing parameters  
 SI 65536  
 SF 400.1500037 MHz  
 WDW EM  
 SSB 0  
 LB 0.30 Hz  
 GB 0  
 PC 1.00

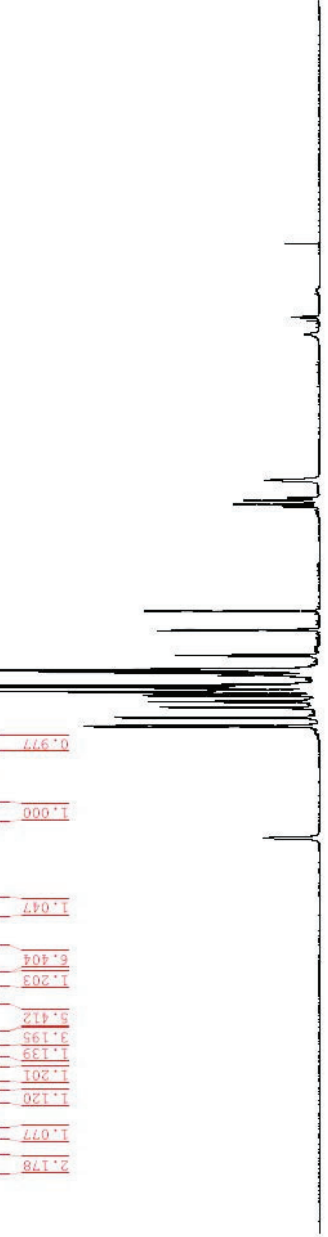
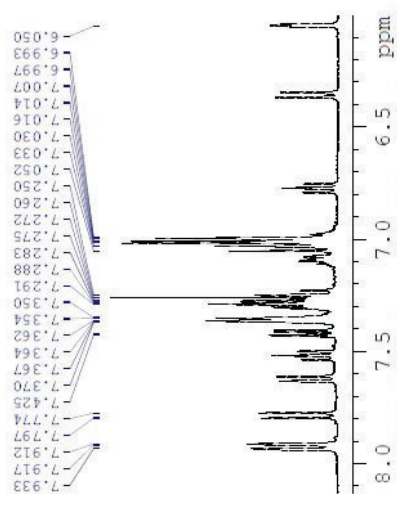
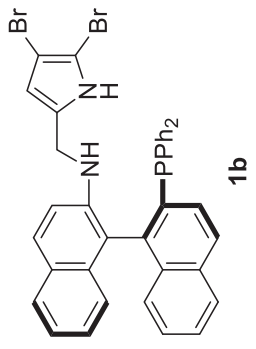


Figure 4. <sup>1</sup>H NMR spectra of catalyst **1b** with the extended aromatic region.



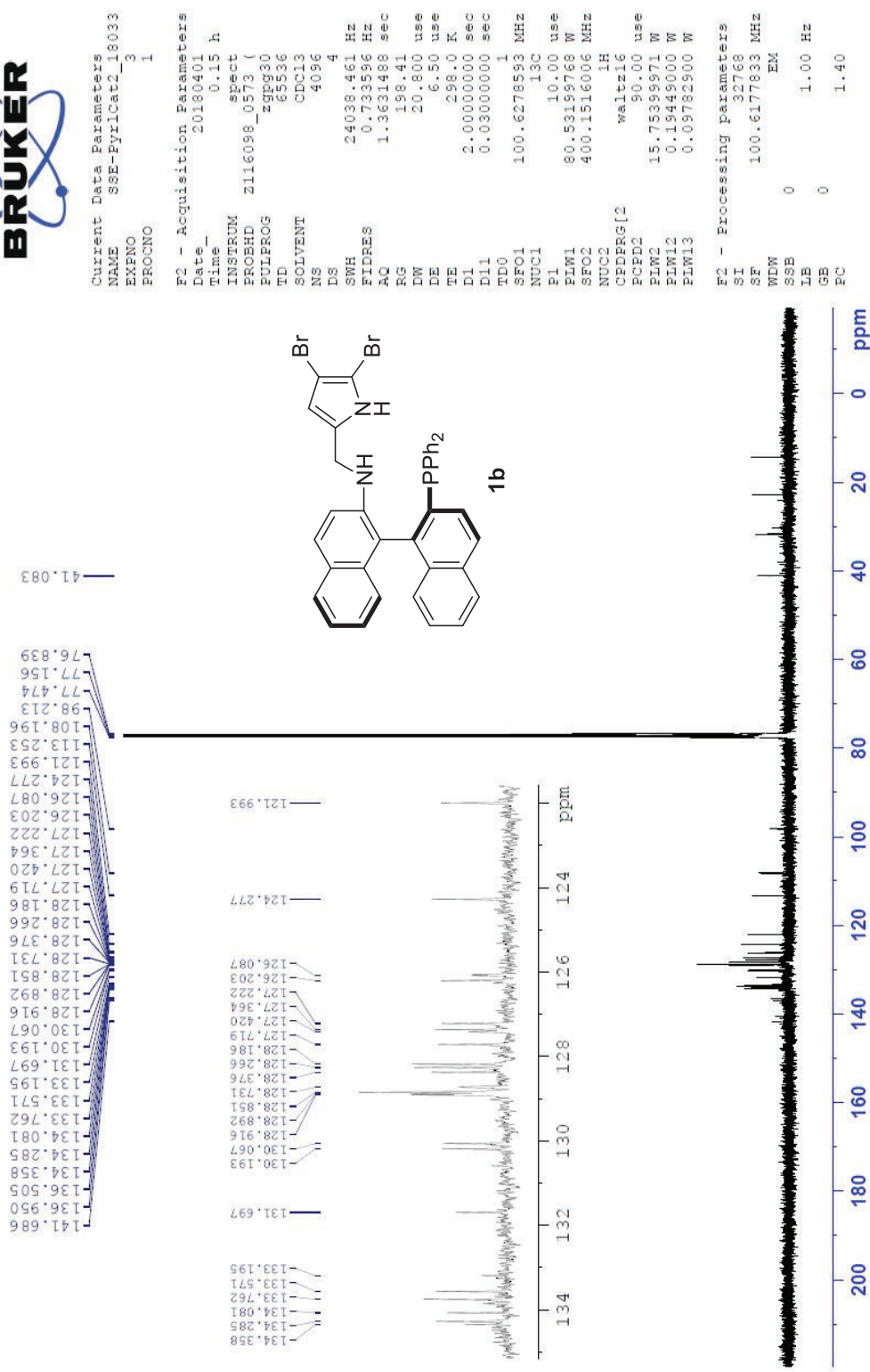
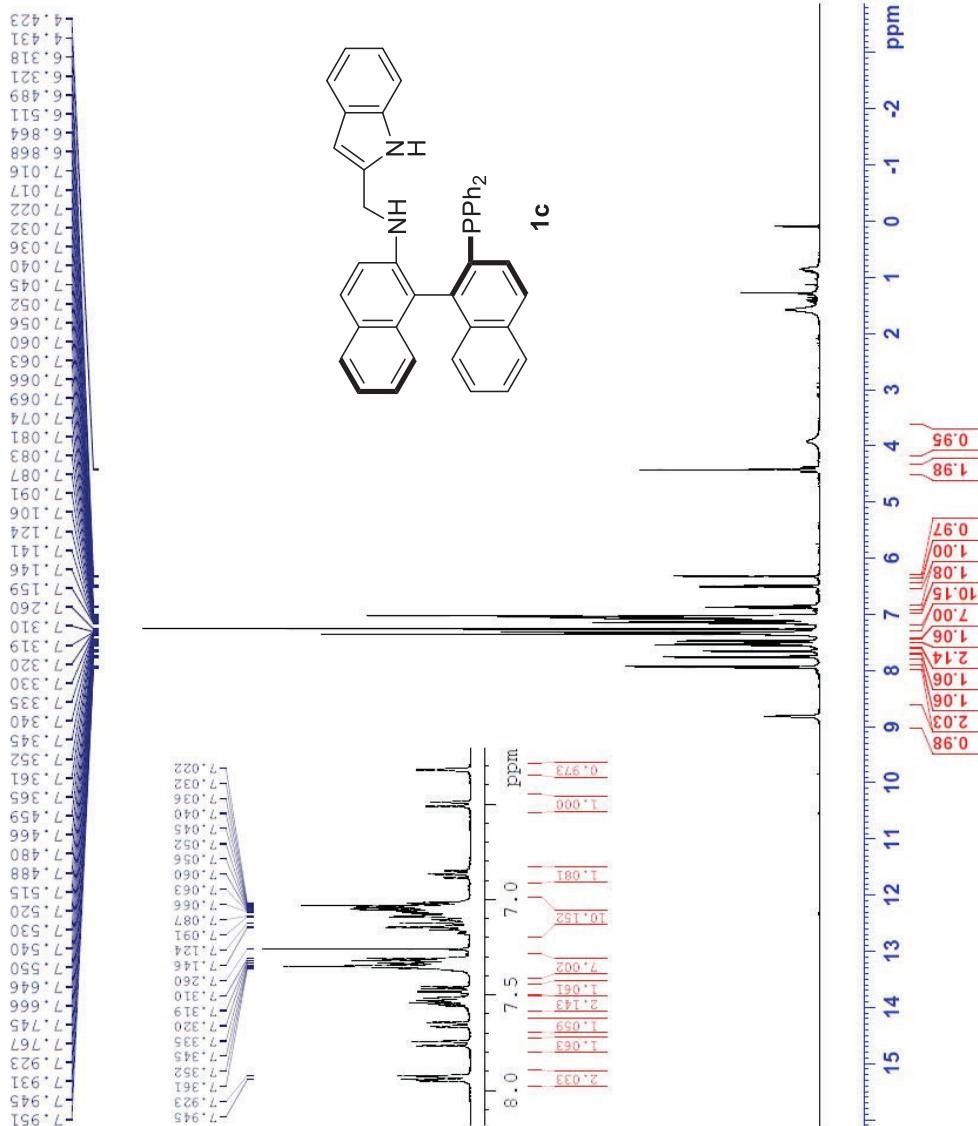


Figure 6. <sup>13</sup>C NMR spectra of catalyst **1b** with the extended aromatic region. The toluene peaks are observed after column purification. The catalyst is unstable under extended exposure of high vacuum.





Current Data Parameters  
NAME SSE-263colF19-33\_Py  
EXPNO 2  
PROCNO 1

F2 - Acquisition Parameters  
Date\_ 20171017  
Time\_ 19.02 h  
INSTRUM spect  
PROBHD zll6098\_0573 (zppg30)  
PULPROG zgpg30  
TD 65536  
SOLVENT CDCl3  
NS 16  
DS 4  
SWH 64102.563 Hz  
FIDRES 1.956255 Hz  
AQ 0.5111808 sec  
RG 198.41  
DM 7.800 usec  
DE 6.50 usec  
TE 298.0 K  
D1 2.0000000 sec  
D11 0.0300000 sec  
TD0 1  
SFO1 161.9753899 MHz  
NUC1 31P  
P1 8.00 usec  
PLW1 55.6020119 W  
SFO2 400.1516006 MHz  
NUC2 1H  
CEPRG[2] waltz16  
PCPD2 90.00 usec  
PLW2 15.75393971 W  
PLW12 0.19449000 W  
PLW13 0.09782900 W

F2 - Processing Parameters  
SI 32768  
SF 161.9836234 MHz  
WDW EM  
SSB 0  
LB 1.00 Hz  
GB 0  
PC 1.40

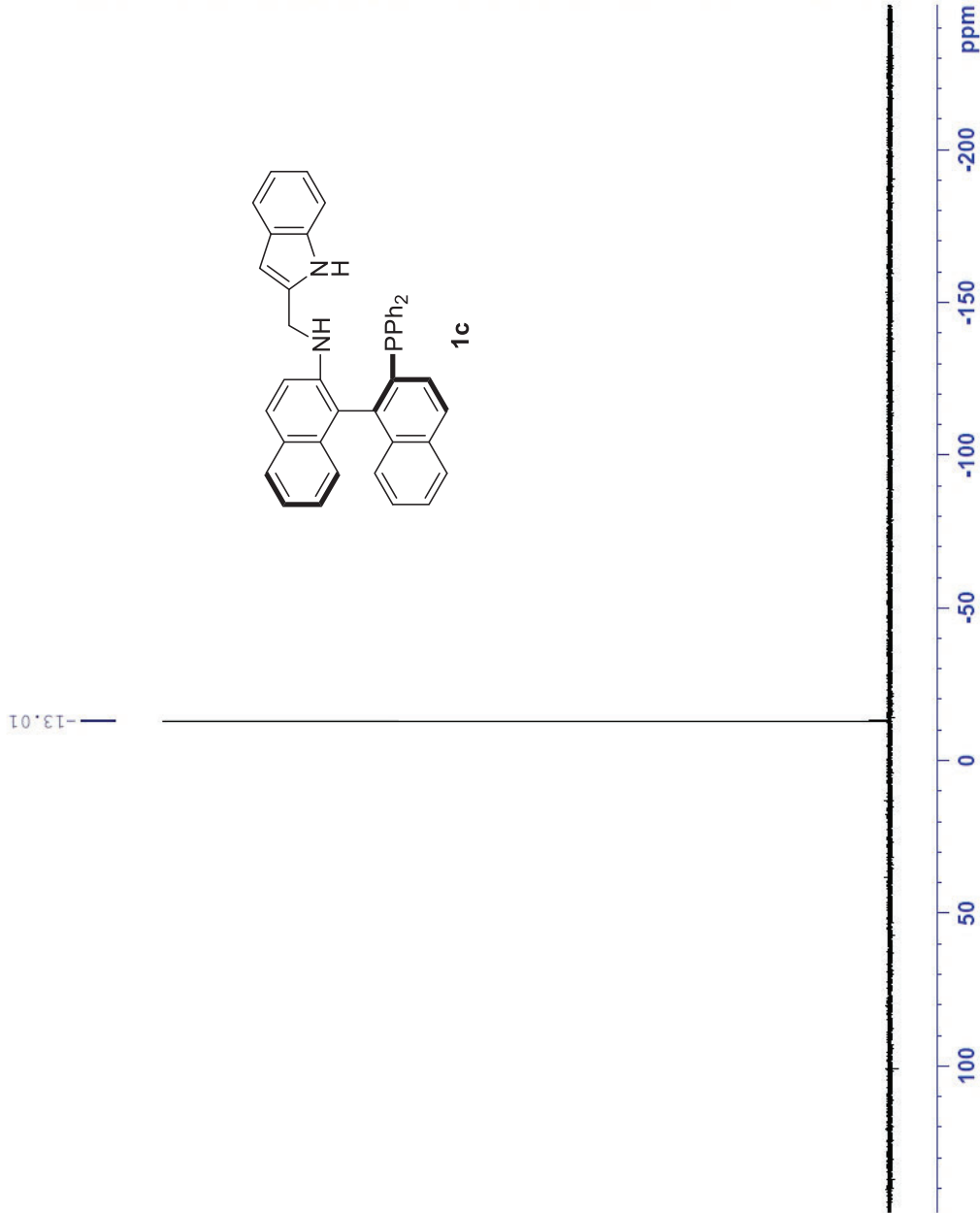


Figure 8. <sup>31</sup>P NMR spectra of catalyst **1c**.



Current Data Parameters  
 NAME SSE-PyrCat3\_col\_F  
 EXENO 3  
 PROCNO 1

F2 - Acquisition Parameters  
 Date\_ 20180312  
 Time\_ 21.59 h

INSTRUM spect  
 PROBHD Z116098\_0573 (  
 FULLPRG zppp30  
 TD 65836  
 SOLVENT CDCl3  
 NS 2048  
 DS 4

SWH 24038.461 Hz  
 FIDRES 0.733596 Hz  
 AQ 1.3631488 sec  
 RG 198.41  
 DW 20.800 use  
 DE 6.50 use  
 TE 298.0 K

D1 2.00000000 sec  
 D11 0.03000000 sec  
 TDO 1  
 SFO1 100.6278593 MHz  
 NUC1 13C

PI 10.00 use  
 PLW1 80.53199768 W  
 SFO2 400.1516006 MHz  
 NUC2 1H  
 CPDPRG12 waltz16  
 PCDP2 90.00 use  
 PLW2 15.75399971 W  
 PLW12 0.19449000 W  
 PLW13 0.09782900 W

F2 - Processing parameters  
 SI 32768  
 SF 100.6177860 MHz  
 WDW EM  
 SSB 0  
 LB 1.00 Hz  
 GB 0  
 FC 1.40

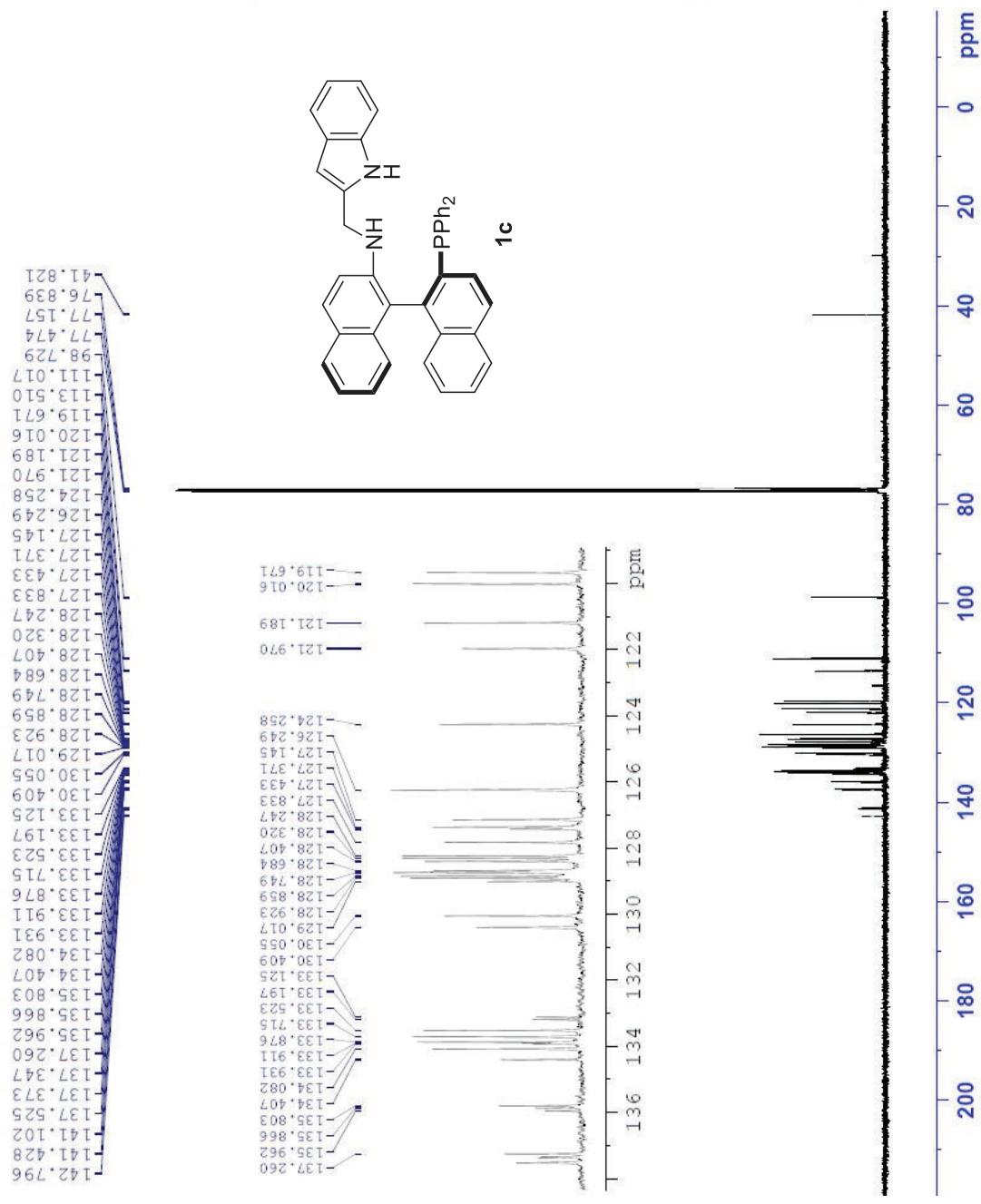


Figure 9. <sup>13</sup>C NMR spectra of catalyst **1c** with the extended aromatic region.





Current Data Parameters  
NAME SSE-280col2\_F51-55\_  
EXPNO 2  
PROCNO 1

F2 - Acquisition Parameters  
Date\_ 20180308  
Time\_ 3.40 h  
INSTRUM spect  
PROBHD Z116098\_0573 (  
PULPROG zgpg30  
TD 65336  
SOLVENT CDCl3  
NS 16  
DS 4  
SWH 64102.563 Hz  
FIDRES 1.956255 Hz  
AQ 0.5111808 sec  
RG 198.41  
DW 7.800 usec  
DE 6.50 usec  
TE 288.0 K  
D1 2.00000000 sec  
D11 0.03000000 sec  
TD0 1  
SF01 161.9755899 MHz  
NUC1 31P  
P1 8.00 usec  
PLW1 55.60200119 W  
SF02 400.1516006 MHz  
NUC2 1H  
CPDPRG[2] waltz16  
PCPD2 90.00 usec  
PLW2 15.75398971 W  
PLW12 0.19449000 W  
PLW13 0.09782900 W

F2 - Processing Parameters  
SI 32768  
SF 161.9836392 MHz  
WDW EM  
SSB 0  
LB 1.00 Hz  
GB 0  
FC 1.40

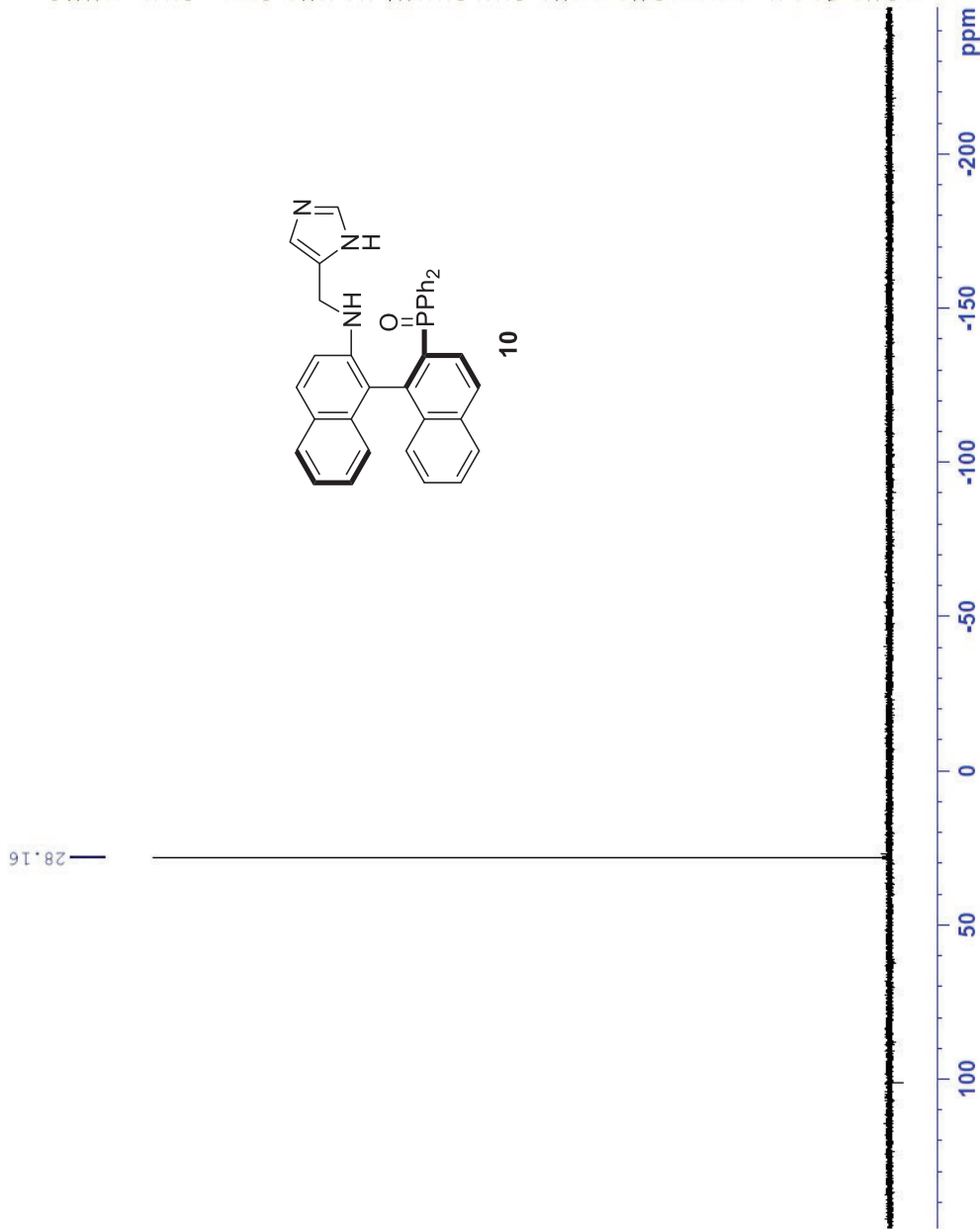
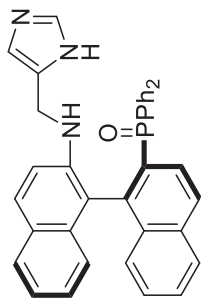


Figure 11. <sup>31</sup>P NMR spectra of catalyst precursor **10**.



Current Data Parameters  
 NAME SSE-280cc12\_F51-55  
 EXENO 3  
 PROCNO 1

F2 - Acquisition Parameters  
 Date\_ 20180308  
 Time 4.40 h  
 INSTRUM spect  
 PROBHD Z116098\_0573 (zpgpg30)  
 PULPROG zgpg30  
 TD 65536  
 SOLVENT CDCl3  
 NS 1024  
 DS 4  
 SWH 24038.461 Hz  
 FIDRES 0.733596 Hz  
 AQ 1.3631488 sec  
 RG 198.41  
 DW 20.800 use  
 DE 6.50 use  
 TE 298.0 K  
 D1 2.00000000 sec  
 D11 0.03000000 sec  
 TDO 1  
 SFO1 100.6278593 MHz  
 NUC1 13C  
 P1 10.00 use  
 PLW1 80.53199768 W  
 SFO2 400.1516006 MHz  
 NUC2 1H  
 CPDPRG2 waltz16  
 PCPD2 90.00 use  
 PLW2 15.75399971 W  
 PLW12 0.19449000 W  
 PLW13 0.09782900 W

F2 - Processing parameters  
 SI 32768  
 SF 100.6177846 MHz  
 WDW EM  
 SSB 0  
 LB 1.00 Hz  
 GB 0  
 PC 1.40

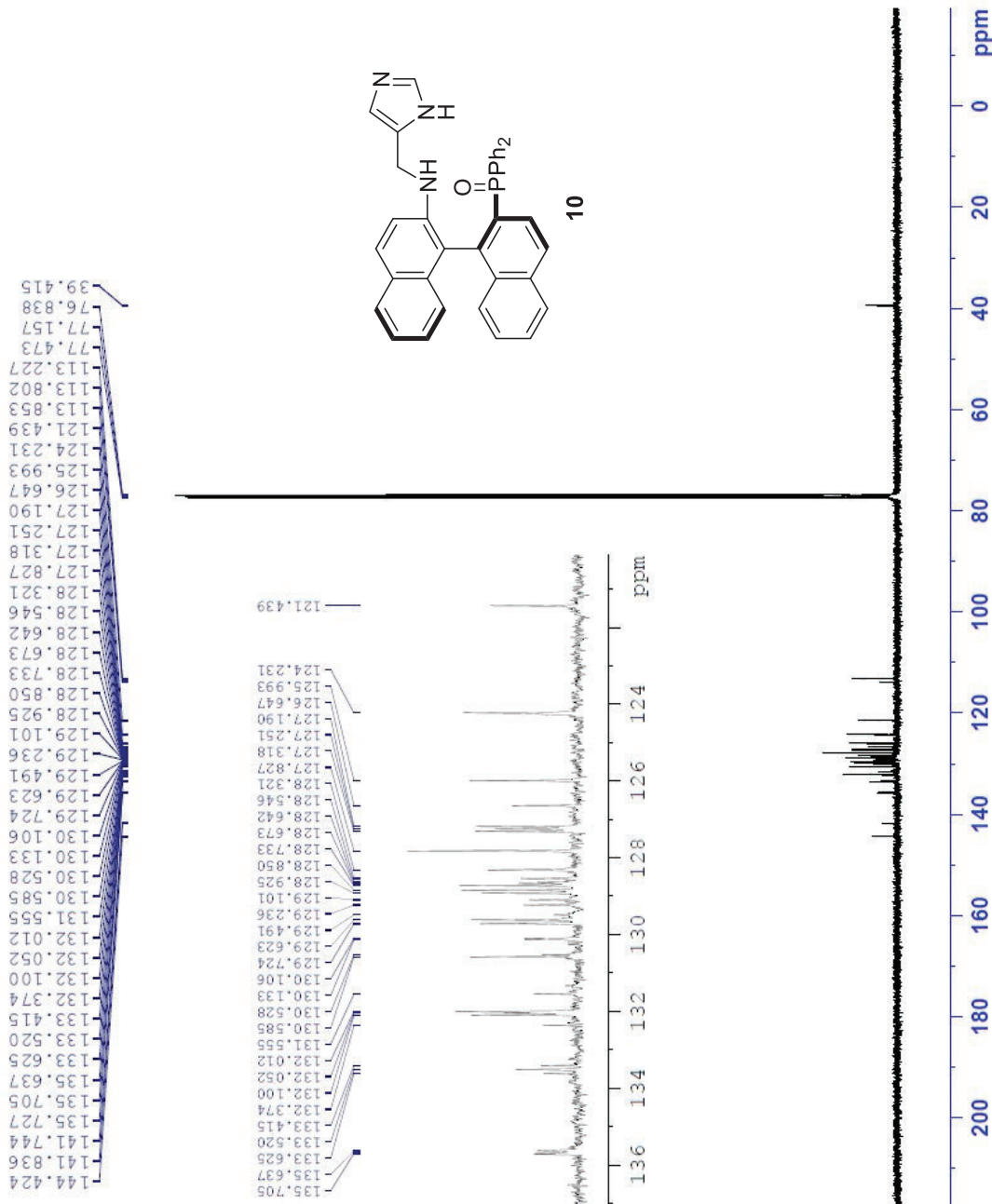
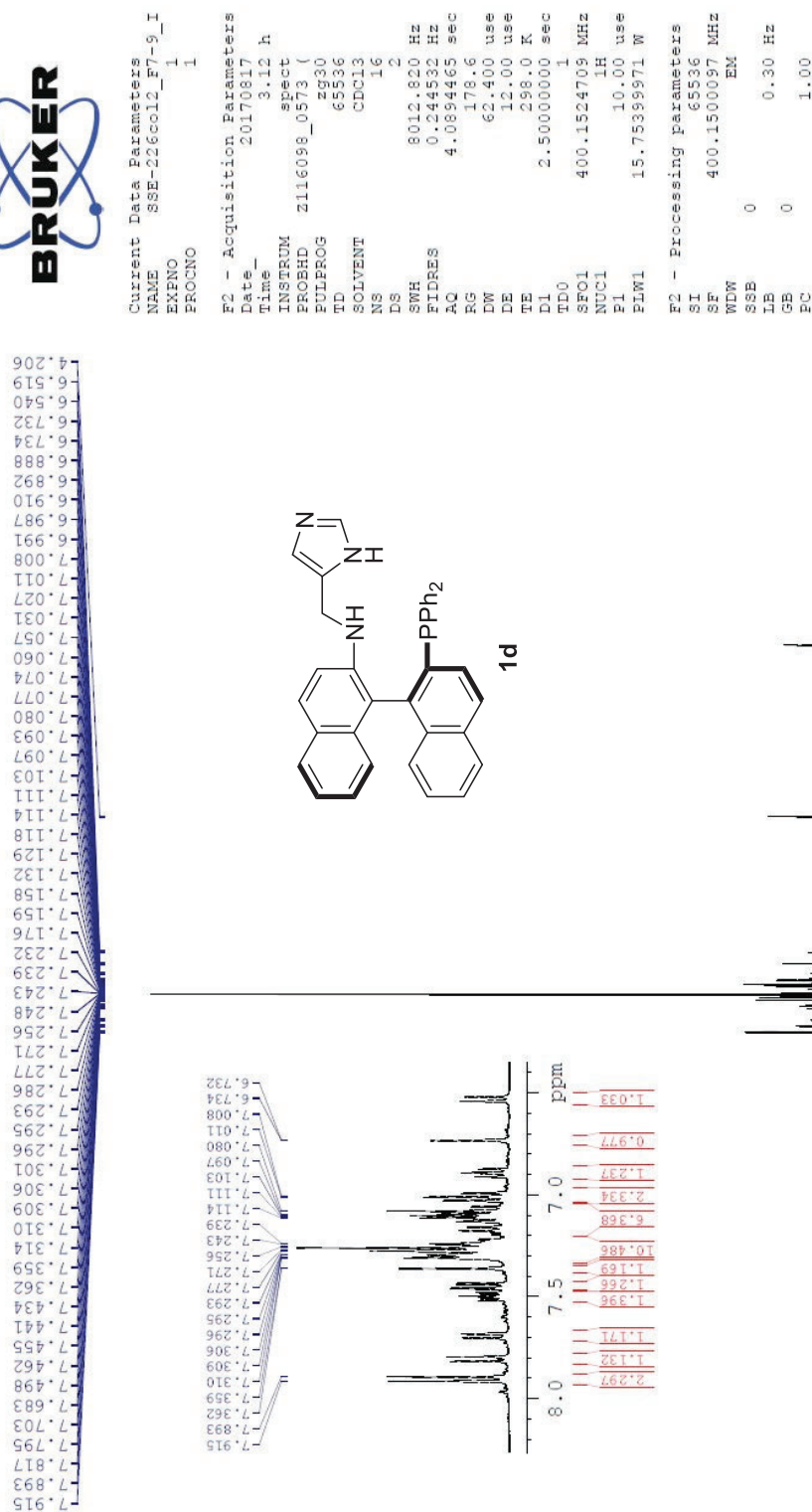


Figure 12. <sup>13</sup>C NMR spectra of catalyst precursor **10** with the extended aromatic region.



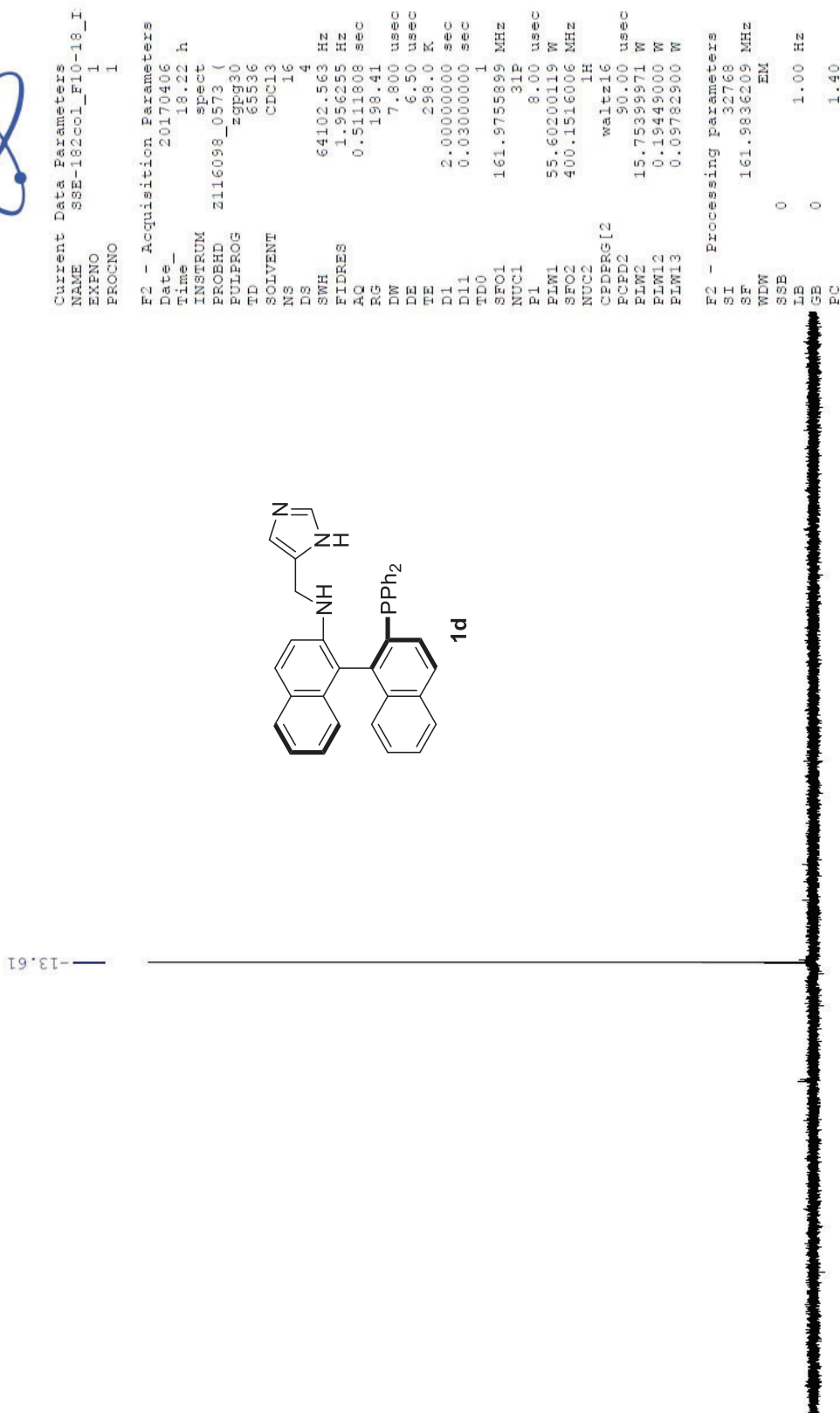


Figure 14. <sup>31</sup>P NMR spectra of catalyst **1d**.



Current Data Parameters  
 NAME SSE-226ccol2\_F7-9\_I  
 EXPNO 3  
 PROCNO 1

F2 - Acquisition Parameters  
 Date\_ 20170817  
 Time\_ 4.15 h

INSTRUM spect  
 PROBRD z116098\_0573 (zcpwg30)  
 PULPROG zgpg30  
 TD 65536  
 SOLVENT CDCl3  
 NS 1024  
 DS 4

SWH 24038.461 Hz  
 FIDRES 0.733596 Hz  
 AQ 1.3631488 sec  
 RG 188.41  
 DW 20.800 use  
 DE 6.50 use  
 TE 298.0 K  
 DT 2.0000000 sec  
 D11 0.0300000 sec

TD0 1  
 SFO1 100.6278593 MHz  
 NUC1 13C  
 P1 10.00 use  
 PLW1 80.53199768 W  
 SFO2 400.1516006 MHz  
 NUC2 1H  
 CPDPRG[2] waltz16  
 PCPD2 90.00 use  
 PLW2 15.75399971 W  
 PLW12 0.19449000 W  
 PLW13 0.09782900 W

F2 - Processing parameters  
 SI 32768  
 SF 100.6177853 MHz  
 WDW EM  
 SSB 0  
 LB 1.00 Hz  
 GB 0  
 FC 1.40

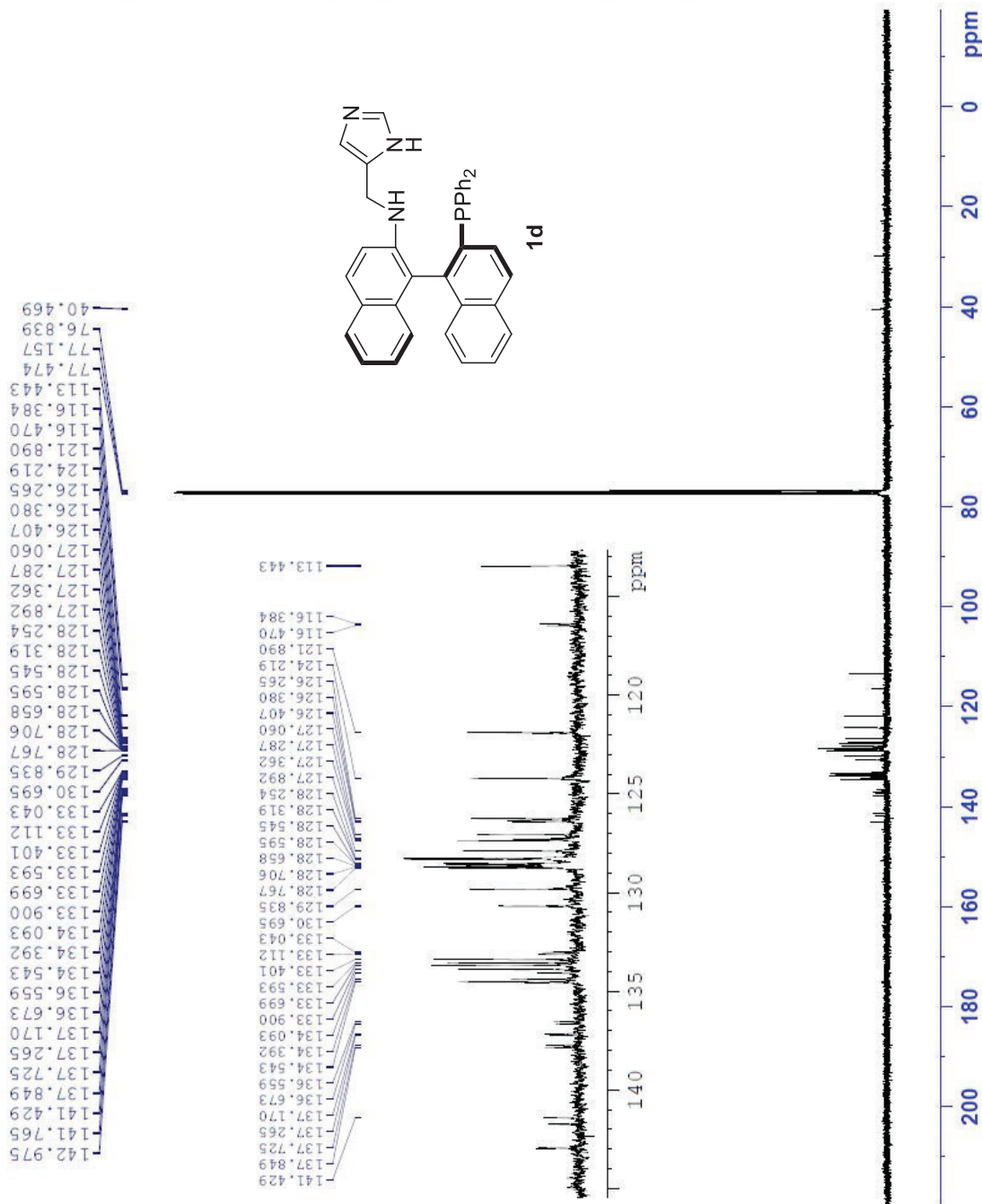


Figure 15. <sup>13</sup>C NMR spectra of catalyst **1d** with the extended aromatic region.





Current Data Parameters  
NAME SSE-Imcat2\_P=O\_rech  
EXPNO 2  
PROCNO 1

F2 - Acquisition Parameters  
Date\_ 20180321  
Time 21:58 h

INSTRUM spect  
PROBHD Z116098\_0573 (z9p930)  
PULPROG zgpg30  
TD 65536

SOLVENT CDCl3  
NS 16  
DS 4

SWH 64102.563 Hz  
FIDRES 1.956255 Hz  
AQ 0.5111808 sec  
RG 198.41

DW 7.800 usec  
DE 6.50 usec  
TE 298.0 K  
D1 2.00000000 sec  
D11 0.03000000 sec

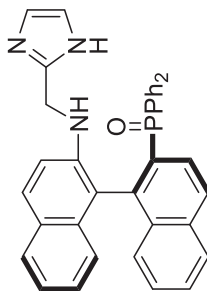
TD0 1  
SF01 161.9755899 MHz  
NUC1 31P

P1 8.00 usec  
PLW1 55.60200119 W  
SFO2 400.1516006 MHz  
NUC2 1H

CPDPRG2 waltz16  
PCPD2 90.00 usec  
PLW2 15.75399971 W  
PLW12 0.19449000 W  
PLW13 0.09782900 W

F2 - Processing parameters  
SI 32768  
SF 161.9836326 MHz  
WDW EM

SSB 0  
IB 1.00 Hz  
GB 0  
PC 1.40



11

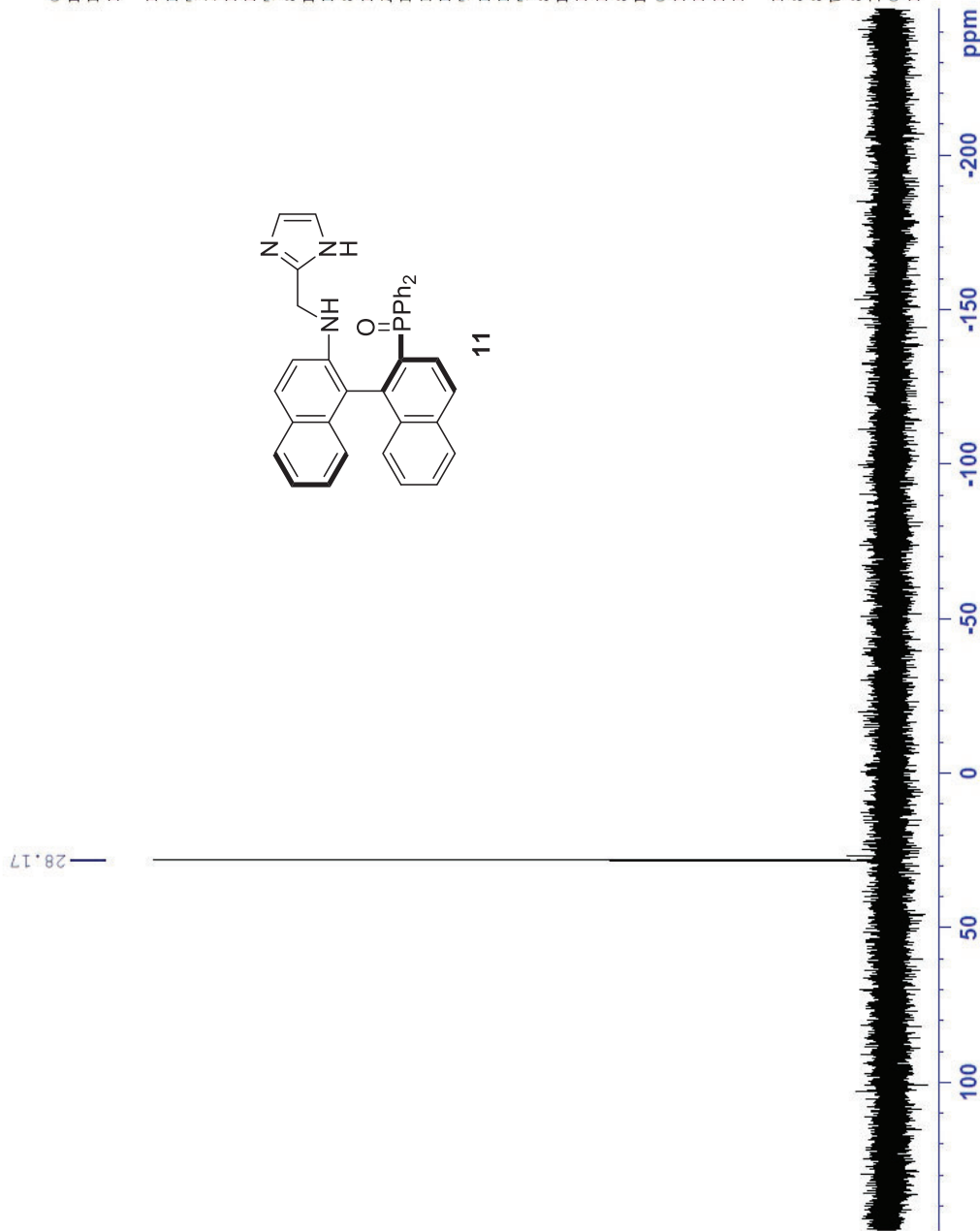
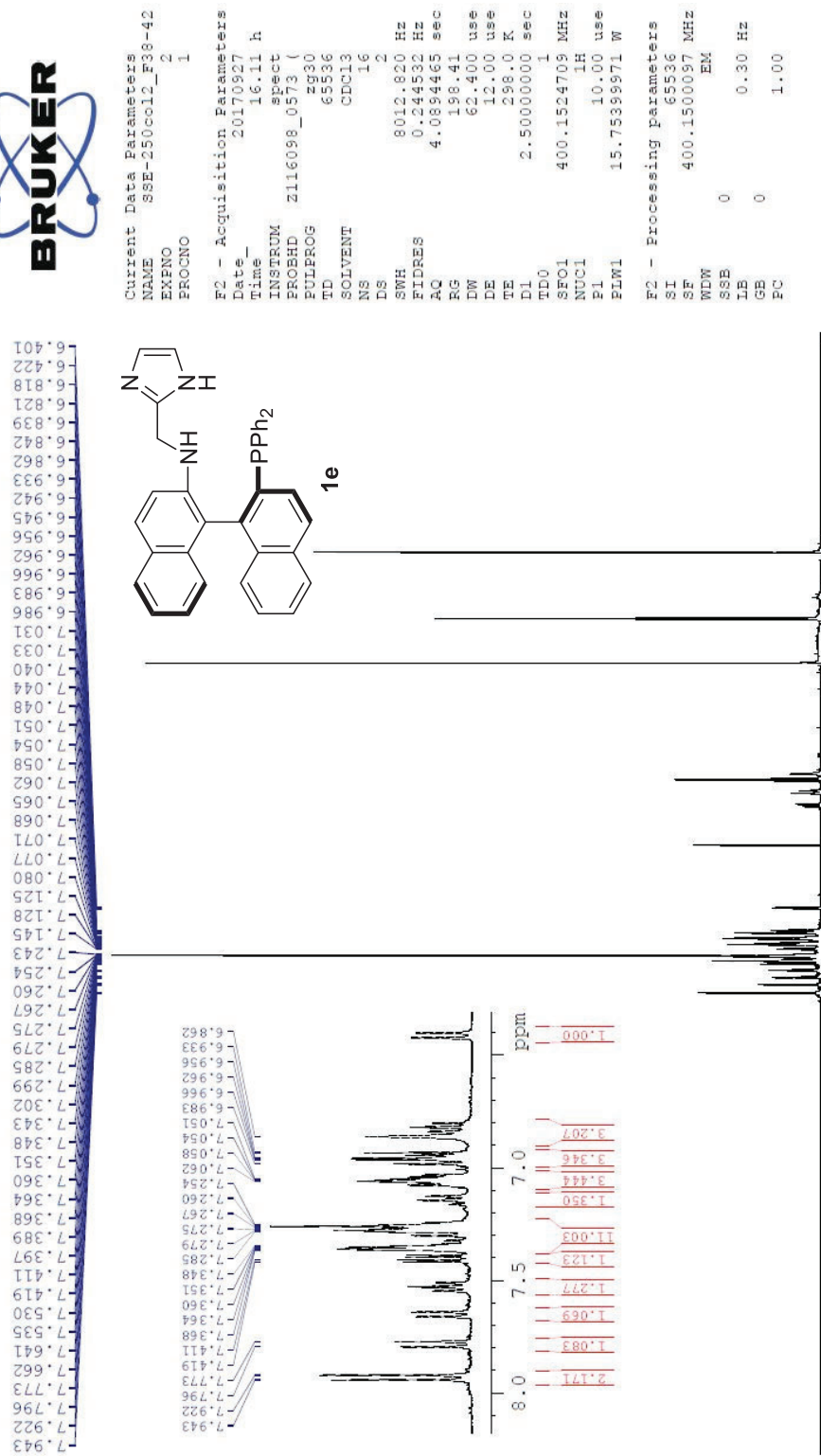


Figure 17. <sup>31</sup>P NMR spectra of catalyst precursor 11.



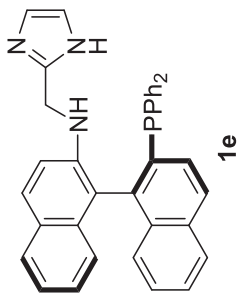




Current Data Parameters  
NAME SSE-302ccl\_F02-35\_I  
EXPNO 3  
PROCNO 1

F2 - Acquisition Parameters  
Date\_ 20180804  
Time 16.36 h  
INSTRUM spect  
PROBHD z116098\_0573 (zg30)  
PULPROG zg30  
TD 65536  
SOLVENT CDCl3  
NS 32  
DS 4  
SWH 64102.563 Hz  
FIDRES 1.856255 Hz  
AQ 0.5111808 sec  
RG 198.41  
DW 7.800 usec  
DE 6.50 usec  
TE 298.0 K  
D1 2.00000000 sec  
TD0 1  
SFO1 161.9755899 MHz  
NUC1 31P  
P1 8.00 usec  
PLW1 55.60200119 W

F2 - Processing parameters  
SI 32768  
SF 161.9836211 MHz  
WDW EM  
SSB 0  
LB 1.00 Hz  
GB 0  
PC 1.40



-12.79

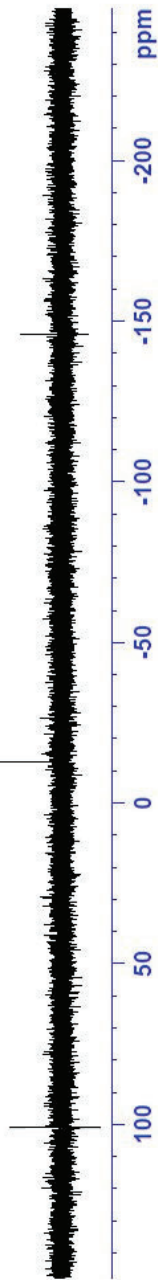


Figure 20. <sup>31</sup>P NMR spectra of catalyst **1e**.



Current Data Parameters  
 NAME SSE-290ccol\_FL17\_Imc  
 EXPNO 7  
 PROCNO 1

F2 - Acquisition Parameters  
 Date\_ 20180401  
 Time 5.31 h  
 INSTRUM spect  
 PROBHD Z116098\_0573 (z9E930)  
 PULPROG zgpg30  
 TD 65536  
 SOLVENT CDCl3  
 NS 4096  
 DS 4  
 SWH 24038.461 Hz  
 FIDRES 0.733596 Hz  
 AQ 1.3631488 sec  
 RG 198.41  
 DW 20.800 use  
 DE 6.50 use  
 TE 298.0 K  
 D1 2.00000000 sec  
 D11 0.03000000 sec  
 TDO 1  
 SFO1 100.6278593 MHz  
 NUC1 13C  
 P1 10.00 use  
 PL1 80.53193768 W  
 SFO2 400.1516006 MHz  
 NUC2 1H  
 CPDPRG2 waltz16  
 PCPD2 90.00 use  
 PL2 15.75339971 W  
 PLW2 0.19449000 W  
 PLW13 0.09782900 W

F2 - Processing parameters  
 SI 32768  
 SF 100.6177838 MHz  
 WDW EM  
 SSB 0  
 LB 1.00 Hz  
 GB 0  
 PC 1.40

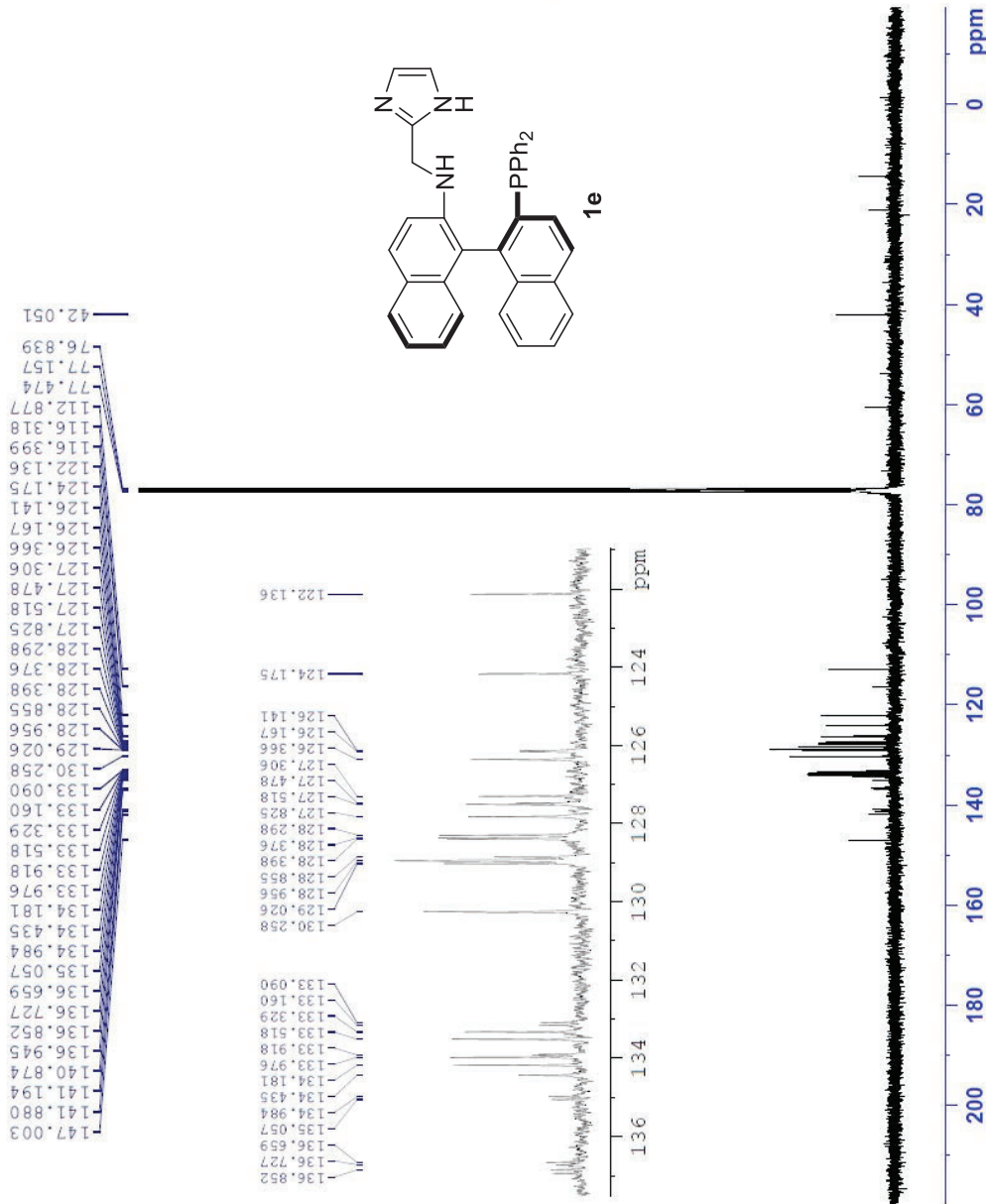


Figure 21. <sup>13</sup>C NMR spectra of catalyst **1e** with the extended aromatic region. The ethyl acetate peaks are observed after column purification. The catalyst is unstable under extended exposure of high vacuum.



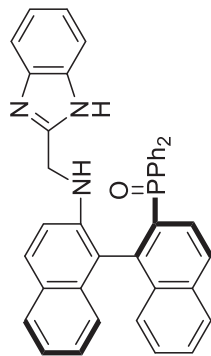


27.87

Current Data Parameters  
NAME SSE-Imcat3\_P=O\_rec1  
EXPNO 2  
PROCNO 1

F2 - Acquisition Parameters  
Date\_ 20180321  
Time 12.53 h  
INSTRUM spect  
PROBHD Z116098\_0573 (zgp930)  
PULPROG zgpg30  
TD 65536  
SOLVENT CDCl3  
NS 16  
DS 4  
SWH 64102.563 Hz  
FIDRES 1.956255 Hz  
AQ 0.5111808 sec  
RG 198.41  
DM 7.800 usec  
DE 6.50 usec  
TE 298.0 K  
D1 2.00000000 sec  
D11 0.03000000 sec  
TD0 1  
SFO1 161.9755899 MHz  
NUC1 31P  
P1 8.00 usec  
PLW1 55.60200119 W  
SFO2 400.1516006 MHz  
NUC2 1H  
CPDPRG2 waltz16  
PCPD2 90.00 usec  
PLW2 15.75399971 W  
PLW12 0.19449000 W  
PLW13 0.097822900 W

F2 - Processing parameters  
SI 32768  
SF 161.9836310 MHz  
WDW EM  
SSB 0  
LB 1.00 Hz  
GB 0  
PC 1.40



12

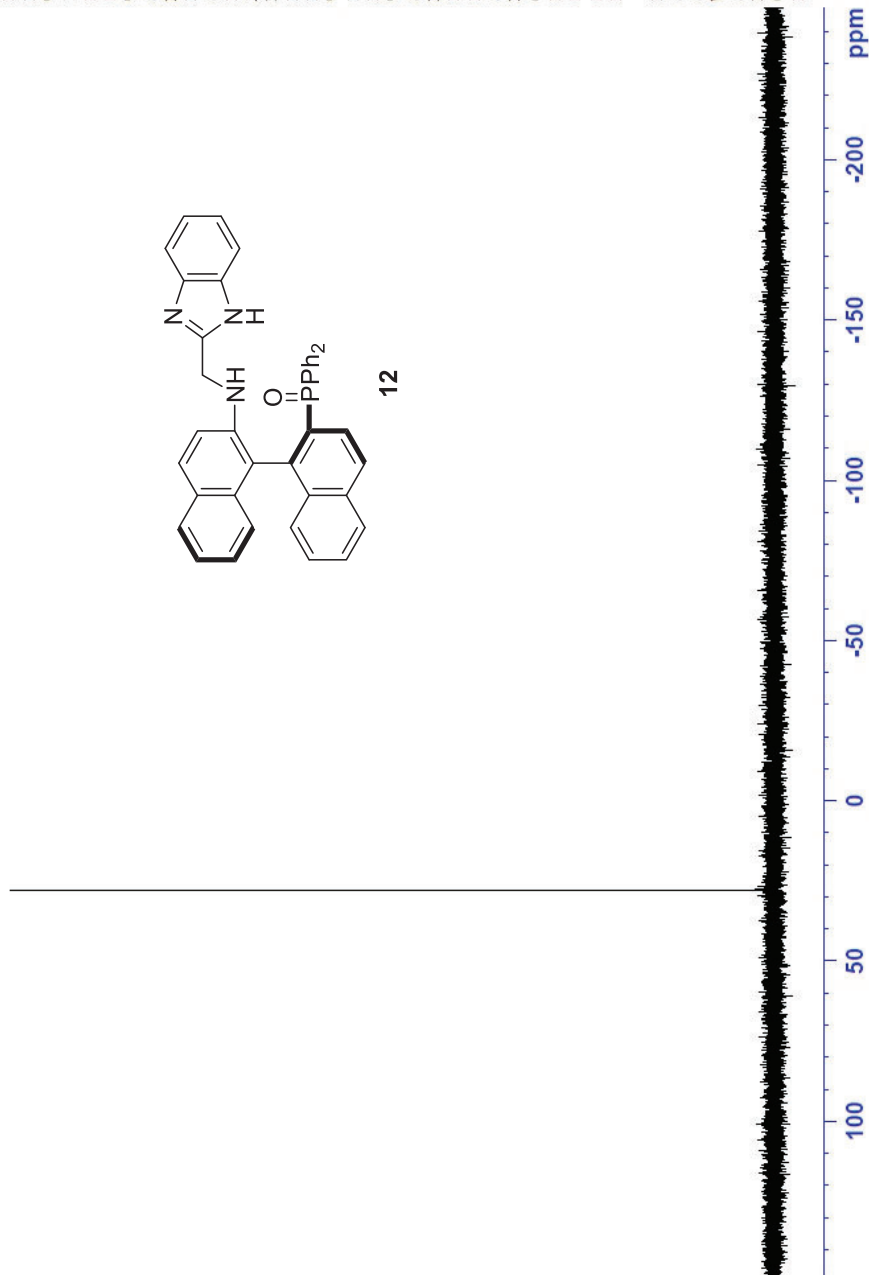


Figure 23. <sup>31</sup>P NMR spectra of catalyst precursor 12.



Current Data Parameters  
 NAME SSE-ImCat3\_PFO\_rec  
 EXPNO 3  
 PROCNO 1

F2 - Acquisition Parameters

Date\_ 20180321  
 Time\_ 20.04 h  
 INSTRUM spect  
 PROBD Z116098\_0573 (   
 PULPROG zgpg30  
 TD 65536  
 SOLVENT CDCl3  
 NS 1024  
 DS 4  
 SWH 24038.461 Hz  
 FIDRES 0.733596 Hz  
 AQ 1.3631488 sec  
 RG 198.41  
 DW 20.800 use  
 DE 6.50 use  
 TE 298.0 K  
 D1 2.00000000 sec  
 D11 0.03000000 sec  
 TD0 1  
 SFO1 100.6278593 MHz  
 NUC1 13C  
 P1 10.00 use  
 PLW1 80.53199768 W  
 SFO2 400.1516006 MHz  
 NUC2 1H  
 CPDPRG2 waltz16  
 PCPD2 90.00 use  
 PLW2 15.75399971 W  
 PLW12 0.19449000 W  
 PLW13 0.09782900 W

F2 - Processing Parameters

SI 32768  
 SF 100.6177841 MHz  
 EM  
 SSB 0  
 LB 1.00 Hz  
 GB 0  
 PC 1.40

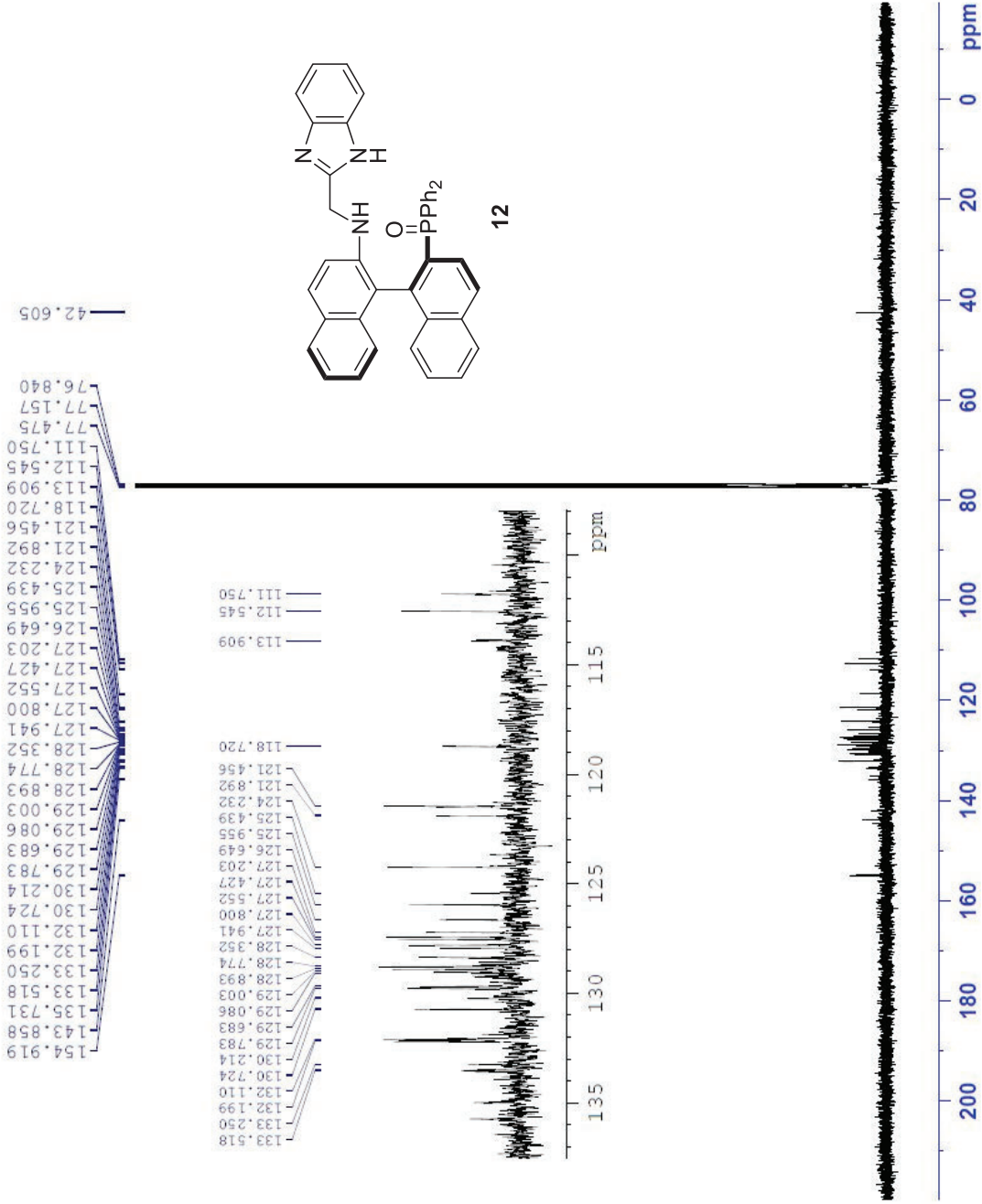


Figure 24. <sup>13</sup>C NMR spectra of catalyst precursor 12 with the extended aromatic region.



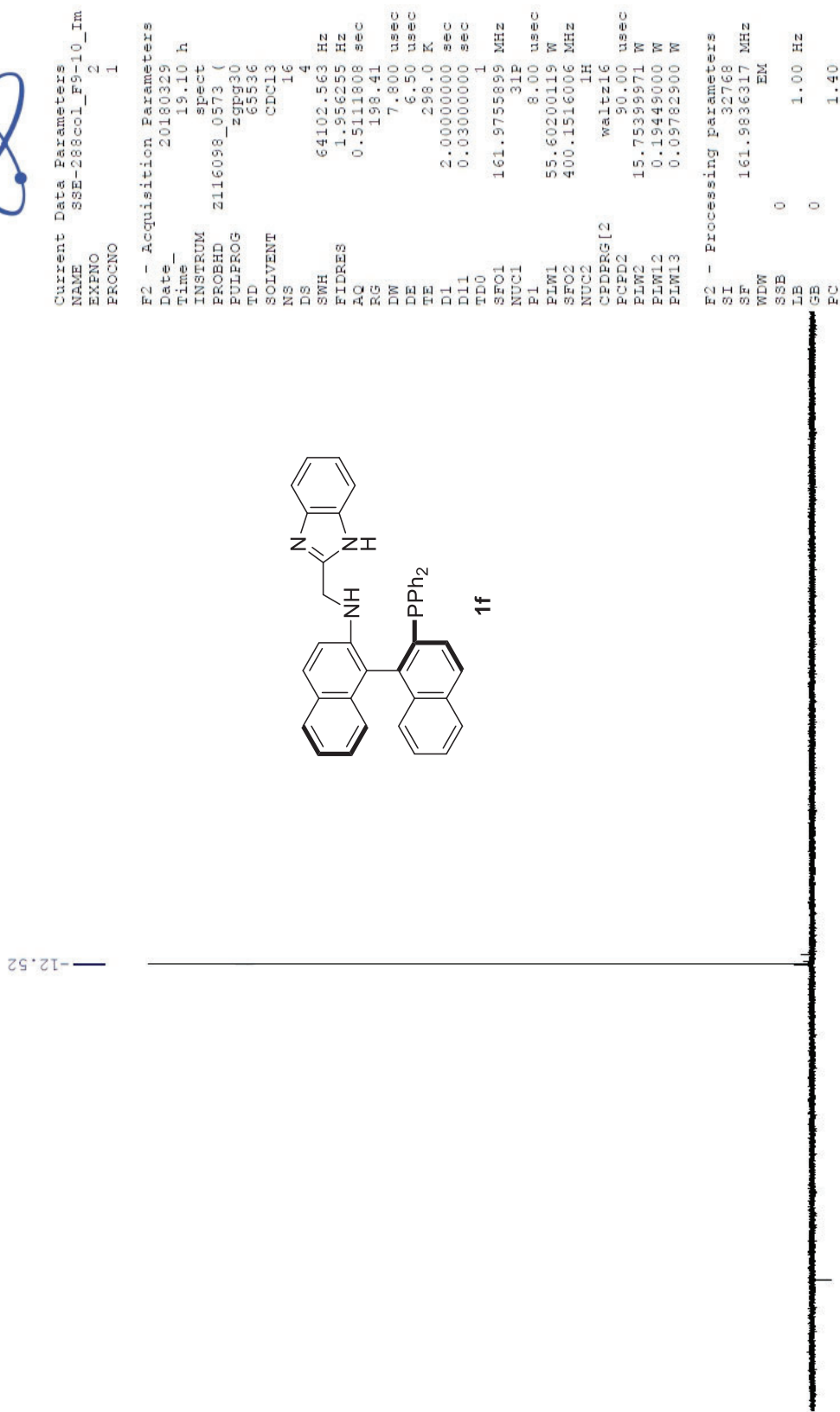


Figure 26. <sup>31</sup>P NMR spectra of catalyst **1f**.



Current Data Parameters  
 NAME SSE-288cool\_F9-10\_I  
 EXPNO 3  
 PROCNO 1

F2 - Acquisition Parameters  
 Date\_ 20180330  
 Time 3.11 h  
 INSTRUM spect  
 PROBHD Z116098\_0573 (  
 PULPROG zgpg30  
 TD 65536  
 SOLVENT CDCl3  
 NS 2048  
 DS 4  
 SWH 24038.461 Hz  
 FIDRES 0.733596 Hz  
 AQ 1.3631488 sec  
 RG 198.41  
 DW 20.800 use  
 DE 6.50 use  
 TE 298.0 K  
 D1 2.00000000 sec  
 D11 0.03000000 sec  
 TD0 1  
 SFO1 100.6278593 MHz  
 NUC1 13C  
 F1 10.00 use  
 PLW1 80.5319768 W  
 SFO2 400.1516006 MHz  
 NUC2 1H  
 CPDPRG2 waltz16  
 ECPD2 90.00 use  
 PLW2 15.75399371 W  
 PLW12 0.19449000 W  
 PLW13 0.09782900 W

F2 - Processing parameters  
 SI 32768  
 SF 100.6177848 MHz  
 WDW EM  
 SSB 0  
 LB 1.00 Hz  
 GB 0  
 PC 1.40

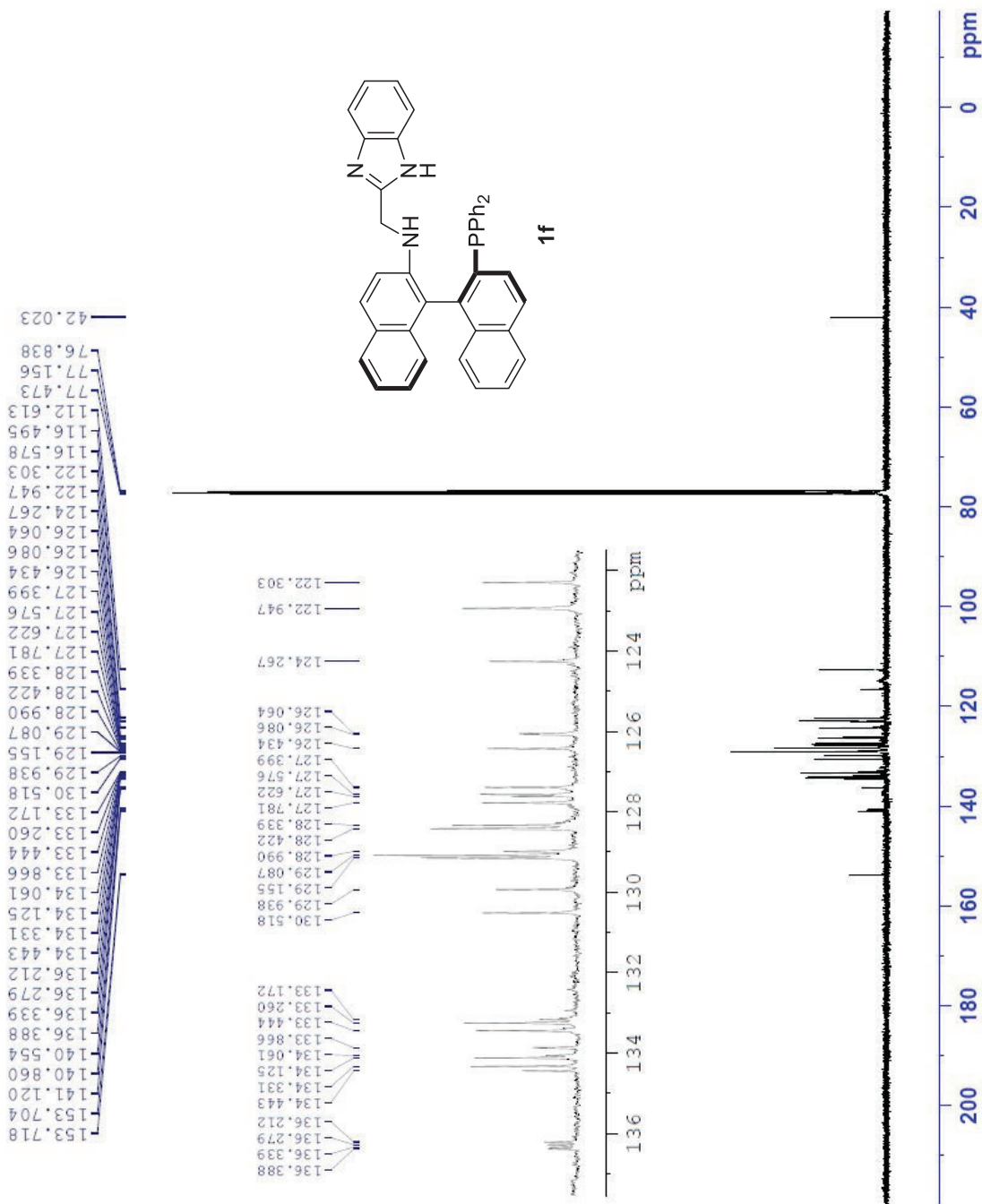


Figure 27. <sup>13</sup>C NMR spectra of catalyst **1f** with the extended aromatic region.

### 3. Chiral HPLC traces for $\alpha\alpha$ -MBH adducts 14a, c and MBH adducts 16a, c

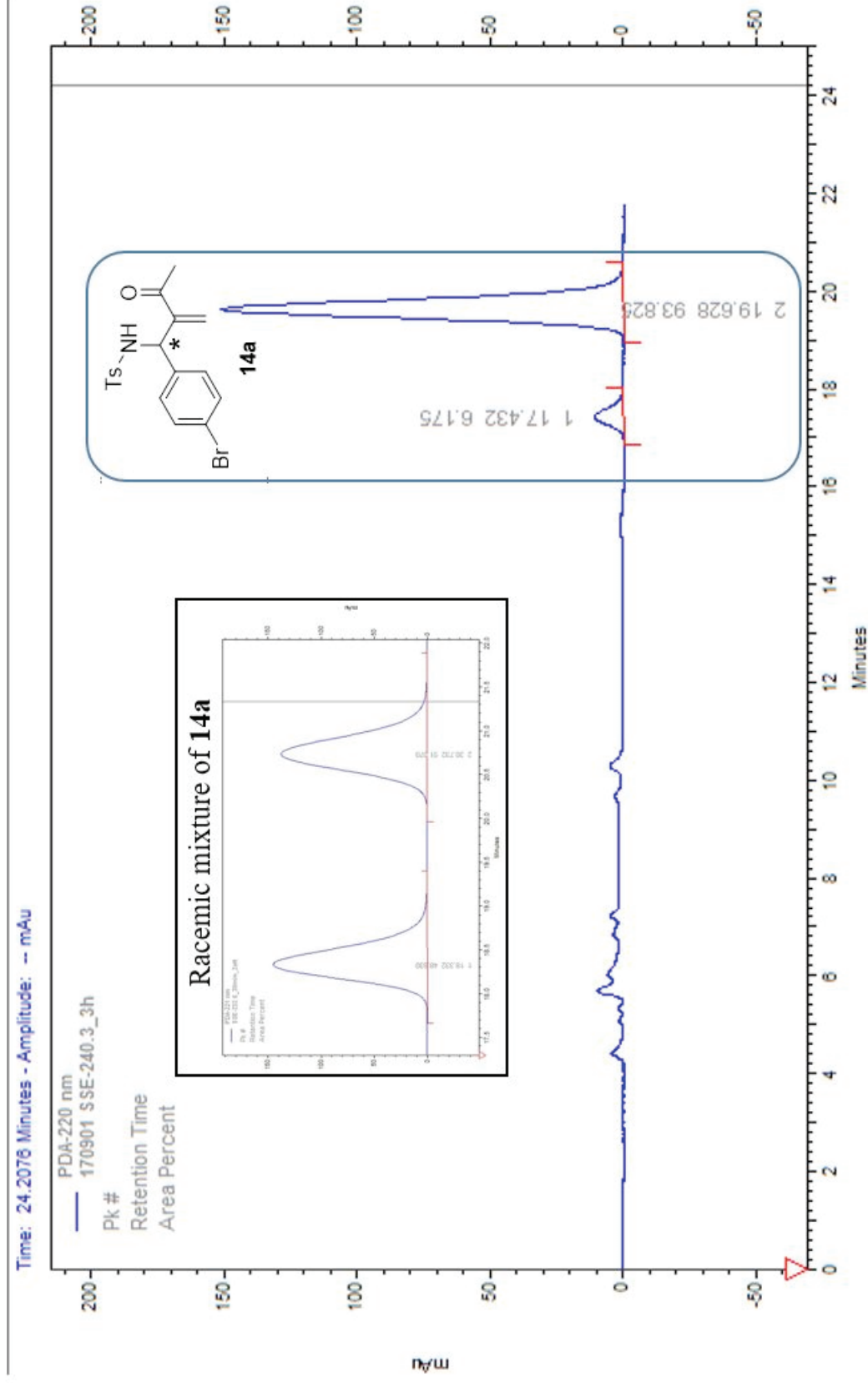


Figure 28. HPLC trace of MBH adduct **14a** and the HPLC trace of the corresponded racemic control in the extension.

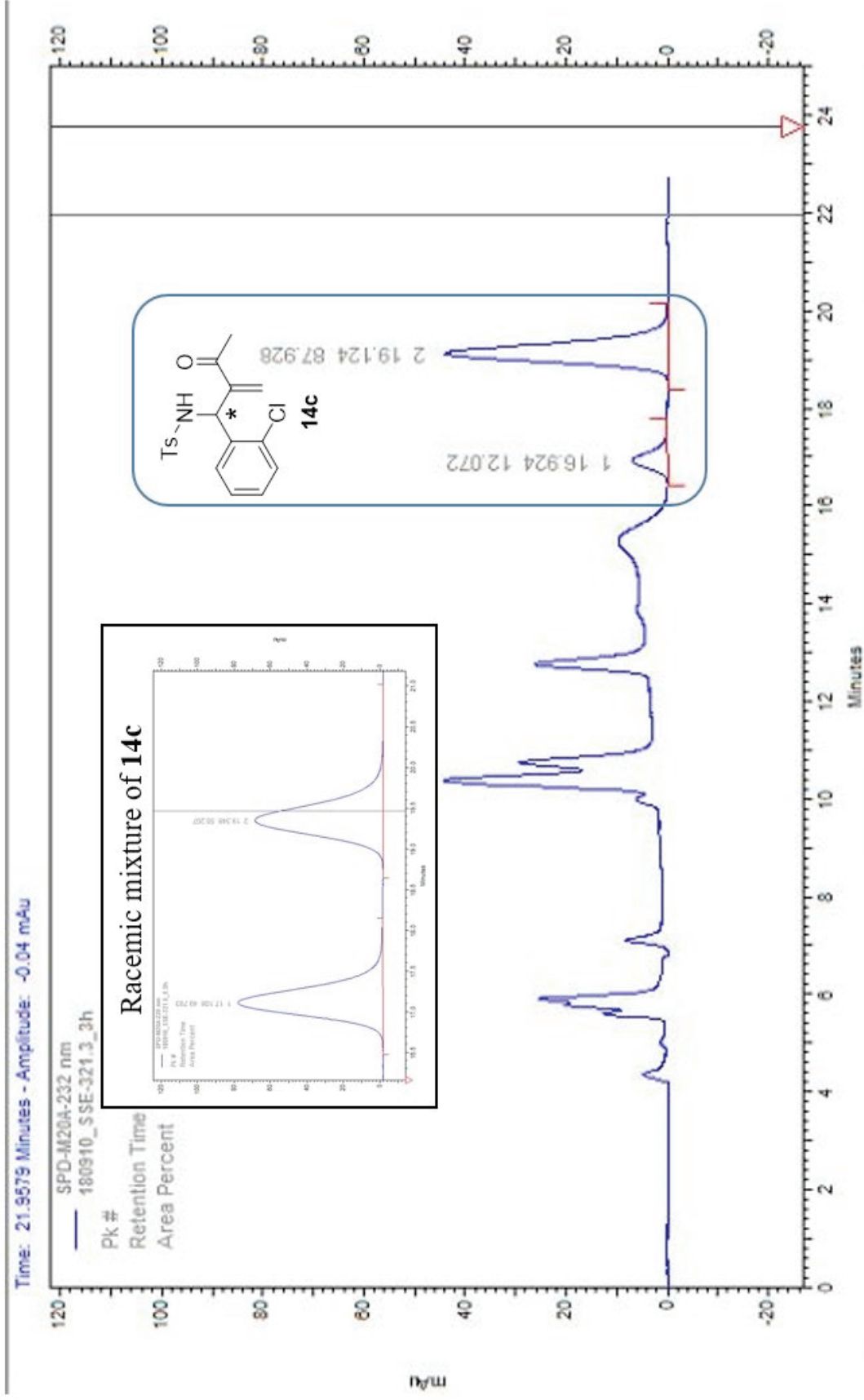


Figure 29. HPLC trace of MBH adduct **14c** and the HPLC trace of the corresponded racemic control in the extension.

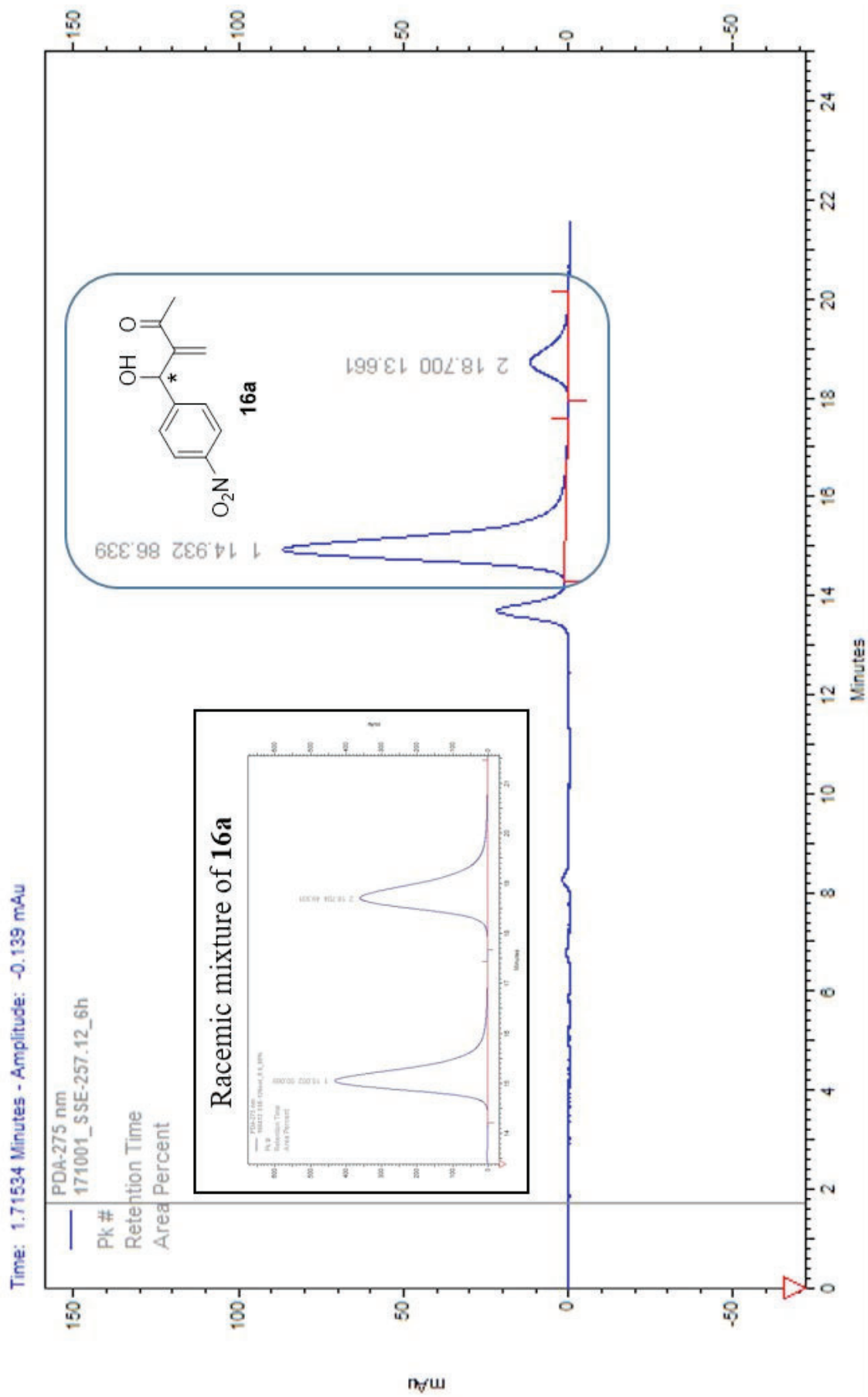


Figure 30. HPLC trace of MBH adduct **16a** and the HPLC trace of the corresponded racemic control in the extension.

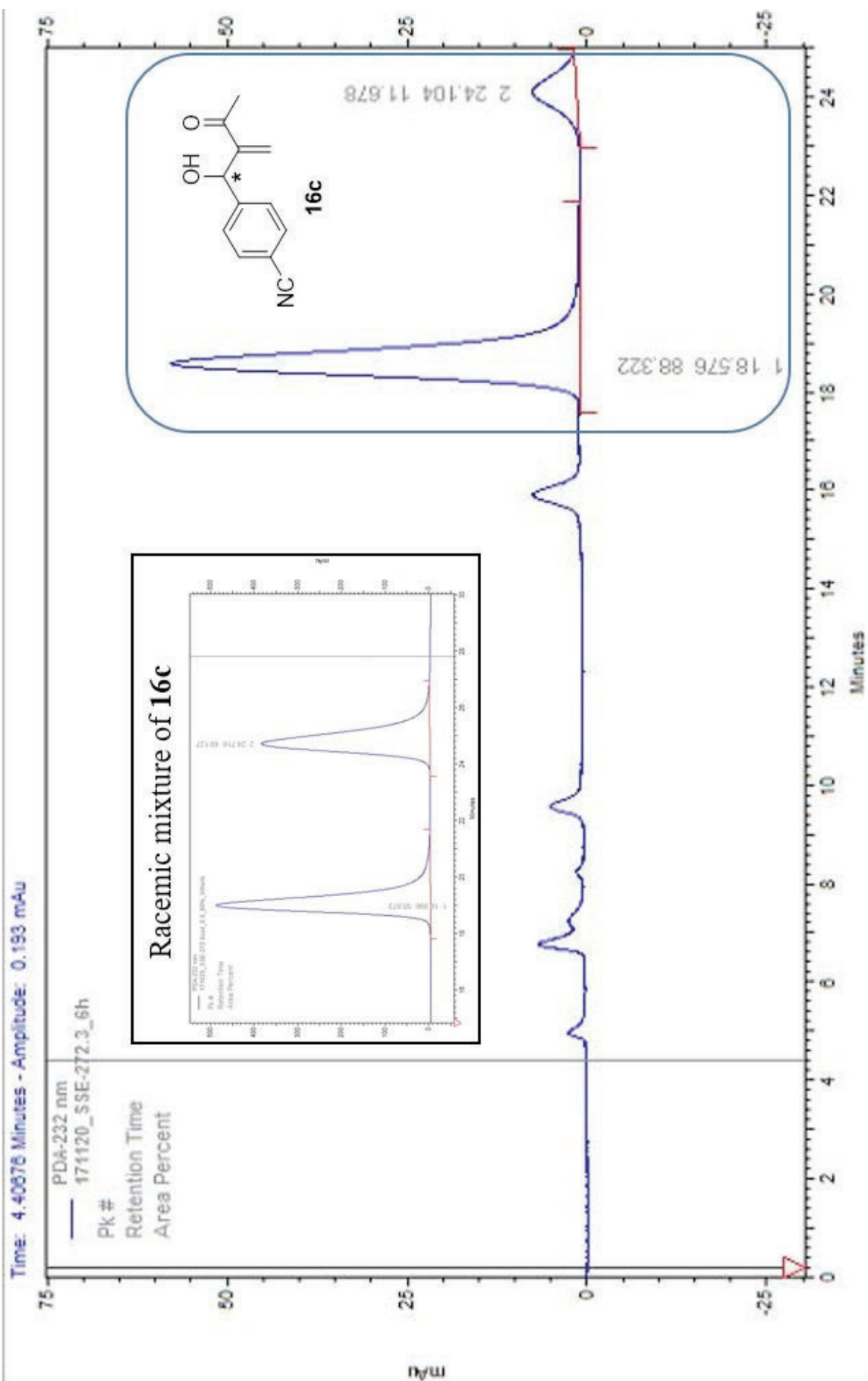
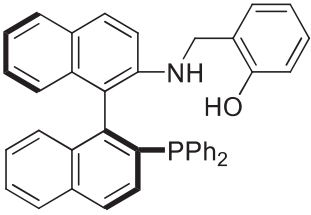
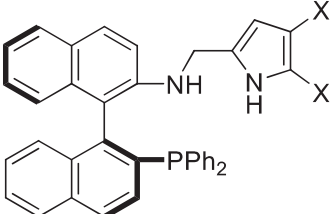
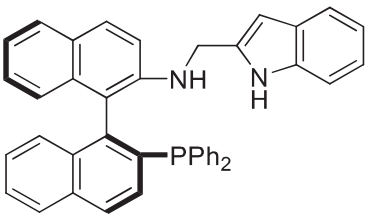
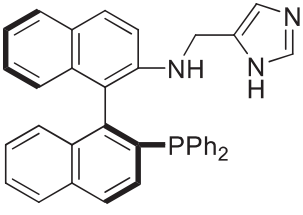
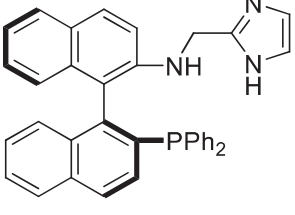
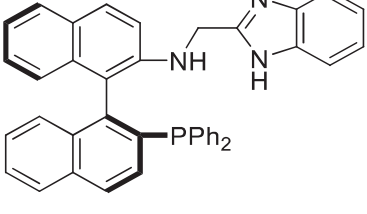
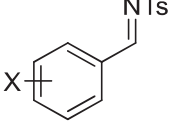


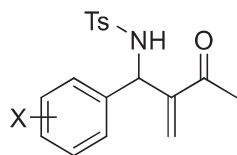
Figure 31. HPLC trace of MBH adduct **16c** and the HPLC trace of the corresponded racemic control in the extension.

#### 4. References

1. Armarego, W. L. F.; Chai, C. L. L., *Purification of Laboratory Chemicals, 6th Edition*. 6 ed.; Butterworth-Heinemann: 2009; p 1-743.
2. Handy, S. T.; Sabatini, J. J., Regioselective Dicyouplings: Application to Differentially Substituted Pyrroles. *Org. Lett.* **2006**, *8* (8), 1537-1539.
3. Anstiss, C.; Karuso, P.; Richardson, M.; Liu, F., Synthesis of New BINAP-Based Aminophosphines and Their <sup>31</sup>P-NMR Spectroscopy. *Molecules* **2013**, *18* (3), 2788.
4. Garnier, J.-M.; Anstiss, C.; Liu, F., Enantioselective Trifunctional Organocatalysts for Rate- Enhanced Aza-Morita-Baylis-Hillman Reactions at Room Temperature. *Adv. Synth. Catal.* **2009**, *351* (3), 331-338.
5. Cheng, L.; Liu, L.; Jia, H.; Wang, D.; Chen, Y.-J., Enantioselective Organocatalytic anti-Mannich-Type Reaction of N- Unprotected 3-Substituted 2-Oxindoles with Aromatic N-Ts-aldimines. *J. Org. Chem.* **2009**, *74* (12), 4650-4653.
6. Cai, H.; Zhou, Y.; Zhang, D.; Xu, J.; Liu, H., A Mannich/cyclization cascade process for the asymmetric synthesis of spirocyclic thioimidazolidoneoxindoles. *Chem. Commun.* **2014**, *50* (94), 14771-14774.

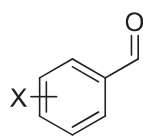
### 2.3 Cross Reference of Compounds in Tetrahedron paper and Thesis

Structure	Number in reference <sup>26</sup>	Number in thesis
	<b>TF-1</b>	<b>1.46a</b>
	<b>1: X = H (a), Br (b)</b>	<b>2.4: X = H (a), Br (b)</b>
	<b>1c</b>	<b>2.4c</b>
	<b>1d</b>	<b>2.4d</b>
	<b>1e</b>	<b>2.4e</b>
	<b>1f</b>	<b>2.4f</b>
	<b>13: X = 4-Br (a), 3-NO<sub>2</sub> (b), 2-Cl (c), 4-Me (d), 2-NO<sub>2</sub> (e), 4-Cl (f), 4-F (g)</b>	<b>1.36: X = 4-Br (b), 3-NO<sub>2</sub> (d), 2-Cl (h), 4-Me (i), 2-NO<sub>2</sub> (e), 4-Cl (g), 4-F (f)</b>



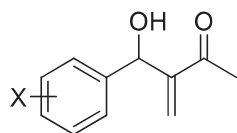
**14:** X = 4-Br (a), 3-NO<sub>2</sub> (b),  
2-Cl (c), 4-Me (d), 2-NO<sub>2</sub> (e),  
4-Cl (f), 4-F (g)

**1.37:** X = 4-Br (b), 3-NO<sub>2</sub>  
(d), 2-Cl (h), 4-Me (i), 2-NO<sub>2</sub>  
(e), 4-Cl (g), 4-F (f)



**15:** X = 4-NO<sub>2</sub> (a), 3-NO<sub>2</sub>  
(b), 4-CN (c), 4-Br (d), 2-  
NO<sub>2</sub> (e), 3-Br (f)

**1.15a:** X = 4-NO<sub>2</sub> (a), 3-NO<sub>2</sub>  
(b), 4-CN (c), 4-Br (d), 2-  
NO<sub>2</sub> (e), 3-Br (f)



**16:** X = 4-NO<sub>2</sub> (a), 3-NO<sub>2</sub>  
(b), 4-CN (c), 4-Br (d), 2-  
NO<sub>2</sub> (e), 3-Br (f)

**2.1:** X = 4-NO<sub>2</sub> (a), 3-NO<sub>2</sub>  
(b), 4-CN (c), 4-Br (d), 2-  
NO<sub>2</sub> (e), 3-Br (f)

---

## 2.4 References

1. R. Kenny and F. Liu, *Chem. Rec.*, 2017, **17**, 535-553.
2. M. C. Gimeno and R. P. Herrera, *Eur. J. Org. Chem.*, 2020, 1057-1068.
3. R. Kenny and F. Liu, *Eur. J. Org. Chem.*, 2015, 5304-5319.
4. F. Zhong, G.-Y. Chen and Y. Lu, *Org. Lett.*, 2011, **13**, 82-85.
5. Y.-L. Liu, B.-L. Wang, J.-J. Cao, L. Chen, Y.-X. Zhang, C. Wang and J. Zhou, *J. Am. Chem. Soc.*, 2010, **132**, 15176-15178.
6. X.-Y. Guan, Y. Wei and M. Shi, *Eur. J. Org. Chem.*, 2010, 4098-4105.
7. X.-Y. Guan, Y. Wei and M. Shi, *Chem. Eur. J.*, 2010, **16**, 13617-13621.
8. N. Abermil, G. Masson and J. Zhu, *Org. Lett.*, 2009, **11**, 4648-4651.
9. M. Shi, M.-J. Qi and X.-G. Liu, *Chem. Commun.*, 2008, 6025-6027.
10. N. Abermil, G. Masson and J. Zhu, *J. Am. Chem. Soc.*, 2008, **130**, 12596-12597.
11. N. Utsumi, H. Zhang, F. Tanaka and C. F. Barbas, *Angew. Chem., Int. Ed.*, 2007, **46**, 1878-1880.
12. A. Nakano, S. Kawahara, S. Akamatsu, K. Morokuma, M. Nakatani, Y. Iwabuchi, K. Takahashi, J. Ishihara and S. Hatakeyama, *Tetrahedron*, 2006, **62**, 381-389.
13. M. Shi, Y.-M. Xu and Y.-L. Shi, *Chem. Eur. J.*, 2005, **11**, 1794-1802.
14. S.-H. Chen, B.-C. Hong, C.-F. Su and S. Sarshar, *Tetrahedron Lett.*, 2005, **46**, 8899-8903.
15. S. Kawahara, A. Nakano, T. Esumi, Y. Iwabuchi and S. Hatakeyama, *Org. Lett.*, 2003, **5**, 3103-3105.
16. D. Balan and H. Adolfsson, *Tetrahedron Lett.*, 2003, **44**, 2521-2524.
17. M. Shi and Y.-M. Xu, *Angew. Chem., Int. Ed.*, 2002, **41**, 4507-4510.
18. M. Shi and J.-K. Jiang, *Tetrahedron: Asymmetry*, 2002, **13**, 1941-1947.
19. Y. Iwabuchi, M. Nakatani, N. Yokoyama and S. Hatakeyama, *J. Am. Chem. Soc.*, 1999, **121**, 10219-10220.
20. M. Shi, Y.-H. Liu and L.-H. Chen, *Chirality*, 2007, **19**, 124-128.
21. Y.-H. Liu, L.-H. Chen and M. Shi, *Adv. Synth. Catal.*, 2006, **348**, 973-979.
22. C. Wang, L. Wang, S. Zeng, S. Xu and Z. He, *Phosphorus, Sulfur Silicon Relat. Elem.*, 2013, **188**, 1548-1554.
23. J.-M. Garnier, C. Anstiss and F. Liu, *Adv. Synth. Catal.*, 2009, **351**, 331-338.
24. J.-M. Garnier and F. Liu, *Org. Biomol. Chem.*, 2009, **7**, 1272-1275.
25. C. Anstiss and F. Liu, *Tetrahedron*, 2010, **66**, 5486-5491.
26. S. S. Eliseenko and F. Liu, *Tetrahedron*, 2019, **75**, 518-526.
27. Y. Wei and M. Shi, in *Comprehensive Enantioselective Organocatalysis*, Wiley-VCH Verlag GmbH & Co. KGaA, 2013, pp. 899-939.
28. H. Sasai and S. Takizawa, in *Comprehensive Chirality*, eds. E. M. Carreira and H. Yamamoto, Elsevier, Amsterdam, 2012, pp. 234-263.
29. T. Oishi, H. Oguri and M. Hiramata, *Tetrahedron: Asymmetry*, 1995, **6**, 1241-1244.
30. G. Masson, C. Housseman and J. Zhu, *Angew. Chem., Int. Ed.*, 2007, **46**, 4614-4628.
31. G. Guillena, D. J. Ramon and M. Yus, in *Catalysis: Volume 24*, The Royal Society of Chemistry, 2012, vol. 24, pp. 223-252.
32. J. Mansilla and J. M. Saá, *Molecules*, 2010, **15**, 709-734.
33. N. Grüger, H. Wadepohl and L. H. Gade, *Dalton Trans.*, 2012, **41**, 14028-14030.
34. A. Gualandi, L. Cerisoli, H. Stoeckli-Evans and D. Savoia, *J. Org. Chem.*, 2011, **76**, 3399-3408.
35. C. A. Caputo and N. D. Jones, *Dalton Trans.*, 2007, 4627-4640.
36. C. Mazet and L. H. Gade, *Chem. Eur. J.*, 2002, **8**, 4308-4318.
37. G. Hirata and H. Maeda, *Org. Lett.*, 2018, **20**, 2853-2856.
38. M. Roucan, M. Kielmann, S. J. Connon, S. S. R. Bernhard and M. O. Senge, *Chem. Commun.*, 2018, **54**, 26-29.

39. J. G. Planas, C. Masalles, R. Sillanpää, R. Kivekäs, F. Teixidor and C. Viñas, *CrystEngComm*, 2006, **8**, 75-83.
40. M. Nishio, Y. Umezawa, K. Honda, S. Tsuboyama and H. Suezawa, *CrystEngComm*, 2009, **11**, 1757-1788.

## **CHAPTER 3**

# **Multifunctional MAP-based Systems as Ligands in Enantiodivergent Catalysis**

## CHAPTER 3. Multifunctional MAP-based Systems as Ligands in Enantiodivergent Catalysis

### 3.1 Introduction

#### 3.1.1 Catalytic dualism: organocatalysts as ligands

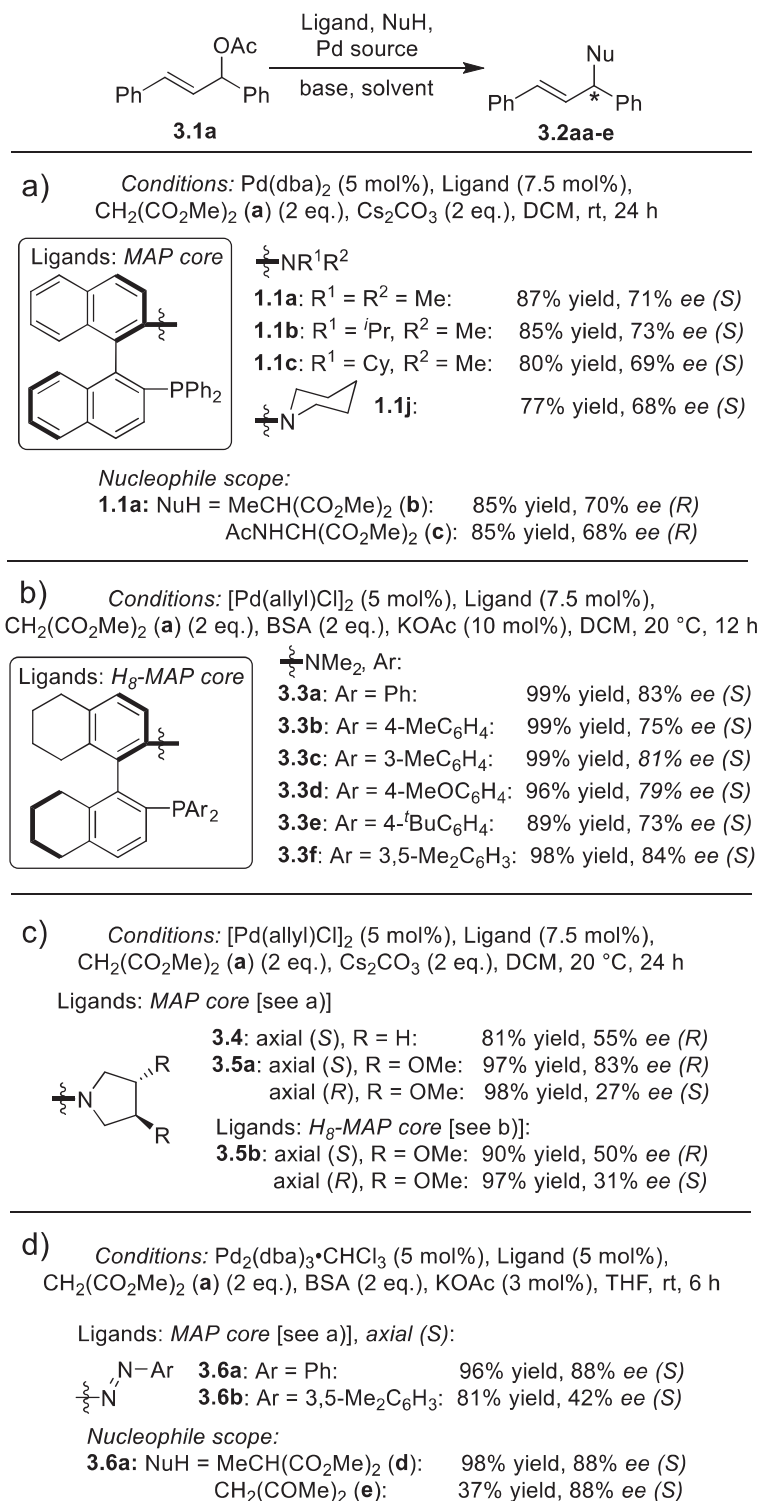
Catalytic dualism where efficient organocatalysts are able to behave as ligands has been discussed in Chapter 1. MAP scaffold, in particular structure **1.17** (Chapter 1, Scheme 2b and Scheme 7a), has already demonstrated the ability to efficiently serve as a ligand and organocatalyst. These examples and a wide application of MAP structures in metal- and organocatalysed processes set the stage for investigating our trifunctional MAP systems in metal-catalysed reactions. The multifunctional nature of the trifunctional system potentially may provide the multidentate, metal-complexation as well as H-bonding catalysis organization. This H-bonding activation, supported by a metal environment, may influence the degree and sense of the asymmetric induction.<sup>1-3</sup>

The coordination of the trifunctional system to metal could occur through the phosphine fragment. Palladium-catalysed asymmetric allylic alkylation (AAA) processes have been thoroughly studied over the last four decades.<sup>4-7</sup> Here, we focus on palladium-catalysed allylic processes as a classical test reaction for multidentate MAP-based ligand investigation.

#### 3.1.2 MAP-based ligands in Pd-catalysed asymmetric allylic substitution

In the seminal report,<sup>8</sup> Kočovský *et al.* demonstrated the ability of palladium complexes from MAP **1.1a** and its derivatives with bulkier *N*-substituents **1.1 b, c, j** to catalyze the allylic substitution of 1,3-diphenylprop-2-en-1-yl acetate **3.1a** with malonate nucleophiles (Scheme 15a) with up to 73% *ee* after 24 h at room temperature. The increased steric congestion around the nitrogen atom of the MAP-based ligands did not improve the enantioselectivity. However,

the application of bulkier malonates as nucleophiles provided the alkylation products **3.2ab,ac** in the opposite configuration (Scheme 15a nucleophile scope). This work was also the first investigation of MAP's "memory effect" in allylic substitution reactions.<sup>8-11</sup>

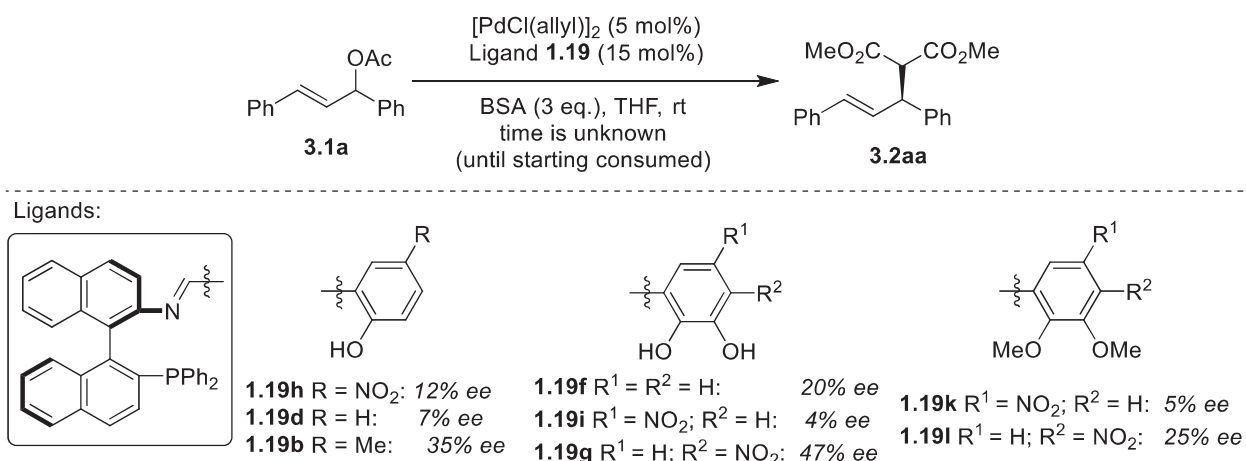


Scheme 15 a) Kocovsky's work; b) and c) Ding's works; d) Kudo's work.

Improvement in Pd-catalysed allylic substitution was made by Ding *et al.* (Scheme 15b) who presented a new type of MAP ligand **3.3** with partially reduced naphthyl rings (H<sub>8</sub>-MAP ligands) and allowed product formation in up to 84% *ee* over 12 h at 20 °C.<sup>12</sup> Later, new MAP-derived ligands **3.4** and **3.5** with additional central chirality were developed (Scheme 15c).<sup>13</sup> The central chirality in **3.5** was found necessary for enantioselective catalysis. Thus, ligand **3.4** without the chirality in the pyrrolidine fragment provided the alkylation product **3.2aa** in only 55% *ee*. At the same time, new ligands **3.5** did not improve MAP-catalysed allylic substitution outcomes and showed comparable selectivities to that of H<sub>8</sub>-MAP **3.3** (up to 83% *ee*) albeit at a lower reaction rate (24 h at 20 °C) (Scheme 15c).

During the same period, Kudo *et al.* reported new arylazo-substituted MAP-based ligands **3.6** (Scheme 15d).<sup>14</sup> New AZOP generation **3.6** enhanced the reaction rate and enantioselectivity of Pd-catalysed allylic substitution, providing product **3.2aa** in up to 88% *ee* over 6 h at room temperature. Interestingly, (*S*)-AZOP provided AAA product **3.2aa** in the *S* configuration that differs from MAP and H<sub>8</sub>-MAP cores that provided the *S* product **3.2aa** from the *R* axial chirality. It was proposed that the *azo*-moiety changed the Pd-coordination pattern from the usual P,C<sub>σ</sub> mode (Chapter 1, Figure 2a) to P,(C<sub>1</sub>-C<sub>2</sub>) η<sup>2</sup>-coordination<sup>15</sup> that is similar to the case of MeO-MOP ligand providing (*S*)-**3.2aa** from the *S* axial chirality.<sup>16</sup> Another key feature of new AZOPs **3.6** was the photoinduced *trans*-to-*cis* isomerization of the *azo*-fragment, however, the photoresponse of catalysis was not observed in a control test.

In conclusion, the chirality transfer of MAP-based structures in AAA can be significantly improved by the ligand's bite angle expansion (H<sub>8</sub>-MAP **3.3**) or by the introduction of additional central chirality. The reversed enantioselectivity can be additionally achieved by the modification of MAP's dimethylamine moiety as it was demonstrated on the AZOP ligands **3.6**. The insertion of additional H-bonding motifs into the MAP core may improve the chirality transfer further via a higher level of the reaction organization.<sup>17-21</sup>



Scheme 16 MAP-based imine ligands **1.19** with phenol moieties in AAA.

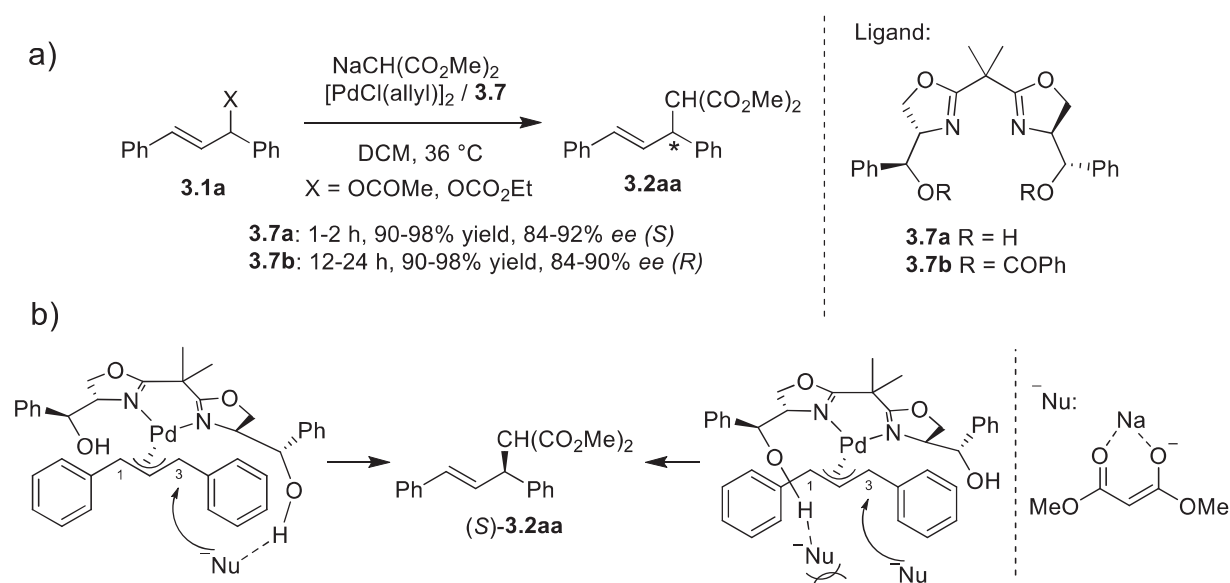
Almost a decade later, imine-based MAP ligands **1.19** bearing phenol fragments were tested in Pd-catalysed allylic substitution reactions (Scheme 16).<sup>22</sup> As shown in Chapter 1, Figure 3, a protic phenolic fragment is not coordinating palladium and may potentially serve as an additional Brønsted acid catalytic motif participating in H-bonding interactions. The reaction enantioselectivity depends on changing phenolic hydroxyl acidities in ligands **1.19h**, **d**, **b** that may indicate the formation of hydrogen bonding interactions important for catalysis. The introduction of an additional hydroxyl group at a  $\beta$ -position to the imine improved the enantioselectivity due to an elongated H-bonding chain. The insertion of a strongly electron-withdrawing nitro group at the *para* position to the  $\alpha$ -hydroxyl position in ligands **1.19i** and **1.19k** turned off the enantioselective pathways completely. However, the shift of the nitro group position from *para* to *meta* in ligand **1.19g** afforded the highest enantioselective outcome. The pivotal role of the hydroxyl protons in ligand **1.19** has been additionally confirmed by a control ligand **1.19k**, **l** with methylated hydroxyls. The *ee* value dropped from 47% for **1.19g** to 25% for the control **1.19l** (Scheme 16). It demonstrated how an appropriate phenolic motif could support the metal catalysis and help with chirality transfer via H-bonding interactions.

### 3.1.3 H-bonding ligands for enantiodivergency in asymmetric allylic substitution

Enantiodivergent catalysis can be performed by H-bonding ligands. The enantioselectivity switch often can be achieved by using different metal sources, ligand properties, additives, loading order, and reaction parameters.<sup>1-3, 23, 24</sup> Ligand-induced enantiodivergency in allylic substitution reactions can be attributed to a ligand's electronic properties,<sup>25, 26</sup> steric hindrances,<sup>27</sup> and ability to form weak interactions with substrates.<sup>28-32</sup> Here we focus on enantiodivergent catalysis, provided by H-bonding interactions between the ligand and substrates in allylic substitution processes.

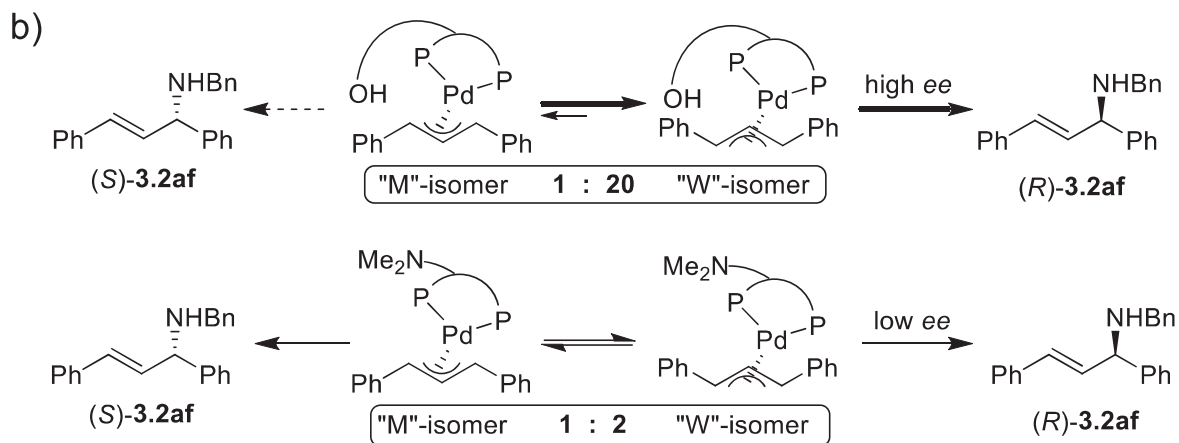
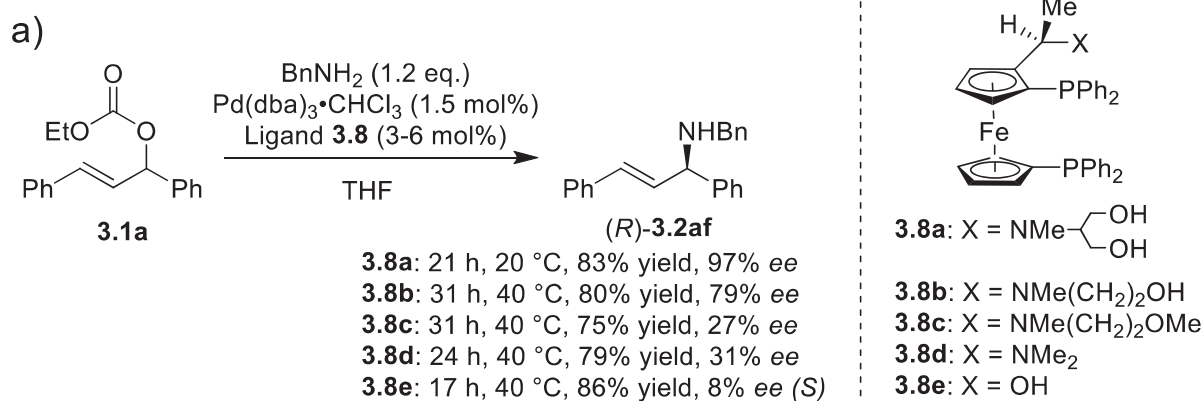
Aït-Haddou *et al.* demonstrated the ability of bis(oxazoline) ligands **3.7** to provide enantiodivergent catalysis in Pd-catalysed asymmetric allylic alkylations (Scheme 17a).<sup>29</sup> Ligand **3.7a**, bearing free hydroxy groups, provided products (*S*)-**3.2aa** in up to 92% *ee* while ligand **3.7b** with protected hydroxyls furnished the product (*R*)-**3.2aa** in up to 90% *ee* under comparable conditions. The ability of hydroxyls to form an H-bond with the tetrafluoroborate counterion was confirmed by X-ray investigations of Pd/**3.7a**-allyl complex.<sup>29</sup> Further investigation showed the presence of both stereogenic centers (in the oxazoline cycles and in the side chains) and free hydroxy groups in ligand structure were found crucial for the enantiodivergent catalysis.<sup>30</sup>

Two hypothetical scenarios were proposed to explain the origin of the enantiodivergency (Scheme 17b). To form (*S*)-**3.2aa**, the attack of the nucleophile needs to occur at the C3 allyl carbon. A hydroxy group proximal to C3 allyl carbon may form a hydrogen bond with the malonate for the C3-attack (Scheme 17b left) or the malonate may bind to the hydroxy group proximal to the C1 allyl carbon and sterically shield the attack of another nucleophile to the C1 carbon (Scheme 17b right).



Scheme 17 a) Enantiodivergency of AAA by bis(oxazole) H-bonding ligand **3.7a**; b) The proposed origin of the enantiodivergency.

Another interesting type of ligand-induced H-bonding stabilization of a palladium-allyl isomer for enantiodivergency was reported by Hayashi *et al.*<sup>28, 32, 33</sup> The ferrocenylphosphine ligands **3.8** with a pendant side chain were able to furnish allylic amination product **3.2af** (Scheme 18a). The characteristics of the hydroxy groups were important for the enantioselective catalysis. Thus **3.8a** containing two hydroxyls provided product (*R*)-**3.2af** in 97% *ee*, while ligand **3.8b** with only one hydroxyl gave (*R*)-**3.2af** in only 79% *ee*. Ligands with protected hydroxyl (**3.8c**) or without the pendant chain (**3.8d**) demonstrated significant erosion in enantioselectivity. The switch of the product **3.2af** in the sense of asymmetric induction occurred in the case of ligand **3.8e**. X-ray investigations and <sup>31</sup>P NMR analysis demonstrated that the remote hydroxyl of **3.8a** would stabilize the “W”-isomer of the allyl-palladium complex, leading to the formation of (*R*)-**3.2af**. Thus, ligand **3.8a** provides a “W” to “M” isomer ratio of 20:1 (Scheme 18b, top), while ligand **3.8d** without the pendant chain gives only 2:1 ratio of “W” and “M” isomers, respectively (Scheme 18b, bottom).

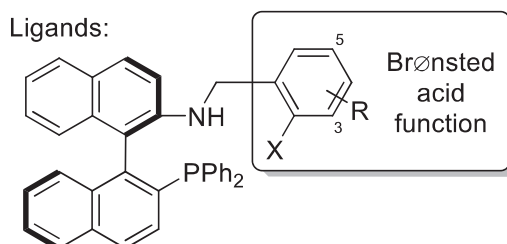
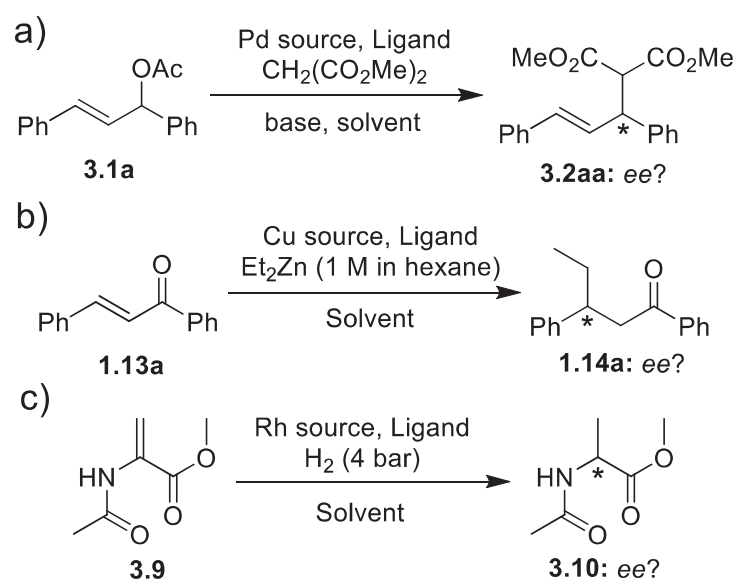


Scheme 18 a) H-bonding ligands **3.8a, b** and control ligands **3.8c–e** in asymmetric allylic amination; b) Stabilization of the “W”-isomer by the remote hydroxy the group.

In conclusion, MAP-based structures were extensively studied and found efficient in palladium-catalysed asymmetric allylic substitution processes. It makes AAA a good candidate for the investigation of dual catalytic properties of our trifunctional MAP-based systems. Moreover, the presence of H-bonding motifs in the ligand structure can improve enantioselectivity and switch the sense of asymmetric induction in AAA.

### 3.1.4 Chapter 3 goals and plan

To test their capability in dual metal/organic catalysis, multidentate MAP-based systems **1.46a,d,h,i** and **1.48a** are studied in palladium-catalysed asymmetric allylic substitution between 1,3-diphenyl-2-propylacrylate **3.1a** and dimethylmalonate (Scheme 19a). In case of successful AAA catalysis, the reaction scope of trifunctional ligands **1.46a,d,h,i** and **1.48a** can also be investigated in Cu-catalysed diethylzinc addition to chalcone **1.13a** (Scheme 19b) and Rh-catalysed hydrogenation of methyl 2-acetamidoacrylate **3.9** (Scheme 19c).



X = OH: R = H (**1.46a**); 5-*t*Bu (**1.46d**); 3-F,5-Br (**1.46h**); 3-*t*Bu,5-Br (**1.46i**)  
 X = NHTs: R = H (**1.48a**)

Scheme 19 Planned a) Pd-catalysed AAA; b) Cu-catalysed diethylzinc addition; c) Rh-catalysed hydrogenation.

## 3.2 Results and Discussion

### 3.2.1 MAP-based structures **1.46a,d,h,i** and **1.48a** in Pd-catalysed allylic substitution

MAP-based structures **1.46a,d,h,i** and **1.48a** were synthesized and tested as multidentate ligands in Pd-catalysed asymmetric allylic alkylation. Catalytic proficiency was dependent on the ligand's Brønsted acid acidity. This may be attributed to the weak, non-covalent H-bonding interactions between the ligand and substrate. The switch of the sense of asymmetric induction from *R* to *S* was achieved by the change of ligand's H-bonding fragment from phenol to tosylamide. Crystals of ligands **1.46a** and **1.48a** complexes to palladium were investigated by X-ray crystallography and demonstrated unusual *P,N*-coordination mode. The detailed discussion of results in terms of chirality switch is provided in the following manuscript submitted to review in Chirality journal.

# Multifunctional chiral aminophosphines for enantiodivergent catalysis in a palladium-catalyzed allylic alkylation reaction

Sviatoslav S. Eliseenko,<sup>[a]</sup> Mohan Bhadbhade,<sup>[b]</sup> and Fei Liu\*<sup>[a]</sup>

**Abstract:** Trifunctional MAP-based chiral phosphines were tested as new ligands in a Pd-catalyzed asymmetric allylic alkylation, demonstrating fast and enantiodivergent catalysis. The palladium complexes of representative ligands by X-ray analysis revealed a novel mode of P, N-coordination of the ligand to the palladium center, which may contribute to switching the sense of the asymmetric induction via combined steric and tunable H-bonding interactions between the metal complex and the substrates.

**Keywords:** Enantiodivergent catalysis, Catalytic dualism, H-bonding ligands.

## 1. Introduction

Chiral compounds are essential in chemical research, and asymmetric catalysis remains the main avenue for efficiently accessing chiral compounds. While a high performing chiral catalyst can readily enable reaction conversion with the preferred sense of asymmetric induction, a more versatile goal is to achieve enantiodivergent or stereodivergent asymmetric catalysis in which the sense of asymmetric induction can be switched to access either enantiomeric product without changing the catalyst's initial chirality.<sup>1</sup> This atom economic mode of asymmetric catalysis, however, is also very challenging in reaction design in both metal-catalyzed and organocatalyzed processes. Interestingly, given that the combination of metal catalysis and organocatalysis is a rapidly developing field,<sup>2-4</sup> in which an organocatalyst can serve as either a catalyst or a ligand, exploring enantiodivergent catalysis in this hybrid mode of catalysis may present new opportunities in finding cooperative catalytic modes. Here we report an enantiodivergent catalysis in a Pd-catalyzed asymmetric allylic alkylation reaction, induced by a multifunctional chiral phosphine ligand. The novel chelation mode of Pd to the P, N ligand, as shown by X-ray analysis, suggested potential cooperativity in substrate activation and direction, from tuning hydrogen-bonding interactions within the multifunctional ligand coordinated to the palladium center, for switching the sense of the asymmetric induction in the reaction even when the chirality of the ligand remained unchanged.

In combined metal/organo-catalysis, the dominant concepts include the cooperative mode (both types of catalysts participate in the same catalytic cycle), the synergistic mode (distinct metal- and organocatalytic cycles in cooperation), and the sequential or relay mode (two detached catalytic cycles are performed in a consecutive manner through the formation of an intermediate).<sup>3</sup> The use of one chiral structure as a ligand and a catalyst may improve both catalytic compatibility and cooperativity in the cooperative mode. Despite the simplicity of the idea, an efficient combination of organocatalytic and metal-ligating properties in a structure (catalytic dualism) is challenging with only limited examples known from carbene-,<sup>5,6</sup> urea-,<sup>7</sup> pyrrolidine-containing structures,<sup>8</sup> *N,N'*-dioxides,<sup>9</sup> aminophosphines,<sup>10-20</sup> and 1,4-hydroxyarylalcohols (also known as HAROLs).<sup>21</sup> Therefore, one current challenge is to design catalytic roles with a more complex organization in the reaction environment to enable not

just efficient asymmetric catalysis but also dynamic properties such as catalytic dualism and chiral induction switching.

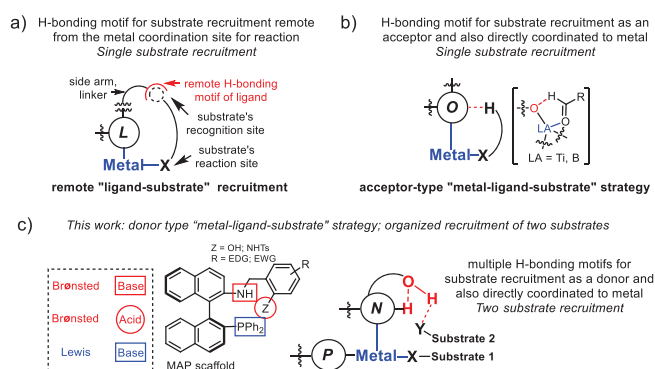


FIGURE 1 a–b) Types of known H-bonding ligands in metal-catalyzed reactions; c) Proposed catalytic dualism by the MAP-based trifunctional system in H-bonding assisted metal-catalysis with more organization.

Ligands with H-bonding properties are excellent candidates for designing more organized catalysis, and existing H-bonding ligands may be broadly classified into two different approaches of substrate recruitment. The first "ligand–substrate" approach is provided by ligands with metal-binding fragment and an H-bonding moiety, located in a remote position away from the metal center (Figure 1a). This strategy allows the binding of a specific substrate by a certain H-bonding moiety of the ligand

[a] Department of Molecular Sciences,  
Macquarie University  
Sydney, Australia  
E-mail: fei.liu@mq.edu.au  
<https://feiliu0.wixsite.com/lrg-site>

[b] Solid State & Elemental Analysis Unit,  
Mark Wainwright Analytical Centre, Division of Research,  
The University of New South Wales  
Sydney, Australia

through a set of weak interactions in order to orient the substrate's reactive site to the coordinated metal center selectively. This approach was successfully applied in a series of highly enantioselective processes (mostly >95% ee) such as Pd-catalyzed allylic substitution<sup>22,23</sup> (including enantiodivergent examples),<sup>24-28</sup> Mn-sulfoxidation,<sup>29</sup> Ru-epoxidation,<sup>30</sup> Pd-arylation and vinylation,<sup>31,32</sup> and Rh-hydrogenation.<sup>33-37</sup>

The second acceptor type "metal–ligand–substrate" strategy is provided by a ligand where its metal-binding fragment also serves as an H-bonding acceptor in close proximity to the metal coordination site. This strategy allows the formation of a planar pseudo cycle (Figure 1b) and is mostly applied in aldehyde recruitment.<sup>38-40</sup> The coordination of the aldehyde oxygen to boron or titanium enhances the electron density on the ligand's oxygen atom attached to the Lewis acid. It makes the oxygen atom more susceptible to form the H-bond with the formyl hydrogen where the positive charge is increased due to the coordination. The five-membered cycle formed keeps the aldehyde in a specific position that favours enantioselective outcomes in allylation, aldol, Diels-Alder, hydrocyanation, and ene-reactions.<sup>38-40</sup>

In this work, a new type of "metal–ligand–substrate" donor-type ligands is investigated (Figure 1c). These ligands are multifunctional chiral phosphines, studied as trifunctional organocatalysts in our previous work<sup>41-48</sup> that have demonstrated proficient catalysis in Morita–Baylis–Hillman model reactions. Our trifunctional system, which combines catalytic motifs such as phosphine Lewis base, amine Brønsted base, and phenol or sulfonamide Brønsted acid, can now be tested for its ability to provide potential metal-coordination sites and H-bonding interactions concurrently for dual activation in a model Pd-catalyzed allylic alkylation. The multifunctional chiral phosphine may act as a ligand to the metal and also organize H-bonding interactions for synergistic substrate direction.

We used the well-established Pd-catalyzed asymmetric allylic alkylation (AAA) to test the applicability of our multifunctional chiral phosphines as ligands as well as H-bonding activators, with the phosphine center as the expected metal coordination site.<sup>24-28</sup> We found that trifunctional MAP-based ligands provide unusual P, N-coordination sites for the palladium center. The tuning of the trifunctional ligand's Brønsted acid motif resulted in responses from both the enantioselectivity and reaction rate. Further alteration of the Brønsted acid type allowed switching of the sense of the asymmetry induction and demonstrated the ability of the trifunctional MAP system to provide enantiodivergent catalysis.

## 2. Materials and Methods

**2.1. General information:** All reagents unless specified are commercially available and purified by standard procedures.<sup>49</sup> Deuterated solvents were purchased from Cambridge Isotope Laboratories, USA. Potassium carbonate, potassium acetate, and BSA were used in a glovebox under nitrogen atmosphere. Air and moisture sensitive reactions were performed under nitrogen or argon atmosphere. Flash column chromatography was performed on Merck silica gel 60 (0.015–0.040 mm). <sup>1</sup>H, <sup>13</sup>C, and <sup>31</sup>P experiments were performed at 298 K on a Bruker DPX 400 MHz spectrometer equipped with a 5mm QNP probe. Chemical shifts were reported in ppm using the residual CHCl<sub>3</sub> ( $\delta_{\text{H}} = 7.26$  ppm,  $\delta_{\text{C}} = 77.16$  ppm) or CH<sub>2</sub>Cl<sub>2</sub> ( $\delta_{\text{H}} = 5.32$  ppm,  $\delta_{\text{C}} =$

53.8 ppm) peaks as an internal reference. All <sup>31</sup>P NMR spectroscopy was performed on a Bruker DPX 400 MHz spectrometer at 298 K, and all spectra were referenced to external H<sub>3</sub>PO<sub>4</sub> (0 ppm). All spectra were processed using Bruker TOPSPIN software versions 4.0.7. High resolution mass analysis was provided by the Australian Proteome Analysis Facility (APAF), Macquarie University, Sydney, Australia. HPLC analysis was performed using a Shimadzu Prominence system with CHIRALPAK® AD–H column. HPLC grade solvents were degassed before use. The X-ray diffraction measurements were carried out on a Bruker D8 Quest Single Crystal diffractometer with Photon II detector at 150 K by using  $\mu\text{S}$  3.0 Microfocus Source with Mo-K $\alpha$  radiation ( $\lambda = 0.710723$  Å). Starting acetate **6** was synthesized by a known procedure.<sup>50</sup>

## 2.2. Experimental Details

**General procedure for Pd-catalyzed asymmetric allylic alkylation (diethylzinc conditions):** Ligand (3.0  $\mu\text{mol}$ ) and palladium(II) dichloride diprop-2-en-1-ide (0.73 mg, 2.0  $\mu\text{mol}$ ) were placed in a 2-mL amber, oven-dried vial ("Catalyst" vial) as stock solutions in freshly distilled dioxane. The volume of dioxane was adjusted to 150  $\mu\text{L}$  and the mixture left to stir for 40 min at room temperature. Acetate **8** (10 mg, 40  $\mu\text{mol}$ ) was then added into the vial as a solution in dioxane and the mixture left to stir for 10 min more at room temperature. Dimethyl malonate (9.1  $\mu\text{L}$ , 80  $\mu\text{mol}$ ) was placed in a separate 2-mL amber, oven-dried vial ("Nucleophile" vial), diluted with 100  $\mu\text{L}$  of dioxane, and cooled down in an ice bath. Then diethylzinc (9.8 mg, 80  $\mu\text{mol}$ ) as 1 M solution in hexanes was slowly added into the "Nucleophile" vial with stirring and the volume of dioxane was adjusted to 600  $\mu\text{L}$ . Then the cold mixture from the "Nucleophile" vial was transferred slowly into the "Catalyst" vial. The "Nucleophile" vial was rinsed with 100  $\mu\text{L}$  of dioxane twice, and the resulting solution was added to the "Catalyst" vial. The mixture (final volume ~1 mL) was left to stir at room temperature for 48 h. Then the reaction mixture was diluted with ethyl acetate and quenched with a saturated ammonium chloride solution. The aqueous layer was extracted with ethyl acetate twice, and the combined organic layer was washed with brine, dried over sodium sulfate, and concentrated by nitrogen flow to yield dimethyl-2-(1,3-diphenylallyl)malonate **9** and reduction product **10**.

**General procedure for Pd-catalyzed asymmetric allylic alkylation (BSA conditions):** Ligand (3.0  $\mu\text{mol}$ ) and palladium(II) dichloride diprop-2-en-1-ide (0.73 mg, 2.0  $\mu\text{mol}$ ) were placed in a 2-mL amber, oven-dried vial ("Catalyst" vial) as stock solutions in freshly distilled dichloromethane. The volume of dichloromethane was adjusted to 100  $\mu\text{L}$  and the mixture left to stir at room temperature for 1 h. Potassium carbonate (0.41 mg, 3.0  $\mu\text{mol}$ ) was placed in a separate 2-mL amber, oven-dried vial ("Nucleophile" vial) in a glovebox under nitrogen atmosphere following by the addition of 100  $\mu\text{L}$  of dichloromethane, BSA (29  $\mu\text{L}$ , 119  $\mu\text{mol}$ ), and dimethyl malonate (14  $\mu\text{L}$ , 119  $\mu\text{mol}$ ). The volume was adjusted to 250  $\mu\text{L}$  and the mixture left to stir at room temperature for 1 h. Acetate **8** (10 mg, 40  $\mu\text{mol}$ ) was added into the "Catalyst" vial as a solution in dichloromethane and the mixture left to stir for 0.5 h more at room temperature. Then the mixture from the "Catalyst" vial was transferred slowly into the "Nucleophile" vial. The "Catalyst" vial was rinsed with 100  $\mu\text{L}$  of dichloromethane twice, and the resulting solution was added to the "Nucleophile" vial and the mixture (final volume 500  $\mu\text{L}$ ) left to stir at room temperature for an indicated time. During the reaction time, 30  $\mu\text{L}$  aliquots were taken at 0.5, 1.5, 3, and 6

h for the conversion and enantioselectivity analysis. Then the reaction mixture was dissolved in ethyl acetate and treated with saturated ammonia chloride solution. The aqueous layer was extracted with ethyl acetate twice, and the combined organic layer was washed with brine, dried over magnesium sulfate, filtered, and concentrated by nitrogen flow to yield dimethyl-2-(1,3-diphenylallyl)malonate **9**. A pure product sample for characterization was obtained by purification of the crude mixture on a silica gel pipette column (gradient hexanes/ethyl acetate).

**Ligand 6:** Aminophosphine **7** (49 mg, 0.11 mmol) was placed into a dry 4-mL amber HPLC vial with septa in glovebox under nitrogen atmosphere and dissolved in 0.3 mL of freshly distilled 1,2-dichloroethane under argon environment. Neat distilled *p*-methoxy benzaldehyde (29 mg, 0.22 mmol) and acetic acid (16 mg, 0.27 mmol) were added and the mixture left to stir at room temperature for 3.5 h then cooled down by ice bath, and sodium triacetoxyborohydride (85 mg, 0.40 mmol) was added in one portion. The mixture left to stir at room temperature for another 40 minutes then cooled down by ice bath and sodium tetrahydroborate (33 mg, 0.86 mmol) was added in one portion. The mixture left to stir at room temperature for 25 minutes then cooled down by ice bath and 1 mL MilliQ water was added slowly. The mixture was transferred to a separating funnel and extracted with DCM three times. The combined organic layer was treated with brine, dried over magnesium sulfate and concentrated by nitrogen flow. The crude mixture was purified by column chromatography (gradient hexanes / ethyl acetate) yielding product **6** in 25 mg (41% yield). <sup>1</sup>H NMR (400 MHz, CDCl<sub>3</sub>) δ 3.64 (br. s., 1H), 3.74 (s, 3H), 3.96 (dd, *J* = 4.3, 15.3 Hz, 1H), 4.07–4.18 (m, 1H), 6.60 (d, *J* = 8.5 Hz, 1H), 6.70 (d, *J* = 8.7 Hz, 2H), 6.89–6.95 (m, 1H), 6.98 (d, *J* = 8.6 Hz, 2H), 7.02–7.11 (m, 4H), 7.12–7.38 (m, 10H), 7.44–7.55 (m, 2H), 7.71 (d, *J* = 8.0 Hz, 1H), 7.82 (d, *J* = 8.6 Hz, 1H), 7.88 (d, *J* = 8.5 Hz, 1H), 7.89 (d, *J* = 8.1 Hz, 1H); <sup>13</sup>C NMR (100 MHz, CDCl<sub>3</sub>) δ 47.27, 55.35, 113.73, 113.90, 116.16 (d), 121.62, 124.23, 126.17, 126.66 (d), 126.91, 127.13, 127.26, 127.92, 128.09, 128.20, 128.26, 128.33, 128.49, 128.55, 129.64, 130.87 (d), 131.85, 133.08 (d), 133.53, 133.59, 133.73, 133.79, 134.21 (d), 134.36, 137.61, 137.74 (d), 138.16, 138.30, 141.76, 142.11, 143.85 (d), 158.61; <sup>31</sup>P NMR (162 MHz, CDCl<sub>3</sub>) δ -14.21; IR (ATR, cm<sup>-1</sup>) ν 3426, 3050, 2927, 1742, 1616, 1597, 1510, 1430, 1339, 1299, 1244, 1172, 1151, 1093, 1027, 953, 915, 808, 773, 739, 695, 628; HRMS (ESI, *m/z*): [*M* + *H*]<sup>+</sup>, calcd. for C<sub>40</sub>H<sub>33</sub>NOP 574.22997; found, 574.22914; [α]<sub>D</sub><sup>20</sup> = +33.81° (c 1.0, CHCl<sub>3</sub>).

**Complex Pd/1:** To a solution of ligand **1** (31.8 mg, 56.82 μmol) in 0.57 mL of degassed dry dichloromethane was added bis(benzonitrile)palladium(II) chloride (21.79 mg, 56.82 μmol) over argon. The reaction was stirred for 5 minutes at room temperature in an inert atmosphere providing a suspension. The precipitate was filtered out and washed with dichloromethane, providing 17 mg (41% yield) of the desired product as a yellow solid. The precipitate was dissolved in 0.9 mL of degassed dichloromethane and filtered through KimVap into a 2 mL clear HPLC vial. Then 0.3 mL of degassed hexane was added to the solution through a KimVap filter. The resulting solution was shaken to mix the solvent layers and left in a fridge for slow evaporation. After 6 days, yellow crystals of compound **Pd/1** were formed. <sup>1</sup>H NMR (400 MHz, CD<sub>2</sub>Cl<sub>2</sub>, δ) 3.92 (br.s, 1H), 4.66 (dd, *J* = 14.5, 2.9 Hz, 1H), 4.82 (dd, *J* = 14.5, 9.9 Hz, 1H), 5.71 (d, *J* = 8.0 Hz, 1H), 6.22 (d, *J* = 8.4 Hz, 1H), 6.24 (br.s, 1H), 6.28 (d, *J* = 8.6 Hz, 1H); 6.54 (td, *J* = 7.5, 0.9 Hz, 1H), 6.74–6.89 (m, 6H), 6.94–7.00 (m, 1H), 7.13–7.19 (m, 1H), 7.25 (t, *J* = 8.5 Hz, 1H), 7.48–7.64 (m, 8H), 7.96–8.04 (m, 3H), 8.20 (d, *J* = 9.0 Hz,

1H); <sup>13</sup>C NMR (100 MHz, CD<sub>2</sub>Cl<sub>2</sub>, δ) 54.03, 115.47, 120.47, 121.09, 121.24, 123.89, 124.36, 124.95, 125.34, 125.80, 126.43, 126.50, 126.92, 128.02, 128.24, 128.29, 128.41, 128.51, 128.60, 128.71, 128.78, 128.85, 128.88, 128.95, 130.03, 130.28, 130.35, 131.35, 131.65, 131.72, 131.80, 131.93, 132.02, 134.00, 134.79, 135.58, 138.92, 139.86, 153.42; <sup>31</sup>P NMR (162 MHz, CD<sub>2</sub>Cl<sub>2</sub>, δ) 24.97; IR (ATR, cm<sup>-1</sup>) ν 3222, 3054, 2918, 1595, 1502, 1456, 1436, 1337, 1261, 1227, 1184, 1099, 1028, 995, 894, 869, 817, 746, 688, 628; UV (λ<sub>max</sub>, nm [ε, M<sup>-1</sup>cm<sup>-1</sup>]): 278 [21534], 292 [18022], 320 [9231], 350 [4423]; HRMS (ESI, *m/z*): [*M* - Cl]<sup>+</sup> calcd. for C<sub>39</sub>H<sub>30</sub>ClNOPd 700.07828; found, 700.07848; [α]<sub>D</sub><sup>25</sup> = -461.93° (c 0.4, CH<sub>2</sub>Cl<sub>2</sub>).

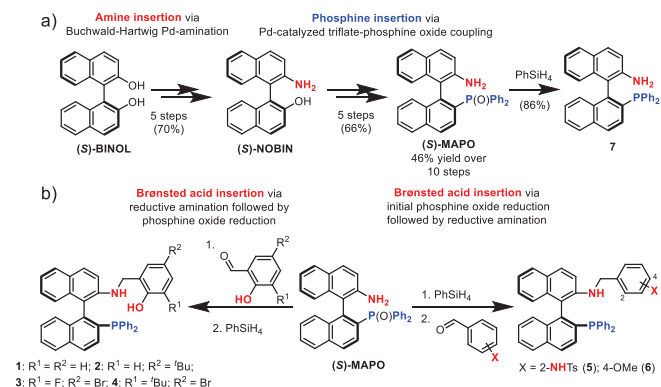
**Complex Pd/5:** To a solution of ligand **5** (37.5 mg, 526 μL, 52.6 μmol) in 0.53 mL of degassed dry dichloromethane was added bis(benzonitrile)palladium(II) chloride (20.18 mg, 52.6 μmol) over argon. The reaction was stirred for 5 minutes at room temperature in an inert atmosphere and then filtered through KimVap and washed with dichloromethane. Degassed hexane was added to the solution to form a double-layer mixture that left to stay overnight. Next morning, the clusters of yellow solid formed on the bottom of the vial. The clusters were filtered out, providing 31.4 mg (67% yield) of the desired product. The aliquot of solid was dissolved in 0.9 mL of degassed dichloromethane and filtered through KimVap into a 2 mL clear HPLC vial. Then 0.3 mL of degassed hexane was added to the solution through KimVap filter. The resulted solution was shaken to mix the solvent layers and left in a fridge for slow evaporation. After 3 days, yellow crystals of compound **Pd/5** were formed. <sup>1</sup>H NMR (500 MHz, CDCl<sub>3</sub>, δ) 2.34 (s, 3H), 5.01 (dd, *J* = 14.5, 10.0 Hz, 1H), 5.11 (dd, *J* = 14.5, 2.0 Hz, 1H), 5.93 (d, *J* = 7.7 Hz, 1H), 6.02 (d, *J* = 8.4 Hz, 1H), 6.51 (s, 1H), 6.55–6.63 (m, 3H), 6.70–6.85 (m, 8H), 6.95–7.02 (m, 3H), 7.14–7.20 (m, 1H), 7.25–7.31 (m, 1H), 7.44–7.61 (m, 7H), 7.67 (d, *J* = 8.1 Hz, 1H), 7.83 (d, *J* = 8.8 Hz, 1H), 7.89 (d, *J* = 7.8 Hz, 1H), 8.08 (d, *J* = 9.0 Hz, 1H), 8.46 (d, *J* = 9.0 Hz, 1H); <sup>13</sup>C NMR (100 MHz, CDCl<sub>3</sub>, δ) 21.73, 52.16, 118.92, 118.88, 121.34, 124.14, 125.39, 125.95, 126.33, 126.66, 127.10, 127.65, 127.98, 128.07, 128.10, 128.31, 128.53, 128.81, 129.22, 129.41, 129.55, 129.64, 130.84, 130.86, 131.18, 131.64, 131.77, 131.89, 131.90, 133.14, 133.22, 134.63, 134.65, 134.67, 134.83, 135.34, 135.54, 135.66, 138.59, 139.85, 143.49; <sup>31</sup>P NMR (162 MHz, CDCl<sub>3</sub>, δ) 23.56; IR (ATR, cm<sup>-1</sup>) ν 3055, 2956, 2918, 2850, 1717, 1596, 1455, 1437, 1377, 1329, 1260, 1184, 1158, 1093, 1021, 892, 868, 812, 744, 687; UV (λ<sub>max</sub>, nm [ε, M<sup>-1</sup>cm<sup>-1</sup>]): 294 (15346), 319 (7355); HRMS (ESI, *m/z*): [*M* - Cl]<sup>+</sup> calcd. for C<sub>46</sub>H<sub>37</sub>ClN<sub>2</sub>O<sub>2</sub>PPdS 853.10312; found, 853.10308; [α]<sub>D</sub><sup>25</sup> = -137.3° (c 0.5, CH<sub>2</sub>Cl<sub>2</sub>).

### 3. Results and Discussion

#### 3.1 Synthesis of ligands.

A set of trifunctional ligands **1–6** was synthesized by reported earlier procedures<sup>45,47,48</sup> and tested in palladium-catalyzed AAA. The late-stage precursor (S)-MAPO was synthesized from commercially available (S)-BINOL via Buchwald-Hartwig amination (amine insertion) and triflate–phosphine oxide coupling (phosphine insertion) in 46% yield over 10 steps (Scheme 1a). The final multidentate ligands **1–6** can be further obtained from (S)-MAPO in 2 steps via phosphine oxide reduction and reductive amination of a corresponding aromatic aldehyde (Brønsted acid insertion) (Scheme 1b). The different acidities of H-bonding motifs in ligands **1–4** may influence enantioselectivity of the reaction as observed earlier for

organocatalysis.<sup>45,47</sup> Ligands **2** and **4** bearing bulky *tert*-butyl groups in different positions were tested for assessing the potential steric requirements on the reaction outcome. Ligand **5** has a tosylamide Brønsted acid motif that significantly differs from the phenolic moiety in ligands **1–4** and may alter the level and sense of the asymmetric induction. The ligand **6** does not have an H-bonding fragment and was synthesized as a control ligand.



SCHEME 1 Synthesis of ligands **1–6**.

### 3.2. Palladium complexation: novel “metal–ligand–substrate” donor-type P, N-mode.

In the seminal investigations of palladium coordination on 2-dimethylamino-2'-diphenylphosphino-1,1'-binaphthyl (MAP) ligand, Kocovsky<sup>51</sup> and Ding<sup>52</sup> described the predominant formation of P, C<sub>σ</sub>-complexes (Figure 2a). The further partial reduction of ligand's binaphthyl core<sup>52</sup> or the change of the amino group to imine fragment<sup>53</sup> allowed the formation of P, N-coordination to the palladium center, consistent with the expectation for a more basic nitrogen donor (Figure 2b). Furthermore, a recent study confirmed again that unreduced binaphthyl-containing aminophosphines tend to form the Pd complex in the P, C<sub>σ</sub>-coordination mode.<sup>54</sup>

The structure of palladium complexes of multifunctional ligands **1** and **5** was investigated by X-Ray crystallography (Figure 2c). The complexes Pd/**1** and Pd/**5** were synthesized by equimolar addition of bis(benzonitrile)palladium(II) chloride to a corresponding ligand in dichloromethane at room temperature. The X-ray investigation showed a P, N-coordination pattern of palladium in Pd/**1** and Pd/**5** that is novel for unreduced binaphthyl-containing aminophosphines. The crystal structures have also revealed the ability of ligands **1** and **5** to form hydrogen bond networks. Ligand **1** provides the hydrogen bond using the phenolic oxygen and the hydrogen of the *exo*-amino group that is ligated to the metal. Ligand **5** forms a different type of hydrogen bonding. The sulfonamide group (a different Brønsted acid compared to the phenol in Pd/**1**) in Pd/**5** demonstrated H-bonding interaction between one of the sulfonyl oxygen atoms and again the *exo*-amino group that is ligated to palladium. In both cases, the nitrogen coordinated to the palladium center is shown to be involved in H-bonding network, suggesting that the H-bonding interactions from the ligand may influence the ligand-metal coordination interactions. This novel complex type, in which the palladium coordination site is also part of an H-bonding network through a ligating protic motif, can provide a new donor-type “metal–ligand–substrate” strategy for

potentially cooperative catalysis (Figure 1c). Both complexes Pd/**1** and Pd/**5** also showed the ability to form halogen bond networks between two dichloromethane molecules and aromatic hydrogens (H8A, H19B for Pd/**1** and H8A for Pd/**5**) through chlorine atoms of the complexes (Figure 2c).

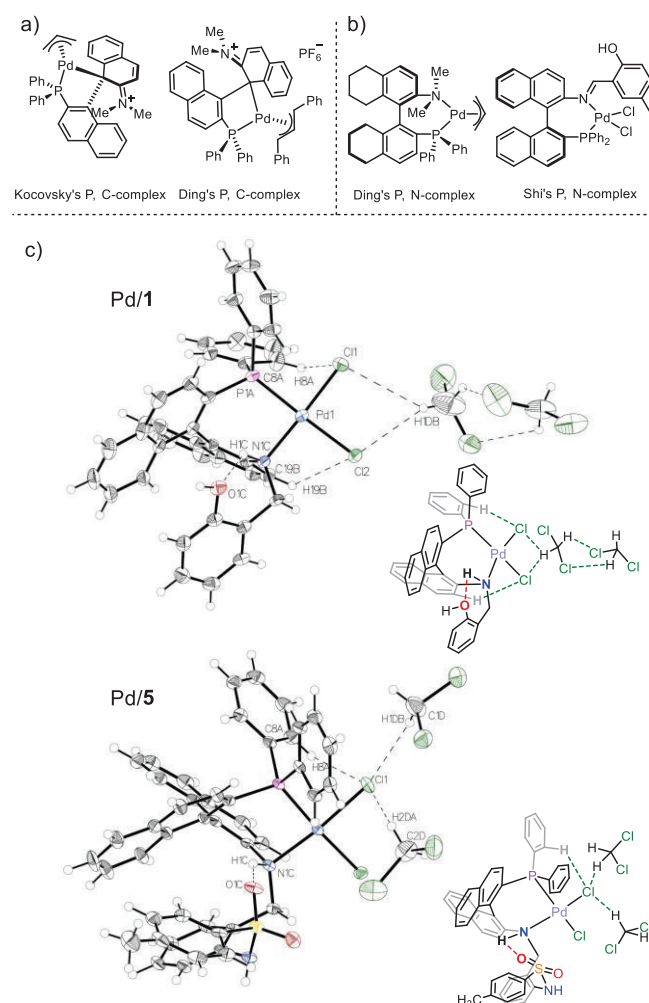
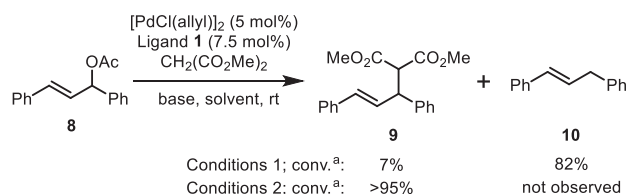


FIGURE 2 a) MAP complexes with P, C<sub>σ</sub>-coordination mode of palladium;<sup>51,52</sup> b) Modified MAP ligands in P, N-complexes with palladium;<sup>52,53</sup> c) ORTEP drawings of Pd/**1** and Pd/**5** complexes with hydrogen and halogen bond networks.

### 3.3. Pd-catalyzed asymmetric allylic substitution: suppression of elimination competition.

Symmetrically disubstituted allyl precursor 1,3-diphenyl-2-propylacetate **8** was chosen as a standard test case to avoid unnecessary regioselectivity complications. Dimethyl malonate was used as a classic representative of C-nucleophiles for model allylic alkylation of acetate **8**. Diethyl zinc was reported to promote enantiomeric excess in AAA for biindane-based diphosphine ligands<sup>55</sup> and therefore tested along with *N,O*-bis(trimethylsilyl)acetamide (BSA). Ligand **1** with unsubstituted phenolic fragment was chosen as a model for the initial optimization process. It was initially tested in dry 1,4-dioxane but demonstrated only 7% conversion to the desired diester **9** over 48 h while the unexpected reduction side product **10** was detected in 82% conversion (Scheme 2, Conditions 1).



Conditions 1: **8** (1 equiv), CH<sub>2</sub>(CO<sub>2</sub>Me)<sub>2</sub> (2 equiv), Et<sub>2</sub>Zn (2 equiv), 1,4-dioxane, 48 h  
Conditions 2: **8** (1 equiv), CH<sub>2</sub>(CO<sub>2</sub>Me)<sub>2</sub> (3 equiv), BSA (3 equiv), K<sub>2</sub>CO<sub>3</sub> (7.5 mol%), DCM, 1.5 h

<sup>a</sup> Calculated by <sup>1</sup>H NMR

SCHEME 2 Initial test of ligand **1** in different AAA conditions.

Such palladium-catalyzed reduction of allyl acetates in the presence of alkyl zinc reagents, containing β-hydrogens, has been reported previously.<sup>56</sup> The formation of the reduction side product **10** in AAA conditions, containing diethyl zinc as a base, was also reported for binaphthyl-based<sup>57</sup> and nicotine-based<sup>58</sup> monophosphine ligands but not for diphosphine ligands. This diethyl zinc interruption of the process probably occurs due to more weakly coordinated palladium-allyl intermediate with monophosphines compared to that from diphosphines. The use of another model Trost's AAA conditions,<sup>59</sup> where BSA was used instead of diethyl zinc as a malonate activator, afforded the formation of desired alkylation product **9** selectively over 1.5 h in 2.7:1 *er* as predominantly the *R*-isomer (assigned by analogy with reference<sup>60</sup>) (Scheme 2, Conditions 2).

TABLE 1 Reaction temperature and base additive/loading tests.

Entry	Base (loading), [mol%]	BSA [equiv]	Time [h]	Conv <sup>a</sup> [%]	<i>R</i> : <i>S</i> <i>er</i> <sup>b</sup>
1	K <sub>2</sub> CO <sub>3</sub> (5)	3	1.5	70 (>95) <sup>e</sup>	2.6 : 1
2	K <sub>2</sub> CO <sub>3</sub> (7.5)	3	0.5	30 (>95) <sup>f</sup>	2.7 : 1
3	K <sub>2</sub> CO <sub>3</sub> (10)	3	1.5	>95	2.7 : 1
4	K <sub>2</sub> CO <sub>3</sub> (7.5)	1.05	1.5	69 (>95) <sup>g</sup>	2.6 : 1
5	K <sub>2</sub> CO <sub>3</sub> (7.5)	1.05	1.5	61 (>95) <sup>g</sup>	2.6 : 1
6	KOAc (7.5)	3	0.5	>95	2.4 : 1
7 <sup>c</sup>	KOAc (7.5)	3	6	67 (>95) <sup>g</sup>	2.7 : 1
8 <sup>d</sup>	KOAc (7.5)	3	48	10	n.d.

<sup>a</sup> Calculated by <sup>1</sup>H NMR spectroscopy. <sup>b</sup> Determined by HPLC analysis. <sup>c</sup> Reaction at 0 °C. <sup>d</sup> Reaction at -25 °C. <sup>e</sup> 3 h of reaction. <sup>f</sup> 1.5 h of reaction. <sup>g</sup> 24 h of reaction.

The enantioselectivity of the AAA reaction is known<sup>50,53,61-65</sup> to be influenced by base choice or loading and therefore was also investigated by changing these two parameters in an AAA test reaction with **1** as the ligand (Table 1). The potassium carbonate loading did not alter the enantioselectivity of reaction (Table 1, entries 1–3). However, the decreased loading from 7.5 to 5 mol% reduced the reaction rate, providing 70% conversion to **9** at 1.5 h (Table 1, entry 2 vs 1). The equimolar to substrate loading of BSA also led to a decline of the reaction rate to 61–69% conversion over 1.5 h without change in enantioselectivity (Table 1, entries 4, 5 vs 2). The use of potassium acetate instead of potassium carbonate allowed increasing the reaction rate and afforded >95% conversion over 0.5 h, albeit with little change in enantioselectivity (Table 1, entry 6 vs 2). A previous report of AAA with MAP-based ligands showed enantioselectivity improvement at lower temperatures.<sup>53</sup> However, in our case, the

AAA at 0 °C led to a significant reaction rate decline with little difference in *ee* (Table 1, entry 7 vs 6). Further decrease of reaction temperature to -25 °C decreased the rate further to a negligible level, providing **9** in only 10% conversion over 48 h (Table 1, entry 8). Thus, the most practical conditions for monitoring the model AAA reaction were performed with 7.5 mol% loading of potassium carbonate and 3 equivalents of BSA as the dimethyl malonate activator at room temperature.

### 3.4. Pd-catalyzed asymmetric allylic substitution: enantiodivergent catalysis.

Classic AAA reactions proceed through a symmetrical Pd-allyl intermediate that present as “M” and “W”-isomers in rapid equilibrium (Figure 3a, left panel).<sup>66,67</sup> The “M” and “W”-isomers interconvert readily even at temperatures below zero,<sup>68,69</sup> however, the ratio can be controlled by ligands with bulky substituents, disfavoring the formation of the W-isomers that position the terminal phenyl group of the allyl intermediate closer to the bulkier ligand (Figure 3a, right panel).<sup>70-72</sup> In the case of the P, N-ligands investigated here, it is likely that the “M” isomer may be favoured with the phosphorous center being the ligand side with bulkier substituents (Figure 3b). The following attack by a nucleophilic species can further contribute to the selectivity due to electronic factors, as the nucleophilic attack tends to prefer the allyl carbon *trans* to the better π-accepting phosphorous ligating atom (Figure 3b, paths a/c preferred over paths c/d).<sup>73-75</sup> Given that the enantioselectivity of the reaction is a complex outcome of multiple factors/pathways, ligands **1–6** were tested in a model AAA reaction in order to ascertain how the rate and enantioselectivity of the reaction may respond to the overall steric and electronic environment provided by these ligands.

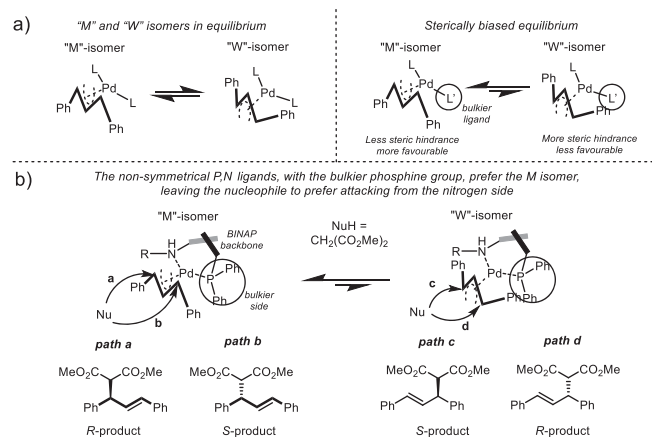


FIGURE 3 a) Factors influencing “M” and “W” Pd-allyl isomer ratio in the AAA; b) Anticipated pathways leading to the *R* and *S* product in the AAA catalysed by the chiral phosphine P, N-ligand system.

Using the optimal condition for the model AAA reaction as investigated earlier, the conversion and enantiomeric ratios of the AAA between acetate **8** and dimethyl malonate were monitored for one hour (Figure 4). Overall, these ligands showed fast conversion of reaction (1 to 6 hr for complete conversion) with moderate enantiomeric ratios (~2–5 to 1) and enantiodivergent catalysis (e.g. ligand **3** preferring the *R* product vs. ligand **5** preferring the *S* product). Ligands **2** and **3**, containing phenolic fragments with altered acidities compared to that of ligand **1**, demonstrated small variations in

enantioselectivity, albeit with more significant differences on the reaction rate for ligand **3** (Figure 4, ligand 2 and 3 vs. ligand 1). Ligand **3**, containing a fluorine substituent *ortho* to the phenol OH group, demonstrated a lower reaction rate than that by ligand **1** or **2** without any *ortho*-substituent (Figure 4, ligand 3 vs. ligands 1 and 2). However, the reaction rate of ligand **3** was still faster than that for ligand **4**, suggesting that a bulky *ortho-tert*-butyl fragment would drastically reduce the reaction rate, providing full conversion to the desired product **9** only after 6 h (Figure 4, ligand **3** vs. ligand **4**). Furthermore, the sense of the asymmetric induction switched from preferring *R* for ligand **3** to *S* for ligand **4**. Ligand **5**, bearing a different tosylamide Brønsted acid, also exhibited a switch of the sense of the asymmetric induction from *R* to *S*, as compared to ligand **3** (Figure 4, ligand 5 vs. ligand 3), although the rate of conversion for ligand **5** was faster than that of ligand **3** and ligand **4** and close to that of ligand **1** and **2**. The ligand **6** demonstrated almost no reactivity providing only traces of product **9** over 1 h (Figure 4, ligand **6**).

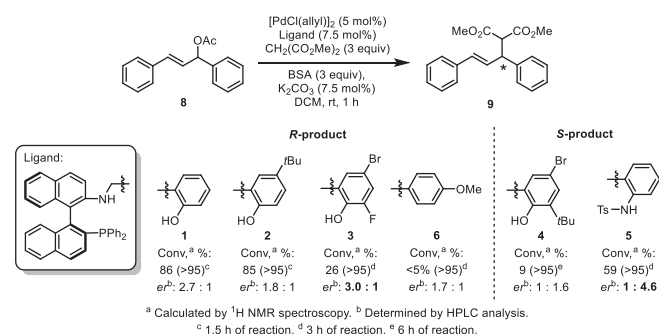


FIGURE 4 Ligands **1–6** used in a model Pd-catalysed AAA.

The relatively fast reaction rate, such as that from ligand **1** (>95% over 1.5 h) compared to previously reported MAP-based ligands<sup>76–79</sup> (>95% conversion over 6–48 h), suggests that this type of P, N-ligands may have different activation modes and potential for further development. The enantiodivergent catalysis from this series, along with the X-ray structural insight, also assisted in hypothesizing on the possible transition structures that may explain the observed reaction outcomes controlled by the complex outcomes of multiple pathways (Figure 3b, path a to d). The fast reaction rate can be attributed to a possible hydrogen-bonding interaction between ligand **1** (or a comparable ligand **2**) and the nucleophile (Figure 5a). The dramatic reduction of reaction rate provided by control ligand **6** may additionally confirm the influence of H-bonding on the reaction rate. However, the moderate *R*-enantioselectivity and high reaction rate of Pd-catalyzed AAA provided by ligand **1** may require consideration of not just the H-bonding capacity of the ligand but also the steric environment in which the H-bonding interactions can be organized. As discussed earlier, preference for the the “M”- over the “W”-isomer for the geometry of the Pd-allyl intermediate can be achieved by steric biasing with a bulkier phosphine group for ligation, along with the favourable nucleophile approach *trans* to the better  $\pi$ -accepting phosphorous ligating atom (Figure 3b, path a), to prefer the *R* product. The low to moderate enantiomeric ratio of product **9** in this series suggests that in this model, the bias for the “M” over the “W” isomer is likely also moderate and possibly prone to alteration of other steric factors also come into play.

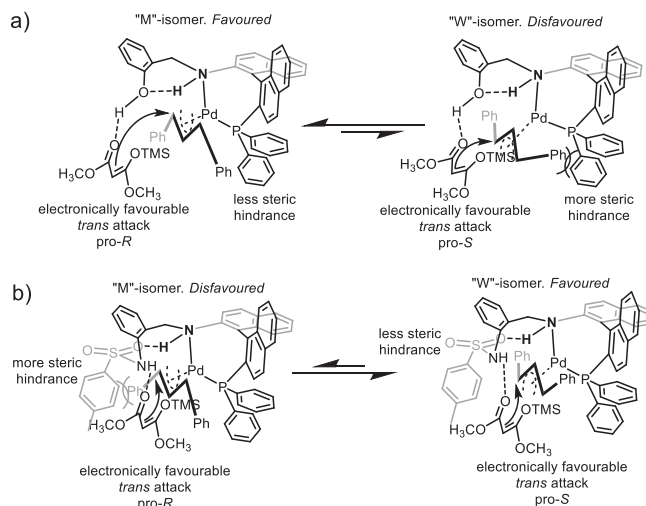


FIGURE 5 Proposed transition structures for ligand **1** (a) and **5** (b).

The moderate reduction of reaction rate in the case of ligand **3**, compared to that of ligand **1** and **2**, may be due to the change in Brønsted acidity and also in the position of the phenolic hydrogen with an *ortho* fluorine substitution. However, the sense and level of the asymmetric induction was not significantly altered and still preferred the *R* product. As the steric bulk around the phenol increased in the case of ligand **4**, the sense of the asymmetric induction was switched to slightly prefer the *S* product, along with a large reduction in the conversion, suggesting the preclusion of H-bonding activation by the steric hindrance in the preferred *trans* nucleophilic approach and also consequentially higher preference for the *cis* approach in both the “M”- and “W”-isomer cases. Ligand **5** delivered a reaction rate comparable to that of ligand **1**, while significantly altering the sense of the asymmetric induction to prefer the *S* product. This enantiodivergence can be most consistently explained by a switched preference for the “W” isomer over the “M” isomer (Figure 5b), due to the large tosylsulfonamide group in closer proximity to the allyl substrate, a supposition consistent with the structural features shown by the X-ray analysis (Figure 2). While the H-bonding interactions between the tosyl NH and the nucleophile would still enhance the reaction rate and prefer the *trans* nucleophilic approach, the switched M/W preference would favour the *S* product overall. Effectively, enantiodivergent catalysis would be possible without changing the ligand chirality, by altering the coordination between the various types of non-covalent interactions such as H-bonding interactions and steric hindrance in this series of multifunctional P, N-ligands.

#### 4. Conclusion

In summary, the ability of MAP-based, multifunctional chiral phosphines **1–6** to serve as ligands in model palladium-catalyzed asymmetric allylic alkylation (AAA) was demonstrated. Crystals of ligands **1** and **5** as palladium complexes were investigated by X-ray analysis and demonstrated an unusual P, N-coordination mode. The ligands in general promoted fast AAA reactions suggesting potential H-bonding activation in a donor-type “metal-ligand-substrate” strategy, with the ligand’s Brønsted acid motif serving as a hydrogen bond donor for recruiting the nucleophile. The switch of the sense of the asymmetric induction to changing the ligand’s Brønsted acid, without ligand chirality

change, can be attributed to non-covalent interactions that alter H-bonding interactions between the ligand and the nucleophile as well as the bias for the preferred geometry of the metal-ligand-allyl complex. Thus, the ligand's set axial chirality, in coordination with non-covalent interactions organised by the ligand's Brønsted acid motif between the metal, ligand, and substrates can lead to enantiodivergent catalysis by tuning both the H-bonding motif and its associated steric environment. Future work will involve tuning this type of ligands for further investigation of this model of organised non-covalent interactions in dynamic chirality translation.

### Acknowledgements

We are grateful to Macquarie University for an iMQRES scholarship (2015071) to Sviatoslav S. Eliseenko.

### Supporting information

Supplementary data (NMR spectra of compounds Pd/1, Pd/5, **6**; X-Ray details of complexes Pd/1 [CCDC 1998913] and Pd/5 [CCDC 1998914]; and HPLC traces of product **9**) associated with this article can be found in the online version at [onlinelibrary.wiley.com/journal/1520636x](http://onlinelibrary.wiley.com/journal/1520636x).

### REFERENCES AND NOTES

1. Beletskaya IP, Nájera C, Yus M. Stereodivergent Catalysis. *Chem. Rev.* **2018**;118(10):5080-5200.
2. Afewerki S, Córdova A. Enamine/Transition Metal Combined Catalysis: Catalytic Transformations Involving Organometallic Electrophilic Intermediates. *Top. Curr. Chem.* **2019**;377(6):38.
3. Du Z, Shao Z. Combining transition metal catalysis and organocatalysis – an update. *Chem. Soc. Rev.* **2013**;42(3):1337-1378.
4. Zhou Q-L. Transition-Metal Catalysis and Organocatalysis: Where Can Progress Be Expected? *Angew. Chem. Int. Ed.* **2016**;55(18):5352-5353.
5. Chen Z, Huo Y, An P, Wang X, Song C, Ma Y. [2.2]Paracyclophane-based N-heterocyclic carbene as efficient catalyst or as ligand for copper catalyst for asymmetric  $\alpha$ -silylation of N-tosylaldimines. *Org. Chem. Front.* **2016**;3(12):1725-1737.
6. Wang L, Chen Z, Ma M, Duan W, Song C, Ma Y. Synthesis and application of a dual chiral [2.2]paracyclophane-based N-heterocyclic carbene in enantioselective  $\beta$ -boration of acyclic enones. *Org. Biomol. Chem.* **2015**;13(43):10691-10698.
7. Hernández-Rodríguez M, Avila-Ortiz CG, del Campo JM, Hernández-Romero D, Rosales-Hoz MJ, Juaristi E. Synthesis of Novel Chiral (Thio)ureas and Their Application as Organocatalysts and Ligands in Asymmetric Synthesis. *Aust. J. Chem.* **2008**;61(5):364-375.
8. Dahlin N, Bøgevig A, Adolfsen H. N-Arenesulfonyl-2-aminomethylpyrrolidines. Novel Modular Ligands and Organocatalysts for Asymmetric Catalysis. *Adv. Synth. Catal.* **2004**;346(9-10):1101-1105.
9. Liu X, Lin L, Feng X. Chiral N,N'-Dioxides: New Ligands and Organocatalysts for Catalytic Asymmetric Reactions. *Acc. Chem. Res.* **2011**;44(8):574-587.
10. Ni H, Tang X, Zheng W, Yao W, Ullah N, Lu Y. Enantioselective Phosphine-Catalyzed Formal [4+4] Annulation of  $\alpha,\beta$ -Unsaturated Imines and Allene Ketones: Construction of Eight-Membered Rings. *Angew. Chem. Int. Ed.* **2017**;56(45):14222-14226.
11. Krauss IJ, Leighton JL. Highly Practical and Enantioselective Cu-Catalyzed Conjugate Addition of Alkylzinc Reagents to Cyclic Enones at Ambient Temperature. *Org. Lett.* **2003**;5(18):3201-3203.
12. Albrecht A, Skrzyńska A, Przydacz A, Albrecht Ł. Nucleophilic Catalysis in the Enantioselective Synthesis of  $\alpha$ -Methylidene- $\delta$ -lactones. *Synlett* **2015**;26(19):2679-2684.
13. Takizawa S, Nguyen TM-N, Grossmann A, Suzuki M, Enders D, Sasai H. Facile synthesis of  $\alpha$ -methylidene- $\gamma$ -butyrolactones: intramolecular Rauhut–Currier reaction promoted by chiral acid–base organocatalysts. *Tetrahedron* **2013**;69(3):1202-1209.
14. Takizawa S, Nguyen TM-N, Grossmann A, Enders D, Sasai H. Enantioselective Synthesis of  $\alpha$ -Alkylidene- $\gamma$ -Butyrolactones: Intramolecular Rauhut–Currier Reaction Promoted by Acid/Base Organocatalysts. *Angew. Chem. Int. Ed.* **2012**;51(22):5423-5426.
15. Gong J-J, Li T-Z, Pan K, Wu X-Y. Enantioselective intramolecular Rauhut–Currier reaction catalyzed by chiral phosphinothiourea. *Chem. Commun.* **2011**;47(5):1491-1493.
16. Zhong F, Wang Y, Han X, Huang K-W, Lu Y. l-Threonine-Derived Novel Bifunctional Phosphine–Sulfonamide Catalyst-Promoted Enantioselective Aza-Morita–Baylis–Hillman Reaction. *Org. Lett.* **2011**;13(6):1310-1313.
17. Han X, Wang Y, Zhong F, Lu Y. Enantioselective Morita–Baylis–Hillman reaction promoted by l-threonine-derived phosphine–thiourea catalysts. *Org. Biomol. Chem.* **2011**;9(19):6734-6740.

18. Takizawa S, Kishi K, Kusaba M, Jianfei B, Suzuki T, Sasai H. Facile Synthesis of Spirooxindoles via an Enantioselective Organocatalyzed Sequential Reaction of Oxindoles with Ynone. *Heterocycles* **2017**;95(2):761-767.
19. Li E, Huang Y. Phosphine-Catalyzed Domino Reactions: A Route to Functionalized Bicyclic Skeletons. *Chem. Eur. J.* **2014**;20(12):3520-3527.
20. Jin Z, Yang R, Du Y, Tiwari B, Ganguly R, Chi YR. Enantioselective Intramolecular Formal [2 + 4] Annulation of Acrylates and  $\alpha,\beta$ -Unsaturated Imines Catalyzed by Amino Acid Derived Phosphines. *Org. Lett.* **2012**;14(12):3226-3229.
21. Dilek Ö, Tezeren MA, Tilki T, Ertürk E. Chiral 2-(2-hydroxyaryl)alcohols (HAROLs) with a 1,4-diol scaffold as a new family of ligands and organocatalysts. *Tetrahedron* **2018**;74(2):268-286.
22. Théveau L, Bellini R, Dydio P, Szabo Z, van der Werf A, Afshin Sander R, Reek JNH, Moberg C. Cofactor-Controlled Chirality of Tropoisomeric Ligand. *Organometallics* **2016**;35(11):1956-1963.
23. Höke T, Herdtweck E, Bach T. Hydrogen-bond mediated regio- and enantioselectivity in a C–H amination reaction catalysed by a supramolecular Rh(II) complex. *Chem. Commun.* **2013**;49(73):8009-8011.
24. Hayashi T, Kanehira K, Hagihara T, Kumada M. Asymmetric synthesis catalyzed by chiral ferrocenylphosphine-transition metal complexes. 5. Palladium-catalyzed asymmetric allylation of active methine compounds. *J. Org. Chem.* **1988**;53(1):113-120.
25. Hayashi T, Yamamoto A, Ito Y, Nishioka E, Miura H, Yanagi K. Asymmetric synthesis catalyzed by chiral ferrocenylphosphine - transition-metal complexes. 8. Palladium-catalyzed asymmetric allylic amination. *J. Am. Chem. Soc.* **1989**;111(16):6301-6311.
26. Hayashi T, Kishi K, Yamamoto A, Ito Y. Asymmetric allylic amination catalyzed by chiral ferrocenylphosphine-palladium complexes. *Tetrahedron Lett.* **1990**;31(12):1743-1746.
27. Hoarau O, Ait-Haddou H, Daran J-C, Cramailère D, Balavoine GGA. Asymmetric Palladium-Catalyzed Allylic Alkylation Using Bis(Oxazoline) Ligands: Phenomenal Reversal of Enantioselectivity with a Single Chiral Backbone. *Organometallics* **1999**;18(23):4718-4723.
28. Ait-Haddou H, Hoarau O, Cramailère D, Pezet F, Daran J-C, Balavoine GGA. New Dihydroxy Bis(Oxazoline) Ligands for the Palladium-Catalyzed Asymmetric Allylic Alkylation: Experimental Investigations of the Origin of the Reversal of the Enantioselectivity. *Chem. Eur. J.* **2004**;10(3):699-707.
29. Voss F, Herdtweck E, Bach T. Hydrogen bond induced enantioselectivity in Mn(salen)-catalysed sulfoxidation reactions. *Chem. Commun.* **2011**;47(7):2137-2139.
30. Fackler P, Huber SM, Bach T. Enantio- and Regioselective Epoxidation of Olefinic Double Bonds in Quinolones, Pyridones, and Amides Catalyzed by a Ruthenium Porphyrin Catalyst with a Hydrogen Bonding Site. *J. Am. Chem. Soc.* **2012**;134(30):12869-12878.
31. Huang Z, Lim LH, Chen Z, Li Y, Zhou F, Su H, Zhou J. Arene CH-O Hydrogen Bonding: A Stereocontrolling Tool in Palladium-Catalyzed Arylation and Vinylation of Ketones. *Angew. Chem. Int. Ed.* **2013**;52(18):4906-4911.
32. Huang Z, Chen Z, Lim LH, Quang GCP, Hirao H, Zhou J. Weak Arene C-H...O Hydrogen Bonding in Palladium-Catalyzed Arylation and Vinylation of Lactones. *Angew. Chem. Int. Ed.* **2013**;52(22):5807-5812.
33. Wen J, Fan X, Tan R, Chien H-C, Zhou Q, Chung LW, Zhang X. Brønsted-Acid-Promoted Rh-Catalyzed Asymmetric Hydrogenation of N-Unprotected Indoles: A Cocatalysis of Transition Metal and Anion Binding. *Org. Lett.* **2018**;20(8):2143-2147.
34. Liu G, Han Z, Dong X-Q, Zhang X. Rh-Catalyzed Asymmetric Hydrogenation of  $\beta$ -Substituted- $\beta$ -thio- $\alpha,\beta$ -unsaturated Esters: Expedient Access to Chiral Organic Sulfides. *Org. Lett.* **2018**;20(18):5636-5639.
35. Wen J, Jiang J, Zhang X. Rhodium-Catalyzed Asymmetric Hydrogenation of  $\alpha,\beta$ -Unsaturated Carbonyl Compounds via Thiourea Hydrogen Bonding. *Org. Lett.* **2016**;18(18):4451-4453.
36. Li P, Zhou M, Zhao Q, Wu W, Hu X, Dong X-Q, Zhang X. Synthesis of Chiral  $\beta$ -Amino Nitroalkanes via Rhodium-Catalyzed Asymmetric Hydrogenation. *Org. Lett.* **2016**;18(1):40-43.
37. Zhao Q, Li S, Huang K, Wang R, Zhang X. A Novel Chiral Bisphosphine-Thiourea Ligand for Asymmetric Hydrogenation of  $\beta,\beta$ -Disubstituted Nitroalkenes. *Org. Lett.* **2013**;15(15):4014-4017.
38. Corey EJ, Lee TW. The formyl C–H...O hydrogen bond as a critical factor in enantioselective Lewis-acid catalyzed reactions of aldehydes. *Chem. Commun.* **2001**(15):1321-1329.
39. Marshall JA, Palovich MR. Enantioselective and Diastereoselective Additions of Allylic Stannanes to Aldehydes Promoted by a Chiral (Acyloxy)borane Catalyst. *J. Org. Chem.* **1998**;63(13):4381-4384.
40. Paton RS, Goodman JM. 1,5-Anti Stereocontrol in the Boron-Mediated Aldol Reactions of  $\beta$ -Alkoxy Methyl Ketones: The Role of the Formyl Hydrogen Bond. *J. Org. Chem.* **2008**;73(4):1253-1263.
41. Eliseenko SS, Liu F. Switchable pyrrole-based hydrogen bonding motif in enantioselective trifunctional organocatalysis. *Tetrahedron* **2019**;75(4):518-526.
42. Kenny R, Liu F. Cooperative Trifunctional Organocatalysts for Proficient Proton Transfer Reactions. *Chem. Rec.* **2017**;17(5):535-553.
43. Liu F. The Upside of Downsizing: Asymmetric Trifunctional Organocatalysts as Small Enzyme Mimics for Cooperative Enhancement of Both Rate and Enantioselectivity With Regulation. *Chirality* **2013**;25(11):675-683.
44. Anstiss C, Karuso P, Richardson M, Liu F. Synthesis of New BINAP-Based Aminophosphines and Their 31P-NMR Spectroscopy. *Molecules* **2013**;18(3):2788.
45. Anstiss C, Liu F. Cooperativity in the counterion catalysis of Morita/Baylis/Hillman reactions promoted by enantioselective trifunctional organocatalysts. *Tetrahedron* **2010**;66(29):5486-5491.
46. Anstiss C, Garnier J-M, Liu F. Mechanistic investigations of multidentate organocatalyst-promoted counterion catalysis for fast and enantioselective aza-Morita-Baylis-Hillman reactions at ambient temperature. *Org. Biomol. Chem.* **2010**;8(19):4400-4407.
47. Garnier J-M, Liu F. Trifunctional organocatalyst-promoted counterion catalysis for fast and enantioselective aza-Morita-Baylis-Hillman reactions at ambient temperature. *Org. Biomol. Chem.* **2009**;7(7):1272-1275.
48. Garnier J-M, Anstiss C, Liu F. Enantioselective Trifunctional Organocatalysts for Rate-Enhanced Aza-Morita-Baylis-Hillman Reactions at Room Temperature. *Adv. Synth. Catal.* **2009**;351(3):331-338.
49. Armarego WLF, Chai CLL. Purification of Laboratory Chemicals, 6th Edition: Butterworth-Heinemann; **2009**. 1-743 p.
50. Watson IDG, Yudin AK. New Insights into the Mechanism of Palladium-Catalyzed Allylic Amination. *J. Am. Chem. Soc.* **2005**;127(49):17516-17529.
51. Kočovský P, Vyskočil Š, Císařová I, Sejbal J, Tišlerová I, Smrčina M, Lloyd-Jones GC, Stephen SC, Butts CP,

- Murray M and others. Palladium(II) Complexes of 2-Dimethylamino-2'-diphenylphosphino-1,1'-binaphthyl (MAP) with Unique P,Co-Coordination and Their Catalytic Activity in Allylic Substitution, Hartwig-Buchwald Amination, and Suzuki Coupling. *J. Am. Chem. Soc.* **1999**;121(33):7714-7715.
52. Wang Y, Li X, Sun J, Ding K. Backbone Effect of MAP Ligands on Their Coordination Patterns with Palladium(II). *Organometallics* **2003**;22(9):1856-1862.
53. Sun Y-W, Jiang J-J, Zhao M-X, Wang F-J, Shi M. Palladium-catalyzed asymmetric allylic substitutions in the presence of chiral phosphine-imine type ligands. *J. Organomet. Chem.* **2011**;696(15-16):2850-2856.
54. Ding L, Sui X, Gu Z. Enantioselective Synthesis of Biaryl Atropisomers via Pd/Norbornene-Catalyzed Three-Component Cross-Couplings. *ACS Catal.* **2018**;8(6):5630-5635.
55. Xie J-H, Duan H-F, Fan B-M, Cheng X, Wang L-X, Zhou Q-L. Application of SDP Ligands for Pd-Catalyzed Allylic Alkylation. *Adv. Synth. Catal.* **2004**;346(6):625-632.
56. Matsushita H, Negishi E. Palladium-catalyzed reactions of allylic electrophiles with organometallic reagents. A regioselective 1,4-elimination and a regio- and stereoselective reduction of allylic derivatives. *J. Org. Chem.* **1982**;47(21):4161-4165.
57. Kinoshita N, Kawabata T, Tsubaki K, Bando M, Fujii K. Use of zinc enolate, free from other metals, in enantioselective palladium-catalyzed allylic alkylation. *Tetrahedron* **2006**;62(8):1756-1763.
58. Comins DL, Capracotta SS; Nicotine-Based Compounds Useful for Asymmetric Synthesis patent WO2010040059 (A1). **2010**.
59. Trost BM, Murphy DJ. A model for metal-templated catalytic asymmetric induction via  $\pi$ -allyl fragments. *Organometallics* **1985**;4(6):1143-1145.
60. Enders D, Peters R, Lochtmann R, Runsink J. Enantioselective Synthesis of Planar Chiral ortho-Functionalized Ferrocenyl Ketones. *Eur. J. Org. Chem.* **2000**(16):2839-2850.
61. Long P-W, Xu J-X, Bai X-F, Xu Z, Zheng Z-J, Yang K-F, Li L, Xu L-W. Palladium-catalyzed tandem allylic substitution/cyclization and cascade hydrosilylated reduction: the influence of reaction parameters and hydrosilanes on the stereoselectivity. *RSC Adv.* **2018**;8(41):22944-22951.
62. Ghorpade SA, Sawant DN, Makki A, Sekar N, Eppinger J. Water promoted allylic nucleophilic substitution reactions of (E)-1,3 diphenylallyl acetate. *Green Chem.* **2018**;20(2):425-430.
63. Rovira L, Fernández-Pérez H, Vidal-Ferran A. Palladium-Based Supramolecularly Regulated Catalysts for Asymmetric Allylic Substitutions. *Organometallics* **2016**;35(4):528-533.
64. Chen M, Hartwig JF. Iridium-Catalyzed Enantioselective Allylic Substitution of Enol Silanes from Vinylogous Esters and Amides. *J. Am. Chem. Soc.* **2015**;137(43):13972-13979.
65. Lai Z-W, Yang R-F, Ye K-Y, Sun H, You S-L. Synthesis of 1-[bis(trifluoromethyl)phosphine]-1'-oxazolinyferrocene ligands and their application in regio- and enantioselective Pd-catalyzed allylic alkylation of monosubstituted allyl substrates. *Beilstein J. Org. Chem.* **2014**;10:1261-1266.
66. Trost BM, Van Vranken DL. Asymmetric Transition Metal-Catalyzed Allylic Alkylations. *Chem. Rev.* **1996**;96(1):395-422.
67. Guerrero Rios I, Rosas-Hernandez A, Martin E. Recent Advances in the Application of Chiral Phosphine Ligands in Pd-Catalyzed Asymmetric Allylic Alkylation. *Molecules* **2011**;16(1):970-1010.
68. Sprinz J, Kiefer M, Helmchen G, Reggelin M, Huttner G, Walter O, Zsolnai L. Catalysis of allylic substitutions by Pd complexes of oxazolines containing an additional P, S, or Se Center. X-ray crystal structures and solution structures of chiral  $\pi$ -allyl palladium complexes of phosphinoaryloxazolines. *Tetrahedron Lett.* **1994**;35(10):1523-1526.
69. Granberg KL, Baekvall JE. Isomerization of ( $\pi$ -allyl)palladium complexes via nucleophilic displacement by palladium(0). A common mechanism in palladium(0)-catalyzed allylic substitution. *J. Am. Chem. Soc.* **1992**;114(17):6858-6863.
70. Nakano H, Okuyama Y, Yanagida M, Hongo H. Palladium-Catalyzed Asymmetric Allylic Substitution Reactions Using New Chiral Phosphinooxathiane Ligands. *J. Org. Chem.* **2001**;66(2):620-625.
71. Kraft J, Mill K, Ziegler T. Sugar-Annulated Oxazoline Ligands: A Novel Pd(II) Complex and Its Application in Allylic Substitution. *Molecules* **2016**;21(12):1704.
72. Anderson JC, Cubbon RJ, Harling JD. Investigation of the importance of nitrogen substituents in a N-P chiral ligand for enantioselective allylic alkylation. *Tetrahedron: Asymmetry* **2001**;12(6):923-935.
73. Aakermark B, Hansson S, Krakenberger B, Vitagliano A, Zetterberg K. Alkylation of ( $\pi$ -allyl)palladium systems. Mechanism and regiocontrol. *Organometallics* **1984**;3(5):679-682.
74. Dawson GJ, Williams JMJ, Coote SJ. Enantioselective synthesis of succinic acids and  $\gamma$ -lactones via palladium catalyzed allylic substitution reactions. *Tetrahedron: Asymmetry* **1995**;6(10):2535-2546.
75. Allen JV, Coote SJ, Dawson GJ, Frost CG, Martins CJ, Williams JMJ. Palladium-catalyzed asymmetric allylic substitution: a ligand design incorporating steric and electronic effects. *J. Chem. Soc., Perkin Trans. 1* **1994**(15):2065-2072.
76. Vyskočil Š, Smrčina M, Hanuš V, Poláček M, Kočovský P. Derivatives of 2-Amino-2'-diphenylphosphino-1,1'-binaphthyl (MAP) and Their Application in Asymmetric Palladium(0)-Catalyzed Allylic Substitution. *J. Org. Chem.* **1998**;63(22):7738-7748.
77. Wang Y, Guo H, Ding K. Synthesis of novel N,P chiral ligands for palladium-catalyzed asymmetric allylations: the effect of binaphthyl backbone on the enantioselectivity. *Tetrahedron: Asymmetry* **2000**;11(20):4153-4162.
78. Wang Y, Li X, Ding K. The synthesis of a new generation of MAP ligands containing two types of chiral elements for asymmetric catalysis. *Tetrahedron Lett.* **2002**;43(1):159-161.
79. Kawamura M, Kiyotake R, Kudo K. Synthesis of a novel photoresponsive axially chiral phosphine ligand containing an arylazo group and its application to palladium-catalyzed asymmetric allylic alkylation. *Chirality* **2002**;14(9):724-726.

## Supplementary Information

### **Ligand-induced hydrogen-bonding network interactions for enantiodivergent catalysis in a palladium-catalyzed allylic alkylation reaction**

Sviatoslav S. Eliseenko,<sup>a</sup> Mohan Bhadbhade,<sup>b</sup> and Fei Liu<sup>a\*</sup>

<sup>a</sup> *Department of Molecular Sciences, Macquarie University, Sydney, NSW 2109,  
Australia*

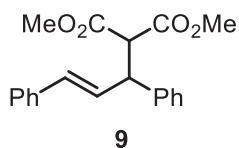
<sup>b</sup> *Solid State & Elemental Analysis Unit, Mark Wainwright Analytical Centre,  
Division of Research, The University of New South Wales, Sydney, NSW 2052,  
Australia*

Corresponding Author – Fax: +61-2-9850-8313; e-mail: fei.liu@mq.edu.au

## Table of Content

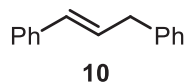
1.	NMR data of Pd-catalyzed AAA products.	3
2.	NMR spectra of ligand <b>6</b> and complexes Pd/ <b>1</b> and Pd/ <b>5</b> .	
	• Figure 1. <sup>1</sup> H NMR spectra of ligand <b>6</b> with the extended aromatic region.	4
	• Figure 2. <sup>31</sup> P NMR spectra of ligand <b>6</b> .	4
	• Figure 3. <sup>13</sup> C NMR spectra of ligand <b>6</b> with the extended aromatic region.	5
	• Figure 4. <sup>1</sup> H NMR spectra of complex Pd/ <b>1</b> with the extended aromatic region.	5
	• Figure 5. <sup>31</sup> P NMR spectra of complex Pd/ <b>1</b> .	6
	• Figure 6. <sup>13</sup> C NMR spectra of complex Pd/ <b>1</b> with the extended aromatic region.	6
	• Figure 7. <sup>1</sup> H NMR spectra of complex Pd/ <b>5</b> with the extended aromatic region.	7
	• Figure 8. <sup>31</sup> P NMR spectra of complex Pd/ <b>5</b> .	7
	• Figure 9. <sup>13</sup> C NMR spectra of complex Pd/ <b>5</b> with the extended aromatic region.	8
3.	Representatives of chiral HPLC traces of diether <b>9</b> .	
	• Figure 10. HPLC trace of product <b>9</b> provided by ligand <b>1</b> and the HPLC trace of the corresponded racemic control in the extension.	9
	• Figure 11. HPLC trace of product <b>9</b> provided by ligand <b>5</b> and the HPLC trace of the corresponded racemic control in the extension.	9
4.	X-Ray Crystallography of complexes Pd/ <b>1</b> and Pd/ <b>5</b>	10
5.	References.	15

## 1. NMR data of Pd-catalyzed AAA products.



Dimethyl-2-(1,3-diphenylallyl)malonate **9**.<sup>1</sup>

<sup>1</sup>H NMR (400 MHz, CDCl<sub>3</sub>) δ 3.52 (s, 3H), 3.71 (s, 3H), 3.96 (d, *J* = 10.9 Hz, 1H), 4.27 (dd, *J* = 10.9, 8.6 Hz, 1H), 6.33 (dd, *J* = 15.7, 8.6 Hz, 1H), 6.48 (d, *J* = 15.7 Hz, 1H), 7.17–7.30 (m, 10H); HPLC conditions: CHIRALPAK<sup>®</sup> AD-H; 0.8 ml/min; hexane/*i*-PrOH 80/20; time: 9.36 min (*R*) and 12.02 min (*S*). Stereochemistry is assigned by analogy with reference<sup>2</sup> where the same chiral column and conditions used.



Prop-1-ene-1,3-diyldibenzene **10**.<sup>3</sup>

<sup>1</sup>H NMR (400 MHz, CDCl<sub>3</sub>) δ 3.55 (d, *J* = 6.7 Hz, 2H), 6.35 (dt, *J* = 16.3, 6.4 Hz, 1H), 6.46 (d, *J* = 16.3 Hz, 1H), 7.38–7.17 (m, 10H).

## 2. NMR spectra of ligand 6 and complexes Pd/1 and Pd/5.

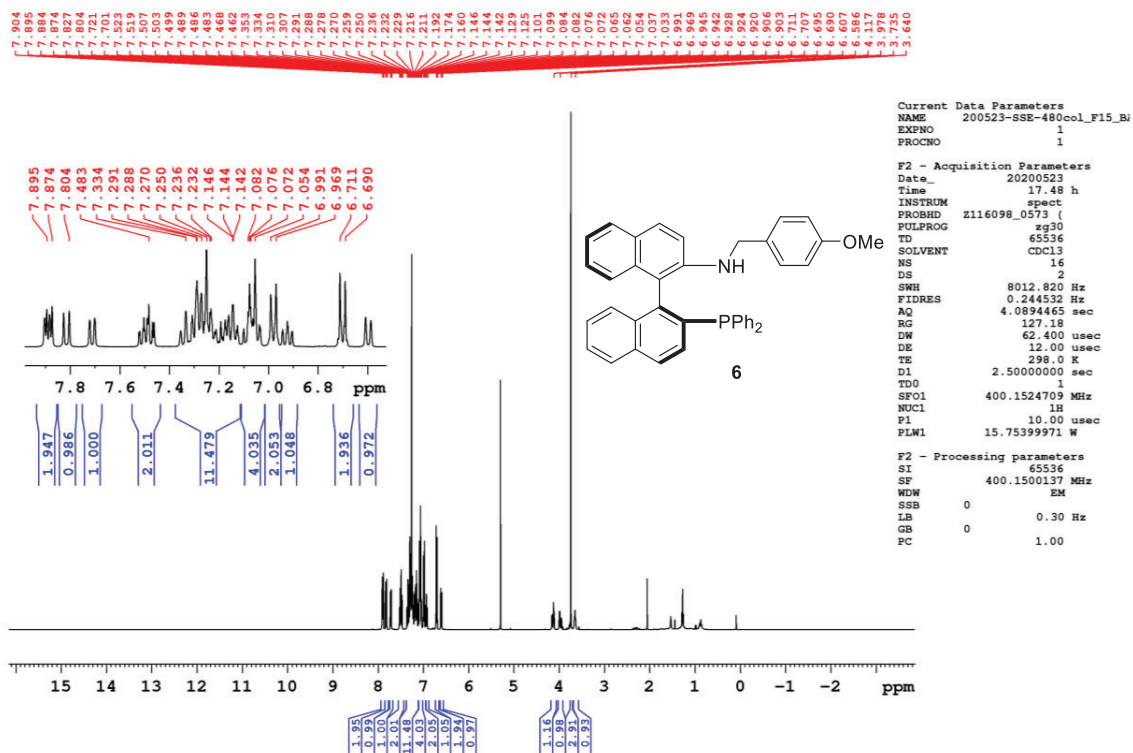


Figure 1.  $^1\text{H}$  NMR spectra of ligand 6 with the extended aromatic region in  $\text{CDCl}_3$ .

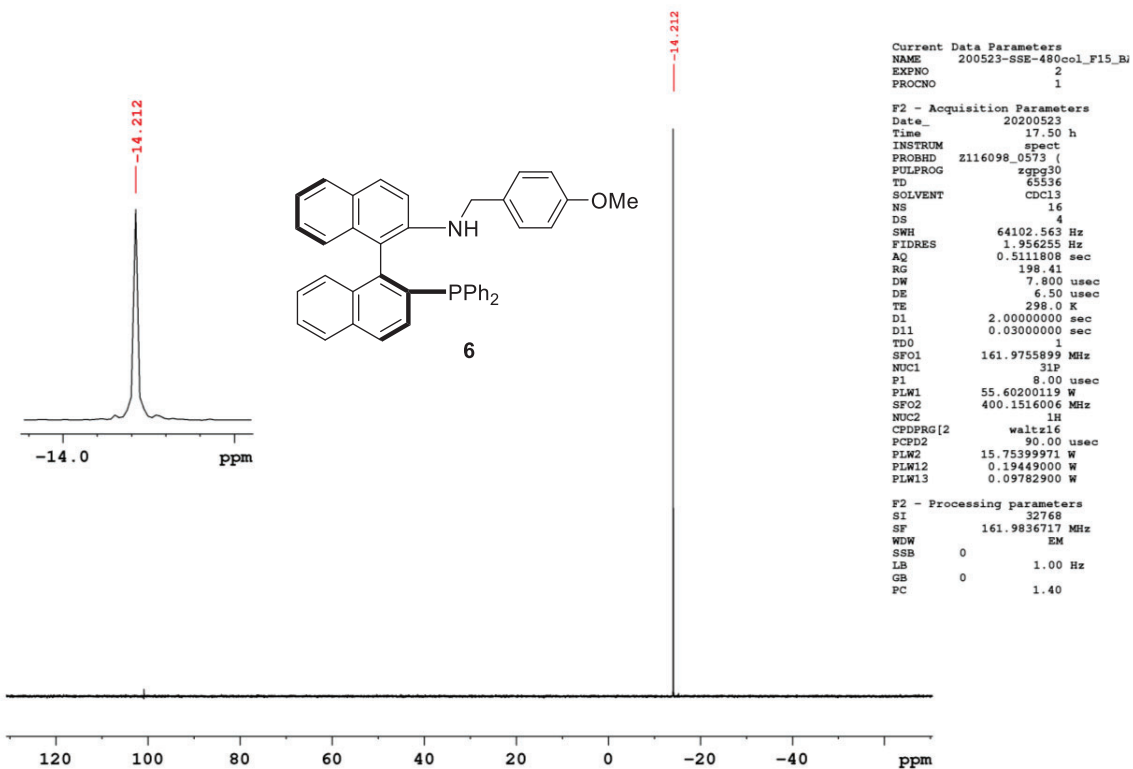


Figure 2.  $^{31}\text{P}$  NMR spectra of ligand 6 in  $\text{CDCl}_3$ .

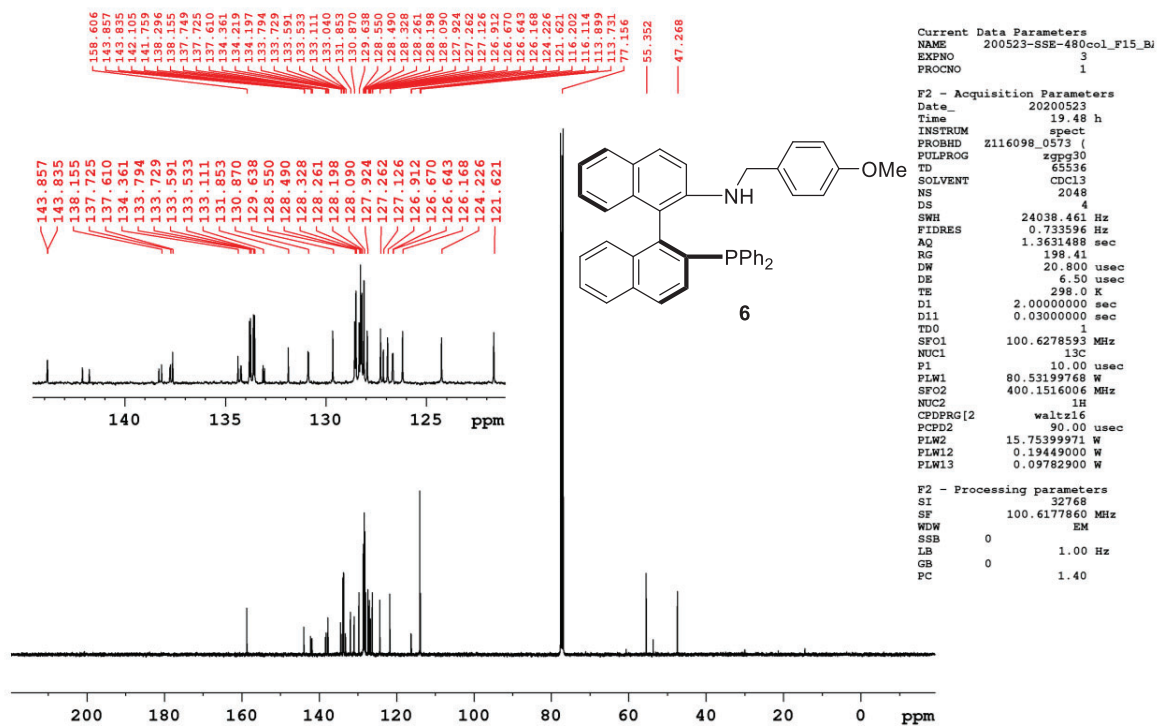


Figure 3.  $^{13}\text{C}$  NMR spectra of ligand **6** with the extended aromatic region in  $\text{CDCl}_3$ .

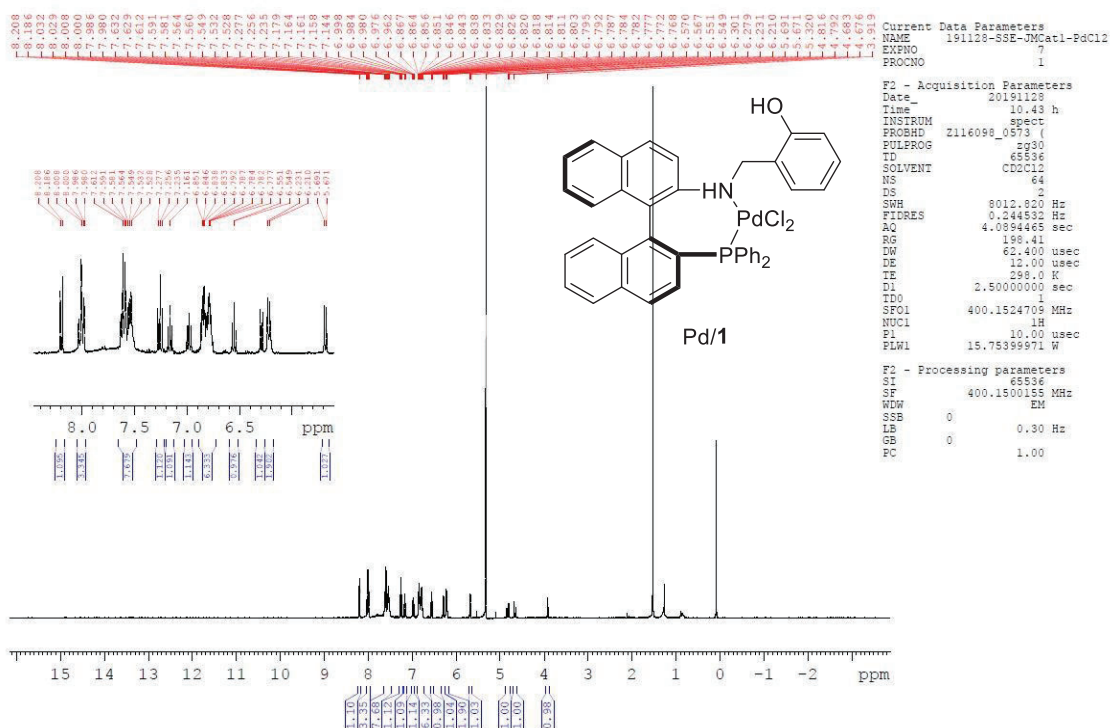


Figure 4.  $^1\text{H}$  NMR spectra of complex **Pd/1** with the extended aromatic region in  $\text{CD}_2\text{Cl}_2$ .

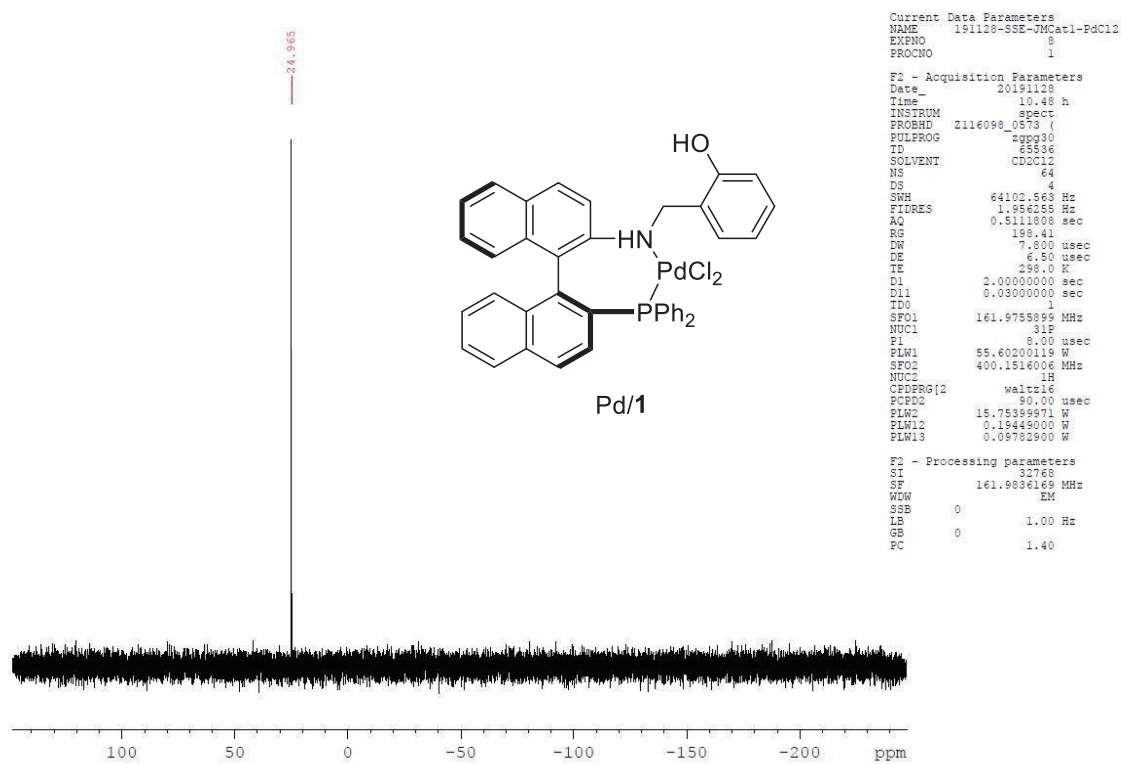


Figure 5. <sup>31</sup>P NMR spectra of complex Pd/1 in CD<sub>2</sub>Cl<sub>2</sub>.

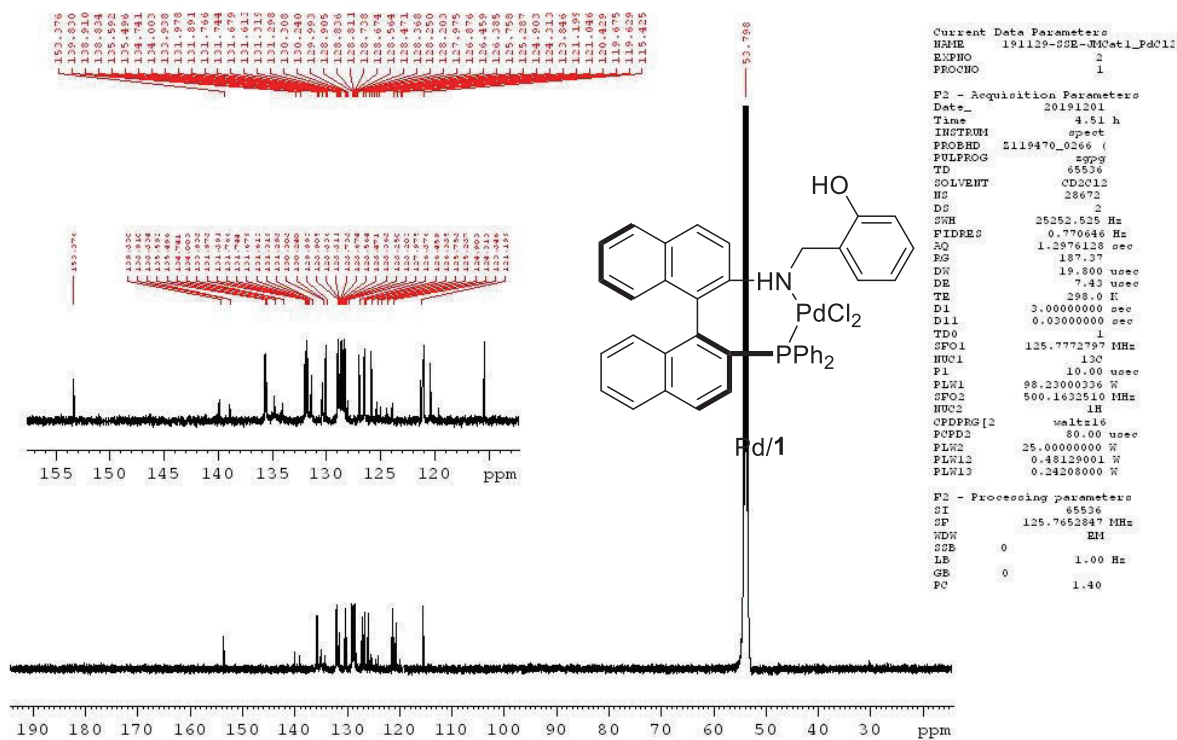


Figure 6. <sup>13</sup>C NMR spectra of complex Pd/1 with the extended aromatic region in CD<sub>2</sub>Cl<sub>2</sub>.

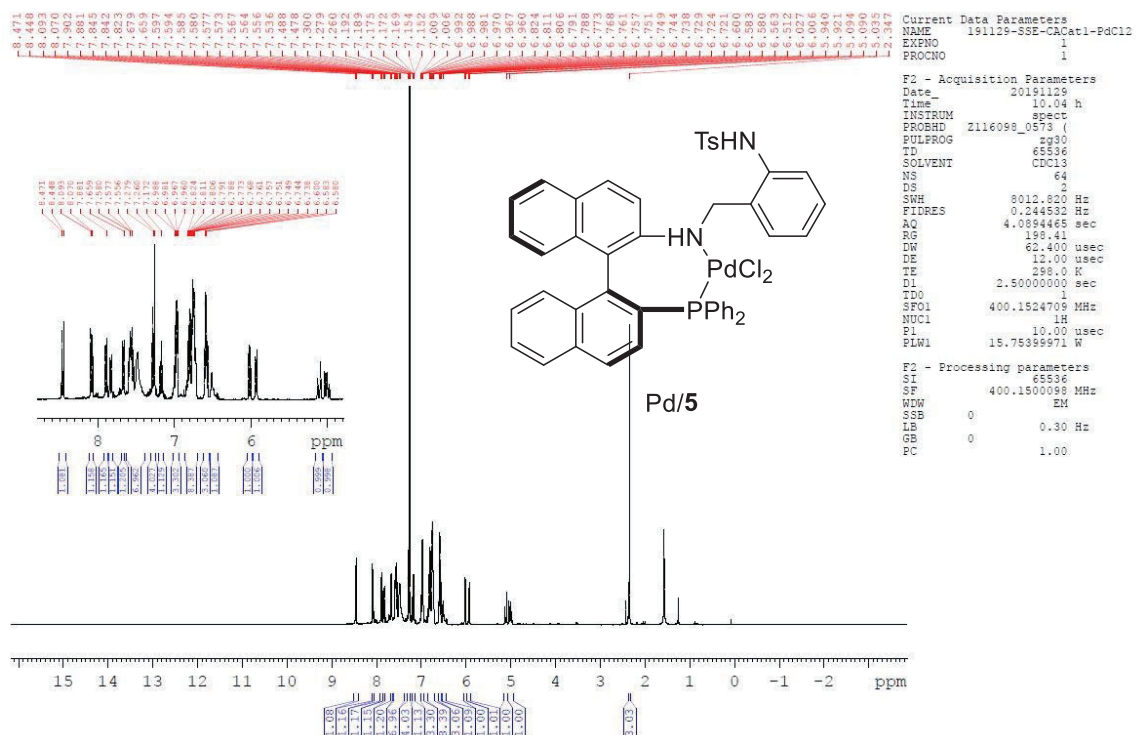


Figure 7.  $^1\text{H}$  NMR spectra of complex Pd/5 with the extended aromatic region in  $\text{CDCl}_3$ .

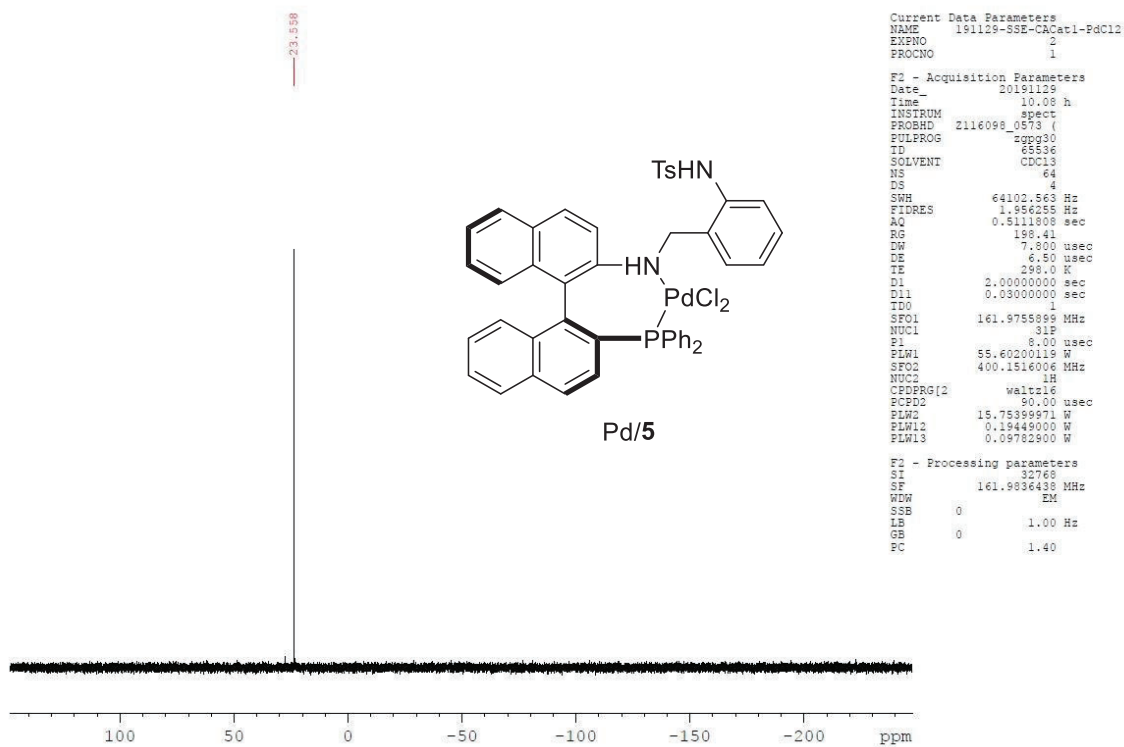


Figure 8.  $^{31}\text{P}$  NMR spectra of complex Pd/5 in  $\text{CDCl}_3$ .

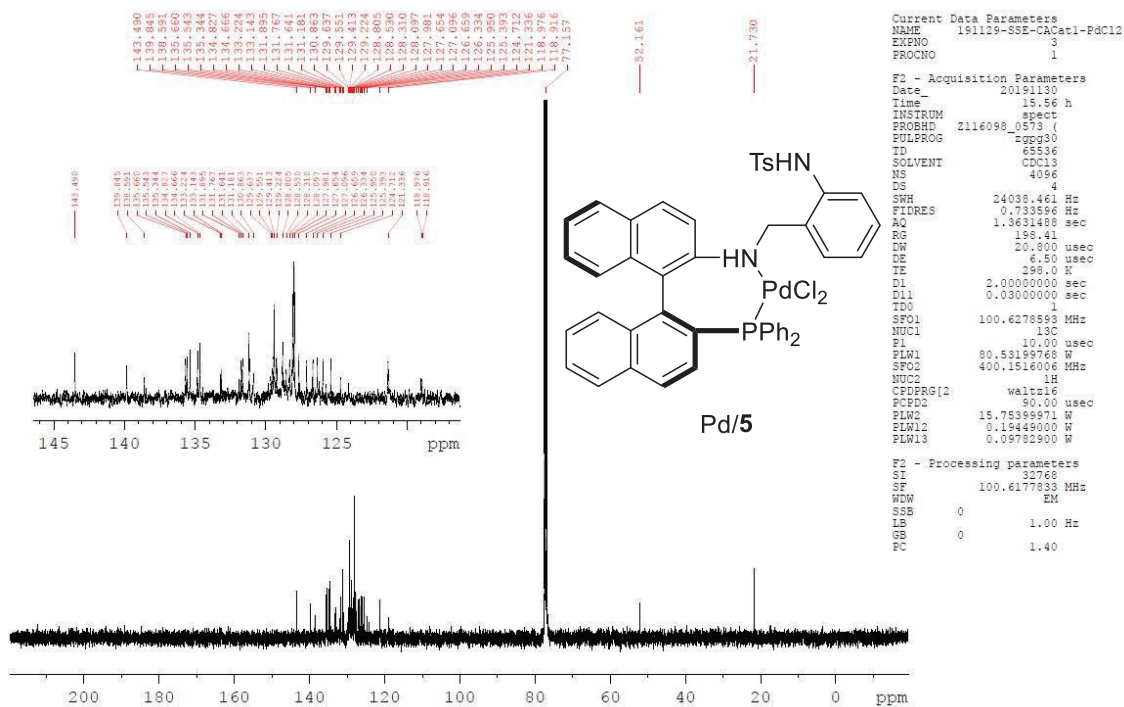


Figure 9.  $^{13}\text{C}$  NMR spectra of complex Pd/5 with the extended aromatic region in  $\text{CDCl}_3$ .

### 3. Chiral HPLC traces for product **9** provided by ligands **1** and **5**.

The UV traces of the product **9** on Figures 10 and 11 were obtained using the same HPLC column and conditions on the same day. The samples have been prepared from products, obtained in the same set of experiments.

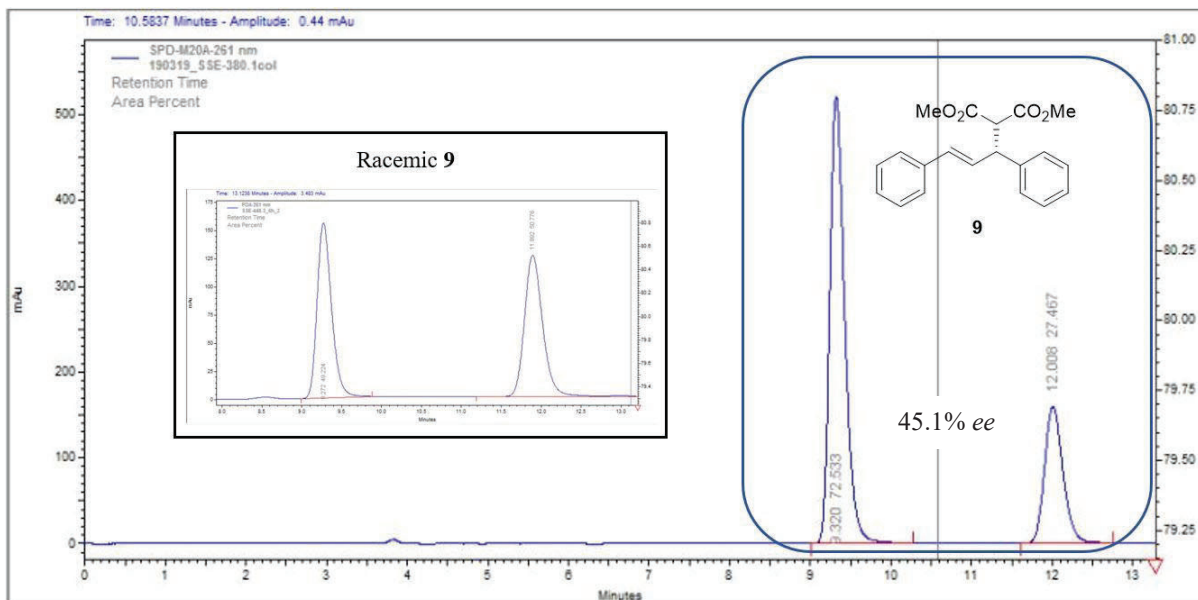


Figure 10. HPLC trace of product **9** provided by ligand **1** and the HPLC trace of the corresponded racemic control in the extension.

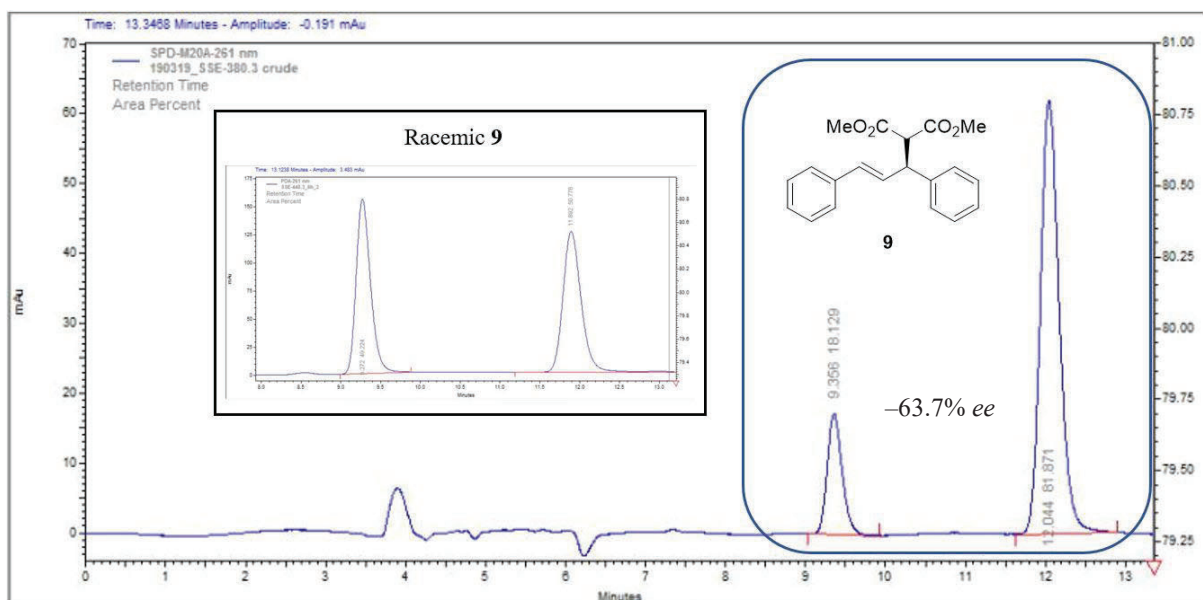


Figure 11. HPLC trace of product **9** provided by ligand **5** and the HPLC trace of the corresponded racemic control in the extension.

#### 4. X-Ray Crystallography

Suitable single crystals of Pd/1 were selected under the polarizing microscope (Leica M165Z), mounted on a MicroMount (MiTeGen, USA) consisting of a thin polymer tip with a wicking aperture. The X-ray diffraction measurements were carried out on a Bruker D8 Quest Single Crystal diffractometer with Photon II detector at 150 K by using I $\mu$ S 3.0 Microfocus Source with Mo-K $\alpha$  radiation ( $\lambda = 0.710723 \text{ \AA}$ ). The single crystal, mounted on the goniometer using cryo loops for intensity measurements, was coated with paraffin oil and then quickly transferred to the cold stream using an Oxford Cryo stream 800 attachment.

Yellowish orange plate like crystal of Pd/5 was selected under the polarizing microscope (Leica M165Z), was picked up on a MicroMount (MiTeGen, USA) consisting of a thin polymer tip with a wicking aperture. The X-ray diffraction measurements were carried out on a Bruker kappa-II CCD diffractometer at 150 K using I $\mu$ S Incoatec Microfocus Source with Mo-K $\alpha$  radiation ( $\lambda = 0.710723 \text{ \AA}$ ). The single crystal, mounted on the goniometer using a cryo loop for intensity measurements, was coated with immersion oil type NVH and then quickly transferred to the cold nitrogen stream generated by an Oxford Cryostream 700 series.

For both the data, symmetry related absorption corrections using the program SADABS<sup>1</sup> were applied and the data were corrected for Lorentz and polarisation effects using Bruker APEX3 software.<sup>4</sup> The structures were solved by program SHELXT<sup>5</sup> (with intrinsic phasing) and the full-matrix least-square refinements were carried out using SHELXL-2015<sup>6</sup> through Olex2<sup>7</sup> suite of software. The non-hydrogen atoms were refined anisotropically.

	Pd/1
Crystal data	
Chemical formula	C <sub>39</sub> H <sub>28</sub> Cl <sub>2</sub> NOPPd·1.25(CH <sub>2</sub> Cl <sub>2</sub> )
<i>M</i> <sub>r</sub>	841.05
Crystal system, space group	Orthorhombic, <i>P</i> 2 <sub>1</sub> 2 <sub>1</sub> 2 <sub>1</sub>
Temperature (K)	150
<i>a</i> , <i>b</i> , <i>c</i> (Å)	9.6377 (6), 15.8598 (9), 25.1274 (15)
<i>V</i> (Å <sup>3</sup> )	3840.8 (4)
<i>Z</i>	4
Radiation type	Mo <i>K</i> α
μ (mm <sup>-1</sup> )	0.87
Crystal size (mm)	0.46 × 0.10 × 0.05
Data collection	
Diffractometer	Bruker D8Quest
Absorption correction	Multi-scan <i>SADABS2016/2</i> (Bruker,2016/2) was used for absorption correction. wR2(int) was 0.1546 before and 0.0952 after correction. The Ratio of minimum to maximum transmission is 0.7540. The λ/2 correction factor is Not present.
<i>T</i> <sub>min</sub> , <i>T</i> <sub>max</sub>	0.562, 0.746
No. of measured, independent and observed [ <i>I</i> > 2σ( <i>I</i> )] reflections	100864, 8852, 8226
<i>R</i> <sub>int</sub>	0.085
(sin θ/λ) <sub>max</sub> (Å <sup>-1</sup> )	0.651
Refinement	
<i>R</i> [ <i>F</i> <sup>2</sup> > 2σ( <i>F</i> <sup>2</sup> )], w <i>R</i> ( <i>F</i> <sup>2</sup> ), <i>S</i>	0.037, 0.095, 1.05
No. of reflections	8852
No. of parameters	461
H-atom treatment	H-atom parameters constrained
Δρ <sub>max</sub> , Δρ <sub>min</sub> (e Å <sup>-3</sup> )	0.81, -0.76
Absolute structure	Flack <i>x</i> determined using 3412 quotients [( <i>I</i> <sup>+</sup> )-( <i>I</i> <sup>-</sup> )]/[( <i>I</i> <sup>+</sup> )+( <i>I</i> <sup>-</sup> )] (Parsons, Flack and Wagner, Acta Cryst. B69 (2013) 249-259).
Absolute structure parameter	0.005 (11)

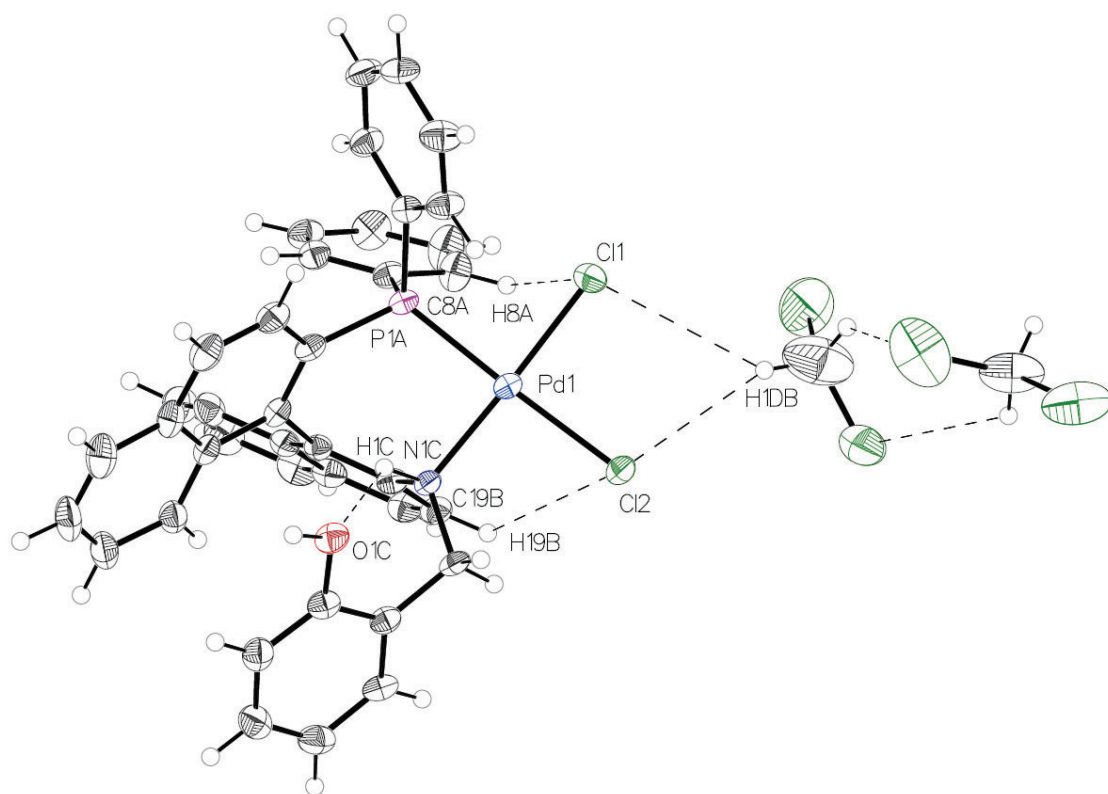


Figure 9. ORTEP drawing of Pd/1 complex (CCDC 1998913).

	Pd/5
Crystal data	
Chemical formula	C <sub>46</sub> H <sub>37</sub> Cl <sub>2</sub> N <sub>2</sub> O <sub>2</sub> PPdS·2(CH <sub>2</sub> Cl <sub>2</sub> )
<i>M</i> <sub>r</sub>	1059.96
Crystal system, space group	Orthorhombic, <i>P</i> 2 <sub>1</sub> 2 <sub>1</sub> 2 <sub>1</sub>
Temperature (K)	150
<i>a</i> , <i>b</i> , <i>c</i> (Å)	15.9582 (9), 16.5600 (8), 17.3772 (9)
<i>V</i> (Å <sup>3</sup> )	4592.2 (4)
<i>Z</i>	4
Radiation type	Mo <i>K</i> α
μ (mm <sup>-1</sup> )	0.88
Crystal size (mm)	0.26 × 0.24 × 0.08
Data collection	
Diffractometer	Bruker <i>APEX</i> -II CCD
Absorption correction	Multi-scan <i>SADABS2016/2</i> (Bruker,2016/2) was used for absorption correction. <i>wR2(int)</i> was 0.1243 before and 0.0692 after correction. The Ratio of minimum to maximum transmission is 0.8621. The λ/2 correction factor is Not present.
<i>T</i> <sub>min</sub> , <i>T</i> <sub>max</sub>	0.643, 0.746
No. of measured, independent and observed [ <i>I</i> > 2σ( <i>I</i> )] reflections	89999, 10576, 9662
<i>R</i> <sub>int</sub>	0.063
(sin θ/λ) <sub>max</sub> (Å <sup>-1</sup> )	0.651
Refinement	
<i>R</i> [ <i>F</i> <sup>2</sup> > 2σ( <i>F</i> <sup>2</sup> )], <i>wR</i> ( <i>F</i> <sup>2</sup> ), <i>S</i>	0.029, 0.099, 0.79
No. of reflections	10576
No. of parameters	551
H-atom treatment	H-atom parameters constrained
Δρ <sub>max</sub> , Δρ <sub>min</sub> (e Å <sup>-3</sup> )	0.43, -0.43
Absolute structure	Flack <i>x</i> determined using 4092 quotients [( <i>I</i> <sup>+</sup> )-( <i>I</i> <sup>-</sup> )]/[( <i>I</i> <sup>+</sup> )+( <i>I</i> <sup>-</sup> )] (Parsons, Flack and Wagner, <i>Acta Cryst.</i> B69 (2013) 249-259).
Absolute structure parameter	-0.024 (9)

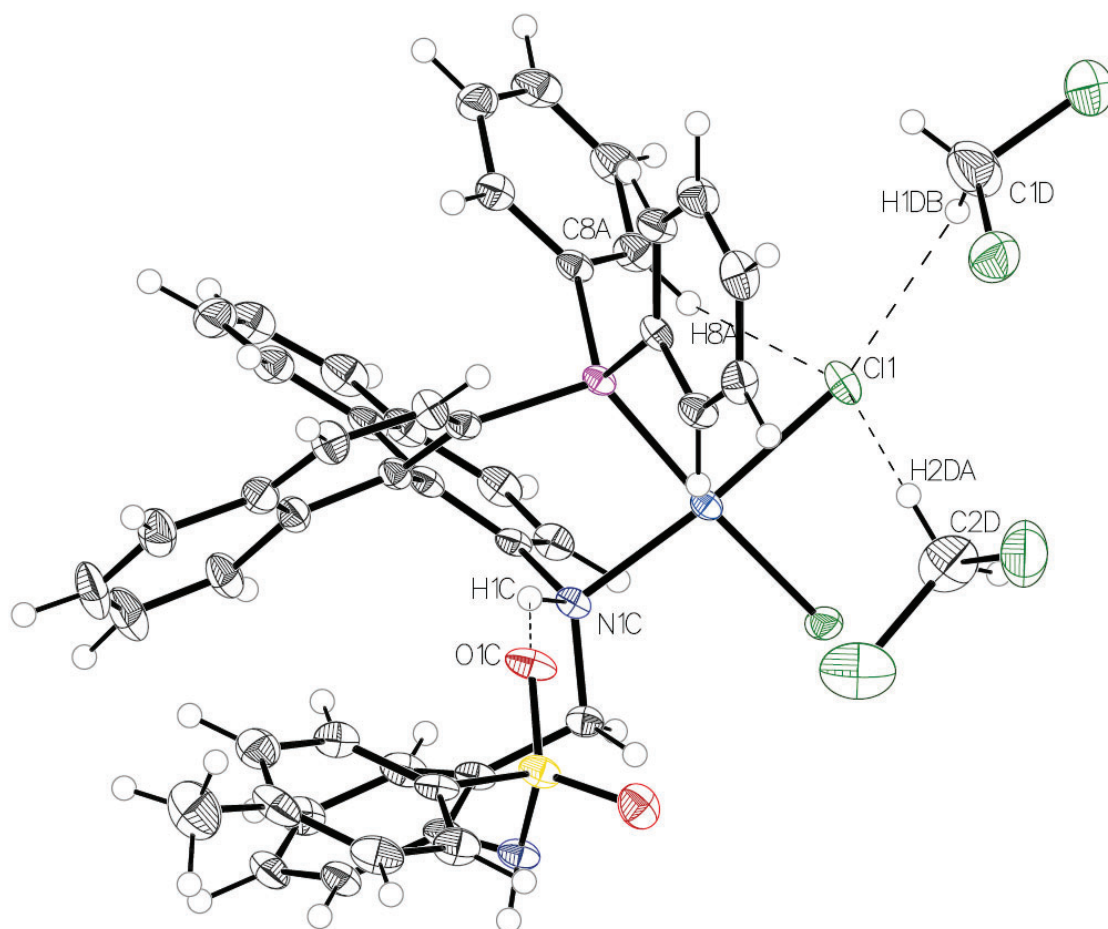


Figure 10. ORTEP drawing of Pd/5 complex (CCDC 1998914).

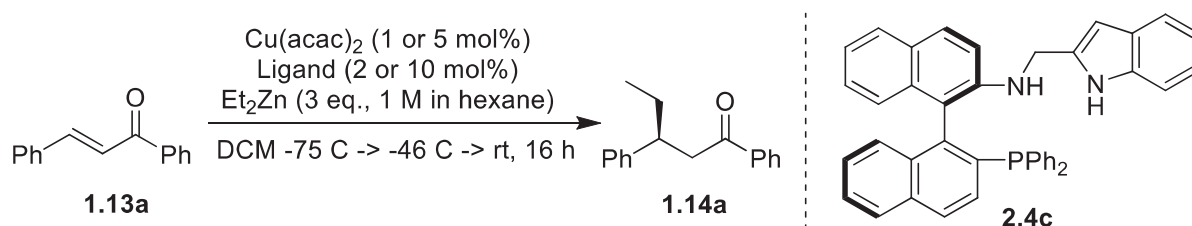
## 5. References.

1. Wang Y, Guo H, Ding K. Synthesis of novel N,P chiral ligands for palladium-catalyzed asymmetric allylations: the effect of binaphthyl backbone on the enantioselectivity. *Tetrahedron: Asymmetry* **2000**;11(20):4153-4162.
2. Enders D, Peters R, Lochtman R, Runsink J. Enantioselective Synthesis of Planar Chiral ortho-Functionalized Ferrocenyl Ketones. *Eur. J. Org. Chem.* **2000**(16):2839-2850.
3. Tang X-L, Wu Z, Li M-B, Gu Y, Tian S-K. Cross-Coupling of N-Allylic Sulfonimides with Organozinc Reagents at Room Temperature. *Eur. J. Org. Chem.* **2012**(22):4107-4109.
4. Bruker. APEX3, SAINT and SADABS. Madison, Wisconsin, USA: Bruker AXS Inc.; **2016**.
5. Sheldrick G. SHELXT - Integrated space-group and crystal-structure determination. *Acta Crystallogr., Sect. A: Found. Adv.* **2015**;71(1):3-8.
6. Sheldrick G. Crystal structure refinement with SHELXL. *Acta Crystallogr., Sect. C: Struct. Chem.* **2015**;71(1):3-8.
7. Dolomanov OV, Bourhis LJ, Gildea RJ, Howard JAK, Puschmann H. OLEX2: a complete structure solution, refinement and analysis program. *J. Appl. Crystallogr.* **2009**;42(2):339-341.

### 3.2.2 MAP-based structures **1.46a,i**, **1.48a**, and **2.4c** in other metal-catalysed reactions

The reaction scope of trifunctional dual catalysts **1.46a,i**, **1.48a**, and **2.4c** was preliminarily investigated in Cu-catalysed diethylzinc addition to chalcone **1.13a** (Table 3) and in Rh-catalysed hydrogenation of methyl 2-acetamidoacrylate **3.9** (Scheme 20).

Table 3 Ligands **1.46a,i**, **1.48a**, and **2.4c** in Cu-catalysed diethylzinc addition to chalcone **1.13a**.

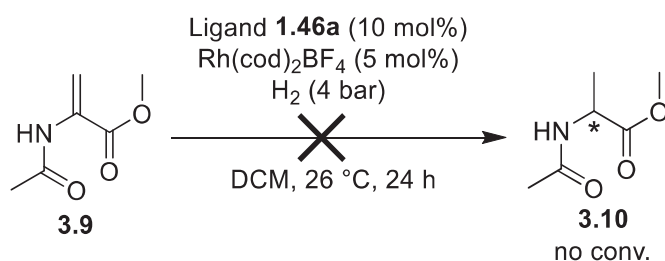


Entry	Ligand	[Cu]/Ligand loading	Conv. <sup>a</sup> , %	ee <sup>b</sup> , %
1	<b>1.46a</b>	5 / 10 mol%	> 95	46
2	<b>1.46a</b>	1 / 2 mol%	> 95	31
3	<b>1.46i</b>	1 / 2 mol%	40	11
4	<b>1.48a</b>	5 / 10 mol%	53	-6
5	<b>2.4c</b>	5 / 10 mol%	65	34
6	no ligand	no copper	27 <sup>c</sup>	rac

<sup>[a]</sup>Calculated by <sup>1</sup>H NMR spectroscopy. <sup>[b]</sup>Determined by HPLC analysis. <sup>[c]</sup>16.6 h of reaction.

The initial tests of Cu-catalysed diethylzinc addition were performed in dichloromethane in the presence of Cu(acac)<sub>2</sub> from -46 °C to room temperature overnight. Ligand **1.46a** demonstrated the cleanest and most proficient reaction providing product **1.14a** in full conversion and 46% *ee* over 16 h (Table 3, Entry 1). The comparison of obtained HPLC data for **1.14a** and UV traces from reference<sup>34</sup> where the same column and condition were used for the analysis of **1.14a** allows assigning the absolute configuration of the product as (*S*)-**1.14a**. Such a practice of a preliminary assignment of absolute configuration is common and also conceded as inferred. The other tested ligands **1.46,i**, **1.48a**, and **2.4c** demonstrated lower activity furnishing **1.14a** in up to 65% conversion and 6–34% *ee* at the comparable conditions (Table 3, Entry 3–5). The decrease

of copper source and ligand loading from 5/10 mol% to 1/2 mol% led to slight erosion in enantioselectivity from 46% to 31% *ee* (Table 3, Entry 1 vs. 2). The control test without a catalyst still demonstrated the formation of racemic product **1.14a** in 27% in comparable conditions (Table 3, Entry 6). Therefore, the poor asymmetric induction provided by ligands **1.46a,i**, **1.48a**, and **2.4c** can be partially explained by a concurrent but non-selective background reaction which “dilutes” the final enantioselective outcome. Despite the unoptimized conditions and the presence of concurrent racemic process, ligand **1.46a** demonstrated promising activity for further investigations. The higher reaction rate, provided by ligand **1.46a**, can potentially be attributed either to H-bonding interactions or to zinc ligation to the phenolic fragment.



Scheme 20 Ligand **1.46a** in Rh-catalysed hydrogenation of methyl 2-acetamidoacrylate **3.9**.

The initial Rh-catalysed hydrogenation of methyl 2-acetamidoacrylate **3.9** was carried out in dichloromethane with 5 mol% of Rh(cod)<sub>2</sub>BF<sub>4</sub> and 10 mol% of ligand **1.46a** under approximately 4 bar of hydrogen gas pressure (Scheme 20). Unfortunately, no conversion of **3.9** was observed after 24 hours. The control experiment with TPP instead of the chiral trifunctional ligand **1.46a** afforded the product **3.10** in 40% conversion in comparable conditions. The low activity of **1.46a** may be due to the lack of hydrogen gas pressure or intrinsic steric hindrance of the ligand.

In summary, trifunctional H-bonding ligands **1.46a,i**, **1.48a**, and **2.4c** demonstrated some ability to transfer chirality in a copper-catalysed process, namely diethylzinc addition to chalcone **1.13a**. The ability of ligand **1.46a** to act in Rh catalysis was not observed in the initial test case.

### 3.3 Experimental

#### 3.3.1 General information

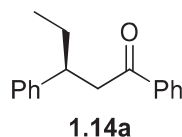
All reagents unless specified are commercially available and purified by standard procedures.<sup>35</sup> Chloroform-*d* was purchased from Cambridge Isotope Laboratories, USA and stored over anhydrous potassium carbonate before use. Air and moisture sensitive reactions were performed under nitrogen or argon atmosphere. Reactions were magnetically stirred and monitored by thin-layer chromatography (TLC) using Merck silica gel 60 F<sub>254</sub> aluminium pre-coated plates (0.25 mm). Flash column chromatography was performed on Merck silica gel 60 (0.015–0.040 mm). <sup>1</sup>H and <sup>13</sup>C, experiments were performed at 298 K on a Bruker DPX 400 MHz spectrometer equipped with a 5mm QNP probe. Chemical shifts were reported in ppm using the residual CHCl<sub>3</sub> peak as an internal reference ( $\delta_{\text{H}} = 7.26$  ppm,  $\delta_{\text{C}} = 77.16$  ppm). All spectra were processed using Bruker TOPSPIN software versions 4.0.7. HPLC analysis was performed using a Shimadzu Prominence system with CHIRALPAK<sup>®</sup> AD–H column. HPLC grade solvents were degassed before use. The peaks of enantiomers in UV traces were integrated and the enantiomeric excess was calculated by the formula:  $ee$  (%) = [(Area A – Area B) / (Area A + Area B)] \* 100%. The  $ee$  difference of less than 3% in the racemic case was considered as racemic. The H-bonding ligands **1.46a,i**, **1.48a**, and **2.4c** were synthesized by known procedures.<sup>36-39</sup>

#### 3.3.2 Experimental part

##### General procedure for Cu-catalysed diethylzinc addition

Ligand (4.8  $\mu\text{mol}$  or 0.96  $\mu\text{mol}$ ) and copper(II) 4-oxopent-2-ene-2-olate (63  $\mu\text{g}$ , 2.4  $\mu\text{mol}$  or 13  $\mu\text{g}$ , 0.48  $\mu\text{mol}$ ) were placed in a 2-mL amber, oven-dried vial as stock solutions in freshly distilled dichloromethane. The volume of dichloromethane was adjusted to 190  $\mu\text{L}$  and the mixture left to stir at room temperature for 1 h. Then chalcone **1.13a** (10 mg, 48  $\mu\text{mol}$ ) was

added as a stock solution in dichloromethane and the mixture left to stir at room temperature for another 30 min. Then the reaction mixture was pre-cooled to -75 °C (dry ice/acetone bath) and diethylzinc (17.8 mg, 144 μmol) was slowly added as 1 M solution in hexanes. The reaction mixture left to stir at -75 °C for 1.6 h and then the temperature was increased to -46 °C (dry ice/acetonitrile Dewar bath) and left to stir at gradually increasing temperature (due to melting of dry ice in acetonitrile) for 16 h. Then the reaction mixture was re-dissolved in ethyl acetate, and 5% hydrochloric acid was added with cooling (ice/acetone bath). The aqueous layer was extracted with ethyl acetate twice, and the combined organic layer was washed with brine, dried over magnesium sulfate, and concentrated *in vacuo*. A pure product **1.14a** sample for characterization was obtained on a silica gel pipette column (gradient hexane/ethyl acetate).



### **1,3-Diphenylpentan-1-one 1.14a**<sup>40</sup>

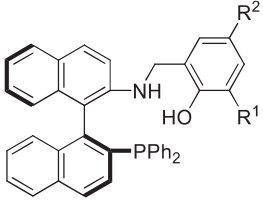
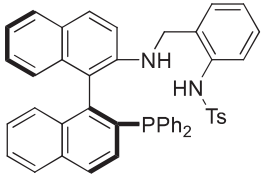
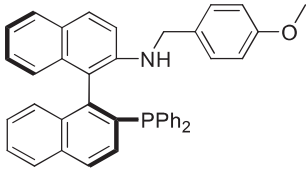
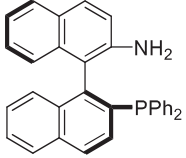
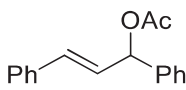
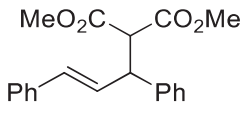
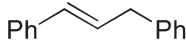
<sup>1</sup>H NMR (400 MHz, CDCl<sub>3</sub>) δ 0.81 (t, *J* = 7.3 Hz, 3H), 1.59–1.72 (m, 1H), 1.73–1.86 (m, 1H), 7.15–7.32 (m, 5H), 7.40–7.46 (m, 2H), 7.51–7.57 (m, 1H), 7.87–7.94 (m, 2H). HPLC conditions: CHIRALPAK<sup>®</sup> AD-H, 0.5 ml/min; 99.5% Hexane / 0.5% *i*PrOH, time: 23.52 min (*S*) and 31.30 (*R*). The integration error was determined as <1% based on the racemic standard.

### **General procedure for Rh-catalysed hydrogenation**

Ligand **1.46a** (3.5 mg, 6.3 μmol), bis(1,5-cyclooctadiene)rhodium(I) tetrafluoroborate (1.3 mg, 3.1 μmol), methyl 2-acetamidoacrylate **3.9** (15 mg, 0.1 mmol), and freshly distilled dichloromethane (1 mL) were placed in a an Ace-glass pressure tube with an equalizing tube connected to a T-shape adapter. One T-adapter shoulder was attached to the vacuum line, and the second shoulder was attached to a hydrogen gas balloon and to a bubbler. The reaction was purged with vacuum/hydrogen gas three times at room temperature. Then the pressure tube was immersed into a liquid nitrogen bath and refilled with hydrogen gas until the bubbler was

bubbling. When the bubbling stopped, the pressure tube was sealed. The reaction mixture was left to stir at 26 °C for 24 h, then the reaction pressure was equalized to 1 atm, and the mixture was concentrated *in vacuo* yielding unreacted starting material **3.9**.

### 3.4 Cross Reference of Compounds in Manuscript and Thesis

Structure	Number in Manuscript	Number in thesis
	<p><math>R_1 = R_2 = H</math> (<b>1</b>)</p> <p><math>R_1 = H; R_2 = 'Bu</math> (<b>2</b>)</p> <p><math>R_1 = 'Bu; R_2 = Br</math> (<b>3</b>)</p> <p><math>R_1 = F; R_2 = Br</math> (<b>4</b>)</p>	<p><b>1.46:</b></p> <p><math>R_1 = R_2 = H</math> (<b>a</b>)</p> <p><math>R_1 = H; R_2 = 'Bu</math> (<b>d</b>)</p> <p><math>R_1 = 'Bu; R_2 = Br</math> (<b>i</b>)</p> <p><math>R_1 = F; R_2 = Br</math> (<b>h</b>)</p>
	<b>5</b>	<b>1.48a</b>
	<b>6</b>	<b>1.46l</b>
	<b>7</b>	<b>1.49</b>
	<b>8</b>	<b>3.1a</b>
	<b>9</b>	<b>3.2aa</b>
	<b>10</b>	<b>3.9</b>

### 3.5 References

1. T. Tanaka and M. Hayashi, *Synthesis*, 2008, **2008**, 3361-3376.
2. W. Cao, X. Feng and X. Liu, *Org. Biomol. Chem.*, 2019, **17**, 6538-6550.
3. I. P. Beletskaya, C. Nájera and M. Yus, *Chem. Rev.*, 2018, **118**, 5080-5200.
4. B. M. Trost and D. L. Van Vranken, *Chem. Rev.*, 1996, **96**, 395-422.
5. B. M. Trost and M. L. Crawley, *Chem. Rev.*, 2003, **103**, 2921-2944.
6. B. M. Trost, M. R. Machacek and A. Aponick, *Acc. Chem. Res.*, 2006, **39**, 747-760.
7. I. Guerrero Rios, A. Rosas-Hernandez and E. Martin, *Molecules*, 2011, **16**, 970-1010.
8. Š. Vyskočil, M. Smrčina, V. Hanuš, M. Polášek and P. Kočovský, *J. Org. Chem.*, 1998, **63**, 7738-7748.
9. I. J. S. Fairlamb, G. C. Lloyd-Jones, Š. Vyskočil and P. Kočovský, *Chem. Eur. J.*, 2002, **8**, 4443-4453.
10. G. C. Lloyd-Jones, S. C. Stephen, M. Murray, C. P. Butts, Š. Vyskočil and P. Kočovský, *Chem. Eur. J.*, 2000, **6**, 4348-4357.
11. L. Gouriou, G. C. Lloyd-Jones, Š. Vyskočil and P. Kočovský, *J. Organomet. Chem.*, 2003, **687**, 525-537.
12. Y. Wang, H. Guo and K. Ding, *Tetrahedron: Asymmetry*, 2000, **11**, 4153-4162.
13. Y. Wang, X. Li and K. Ding, *Tetrahedron Lett.*, 2002, **43**, 159-161.
14. M. Kawamura, R. Kiyotake and K. Kudo, *Chirality*, 2002, **14**, 724-726.
15. P. Kočovský, Š. Vyskočil, I. Čísařová, J. Sejbal, I. Tišlerová, M. Smrčina, G. C. Lloyd-Jones, S. C. Stephen, C. P. Butts, M. Murray and V. Langer, *J. Am. Chem. Soc.*, 1999, **121**, 7714-7715.
16. H. Kodama, T. Taiji, T. Ohta and I. Furukawa, *Tetrahedron: Asymmetry*, 2000, **11**, 4009-4015.
17. N. R. Mote and S. H. Chikkali, *Chem. - Asian J.*, 2018, **13**, 3623-3646.
18. S. Liao, X.-L. Sun and Y. Tang, *Acc. Chem. Res.*, 2014, **47**, 2260-2272.
19. R. Kenny and F. Liu, *Chem. Rec.*, 2017, **17**, 535-553.
20. X. Fang and C.-J. Wang, *Chem. Commun.*, 2015, **51**, 1185-1197.
21. X. Lu and L. Deng, in *Cooperative Catalysis*, ed. R. Peters, 2015, pp. 145-170.
22. Y.-W. Sun, J.-J. Jiang, M.-X. Zhao, F.-J. Wang and M. Shi, *J. Organomet. Chem.*, 2011, **696**, 2850-2856.
23. G. Romanazzi, L. Degennaro, P. Mastrorilli and R. Luisi, *ASC Catal.*, 2017, **7**, 4100-4114.
24. S. Krautwald and E. M. Carreira, *J. Am. Chem. Soc.*, 2017, **139**, 5627-5639.
25. D. S. Clyne, Y. C. Mermet-Bouvier, N. Nomura and T. V. RajanBabu, *J. Org. Chem.*, 1999, **64**, 7601-7611.
26. N. Nomura, Y. C. Mermet-Bouvier and T. V. RajanBabu, *Synlett*, 1996, **1996**, 745-746.
27. A. Togni, U. Burckhardt, V. Gramlich, P. S. Pregosin and R. Salzmann, *J. Am. Chem. Soc.*, 1996, **118**, 1031-1037.
28. T. Hayashi, K. Kanehira, T. Hagihara and M. Kumada, *J. Org. Chem.*, 1988, **53**, 113-120.
29. O. Hoarau, H. Aït-Haddou, J.-C. Daran, D. Cramailère and G. G. A. Balavoine, *Organometallics*, 1999, **18**, 4718-4723.
30. H. Aït-Haddou, O. Hoarau, D. Cramailère, F. Pezet, J.-C. Daran and G. G. A. Balavoine, *Chem. Eur. J.*, 2004, **10**, 699-707.
31. M. Sawamura and Y. Ito, *Chem. Rev.*, 1992, **92**, 857-871.
32. T. Hayashi, A. Yamamoto, Y. Ito, E. Nishioka, H. Miura and K. Yanagi, *J. Am. Chem. Soc.*, 1989, **111**, 6301-6311.
33. T. Hayashi, K. Kishi, A. Yamamoto and Y. Ito, *Tetrahedron Lett.*, 1990, **31**, 1743-1746.
34. X. Hu, H. Chen and X. Zhang, *Angew. Chem., Int. Ed.*, 1999, **38**, 3518-3521.

35. W. L. F. Armarego and C. L. L. Chai, *Purification of Laboratory Chemicals, 6th Edition*, Butterworth-Heinemann, 6 edn., 2009.
36. J.-M. Garnier, C. Anstiss and F. Liu, *Adv. Synth. Catal.*, 2009, **351**, 331-338.
37. J.-M. Garnier and F. Liu, *Org. Biomol. Chem.*, 2009, **7**, 1272-1275.
38. C. Anstiss and F. Liu, *Tetrahedron*, 2010, **66**, 5486-5491.
39. S. S. Eliseenko and F. Liu, *Tetrahedron*, 2019, **75**, 518-526.
40. H. Yu, F. Xie, Z. Ma, Y. Liu and W. Zhang, *Org. Biomol. Chem.*, 2012, **10**, 5137-5142.



## **CHAPTER 4**

### **MAP-based Catalytic Systems**

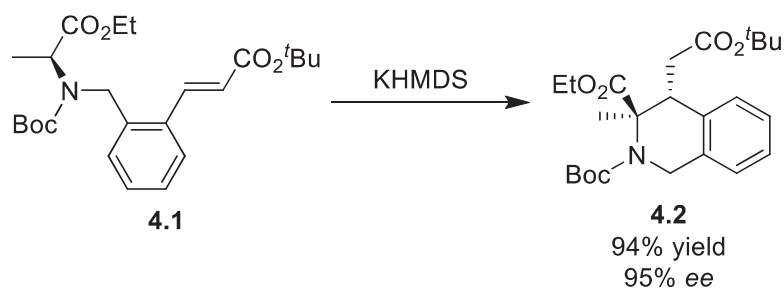
#### **for Cascade Chirality Transfer in Model Reactions**

## CHAPTER 4. MAP-based Catalytic Systems for Cascade Chirality Transfer in Model Reactions

### 4.1 Introduction

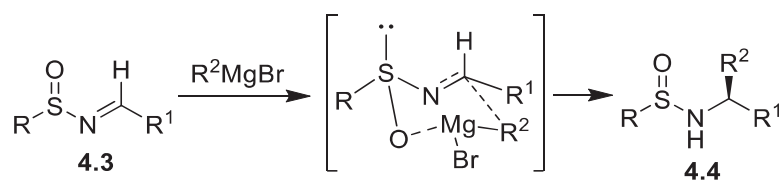
#### 4.1.1 Chirality induction from non-racemic substrates

One of the strategies for the introduction of multiple stereocenters is the use of non-racemic substrates in stereoselective synthesis.<sup>1</sup> In this strategy, the chirality of starting material can be transferred to new asymmetric centers with or without transformation of the original chiral element.<sup>2, 3</sup> The chirality transfer from non-racemic substrates as a variation of the chiral auxiliary strategy has a diverse set of approaches. Main approaches of chiral transfer include 1) atroposelective synthesis which is commonly used for the generation of compounds with axial chirality;<sup>4, 5</sup> 2) self-regeneration of stereocenters;<sup>6, 7</sup> 3) memory of chirality (MOC)<sup>8, 9</sup> that occurs through trigonalized “pseudo-chiral” intermediates; 4) axial-to-central chirality transfer<sup>3, 10</sup> where chiral allenes are mostly used as precursors; 5) stereochemical relay<sup>11</sup> for the stereocontrol over long-chain molecules; and 6) intermolecular chiral transfer.<sup>2</sup> Despite the established reactivity protocols and accumulated research data, these approaches are not always useful for a target stereoselective synthesis as they occur with the transformation of the original chiral center. An example of MOC approach in which the nature of original tertiary chiral element has been transformed with the generation of a new chiral center is presented in Scheme 21.<sup>12</sup> The intramolecular conjugate addition of chiral acrylate **4.1** afforded the highly enantioselective formation of hydroisoquinoline cycle **4.2** with two chiral centers (Scheme 21)



Scheme 21 Example of MOC approach with the transformation of the initial chirality element.

The processes where a non-racemic molecule serves as a chiral auxiliary and also becomes a part of the product structure can be advantageous for the syntheses of molecules with multiple chiral centers. A seminal demonstration of this approach is Cram's chelation model.<sup>13-15</sup> This model was later applied in combination with sulfinimines auxiliary **4.3** in asymmetric amines **4.4** synthesis (Scheme 22).<sup>16, 17</sup>



Scheme 22 Example of the chelation model with maintained nature of the initial chiral center.

Multistep processes in which a chiral center is initially formed by asymmetric catalysis and later serves as an auxiliary in the following steps can be developed with higher efficiency for synthetic utility, as well as model systems for investigating the catalytic organization. In these models, the catalyst may initially transfer the chirality to an intermediate and at later steps can dynamically interact with the pre-formed chiral auxiliary providing highly enantioenriched molecules bearing multiple chiral centers. However, the design of such processes is challenging because of the limited reaction scope from single catalysts and condition compatibility issues in multistep reactions.

#### 4.1.2 Design of processes with complex catalytic organisation

The ability to actively exploit the chirality of the substrates in asymmetric catalytic reactions may lead to new and more efficient synthesis of molecules bearing multiple chiral centers. In a cascade or sequential reaction, the chirality of the substrate, formed *in situ*, may act as an intrinsic chiral bias that influences the formation of subsequent chiral centers on the same substrate, as well as serving as a chiral ligand to interact with the chiral catalyst. The determinants of the stereo-outcome will be complex but may be primarily attributed to two factors: (a) the enantio-biasing effect of the chiral substrate/intermediate and (b) the diastereoselectivity of the subsequent reaction steps. Synergistic relationships between the two factors will likely lead to one dominant enantiomer (high enantioselectivity coupled to high diastereoselectivity).

The trifunctional MAP-based catalytic system **1.46a** is investigated here as a good candidate for designing these hybrid models. First, this catalyst provides highly enantioselective and fast *aza*-MBH reactions at ambient temperature.<sup>18-23</sup> The densely functionalized *aza*-MBH adducts may become excellent chiral intermediates as well as auxiliaries for further modifications during a cascade or a sequential process (Figure 8). Functional groups such as a terminal enone or allylamine provide an opportunity for diverse addition and substitution processes. Moreover, the appropriate R' substituent in the aromatic cycle can enable further intramolecular reactions in a cascade manner.

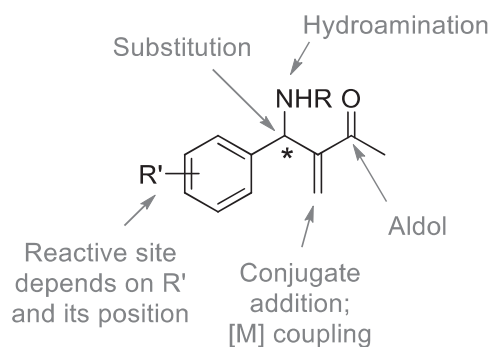


Figure 8 Potential of *aza*-MBH adducts as intermediates and ligands/auxiliaries in multistep processes.

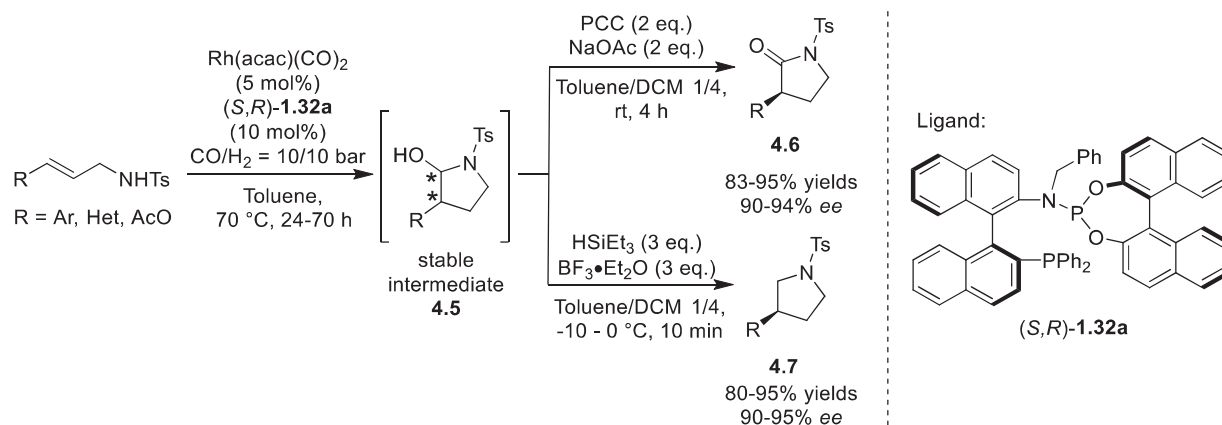
Secondly, trifunctional MAP-based catalytic structures demonstrated catalytic dualism and provided both asymmetric organocatalysis<sup>18, 20, 23, 24</sup> and organometallic catalysis (see Chapter 3). The development of a cascade or a sequential process where a single catalyst provides organo- and metal-catalysed processes is an extraordinarily challenging task and would be the first and unique example of such a type of highly organised catalysis.

#### 4.1.3 MAP-based structures as catalysts in cascade or sequential processes

Despite the intensive investigation of MAP-based ligands in asymmetric metal-catalysed reactions, the reports of a cascade or one-pot reactions with metal/MAP complexes were limited and published two decades after the first MAP synthesis.

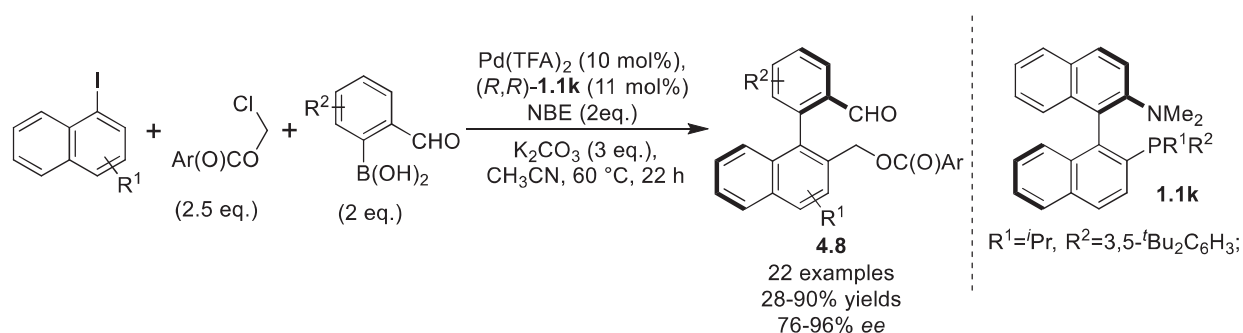
An elegant protocol of one-pot interrupted asymmetric Rh-catalysed hydroaminomethylation (HAM) was reported by Zhang *et al.* using (*S,R*)-**1.32a** as a ligand (Scheme 23).<sup>25</sup> The unavoidable racemization of the iminium intermediate due to a water molecule elimination is common for HAM processes. The described protocol converted the chiral hemiacetal intermediate **4.5** into stable products **4.6** and **4.7** preventing the iminium racemization. The corresponding pyrrolidinones **4.6** (oxidative pathway) and pyrrolidines **4.7** (reductive pathway) were obtained in more than 90% *ee* in most cases (Scheme 23). However, the role of the (*S,R*)-

**1.32a** is limited to the asymmetric hydroformylation step. The ligand does not participate in or influence the following oxidation or reduction stage.



Scheme 23 Cascade of hydroaminomethylation interrupted by oxidation and reduction.

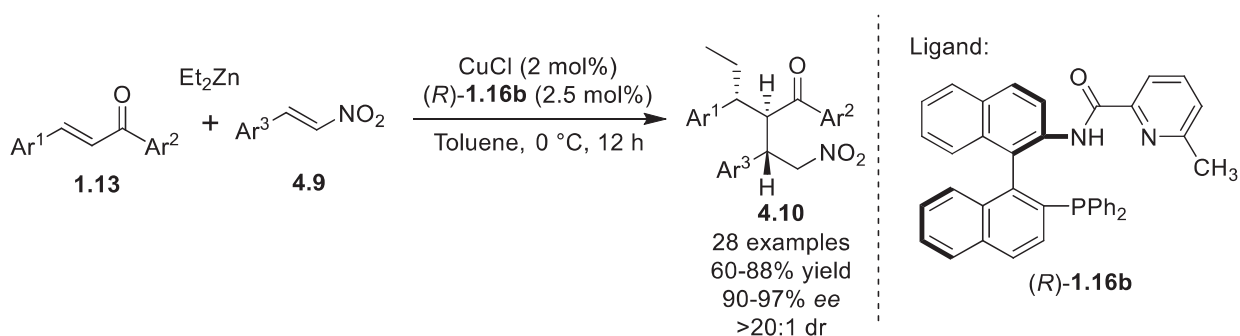
Another example<sup>26</sup> is a three-component cross-coupling cascade providing biaryl atropoisomers **4.8**. (*R,R*)-**1.1k**/Pd-norbornene co-catalytic system was used in the process, furnishing the aldehyde products **4.8** in 28–90% yields and 76–96% *ee* (Scheme 24). (*R,S*)-**1.1k** was also tested in the reaction and demonstrated no enantioselectivity at a slightly lower yield. It was proposed that the (*R,S*)-**1.1k** palladium complex participates in both norbornene co-catalysed Cattelani-type and the following Suzuki steps.



Scheme 24 Pd-catalysed three-component cross-coupling cascade.

The latest example of a tandem double Michael addition was reported by Hu *et al.*<sup>27</sup> The sequence includes the initial Cu-catalysed diethylzinc addition to a chalcone **1.13** followed by trapping of a nitrostyrene **4.9**. This tandem reaction afforded molecules **4.10** with three chiral

centers in excellent diastero- and enantioselectivity (Scheme 25). The catalyst **1.16b** participates in the initial Cu-catalysed diethylzinc addition step and, most probably, is not involved in the subsequent step. However, this hypothesis requires additional substrate-controlled investigations.



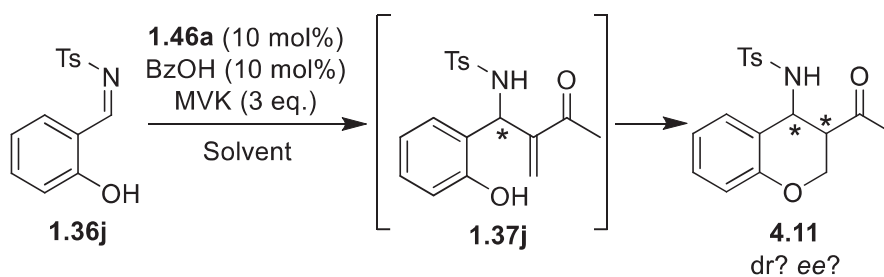
Scheme 25 Asymmetric tandem double Michael reactions catalysed by (*R*)-**1.16b**.

In conclusion, so far only a very limited number of reports describe cascade reactions catalysed by MAP-based structures. In these cases, MAP representatives serve only as ligands, and there are no cascade or sequential processes in which MAP-based systems participate as an organocatalyst and/or as a ligand.

#### 4.1.4 Chapter 4 goals and plan

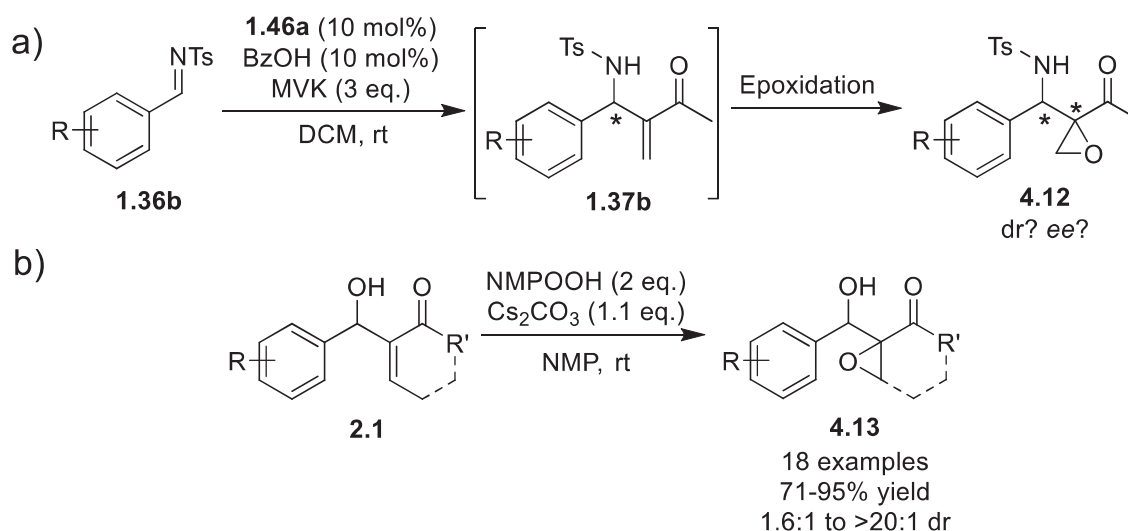
This chapter focuses on the investigation of the organization potential of the trifunctional MAP-based catalysts to transfer chirality from the initially generated benzylic chirality in *aza*-MBH intermediate through the following steps into more complex products with chiral centers.

The first model is the simplest *aza*-MBH initiated cascade reaction that is based on the use of an *ortho*-substituted *N*-tosyl benzaldimine **1.36j** possessing a nucleophilic hydroxy fragment (Scheme 26). This nucleophilic hydroxy group in *ortho*-position, after the formation of the *aza*-MBH adduct **1.37j**, would be capable of an intramolecular attack to the enone fragment providing the cyclized cascade product **4.11**. Such cascades have been previously reported, however only as racemic processes (Scheme 26).<sup>28-30</sup>



Scheme 26 Proposed *aza*-MBH / nucleophilic cyclization cascade.

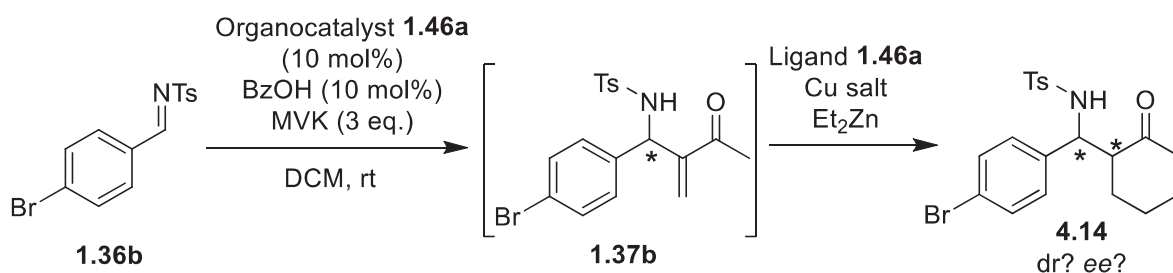
The next step of the investigation will expand from an intramolecular cyclisation to an intermolecular oxidation reaction in a consecutive *aza*-MBH / epoxidation process. The initial formation of a chiral *aza*-MBH adduct **1.37b** between a benzaldimine **1.36b** and MVK is followed by the base-catalysed epoxidation step (Scheme 27a). The enantioselectivity of diastereomers **4.12** will depend on the chiral center of **1.37b** and may also be influenced by the trifunctional catalysts that can provide chelating groups. The epoxidation of racemic MBH adducts **2.1** derived from aldehydes and various activated alkenes was reported previously (Scheme 27b).<sup>31</sup>



Scheme 27 a) Proposed chiral *aza*-MBH / epoxidation sequential process; b) Racemic epoxidation of MBH adducts **2.1**.

The last investigation of organizational catalytic behaviour of MAP-based structures involves metal species in an *aza*-MBH / diethylzinc addition sequential process. As discussed in Chapter

1, Cu-catalysed processes, including the addition of organozinc reagents, are common models for the catalytic dualism investigation. The MAP-based trifunctional system **1.46a** could serve as an organocatalyst during the asymmetric *aza*-MBH step and then participate as a ligand for the Cu-complex in asymmetric diethylzinc addition step that may also be influenced by the chirality of the *aza*-MBH-adduct **1.37b** intermediate (Scheme 28).



Scheme 28 Proposed chiral *aza*-MBH / diethylzinc addition dual catalytic sequential process.

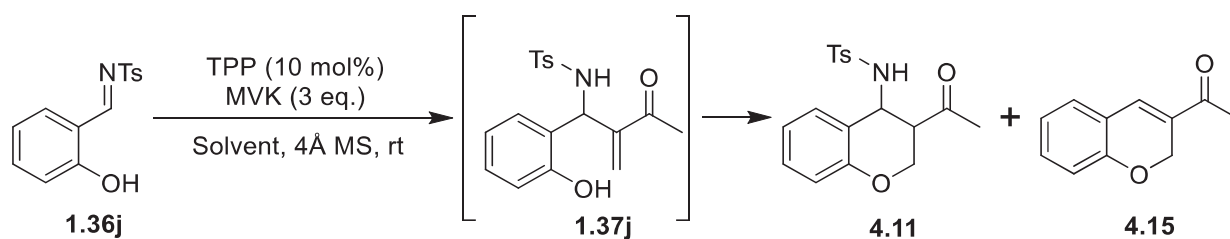
To the best of our knowledge, there have been no prior reports in which a single catalytic structure serves as a chiral organocatalyst and as a chiral ligand in the frame of one process. Such a new level of catalytic organization is extremely challenging to design and achieve by a singular catalyst but can be readily tested in the *aza*-MBH / diethylzinc addition sequential process that may become a unique example of a highly organized hybrid catalysis.

## 4.2 Results and Discussion

### 4.2.1 Trifunctional system in an *aza*-MBH / nucleophilic addition cascade

A known *aza*-MBH / nucleophilic cyclization cascade (Table 4, Scheme) was chosen for the initial investigation of the trifunctional systems organisational ability. The cascade was previously reported<sup>30</sup> and performed in a racemic manner.

Table 4 Conditions investigation for *aza*-MBH / nucleophilic addition cascade.



Entry	Solvent	Time [h]	Conv <sup>a</sup> to <b>1.37j</b> , [%]	Conv <sup>a</sup> to <b>4.11</b> , [%] ( <i>anti/syn</i> ) <sup>a</sup>	Conv <sup>a</sup> to <b>4.15</b> , [%]
1	DCM	24	9.7	42.1 (1.8 : 1)	<5%
2	THF	24	<5%	89.0 (2.92 : 1)	9.5
3	Diethyl ether	24	<5%	32.7 (2.82 : 1)	66.4
4	Toluene	24	no	91.8 (3.4 : 1)	8.2

<sup>[a]</sup>Calculated by <sup>1</sup>H NMR spectroscopy.

The initial racemic test of the cascade was carried out with triphenylphosphine (TPP) as the catalyst. A limited solvent screen was carried out, and toluene was found as the optimal solvent for conversion to the cyclized product **4.11** (Table 4, Entries 1–4). Dichloromethane, while an efficient solvent for the *aza*-MBH processes, provided poor conversion of the starting imine **1.36j** to the product **4.11** over 24 h (Table 4, Entry 1). Diethyl ether facilitated the tosylamide elimination from the cyclized product **4.11**, converting 66% of the starting imine to the elimination side-product **4.15** (Table 4, Entry 3). The reactions in THF and toluene provided the comparable results furnishing **4.11** in 89 and 92% conversion, respectively, over 24 h. However, the diastereomeric ratio of the product **4.11** was slightly higher for the reaction in toluene (Table 4, Entries 2 and 4). The diastereoselectivity of the product **4.11** formed in toluene was found as 3.4 to 1 with the major *anti* diastereomer (Table 4, Entry 1). The sense of diastereoselectivity has been confirmed by the comparison of isolated diastereomers with the reference<sup>30</sup> NMR and X-Ray data and calculated by integration of the following <sup>1</sup>H NMR signals: a quadruplet at 3.27 ppm for *anti*, and by a multiplet at 3.05 ppm for *syn* isomer (Figure 9 for <sup>1</sup>H NMR proton

patterns). The level of the diastereomeric ratio is lower than the reported previously for the cascade in toluene where product **4.11** was obtained as 7:1 *anti* : *syn* diastereomers.<sup>30</sup> Such a significant discrepancy may be due to the reaction conditions here with 4Å molecular sieves and triple excess of methyl vinyl ketone.

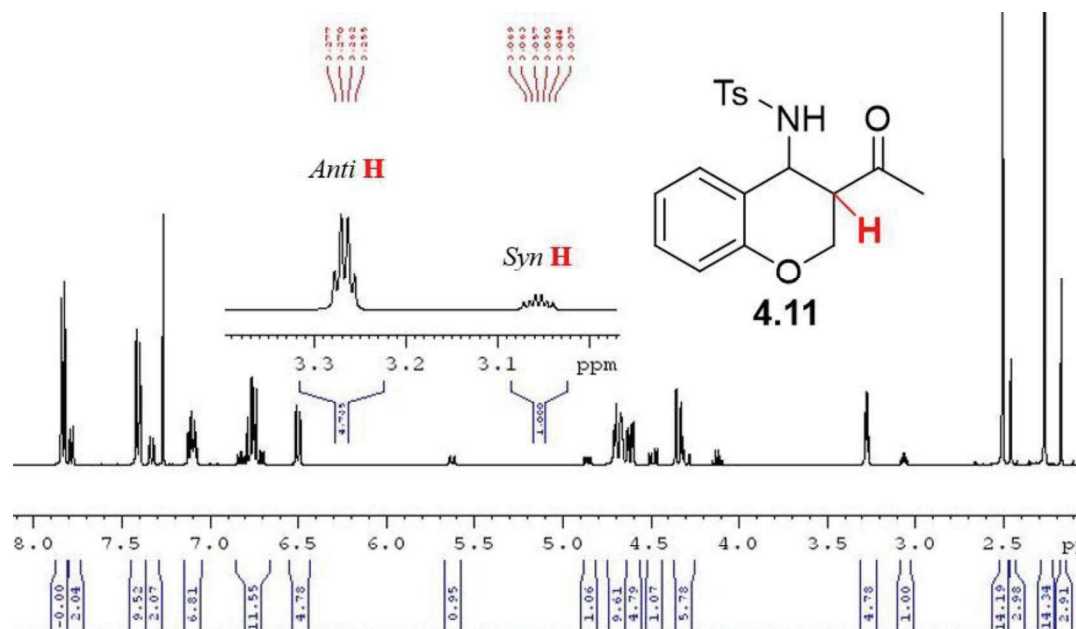
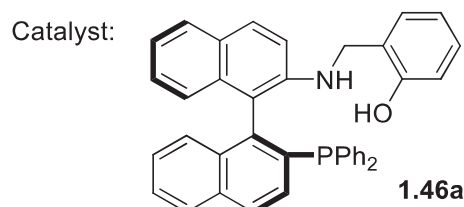
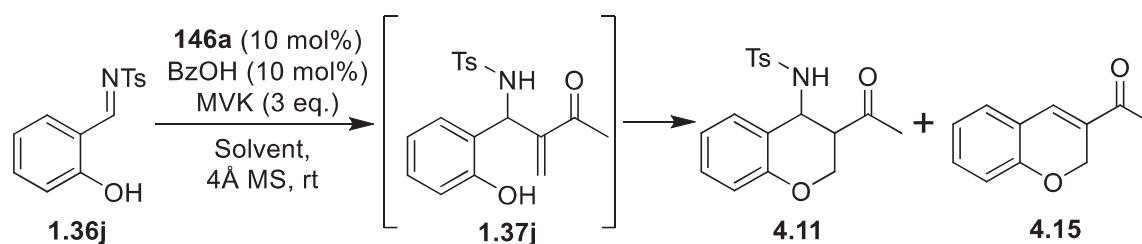


Figure 9 <sup>1</sup>H NMR spectra of **4.11** in CDCl<sub>3</sub> indicating key proton patterns for *anti/syn* diastereomers assignment.

With the racemic control conditions in hand, model trifunctional system **1.46a** was next tested in DCM and toluene with benzoic acid as the activator (Table 5, Scheme). In DCM, reaction version showed poor conversion providing the product **4.11** in only 15% conversion and 1.4:1 dr over 24 h (Table 5, Entry 1). In toluene, the reaction rate was slightly higher furnishing the product **4.11** in 22% conversion over 24 h (Table 5, Entry 2). The reaction in toluene was further continued at 50 °C for 65 h when conversion to **4.11** reached 86% (Table 5, Entry 3). The elimination side product **4.15** was also detected (8.3% conv.).

Table 5 Test of trifunctional organocatalyst **1.46a** in *aza*-MBH / nucleophilic addition cascade.



Entry	Solvent	Time [h]	Conv <sup>a</sup> to <b>1.37j</b> , [%]	Conv <sup>a</sup> to <b>4.11</b> , [%] ( <i>anti/syn</i> . <sup>a</sup> ); <i>lee</i>	Conv <sup>a</sup> to <b>4.15</b> , [%]
1	DCM	24	8.6	15 (1.4 : 1) /n.d./	no
2	Toluene	24	10.8	22 (2.4 : 1) /n.d./	no
3	Toluene	65 <sup>b</sup>	<5%	86.3 (3.5 : 1) / <i>rac</i> /	8.3

<sup>[a]</sup>Calculated by <sup>1</sup>H NMR spectroscopy. <sup>[b]</sup>28h at room temperature then 65 h at 50 °C.

HPLC analysis of product **4.11** demonstrated the equal amount of enantiomers for the major *anti*-diastereomer indicating that it was obtained as a racemic mixture (Figure 10). The *ortho*-positioned hydroxyl of the substrate **1.36j** may form an internal H-bond between the hydroxyl and imine fragments that interferes with the subtle H-bonding system built by the chiral catalyst **1.46a** during the *aza*-MBH catalysis and could lead to the erosion and complete loss of the reaction enantioselectivity.

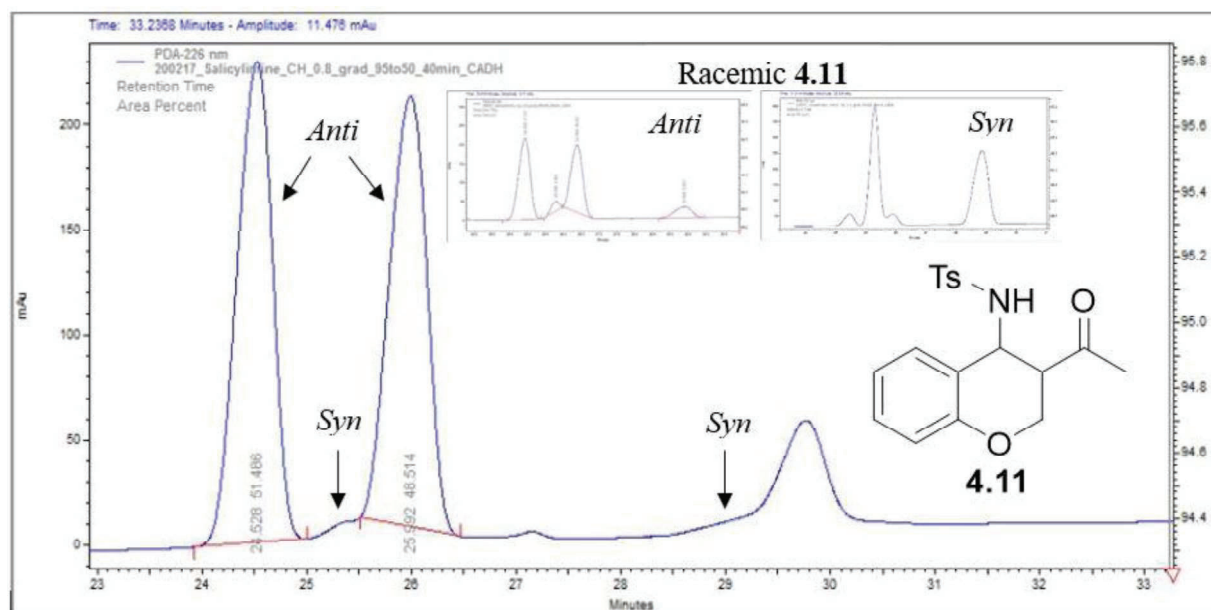
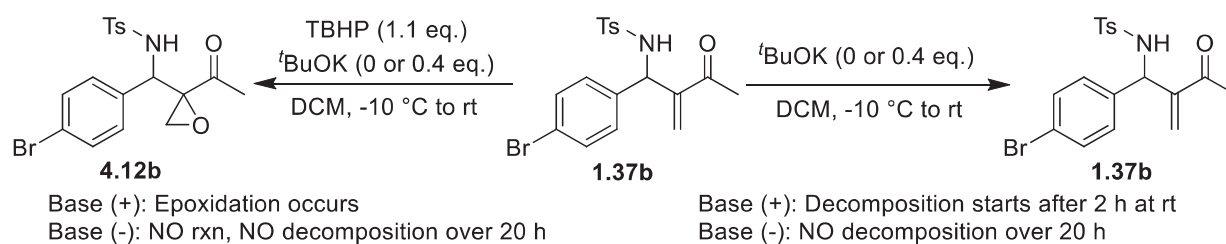


Figure 10 HPLC traces of product **4.11**, obtained from the **1.46a**-catalysed cascade.

#### 4.2.2 Trifunctional system in an aza-MBH / epoxidation sequential process

Based on a literature precedent,<sup>31</sup> the epoxidation of MBH adducts **2.1** required a base as a catalyst for hydroperoxide activation (Scheme 27b). At the same time, a base and a hydroperoxide may induce the decomposition of the intermediate *aza*-MBH adduct **1.37b**. Therefore, the effect of a base on the reaction and *aza*-MBH adduct **1.37b** decomposition was initially investigated (Scheme 29). The control (with or without the addition of 0.4 equivalents of potassium *tert*-butoxide, Scheme 29, right arrow) demonstrated no decomposition of the *aza*-MBH adduct **1.37b** in basic conditions during the first 2 h at room temperature. However, after 20 h decomposition of **1.37b** was observed. It should be noted that without a base, *aza*-MBH adduct **1.37b** did not decompose in dichloromethane even over 20 h at room temperature (Scheme 29, right arrow). The reaction with the base and hydroperoxide addition demonstrated the formation of the product **4.12b** in 30 minutes at room temperature without any decomposition (Scheme 29 left).



Scheme 29 *aza*-MBH adduct **1.37b** decomposition investigation in epoxidation conditions.

The next question was whether the reaction sequence could be performed in one step or one-pot. Unfortunately, the formation of the *aza*-MBH product **1.37b** was not detected in the presence of the base and TBHP. Thus, *aza*-MBH reaction was performed first between *N*-tosyl-*p*-bromobenzaldimine **1.36b** and MVK in dichloromethane at room temperature (Scheme 30). After the full conversion of the starting imine to the *aza*-MBH adduct, potassium *tert*-butoxide in THF and TBHP were added to the pre-cooled (ice/acetone bath) reaction mixture and left to stir for 45 minutes at room temperature, providing the desired epoxide product **4.12b** in 2.4 : 1 dr.

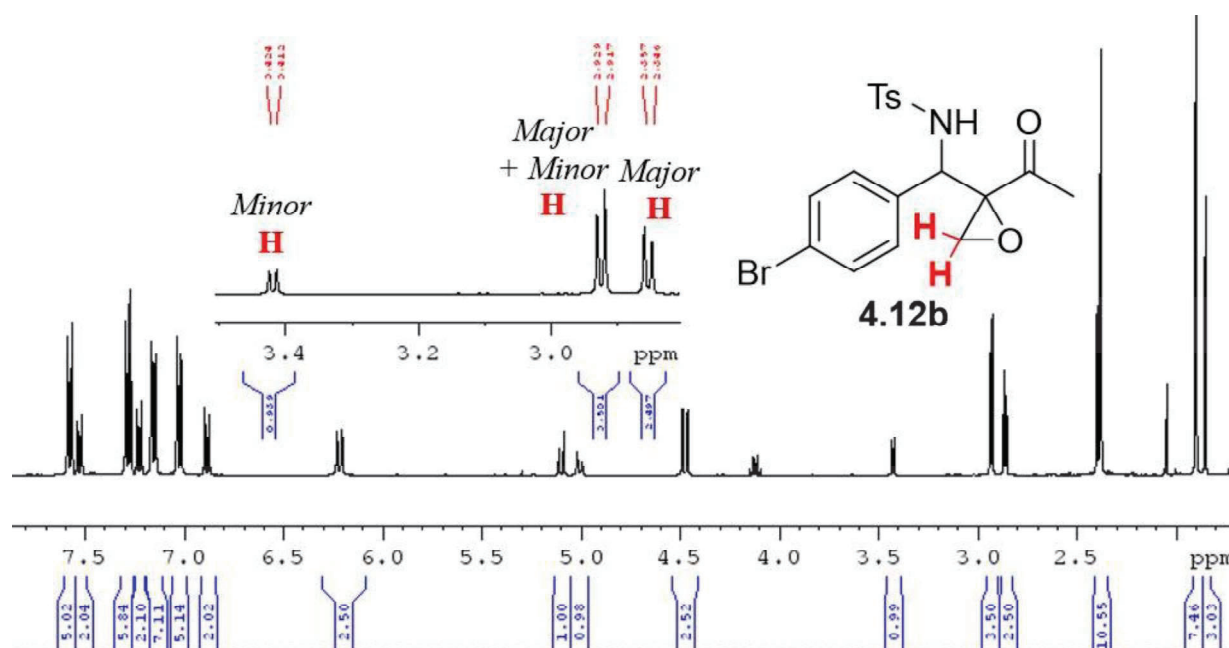
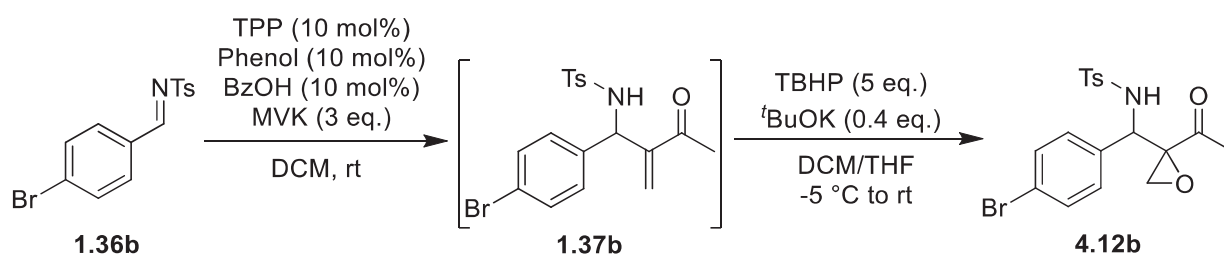


Figure 11 <sup>1</sup>H NMR spectra of **4.12b** in CDCl<sub>3</sub> indicating key proton patterns for diastereomers assignment.

Figure 11 shows the **4.12b** key proton patterns for both major diastereomer at 2.85 (d) and 2.91 (d) ppm ( $J = 4.5$  Hz) and minor diastereomer at 2.91 (d) and 3.41 (d) ppm ( $J = 4.6$  Hz). This pattern is similar for all other **4.12** structures.

The significant excess (5 equivalents) of TBHP was used to increase the rate of epoxidation and shorten the time of the *aza*-MBH intermediate **1.37b** in the basic environment to avoid its decomposition. However, product **4.12b** was isolated in only 41% yield after purification on silica gel. The low yield may be partially attributed to a decomposition of the product during purification as ring-opening of epoxides on silica gel is a known process and can occur in the presence of amines.<sup>32</sup>



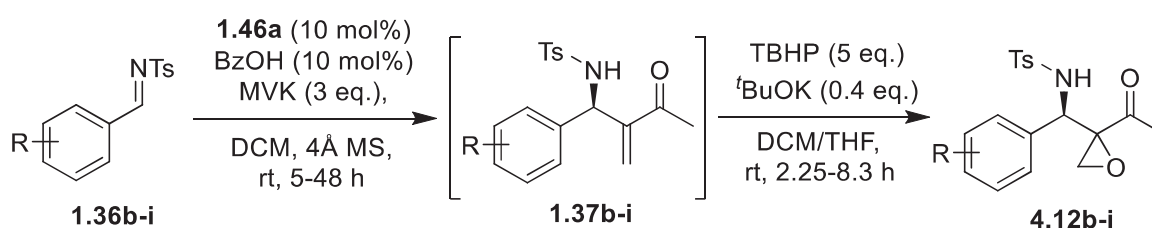
Scheme 30 Model racemic conditions for the MBH / epoxidation sequential process.

With the optimised protocol in hand, a set of *N*-tosylbenzaldimines **1.36b-i** using **1.46a** as the chiral catalyst were subjected to this *aza*-MBH / epoxidation sequence (Table 6).

The chiral sequential tests provided epoxides **4.12b-i** with no diastereoselectivity (1:1 in most cases) that demonstrates the detrimental effect of **1.46a** compared to TPP. This difference may potentially indicate the participation of **1.46a** or TPP in the epoxidation process. Low diastereoselectivity in general could also be explained by the sterically unrestricted rotation of the  $\beta$ -peroxyenolate intermediate. This was observed in the formation of epoxides derived from acyclic MBH adducts **2.1** earlier.<sup>31</sup> The enantioselectivity of epoxides **4.12b-i** is comparable to the *ee* levels of the corresponding *aza*-MBH intermediates **1.37b-i** (Table 6). This may suggest that the enantiomeric excess of the initially formed *aza*-MBH adducts was transferred to the final epoxides. In most cases, it was difficult to separate all four peaks from the enantiomeric pairs of

the epoxide **4.12b-i** completely on the HPLC even though a set of chiral columns (CHIRALPAK® AD-H, Regis Chiral Technologies Whelk-O1, Phenomenex Lux® 5  $\mu$ m Amylose-1, Advanced Separation Technology Inc. Cyclobond I 2000 SN) was screened. However, *m*-nitro- **4.12d** and *o*-chloro **4.12h** substituted epoxides unambiguously demonstrated comparable enantioselectivity of both diastereomers (Table 7, Entries 7, 4).

Table 6 Test of trifunctional organocatalyst **1.46a** in an *aza*-MBH / epoxidation sequence.



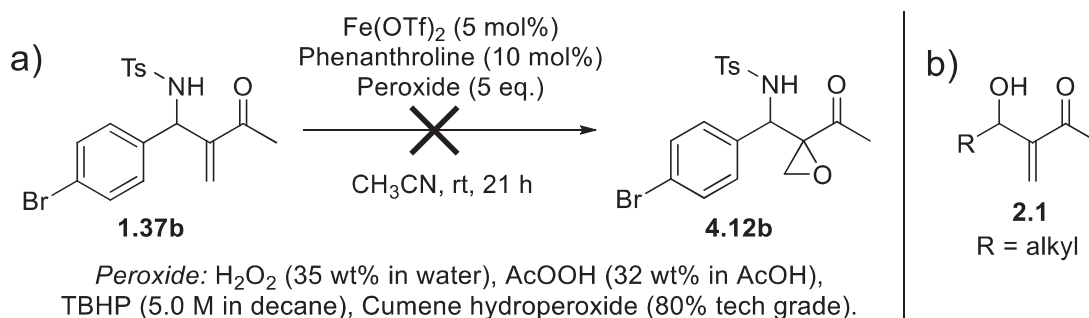
Entry	R	Time of <i>aza</i> -MBH step, [h]	<i>ee</i> of MBH adduct <b>1.37</b> , [%] <sup>c</sup>	Time of Epoxidation step, [h]	Yield of <b>4.12</b> , [%] <sup>a</sup>	dr <sup>b</sup>	<i>ee</i> major (minor), [%] <sup>c</sup>
1	<i>p</i> -Br ( <b>b</b> )	22	86	2.3	63	1.2/1	84 (n.d.)
2	<i>p</i> -NO <sub>2</sub> ( <b>c</b> )	5	81	2.25	46	1.25/1	85 (n.d.)
3	<i>m</i> -NO <sub>2</sub> ( <b>d</b> )	5	81	2.25	51	1/1	83 (84)
4	<i>o</i> -NO <sub>2</sub> ( <b>e</b> )	48	74	8.3	49	1/1	n.d (n.d)
5	<i>p</i> -F ( <b>f</b> )	48	85	3.5	41	1/1	88 (n.d.)
6	<i>p</i> -Cl ( <b>g</b> )	22	89	2.3	26	1/1	91 (n.d.)
7	<i>o</i> -Cl ( <b>h</b> )	48	72	2.8	38	1/1	71 (72)
8	<i>p</i> -Me ( <b>i</b> )	48	77	5	11	1/1	n.d (n.d)

<sup>[a]</sup>Isolated yield after column chromatography. <sup>[b]</sup>Calculated by <sup>1</sup>H NMR spectroscopy of crude mixtures.

<sup>[c]</sup>Determined by HPLC.

The (*R,S*)-**4.12** and (*R,R*)-**4.12** were proposed as major enantiomers based on the predominant formation of (*R*)-**1.37** in the *aza*-MBH step. The epoxidation in this sequence required a longer time for complete conversion to **4.12** than that for the racemic control with TPP, and partial decomposition of *aza*-MBH intermediates in the basic conditions was observed. The poor

yielding of the epoxides **4.12b-i** (11–63% isolated yields) can also be partially attributed to the decomposition of epoxides **4.12** during purification on silica gel.



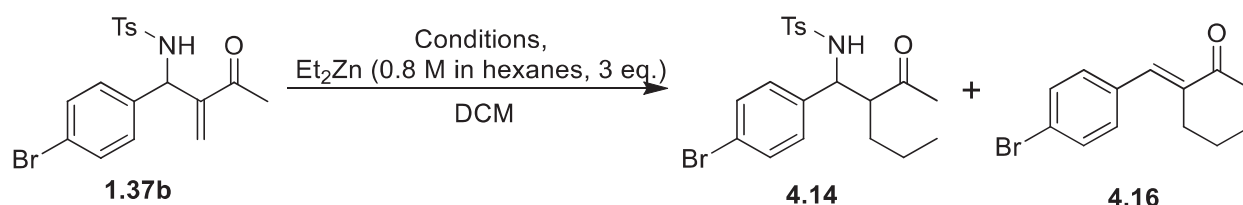
Scheme 31 a) *aza*-MBH adduct **1.37b** for Fe-catalysed epoxidation; b) Active in Sharpless epoxidation conditions MBH adducts **2.1**.

In an attempt to create a hybrid process where **1.46a** could serve as an organocatalyst as well as a ligand, *aza*-MBH / Fe-catalysed epoxidation sequence was further examined. The initial control screening of hydroperoxides in Fe-catalysed epoxidation of racemic *aza*-MBH adduct **1.37b**, however, demonstrated no epoxide **4.12b** formation over 21 h at room temperature (Scheme 31a). The reaction with 3-chloroperbenzoic acid as a peroxide provided product **4.12b** in 26% conversion at room temperature over 1 h and did not require the iron salt and phenanthroline. Sharpless conditions that were efficient in the epoxidation of MBH adducts **2.1** bearing allylic alcohol functionality (Scheme 31b)<sup>33</sup> were tested in allylamine **1.37b** epoxidation. Substrate **1.37b** demonstrated no reactivity over 7 days in Sharpless epoxidation conditions designed for allylic alcohols as starting materials. Therefore, all attempts to apply iron catalysis for **1.37b** epoxidation were not successful.

### 4.2.3 Trifunctional system in an *aza*-MBH / diethylzinc addition sequence

As the initial control, racemic *aza*-MBH adduct **1.37b** was investigated in an *aza*-MBH / diethylzinc addition sequence in various conditions (Table 7, Scheme).

Table 7 Investigation of diethylzinc addition to racemic *aza*-MBH adduct **1.37b**.

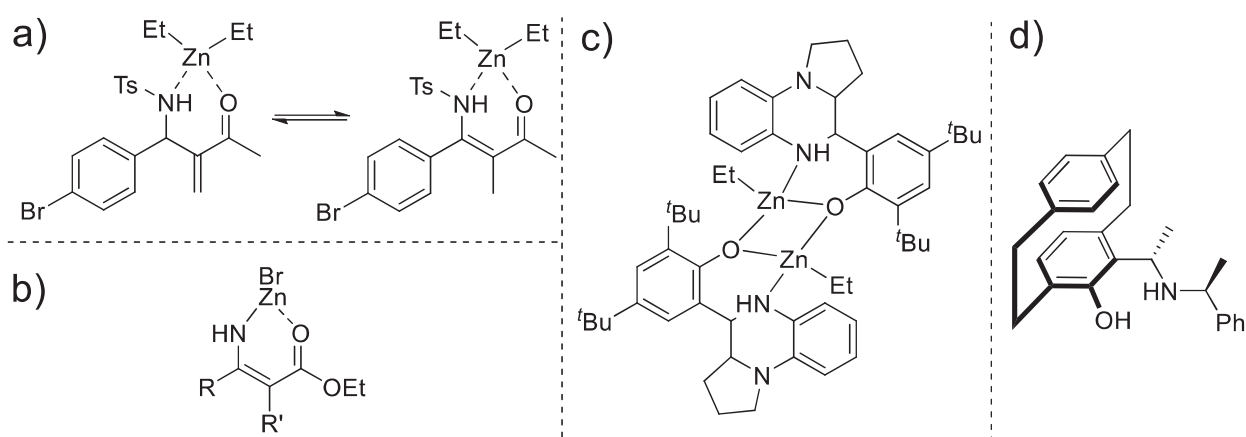


Entry	Catalyst	Temperature, [°C]	Time	Conv. to <b>4.14</b> , [%] <sup>a</sup>	Conv to <b>4.16</b> , [%] <sup>a</sup>	Tosylamide, [%] <sup>a</sup>
1	Cu(acac) <sub>2</sub> (5 mol%), BINOL (5 mol%), TPP (10 mol%).	-25 °C	2.75 h	54 <sup>b</sup>	19	27
2	Cu(acac) <sub>2</sub> (5 mol%), BINOL (5 mol%), TPP (10 mol%),	-66 °C	20 min	63	13%	22
3	Cu(acac) <sub>2</sub> (5 mol%), <i>NO Ligands</i>	-66 °C	20 min	52	31	16
4	<i>NO [Cu]</i> , BINOL (5 mol%), TPP (10 mol%)	-66 °C	20 min	48	26	26
5	none	-66 °C	20 min	63	27	9

<sup>[a]</sup>Calculated by <sup>1</sup>H NMR spectroscopy. <sup>[b]</sup>Isolated yield 38%.

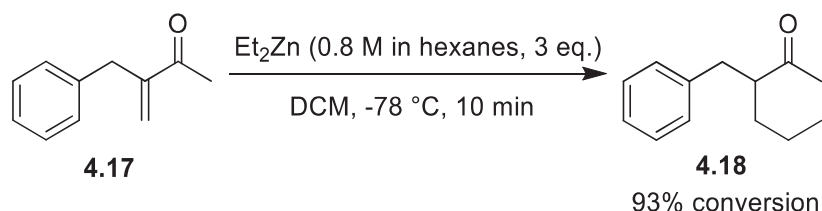
The initial racemic test with the presence of Cu source and co-catalytic system TPP and BINOL demonstrated the formation of the desired product **4.14**. However, NMR analysis of the crude mixture indicated significant presence of side-product **4.16** (19% conversion) and tosylamide (27% conversion) indicating the potential decomposition of **4.14** by elimination (Table 7, entry 1) that may be initialized by diethylzinc as a base. Moreover, after pipette column purification,

significant mass loss was observed, providing only 38% isolated yield of **4.14** and the elimination side-product **4.16** was isolated. Additional controls, including no ligand addition (Table 7, entry 3), no copper source addition (Table 7, entry 4), and no catalyst at all (Table 7, entry 5), were performed at -66 °C to help suppress the decomposition process (Table 7, entry 2–5). All control reactions demonstrated the full consumption of starting material and conversion to product **4.14** and side-products **4.16**, tosylamide. Therefore, the reaction proceeds even without a catalyst addition. Considering that organozinc reagents usually provide sluggish uncatalysed reactions and require ligation to reveal the reactivity,<sup>34, 35</sup> it was hypothesized that the *aza*-MBH adduct **1.37b** and product **4.14** may serve as ligands stabilizing organozinc reagent and promoting the reaction (Scheme 32a). This is consistent with a prior report that *N,O*-stabilisation of zinc reagents is common in Reformatsky processes (Scheme 32b)<sup>36</sup> and that *N,O*-coordinated zinc complexes are active for ring-opening polymerization (Scheme 32c).<sup>37</sup> *N,O*-paracyclophane ligands were previously successfully used in metal-free asymmetric conjugate addition of zinc reagents (Scheme 32d),<sup>38</sup> and numerous aminoalcohols are also known as privileged ligands in organozinc chemistry.<sup>39</sup>



Scheme 32 a) Proposed stabilization of organozinc reagent by *aza*-MBH adduct **1.37b**; b) Six-membered *N,O*-stabilisation of Zn in Reformatsky reaction; c) *N,O*-Zn complex for polymerization processes; d) *N,O*-ligand for conjugate addition of organozinc reagents.

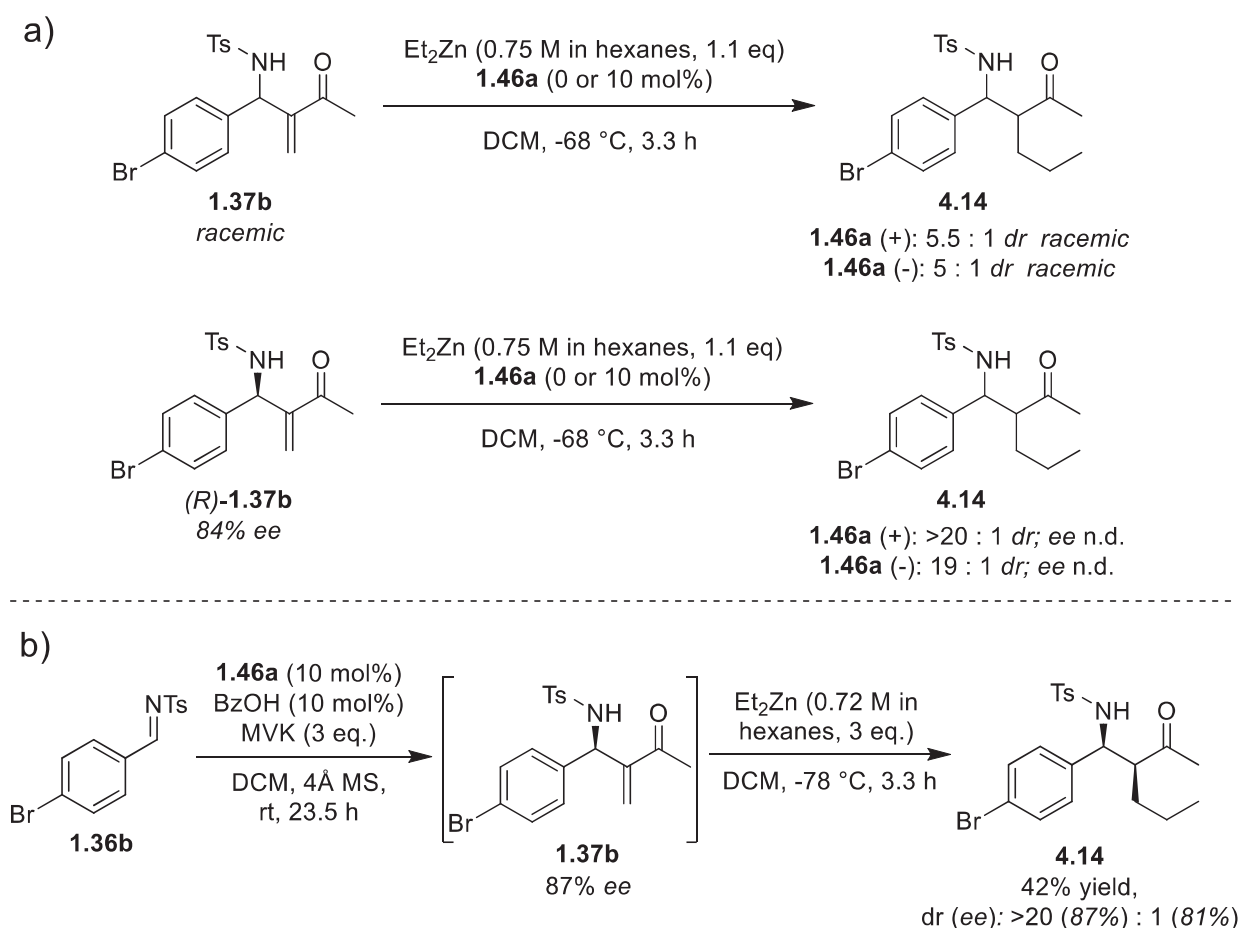
To test this hypothesis, the control substrate **4.17** without a benzylic substituent was synthesized and tested in diethylzinc addition (Scheme 33). Nevertheless, the control substrate **4.17**, without the nitrogen coordination site, provided the corresponding alkylation product **4.18** in 93% conversion over 10 minutes of the reaction at -78 °C.



Scheme 33 A control experiment with substrate **4.17**.

The source of this unusual reactivity is currently unclear. However, it is known that organozinc reactions can be promoted by various factors such as solvents-dependent aggregation<sup>40</sup> and even traces of copper in the starting diethylzinc solution.<sup>38</sup> Given the fast reaction rate in the uncatalysed racemic pathway, the chiral version with **1.46a** was investigated nonetheless (Scheme 34).

To understand the influence of the catalyst **1.46a** on diethylzinc addition, the selectivity of the process starting from racemic and chiral *aza*-MBH adduct **1.37b** in the presence and absence of trifunctional catalyst **1.46a** has been investigated (Scheme 34a). Both diastereoselectivity and enantioselectivity of the process mostly depend on the enantiomeric excess of the starting **1.37b**. The diastereoselectivity of **4.14** is only 5 : 1 *dr* when it is obtained from racemic **1.37b**, and can be increased to 19 : 1 *dr* if chiral (*R*)-**1.37b** (84% *ee*) used as starting material. The addition of the catalyst **1.46a** can marginally improve diastereoselectivity of the diethylzinc addition. It may suggest the **1.46a** can coordinate on zinc, however, a catalytic amount of chiral ligand **1.46a** would not efficiently compete with the stoichiometric amount of the racemic **1.37b** which ligates zinc too. The HPLC analysis of the product **4.14**, obtained from the racemic **1.37b** revealed the racemic mixture of enantiomers (Figure 12 top) meaning that the trifunctional catalytic system **1.46a** was not able to transfer the chirality in the tested conditions.



Scheme 34 a) Control tests of diethylzinc addition to *aza*-MBH adduct **1.37b**; b) A tandem chiral *aza*-MBH / diethylzinc addition sequence.

Further, a chiral *aza*-MBH / diethylzinc addition tandem sequence was tested (Scheme 34b). Interestingly, the product **4.14** was isolated in excellent >20:1 diastereoselectivity with 87% *ee* as a single major isomer (Figure 12 bottom for HPLC traces). The relative configuration of the formed product was preliminarily assigned as (*S,S*)-**4.14**. It is known that catalyst **1.46a** forms the benzylic chiral center in the *R*-configuration in product **1.37b**,<sup>18</sup> and this chiral center should be maintained during the diethylzinc addition step (it becomes *S* in product **4.14** due to the nomenclature rules). The *S*-configuration for the second chiral center was proposed by the comparison of <sup>1</sup>H NMR coupling constants of the ketonic  $\alpha$ -proton which appears as a triplet at 4.38 ppm ( $J = 8.2$  Hz) in the major *syn* diastereomer and as a doublet of doublets at 4.51 ppm ( $J = 9.2, 5.0$  Hz) in the minor *anti* diastereomer (Figure 13).

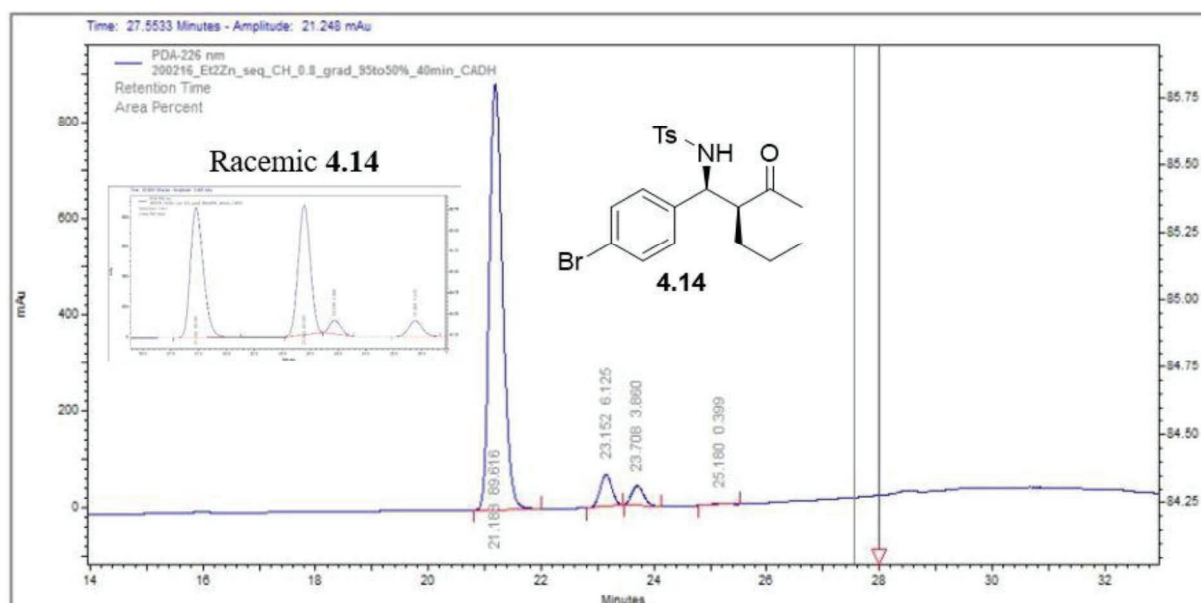
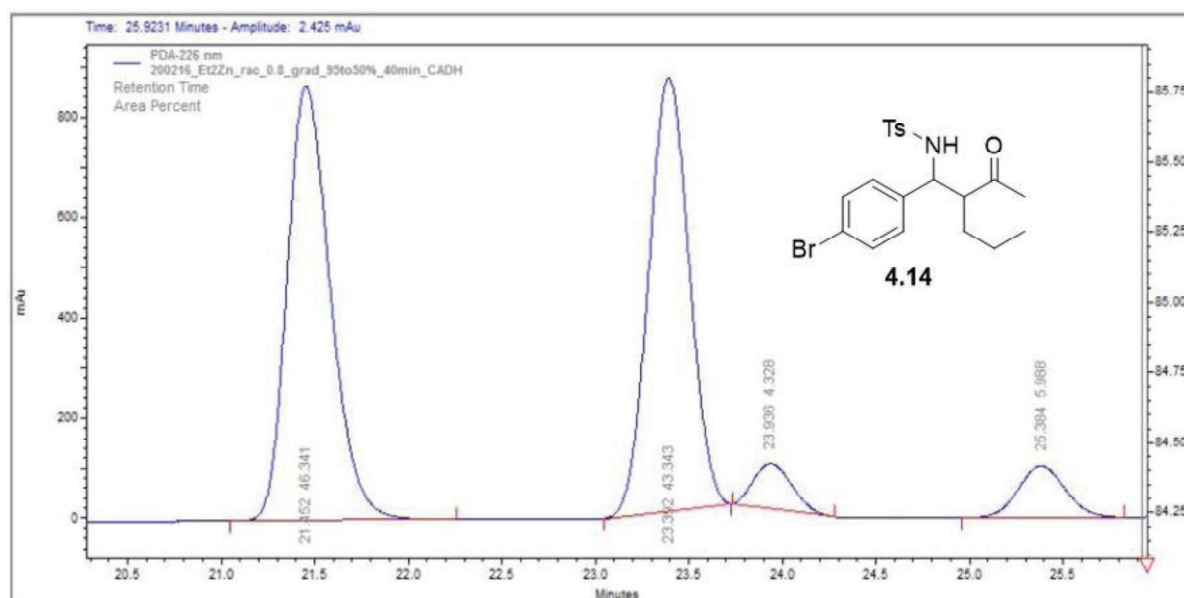


Figure 12 HPLC traces of product **4.14** obtained from **1.46a**-catalysed diethylzinc addition to racemic *aza*-MBH adduct **1.37b** (top) and from the **1.46a**-catalysed *aza*-MBH / diethylzinc addition sequence (bottom).

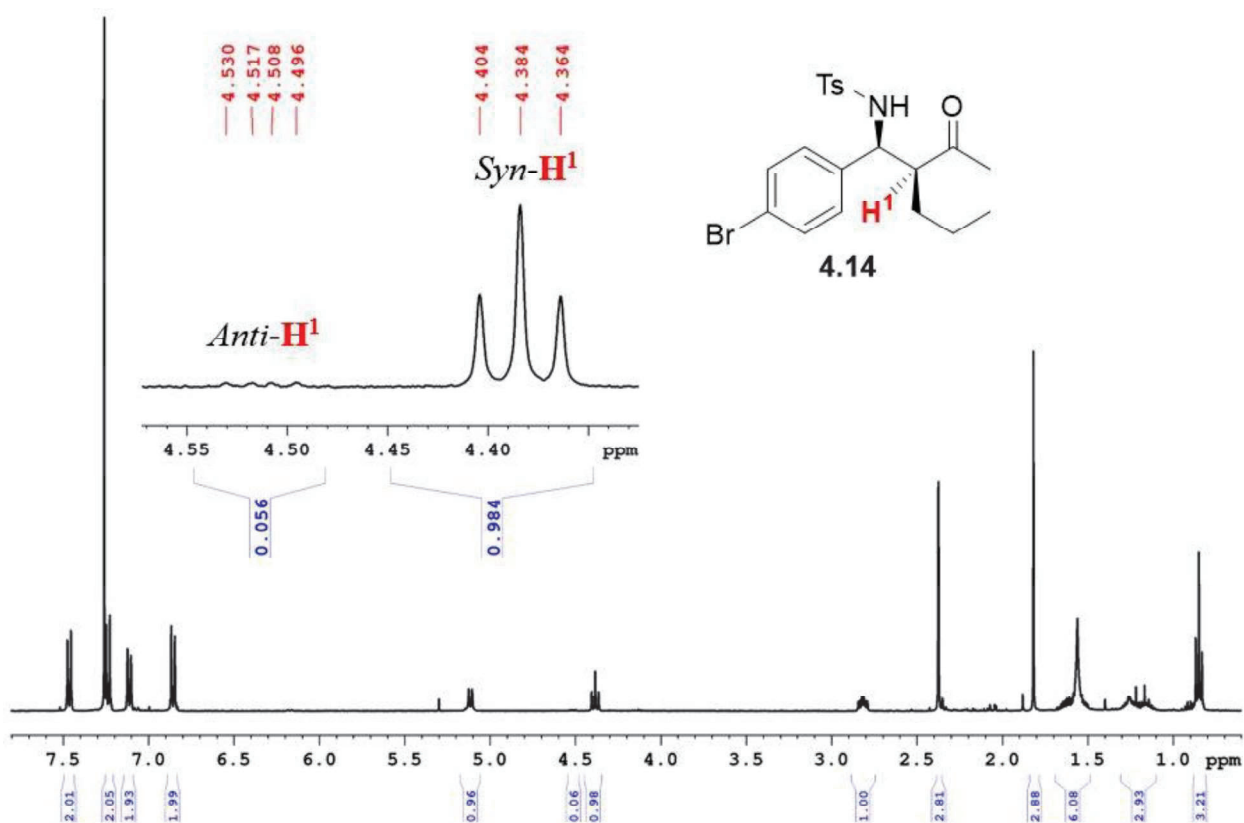


Figure 13  $^1\text{H}$  NMR spectra of **4.14** in  $\text{CDCl}_3$  indicating key proton patterns for diastereomers assignment.

The high stereoselectivity of the sequential process (Scheme 34b) cannot be explained by effects from catalyst **1.46a** alone given the control diethylzinc addition test results (Scheme 34a). Thus, the participation of the *in situ* formed chiral *aza*-MBH intermediate **1.37b** as a ligating agent in the diethylzinc addition step was hypothesized. However, the influence of catalyst **1.46a** on the diethylzinc addition step in the absence of a copper salt cannot be excluded yet and requires future investigation. The unexpected substrate effect observed in the diethylzinc addition step suggests that the highly organized catalytic model where a sub-stoichiometric chiral catalyst is involved in the early, as well as late steps in the cascade, is intrinsically difficult. It may happen because the new pool of chiral intermediates/products continues to grow larger and compete more significantly with the initial catalyst for chiral bias in the diethylzinc addition step.

### 4.3 Conclusions

The ability of a trifunctional, MAP-based system **1.46a** to transfer chirality through multistep processes was investigated in an *aza*-MBH / nucleophilic cyclization cascade, an *aza*-MBH / epoxidation tandem sequence, and an *aza*-MBH / diethylzinc addition sequence. The trifunctional system **1.46a** furnished only a racemic product in the *aza*-MBH / nucleophilic cascade. The failure to transfer chirality from the MAP core to the *aza*-MBH intermediate **1.37j** most likely could be attributed to the presence of the protic *ortho*-substituent in the substrate **1.36j** structure which can potentially interfere with the H-bonding organization created by the catalyst **1.46a**.

For the *aza*-MBH / epoxidation tandem sequence, the chirality information generated by the trifunctional catalyst **1.46a** in *aza*-MBH intermediates **1.37b-i** was preserved and translated into the epoxides **4.12b-i**. The lack of diastereoselectivity of the epoxidation step did not afford the formation of a single enantioenriched epoxide, translating the early benzylic chirality in a linear manner and providing two (*R,S*)- and (*R,R*)-**4.12** species out of four possible stereoisomers. In this process, the trifunctional system **1.46a** catalyses only the initial *aza*-MBH step of the process and does not participate in the organization of the subsequent epoxidation stage. Further investigation may be focused on the improvement of epoxidation step diastereoselectivity by the use of different epoxides or starting cyclic enones.

The unique chiral *aza*-MBH / diethylzinc addition sequence catalysed by the trifunctional catalyst **1.46a** afforded a new product **4.14** as one dominant enantiomer. The preliminary tests demonstrated that the trifunctional system **1.46a** is able to affect both the initial *aza*-MBH step and the subsequent diethylzinc addition step. However, intermediate **1.37b** may out-compete **1.46a** in the diethylzinc addition process either by having better zinc ligating properties or higher stoichiometric presence in the reaction mixture. The diethylzinc addition to a racemic **1.37b** in the various amounts of **1.46a** (or even excess) may be investigated in future to answer this

question. Thus, a new level of complexity in catalytic self-organization of the reaction was demonstrated. Future studies will focus on the optimization, non-linear effect investigation, and mechanistic elucidation of collective chirality induction through the chiral pool formed *in situ* and the confirmation of the absolute configuration of synthesized products **4.12** and **4.14**.

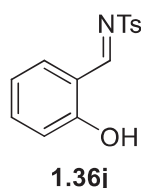
## 4.4 Experimental Section

### 4.4.1 General information

All reagents unless specified are commercially available and purified by standard procedures.<sup>41</sup> Chloroform-*d* was purchased from Cambridge Isotope Laboratories, USA and stored over anhydrous potassium carbonate before use. Potassium *tert*-butoxide was used in glovebox. Air and moisture sensitive reactions were performed under nitrogen or argon atmosphere. Reactions were magnetically stirred and monitored by thin-layer chromatography (TLC) using Merck silica gel 60 F<sub>254</sub> aluminium pre-coated plates (0.25 mm). Flash column chromatography was performed on Merck silica gel 60 (0.015–0.040 mm). <sup>1</sup>H, <sup>13</sup>C, <sup>19</sup>F, and <sup>31</sup>P experiments were performed at 298 K on a Bruker DPX 400 MHz spectrometer equipped with a 5mm QNP probe. Chemical shifts were reported in ppm using the residual CHCl<sub>3</sub> peak as an internal reference ( $\delta_{\text{H}} = 7.26$  ppm,  $\delta_{\text{C}} = 77.16$  ppm). All <sup>31</sup>P NMR spectroscopy was performed on a Bruker DPX 400 MHz spectrometer at 298 K, and all spectra were referenced to external H<sub>3</sub>PO<sub>4</sub> (0 ppm). All <sup>19</sup>F NMR spectroscopy was performed on a Bruker DPX 400 MHz spectrometer at 298 K, and all spectra were referenced to external  $\alpha,\alpha,\alpha$ -trifluorotoluene (-63.8 ppm). All spectra were processed using Bruker TOPSPIN software versions 4.0.7. High resolution mass analysis was provided by the Australian Proteome Analysis Facility (APAF), Macquarie University, Sydney, Australia. HPLC analysis was performed using a Shimadzu Prominence system with CHIRALPAK<sup>®</sup> AD–H column, Regis Chiral Technologies Whelk-O1 column, or Phenomenex Lux<sup>®</sup> 5  $\mu\text{m}$  Amylose-1 column. HPLC grade solvents were degassed before use. The peaks of

enantiomers in UV traces were integrated and the enantiomeric excess was calculated by the formula:  $ee$  (%) = [(Area A – Area B) / (Area A + Area B)] \* 100%. The  $ee$  difference of less than 3% in the racemic case was considered as racemic. *N*-Tosylbenzaldimines **1.36** were synthesized by a known procedures.<sup>42, 43</sup> The trifunctional catalyst **1.46a** was synthesized by a known procedure.<sup>18</sup> Racemic standards of epoxides **4.12b-i** were obtained using a TPP/Phenol co-catalytic system in conditions, indicated further for chiral tests. Standard *aza*-MBH adduct **1.37b** was obtained by known procedure<sup>20</sup> with the use of TPP/Phenol or **1.46a**/BzOH as a catalytic system. The control substrate **4.17** was obtained by known procedure<sup>44</sup> in 6% yield.

#### 4.4.2 *aza*-MBH / nucleophilic cyclization cascade



#### *N*-(2-hydroxybenzylidene)-4-methylbenzenesulfonamide **1.36j**<sup>29</sup>

Salicyl aldehyde (0.87 mL, 8.19 mmol), *p*-toluenesulfonamide (1.40 g, 8.19 mmol), *p*-toluenesulfonic acid monohydrate (15.6 mg, 0.082 mmol), and toluene (20 mL) were combined in a flask equipped with a Dean-Stark adapter filled with toluene. The reaction mixture was refluxed for 21.5 h. The solvent was then evaporated, and the crude mixture recrystallized from hexane/ethyl acetate providing 1.6g (71% yield) of **1.36j** as pink needles.

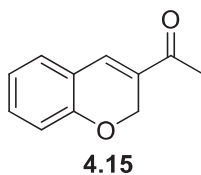
<sup>1</sup>H NMR (400 MHz, CDCl<sub>3</sub>) δ 2.44 (s, 3H), 6.96–7.04 (m, 2H), 7.35 (d, *J* = 8.3 Hz, 2H), 7.46–7.56 (m, 2H), 7.86 (d, *J* = 8.3 Hz, 2H), 9.09 (s, 1H), 10.82 (br s, 1H); <sup>13</sup>C NMR (100 MHz, CDCl<sub>3</sub>) δ 21.81, 116.76, 118.08, 120.43, 128.07, 130.16, 135.20, 135.53, 137.48, 145.20, 162.29, 171.56.



***N*-(3-acetylchroman-4-yl)-4-methylbenzenesulfonamide **4.11**.**<sup>30</sup>

*N*-(2-hydroxybenzylidene)-4-methylbenzenesulfonamide **1.36j** (6.9 mg, 25  $\mu$ mol) was placed in a 2-mL amber, oven-dried vial. The catalyst **1.46a** (1.4 mg, 2.5  $\mu$ mol) and benzoic acid (0.31 mg, 2.5  $\mu$ mol) were added into the reaction vials as stock solutions in freshly distilled dichloromethane. The volume was adjusted to 150  $\mu$ L, and neat but-3-en-2-one (7.2  $\mu$ l, 88.7  $\mu$ mol) was added slowly to the resulting mixture with stirring and left to stir for 28 h at room temperature. The reaction temperature was then increased to 50  $^{\circ}$ C and the mixture left to stir for another 65 h. The resulting mixture was concentrated under nitrogen flow to remove volatiles and the crude mixture analyzed by NMR and purified later on silica gel (gradient hexanes/ethyl acetate) yielding **4.11** in 6.1 mg (71% yield).

*Anti*: <sup>1</sup>H NMR (400 MHz, CDCl<sub>3</sub>)  $\delta$  2.25 (s, 3H), 2.49 (s, 3H), 3.26 (q,  $J$  = 3.0 Hz, 1H), 4.33 (dd,  $J$  = 2.8, 12.0 Hz, 1H), 4.57–4.64 (m, 1H), 4.64–4.69 (m, 1H), 4.72 (d,  $J$  = 5.1 Hz, 1H), 6.47–6.54 (m, 1H), 6.72–6.80 (m, 2H), 7.07–7.14 (m, 1H), 7.40 (d,  $J$  = 8.3 Hz, 2H), 7.83 (d,  $J$  = 8.3 Hz, 2H); *Syn*: <sup>1</sup>H NMR (400 MHz, CDCl<sub>3</sub>)  $\delta$  2.17 (s, 3H), 2.45 (s, 3H), 3.03–3.09 (m, 1H), 4.25–4.33 (m, 1H), 4.49 (dd,  $J$  = 5.0, 12.2 Hz, 1H), 4.85 (dd,  $J$  = 5.0, 9.85 Hz, 1H), 5.60 (d,  $J$  = 9.9 Hz, 1H), 6.68–6.73 (m, 1H), 6.80–6.87 (m, 1H), 7.06–7.13 (m, 2H), 7.33 (d,  $J$  = 8.3 Hz, 2H), 7.79 (d,  $J$  = 8.3 Hz, 2H). **HPLC conditions**: CHIRALPAK<sup>®</sup> AD-H, 0.8 ml/min; gradient from 95% to 50% of Hexane in *i*PrOH, time of *syn* diastereomer: 25.79, 29.39 min; *anti* diastereomer: 24.92, 26.37 min;  $\lambda$  = 226.



### 1-(2H-chromen-3-yl)ethan-1-one **4.15**.<sup>28</sup>

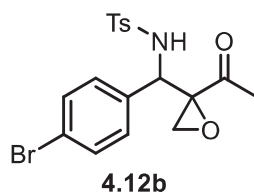
Isolated as an elimination side-product from the synthesis of compound **4.11**.

<sup>1</sup>H NMR (400 MHz, CDCl<sub>3</sub>) δ 2.41 (s, 3H), 5.01 (d, *J* = 1.3 Hz, 2H), 6.86 (d, *J* = 8.2 Hz, 1H), 6.94 (dt, *J* = 7.5, 1.1 Hz, 1H), 7.17 (dd, *J* = 7.5, 1.6 Hz, 1H), 7.23–7.32 (m, 2H).

#### 4.4.3 *aza-MBH / epoxidation sequential process*

##### General Procedure for *aza-MBH / Epoxidation sequential process*

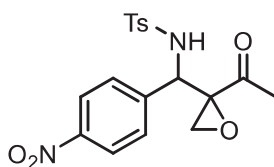
*N*-tosylbenzaldimine **1.36** (30 μmol) was placed in a 2-mL amber, oven-dried vial in a glovebox. Then 140 μl of freshly distilled dichloromethane was added into the vial. The catalyst **1.46a** (1.65 mg, 3 μmol) and benzoic acid (0.36 mg, 3 μmol) were added into the reaction vial as stock solutions in dichloromethane. Then to the resulting mixture neat but-3-en-2-one (7.2 μl, 88.7 μmol) was added at room temperature with stirring and left to stir for an indicated time. The reaction mixture was cooled down by ice/acetone bath, and the potassium *tert*-butoxide (1.66 mg, 14.8 μmol), as 0.1 M solution in freshly distilled THF was added to the reaction mixture followed by the addition of *tert*-butyl hydroperoxide (13.32 mg, 148 μmol) as 5 M solution in decane with stirring. The reaction mixture was left to stir at the reduced temperature for 5 minutes. Then the cooling bath was removed, and the reaction mixture left to stir at room temperature for an indicated time. Then the reaction mixture was diluted with dichloromethane, washed with MiliQ water three times and with brine once. The resulting organic layer was concentrated, and the crude mixture was analyzed by NMR and purified later by a pipette silica gel column (gradient hexanes/ethyl acetate).



***N*-((2-acetyloxiran-2-yl)(4-bromophenyl)methyl)-4-methylbenzenesulfonamide **4.12b** (new)**

*aza*-MBH time: 22 h; Epoxidation time: 2.3 h; Yield 63%. dr: 1.2:1, *ee*: 84% (major), n.d. (minor)

Major:  $^1\text{H NMR}$  (400 MHz,  $\text{CDCl}_3$ )  $\delta$  1.88 (s, 3H), 2.37 (s, 3H), 2.84 (d,  $J = 4.5$  Hz, 1H), 2.91 (d,  $J = 4.5$  Hz, 1H), 4.48 (d,  $J = 10.0$  Hz, 1H), 6.24 (d,  $J = 10.0$  Hz, 1H), 7.02 (d,  $J = 8.6$  Hz, 2H), 7.15 (d,  $J = 8.0$  Hz, 2H), 7.28 (d,  $J = 8.6$  Hz, 2H), 7.57 (d,  $J = 8.0$  Hz, 2H);  $^{13}\text{C NMR}$  (100 MHz,  $\text{CDCl}_3$ )  $\delta$  21.58, 24.55, 51.28, 58.60, 63.48, 122.02, 127.02, 128.54, 129.62, 131.57, 135.55, 137.72, 143.72, 207.48. Minor:  $^1\text{H NMR}$  (400 MHz,  $\text{CDCl}_3$ )  $\delta$  1.84 (s, 3H), 2.38 (s, 3H), 2.91 (d,  $J = 4.6$  Hz, 1H), 3.41 (d,  $J = 4.6$  Hz, 1H), 5.05–5.11 (m, 2H), 6.88 (d,  $J = 8.6$  Hz, 2H), 7.15 (d,  $J = 8.6$  Hz, 2H), 7.21 (d,  $J = 8.6$  Hz, 2H), 7.52 (d,  $J = 8.6$  Hz, 2H);  $^{13}\text{C NMR}$  (100 MHz,  $\text{CDCl}_3$ )  $\delta$  21.60, 24.42, 48.39, 54.04, 64.71, 122.39, 127.17, 129.32, 129.69, 131.84, 136.63, 137.20, 143.86, 205.83; **HRMS** Found  $[\text{M} - \text{H}]^-$ , 422.00644, 424.00429.  $\text{C}_{18}\text{H}_{17}\text{BrNO}_4\text{S}$  requires  $[\text{M} - \text{H}]^-$ , 422.00619, 424.00414; **IR** (ATR,  $\text{cm}^{-1}$ )  $\nu$  3232, 2925, 1718, 1597, 1489, 1438, 1361, 1326, 1244, 1163, 1091, 1063, 1011, 939, 884, 856, 814, 704, 659, 610;  $[\alpha]_{\text{D}}^{25} = -13.98^\circ$  ( $c$  1.0,  $\text{CHCl}_3$ ); **HPLC conditions**: WhelkO-1, 0.8 ml/min; 80% Hexane / 20% *i*PrOH, time of minor diastereomer: 26.99, 28.13 min; major diastereomer: 33.56, 40.68 min;  $\lambda = 226$ .

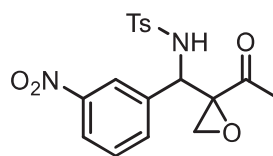


4.12c

***N*-((2-acetyloxiran-2-yl)(4-nitrophenyl)methyl)-4-methylbenzenesulfonamide 4.12c (new)**

*aza*-MBH time: 5 h; Epoxidation time: 2.25 h; Yield 46%. dr: 1.27:1, *ee*: 85%.(major), n.d. (minor)

Major:  $^1\text{H NMR}$  (400 MHz,  $\text{CDCl}_3$ )  $\delta$  1.89 (s, 3H), 2.37 (s, 3H), 2.98 (d,  $J = 4.6$  Hz, 1H), 3.02 (d,  $J = 4.6$  Hz, 1H), 4.50 (d,  $J = 10.0$  Hz, 1H), 6.25 (d,  $J = 10.0$  Hz, 1H), 7.20 (d,  $J = 8.3$  Hz, 2H), 7.39 (d,  $J = 8.8$  Hz, 2H), 7.63 (d,  $J = 8.3$  Hz, 2H), 8.05 (d,  $J = 8.8$  Hz, 2H);  $^{13}\text{C NMR}$  (100 MHz,  $\text{CDCl}_3$ )  $\delta$  21.63, 24.36, 51.55, 59.01, 63.36, 123.70, 127.03, 127.71, 129.86, 137.68, 144.16, 144.18, 147.63, 207.56. Minor:  $^1\text{H NMR}$  (400 MHz,  $\text{CDCl}_3$ )  $\delta$  1.87 (s, 3H), 2.37 (s, 3H), 3.00 (d,  $J = 4.5$  Hz, 1H), 3.43 (d,  $J = 4.5$  Hz, 1H), 4.90 (d,  $J = 10.0$  Hz, 1H), 5.25 (d,  $J = 10.0$  Hz, 1H), 7.17 (d,  $J = 8.3$  Hz, 2H), 7.23 (d,  $J = 8.8$  Hz, 2H), 7.54 (d,  $J = 8.3$  Hz, 2H), 7.99 (d,  $J = 8.8$  Hz, 2H);  $^{13}\text{C NMR}$  (100 MHz,  $\text{CDCl}_3$ )  $\delta$  21.64, 24.23, 48.48, 54.08, 64.41, 123.96, 127.18, 128.66, 129.84, 137.09, 144.30, 144.81, 147.66, 205.56. **HRMS** Found  $[\text{M} - \text{H}]^-$ , 389.08103.  $\text{C}_{18}\text{H}_{17}\text{N}_2\text{O}_6\text{S}$  requires  $[\text{M} - \text{H}]^-$ , 389.08077; **IR** (ATR,  $\text{cm}^{-1}$ )  $\nu$  3270, 2926, 1711, 1599, 1520, 1436, 1345, 1159, 1091, 1070, 1018, 946, 896, 853, 814, 727, 698, 661, 610;  $[\alpha]_{\text{D}}^{25} = -24.5^\circ$  ( $c$  1.0,  $\text{CHCl}_3$ ); **HPLC conditions**: WhelkO-1, 0.8 ml/min; gradient from 95% to 50% of Hexane in *i*PrOH, time of minor diastereomer: 48.29, 52.77 min; major diastereomer: 43.22, 43.93 min (overlaps);  $\lambda = 226$ .

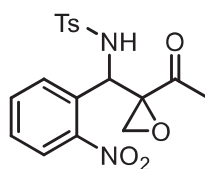


4.12d

***N*-((2-acetyloxiran-2-yl)(3-nitrophenyl)methyl)-4-methylbenzenesulfonamide 4.12d (new)**

*aza*-MBH time: 5 h; Epoxidation time: 2.25 h; Yield 51%. dr: 1:1, *ee*: 83% (major), 84% (minor)

Major:  $^1\text{H NMR}$  (400 MHz,  $\text{CDCl}_3$ )  $\delta$  1.91 (s, 3H), 2.34 (s, 3H), 2.97 (d,  $J = 4.5$  Hz, 1H), 3.04 (d,  $J = 4.5$  Hz, 1H), 4.54 (d,  $J = 9.9$  Hz, 1H), 6.31 (d,  $J = 9.9$  Hz, 1H), 7.16 (d,  $J = 8.3$  Hz, 2H), 7.40 (t,  $J = 8.0$  Hz, 1H), 7.57-7.60 (m, 1H), 7.61 (d,  $J = 8.3$  Hz, 2H), 7.94 (t,  $J = 2.0$  Hz, 1H), 8.01–8.06 (m, 1H);  $^{13}\text{C NMR}$  (100 MHz,  $\text{CDCl}_3$ )  $\delta$  21.57, 24.37, 48.45, 54.06, 64.45, 121.89, 122.94, 127.02, 129.59, 129.87, 133.01, 137.57, 139.96, 144.05, 148.28, 207.46. Minor:  $^1\text{H NMR}$  (400 MHz,  $\text{CDCl}_3$ )  $\delta$  1.88 (s, 3H), 2.35 (s, 3H), 3.01 (d,  $J = 4.5$  Hz, 1H), 3.47 (d,  $J = 4.5$  Hz, 1H), 5.05 (d,  $J = 10.0$  Hz, 1H), 5.24 (d,  $J = 10.0$  Hz, 1H), 7.15 (d,  $J = 8.3$  Hz, 2H), 7.35 (t,  $J = 8.0$  Hz, 1H), 7.46–7.51 (m, 1H), 7.54 (d,  $J = 8.3$  Hz, 2H), 7.69 (t,  $J = 2.1$  Hz, 1H), 7.98–8.02 (m, 1H);  $^{13}\text{C NMR}$  (100 MHz,  $\text{CDCl}_3$ )  $\delta$  21.55, 24.25, 51.49, 58.75, 63.29, 122.87, 123.16, 127.17, 129.83, 129.91, 133.51, 136.98, 139.78, 144.32, 148.14, 205.68. **HRMS** Found  $[\text{M} - \text{H}]^-$ , 389.08107.  $\text{C}_{18}\text{H}_{17}\text{N}_2\text{O}_6\text{S}$  requires  $[\text{M} - \text{H}]^-$ , 389.08077; **IR** (ATR,  $\text{cm}^{-1}$ )  $\nu$  3272, 1709, 1598, 1528, 1419, 1346, 1158, 1089, 1065, 879, 842, 813, 728, 681, 663;  $[\alpha]_{\text{D}}^{25} = -15.61^\circ$  ( $c$  1.0,  $\text{CHCl}_3$ ); **HPLC conditions**: WhelkO-1, 1.0 ml/min; 70% Hexane / 30% *i*PrOH, time of minor diastereomer: 22.21, 19.96 min; major diastereomer: 29.37, 35.82 min;  $\lambda = 229$ ; or Lux Amylose-1, 1.0 ml/min; 70% Hexane / 30% *i*PrOH, time of minor diastereomer: 14.16, 31.59 min; major diastereomer: 13.13, 18.48 min;  $\lambda = 226$ .

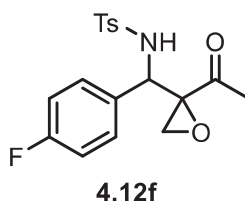


4.12e

***N*-((2-acetyloxiran-2-yl)(2-nitrophenyl)methyl)-4-methylbenzenesulfonamide 4.12e (new)**

*aza*-MBH time: 48 h; Epoxidation time: 8.3 h; Yield 49%. dr: 1:1, *ee*: n.d

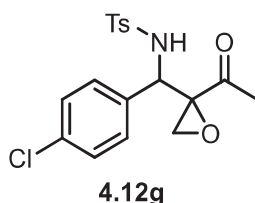
Major: <sup>1</sup>H NMR (400 MHz, CDCl<sub>3</sub>) δ 2.01 (s, 3H), 2.34 (s, 3H), 2.38 (d, *J* = 4.4 Hz, 1H), 2.88 (d, *J* = 4.4 Hz, 1H), 5.89 (d, *J* = 9.6 Hz, 1H), 6.09 (d, *J* = 9.6 Hz, 1H), 7.14 (d, *J* = 8.3 Hz, 2H), 7.33–7.45 (m, 3H), 7.60 (d, *J* = 8.3 Hz, 2H), 7.83 (d, *J* = 8.3 Hz, 1H); <sup>13</sup>C NMR (100 MHz, CDCl<sub>3</sub>) δ 21.62, 24.63, 51.96, 52.22, 63.79, 124.73, 127.23, 127.71, 129.00, 129.56, 129.68, 130.89, 136.92, 143.83, 148.69, 204.72. Minor: <sup>1</sup>H NMR (400 MHz, CDCl<sub>3</sub>) δ 1.87 (s, 3H), 2.36 (s, 3H), 2.93 (d, *J* = 4.5 Hz, 1H), 3.20 (d, *J* = 4.5 Hz, 1H), 5.37 (d, *J* = 8.8 Hz, 1H), 6.14 (d, *J* = 10.0 Hz, 1H), 7.17 (d, *J* = 8.3 Hz, 2H), 7.45–7.58 (m, 3H), 7.65 (d, *J* = 8.3 Hz, 2H), 7.83 (d, *J* = 7.9 Hz, 1H); <sup>13</sup>C NMR (100 MHz, CDCl<sub>3</sub>) δ 21.66, 24.06, 47.82, 50.09, 63.61, 125.15, 127.47, 129.12, 129.32, 129.64, 132.58, 136.67, 143.93, 148.52, 205.27; HRMS Found [M – H]<sup>–</sup>, 389.08084. C<sub>18</sub>H<sub>17</sub>N<sub>2</sub>O<sub>6</sub>S requires [M – H]<sup>–</sup>, 389.08077; IR (ATR, cm<sup>–1</sup>) ν 3235, 1717, 1596, 1579, 1528, 1449, 1349, 1320, 1235, 1188, 1162, 1112, 1089, 1065, 959, 941, 918, 871, 858, 840, 816, 793, 768, 725, 706, 688, 664, 616; [α]<sub>D</sub><sup>25</sup> = –26.46° (*c* 1.0, CHCl<sub>3</sub>); HPLC conditions: CHIRALPAK<sup>®</sup> AD-H, 0.8 ml/min; gradient from 95% to 50% of Hexane in *i*PrOH, time of minor diastereomer: 36.65, 37.58 min; major diastereomer: 35.44, 38.56 min; λ = 227.



***N*-((2-acetyloxiran-2-yl)(4-fluorophenyl)methyl)-4-methylbenzenesulfonamide **4.12f** (new)**

*aza*-MBH time: 48 h; Epoxidation time: 3.5 h; Yield 41%. dr: 1:1, *ee*: 88% (major), n.d. (minor)

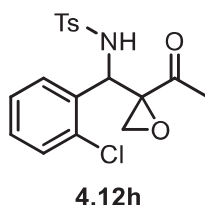
Major: <sup>1</sup>H NMR (400 MHz, CDCl<sub>3</sub>) δ 1.89 (s, 3H), 2.36 (s, 3H), 2.86 (d, *J* = 4.6 Hz, 1H), 2.92 (d, *J* = 4.6 Hz, 1H), 4.48 (d, *J* = 10.1 Hz, 1H), 6.17 (d, *J* = 10.1 Hz, 1H), 6.86 (t, *J* = 8.7 Hz, 2H), 7.10–7.15 (m, 2H), 7.16 (d, *J* = 8.3 Hz, 2H), 7.59 (d, *J* = 8.3 Hz, 2H); <sup>13</sup>C NMR (100 MHz, CDCl<sub>3</sub>) δ 21.60, 24.64, 51.44, 58.67, 63.60, 115.43 (d, *J* = 21.8 Hz), 127.06, 128.52 (d, *J* = 8.2 Hz), 129.64, 132.37 (d, *J* = 3.2 Hz), 137.88, 143.67, 162.41 (d, *J* = 246.7 Hz), 207.76; <sup>19</sup>F NMR (300 MHz, CDCl<sub>3</sub>) δ -115.39. Minor: <sup>1</sup>H NMR (400 MHz, CDCl<sub>3</sub>) δ 1.85 (s, 3H), 2.39 (s, 3H), 2.92 (d, *J* = 4.6 Hz, 1H), 3.43 (d, *J* = 4.6 Hz, 1H), 4.81 (d, *J* = 9.7 Hz, 1H), 5.12 (d, *J* = 9.7 Hz, 1H), 6.78 (t, *J* = 8.7 Hz, 2H), 6.95–7.03 (m, 2H), 7.17 (d, *J* = 8.3 Hz, 2H), 7.55 (d, *J* = 8.3 Hz, 2H). <sup>13</sup>C NMR (100 MHz, CDCl<sub>3</sub>) δ 21.62, 24.48, 48.52, 53.92, 64.88, 115.75 (d, *J* = 21.4 Hz), 127.24, 129.36 (d, *J* = 8.3 Hz), 129.73, 133.73 (d, *J* = 3.2 Hz), 137.30, 143.86, 162.50 (d, *J* = 248.3 Hz), 205.92; <sup>19</sup>F NMR (300 MHz, CDCl<sub>3</sub>): δ -114.21; HRMS Found [M – H]<sup>–</sup>, 362.08663. C<sub>18</sub>H<sub>17</sub>FNO<sub>4</sub>S requires [M – H]<sup>–</sup>, 362.08652; IR (ATR, cm<sup>–1</sup>) ν 3273, 2925, 1711, 1603, 1510, 1431, 1363, 1332, 1226, 1158, 1092, 1065, 1018, 929, 894, 835, 814, 785, 736, 705, 664, 612; [α]<sub>D</sub><sup>25</sup> = –14.11° (*c* 1.0, CHCl<sub>3</sub>); HPLC conditions: CHIRALPAK<sup>®</sup> AD-H, 1.0 ml/min; 70% Hexane / 30% *i*PrOH, time of minor diastereomer: 9.88, 12.48 min; major diastereomer: 10.56, 17.73 min; λ = 257.



***N*-((2-acetyloxiran-2-yl)(2-nitrophenyl)methyl)-4-methylbenzenesulfonamide 4.12e (new)**

*aza*-MBH time: 48 h; Epoxidation time: 8.3 h; Yield 49%. dr: 1:1, *ee*: n.d

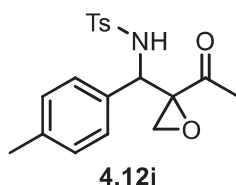
Major:  $^1\text{H NMR}$  (400 MHz,  $\text{CDCl}_3$ )  $\delta$  2.01 (s, 3H), 2.34 (s, 3H), 2.38 (d,  $J = 4.4$  Hz, 1H), 2.88 (d,  $J = 4.4$  Hz, 1H), 5.89 (d,  $J = 9.6$  Hz, 1H), 6.09 (d,  $J = 9.6$  Hz, 1H), 7.14 (d,  $J = 8.3$  Hz, 2H), 7.33–7.45 (m, 3H), 7.60 (d,  $J = 8.3$  Hz, 2H), 7.83 (d,  $J = 8.3$  Hz, 1H);  $^{13}\text{C NMR}$  (100 MHz,  $\text{CDCl}_3$ )  $\delta$  21.62, 24.63, 51.96, 52.22, 63.79, 124.73, 127.23, 127.71, 129.00, 129.56, 129.68, 130.89, 136.92, 143.83, 148.69, 204.72. Minor:  $^1\text{H NMR}$  (400 MHz,  $\text{CDCl}_3$ )  $\delta$  1.87 (s, 3H), 2.36 (s, 3H), 2.93 (d,  $J = 4.5$  Hz, 1H), 3.20 (d,  $J = 4.5$  Hz, 1H), 5.37 (d,  $J = 8.8$  Hz, 1H), 6.14 (d,  $J = 10.0$  Hz, 1H), 7.17 (d,  $J = 8.3$  Hz, 2H), 7.45–7.58 (m, 3H), 7.65 (d,  $J = 8.3$  Hz, 2H), 7.83 (d,  $J = 7.9$  Hz, 1H);  $^{13}\text{C NMR}$  (100 MHz,  $\text{CDCl}_3$ )  $\delta$  21.66, 24.06, 47.82, 50.09, 63.61, 125.15, 127.47, 129.12, 129.32, 129.64, 132.58, 136.67, 143.93, 148.52, 205.27; **HRMS** Found  $[\text{M} - \text{H}]^-$ , 389.08084.  $\text{C}_{18}\text{H}_{17}\text{N}_2\text{O}_6\text{S}$  requires  $[\text{M} - \text{H}]^-$ , 389.08077; **IR** (ATR,  $\text{cm}^{-1}$ )  $\nu$  3274, 1710, 1597, 1492, 1421, 1362, 1331, 1266, 1159, 1090, 1067, 1015, 928, 889, 813, 734, 708, 662, 609;  $[\alpha]_{\text{D}}^{25} = -48.57^\circ$  ( $c$  1.0,  $\text{CHCl}_3$ ); **HPLC conditions**: CHIRALPAK<sup>®</sup> AD-H, 0.8 ml/min; gradient from 95% to 50% of Hexane in *i*PrOH, time of minor diastereomer: 36.65, 37.58 min; major diastereomer: 35.44, 38.56 min;  $\lambda = 227$ .



***N*-((2-acetyloxiran-2-yl)(2-chlorophenyl)methyl)-4-methylbenzenesulfonamide **4.12h** (new)**

*aza*-MBH time: 48 h; Epoxidation time: 2.8 h; Yield 38%. dr: 1:1, *ee*: 71% major, 72% minor

Major:  $^1\text{H NMR}$  (400 MHz,  $\text{CDCl}_3$ )  $\delta$  2.05 (s, 3H), 2.28 (d,  $J = 4.5$  Hz, 1H), 2.31 (s, 3H), 2.80 (d,  $J = 4.5$  Hz, 1H), 5.74–5.82 (m, 2H), 6.98–7.17 (m, 3H), 7.09 (d,  $J = 8.3$  Hz, 2H), 7.21–7.25 (m, 1H), 7.64 (d,  $J = 8.3$  Hz, 2H);  $^{13}\text{C NMR}$  (100 MHz,  $\text{CDCl}_3$ )  $\delta$  21.56, 24.76, 51.23, 53.10, 64.09, 126.90, 127.17, 128.68, 129.23, 129.44, 133.09, 133.46, 137.11, 143.50, 204.92; Minor:  $^1\text{H NMR}$  (400 MHz,  $\text{CDCl}_3$ )  $\delta$  1.87 (s, 3H), 2.34 (s, 3H), 2.92 (d,  $J = 4.5$  Hz, 1H), 3.43 (d,  $J = 4.5$  Hz, 1H), 5.14 (d,  $J = 9.8$  Hz, 1H), 5.67 (d,  $J = 9.8$  Hz, 1H), 6.98–7.17 (m, 3H), 7.11 (d,  $J = 8.3$  Hz, 2H), 7.36–7.40 (m, 1H), 7.64 (d,  $J = 8.3$  Hz, 2H);  $^{13}\text{C NMR}$  (100 MHz,  $\text{CDCl}_3$ )  $\delta$  21.60, 24.67, 48.00, 51.40, 64.38, 127.25, 127.44, 128.85, 129.48, 129.96, 133.62, 135.77, 137.19, 143.55, 205.38;  $[\text{M} - \text{H}]^-$ , 378.05683.  $\text{C}_{18}\text{H}_{17}\text{ClNO}_4\text{S}$  requires  $[\text{M} - \text{H}]^-$ , 378.05670; **IR** (ATR,  $\text{cm}^{-1}$ )  $\nu$  3270, 2925, 1714, 1597, 1474, 1441, 1333, 1267, 1158, 1090, 1037, 939, 892, 849, 813, 735, 703, 664;  $[\alpha]_{\text{D}}^{25} = -16.98^\circ$  ( $c$  0.67,  $\text{CHCl}_3$ ); **HPLC conditions**: Lux Amylose-1, 0.8 ml/min; gradient from 95% to 50% of Hexane in *i*PrOH, time of minor diastereomer: 21.97, 39.93 min; major diastereomer: 29.96, 33.35 min;  $\lambda = 227$ .



***N*-((2-acetyloxiran-2-yl)(*p*-tolyl)methyl)-4-methylbenzenesulfonamide **4.12i** (new)**

*aza*-MBH time: 48 h; Epoxidation time: 5 h; Yield 11%. dr: 1:1, *ee*: n.d.

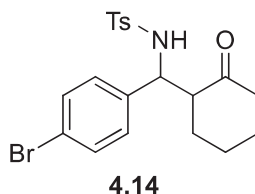
Major:  $^1\text{H NMR}$  (400 MHz,  $\text{CDCl}_3$ )  $\delta$  1.89 (s, 3H), 2.25 (s, 3H), 2.35 (s, 3H), 2.84 (d,  $J = 4.7$  Hz, 1H), 2.88 (d,  $J = 4.7$  Hz, 1H), 4.51 (d,  $J = 10.1$  Hz, 1H), 6.10 (d,  $J = 10.1$  Hz, 1H), 6.95–7.06 (m, 4H), 7.14 (d,  $J = 8.3$  Hz, 1H), 7.60 (d,  $J = 8.3$  Hz, 1H);  $^{13}\text{C NMR}$  (100 MHz,  $\text{CDCl}_3$ )  $\delta$  21.10, 21.58, 24.71, 51.31, 58.82, 63.78, 126.58, 127.09, 129.19, 129.53, 133.52, 137.63, 137.99, 143.39, 207.75; Minor:  $^1\text{H NMR}$  (400 MHz,  $\text{CDCl}_3$ )  $\delta$  1.85 (s, 3H), 2.23 (s, 3H), 2.38 (s, 3H), 2.90 (d,  $J = 4.7$  Hz, 1H), 3.43 (d,  $J = 4.7$  Hz, 1H), 4.79 (d,  $J = 9.4$  Hz, 1H), 5.07 (d,  $J = 9.4$  Hz, 1H), 6.84–6.95 (m, 4H), 7.17 (d,  $J = 8.3$  Hz, 1H), 7.57 (d,  $J = 8.3$  Hz, 1H);  $^{13}\text{C NMR}$  (100 MHz,  $\text{CDCl}_3$ )  $\delta$  21.16, 21.62, 24.57, 48.49, 54.42, 64.91, 127.30, 127.40, 129.50, 129.66, 134.74, 137.37, 138.15, 143.62, 206.10; **HRMS** Found  $[\text{M} - \text{H}]^-$ , 385.11129.  $\text{C}_{19}\text{H}_{20}\text{NO}_4\text{S}$  requires  $[\text{M} - \text{H}]^-$ , 385.11132; **IR** (ATR,  $\text{cm}^{-1}$ )  $\nu$  3281, 2923, 1710, 1598, 1515, 1422, 1362, 1331, 1267, 1185, 1158, 1091, 1066, 1021, 928, 888, 851, 812, 771, 736, 706, 663, 613;  $[\alpha]_{\text{D}}^{25} = -40.83^\circ$  ( $c$  0.67,  $\text{CHCl}_3$ ); **HPLC conditions**: Lux Amylose-1, 1.0 ml/min; 70% Hexane / 30% *i*PrOH, time of minor diastereomer: 10.18, 11.82 min; major diastereomer: 11.07, 15.09 min;  $\lambda = 229$ .

**General Procedure for Fe-catalysed epoxidation.**

Iron(II) trifluoromethane sulfonate (0.17 mg, 0.49  $\mu\text{mol}$ ), phenanthroline (0.17 mg, 0.98  $\mu\text{mol}$ ), and *aza*-MBH adduct **1.37b** (4 mg, 9.8  $\mu\text{mol}$ ) were transferred in a 2-mL amber, oven-dried vial as stock solutions in freshly distilled acetonitrile. The resulting mixture was stirred for 10

minutes at room temperature then it was cooled down by ice/acetone bath and peroxide (49  $\mu\text{mol}$ ) was added with stirring. The reaction mixture was left to stir at room temperature for 21 h then aliquots were taken and analysed by  $^1\text{H}$  NMR demonstrating no epoxide **4.12b** formation.

#### 4.4.4 *aza-MBH / diethylzinc addition sequential process*



#### ***N*-(2-acetyl-1-(4-bromophenyl)pentyl)-4-methylbenzenesulfonamide **4.14** (new)**

##### *Procedure the sequential process:*

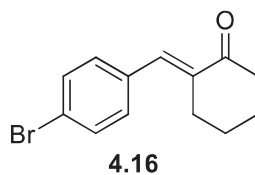
*p*-Bromosubstituted *N*-tosylbenzaldimine **1.36b** (10 mg, 30  $\mu\text{mol}$ ) was placed in a 2-mL amber, oven-dried vial in a glovebox. Then 140  $\mu\text{l}$  of freshly distilled dichloromethane was added into the vial. The catalyst **1.46a** (1.65 mg, 3  $\mu\text{mol}$ ) and benzoic acid (0.36 mg, 3  $\mu\text{mol}$ ) were added into the reaction vials as stock solutions in dichloromethane. Then to the resulting mixture, neat but-3-en-2-one (7.2  $\mu\text{l}$ , 88.7  $\mu\text{mol}$ ) was added at room temperature with stirring and left to stir for 23.5 h. The reaction mixture was cooled down to  $-78\text{ }^\circ\text{C}$  by dry ice/*iso*-propanol bath, and the diethylzinc (4.0 mg, 33  $\mu\text{mol}$ ) was slowly added as 0.71 M solution in hexanes with stirring. The reaction mixture was left to stir at  $-78\text{ }^\circ\text{C}$  for 3.3 h. Then the reaction mixture was quenched by citric acid at cooling, washed with MiliQ water three times and with brine once. The resulting organic layer was concentrated, and the crude mixture was analyzed by NMR and purified later by a pipette silica gel column (gradient hexanes/ethyl acetate) yielding product **4.14** in 5.5 mg (42% yield), dr:  $>20 : 1$ , *ee*: 87% (major), 81% (minor).

##### *Procedure of the diethylzinc addition to aza-MBH adduct:*

The *aza*-MBH adduct **1.37b** (5 mg, 12.25  $\mu\text{mol}$ ) and the catalytic system (TPP and Phenol or **1.46a** and BzOH, 1.225  $\mu\text{mol}$ ) were placed in a 2-mL amber, oven-dried vial as stock solutions

in freshly distilled dichloromethane. The total volume was adjusted to 300  $\mu$ L, the mixture was cooled down to -68  $^{\circ}$ C by dry ice/iso-propanol bath, and the diethylzinc (1.7 mg, 13.5  $\mu$ mol) was slowly added as 0.75 M solution in hexanes with stirring. The reaction mixture was left to stir at -78  $^{\circ}$ C for 3.3 h. Then the reaction mixture was quenched by citric acid at cooling, washed with MiliQ water three times and with brine once. The resulting organic layer was concentrated, and the crude mixture was analyzed by NMR and purified later by a pipette silica gel column (gradient hexanes/ethyl acetate) yielding product **4.14**.

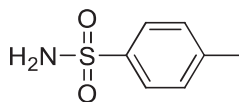
Major:  $^1\text{H NMR}$  (400 MHz,  $\text{CDCl}_3$ )  $\delta$  0.84 (t,  $J = 7.3$  Hz, 3H), 1.06–1.37 (m, 2H), 1.49–1.70 (m, 2H), 1.81 (s, 3H), 2.37 (s, 3H), 2.78–2.86 (m, 1H), 4.38 (t,  $J = 8.2$  Hz, 1H), 5.26 (d,  $J = 8.2$  Hz, 1H), 6.85 (d,  $J = 8.4$  Hz, 2H), 7.11 (d,  $J = 8.3$  Hz, 2H), 7.23 (d,  $J = 8.4$  Hz, 2H), 7.47 (d,  $J = 8.4$  Hz, 2H);  $^{13}\text{C NMR}$  (100 MHz,  $\text{CDCl}_3$ )  $\delta$  14.20, 20.56, 21.61, 30.69, 31.36, 58.13, 58.38, 121.76, 127.31, 128.97, 129.51, 131.62, 137.09, 137.99, 143.66, 210.18; Minor:  $^1\text{H NMR}$  (400 MHz,  $\text{CDCl}_3$ )  $\delta$  4.51 (dd,  $J = 9.2, 5.0$  Hz, 1H); **HRMS** Found  $[\text{M} - \text{H}]^-$ , 436.05835, 438.05614.  $\text{C}_{20}\text{H}_{23}\text{BrNO}_3\text{S}$  requires  $[\text{M} - \text{H}]^-$ , 436.05822, 438.05617; **IR** (ATR,  $\text{cm}^{-1}$ )  $\nu$  3248, 2956, 1710, 1598, 1490, 1446, 1358, 1321, 1239, 1159, 1094, 1073, 1050, 1010, 935, 888, 828, 810, 721, 684, 658, 622;  $[\alpha]_{\text{D}}^{25} = -45.27^{\circ}$  ( $c$  0.67,  $\text{CHCl}_3$ ); **HPLC conditions**: CHIRALPAK<sup>®</sup> AD-H, 0.8 ml/min; gradient from 95% to 50% of Hexane in *i*PrOH, time of major diastereomer: 21.45, 23.39 min; minor diastereomer: 23.94, 25.38 min;  $\lambda = 226$ .



**3-(4-bromobenzylidene)hexan-2-one 4.16**

Isolated as an elimination side-product from the synthesis of compound **4.14**.

**<sup>1</sup>H NMR** (400 MHz, CDCl<sub>3</sub>) δ 0.93 (t, *J* = 7.3 Hz, 3H), 1.39–1.51 (m, 2H), 2.39–2.48 (m, 2H), 2.43 (s, 3H), 7.24 (d, *J* = 8.4 Hz, 2H), 7.34 (s, 1H), 7.54 (d, *J* = 8.4 Hz, 2H).



**4-methylbenzenesulfonamide<sup>45</sup>**

Isolated as an elimination side-product from the synthesis of compound **4.14**.

**<sup>1</sup>H NMR** (400 MHz, CDCl<sub>3</sub>) δ 2.44 (s, 3H), 4.72 (br s, 2H), 7.32 (d, *J* = 8.0 Hz, 2H); 7.82 (d, *J* = 8.0 Hz, 2H).

## 4.5 References

1. M. S. Taylor and E. N. Jacobsen, *Proc. Natl. Acad. Sci. U. S. A.*, 2004, **101**, 5368-5373.
2. C. Wolf, in *Dynamic Stereochemistry of Chiral Compounds: Principles and Applications*, The Royal Society of Chemistry, 2008, pp. 204-330.
3. D. Campolo, S. Gastaldi, C. Roussel, M. P. Bertrand and M. Nechab, *Chem. Soc. Rev.*, 2013, **42**, 8434-8466.
4. B. H. Lipshutz, K. Siegmann, E. Garcia and F. Kayser, *J. Am. Chem. Soc.*, 1993, **115**, 9276-9282.
5. B. H. Lipshutz, F. Kayser and Z.-P. Liu, *Angew. Chem., Int. Ed. Engl.*, 1994, **33**, 1842-1844.
6. D. Seebach, A. R. Sting and M. Hoffmann, *Angew. Chem., Int. Ed. Engl.*, 1996, **35**, 2708-2748.
7. S. A. A. El Bialy, H. Braun and L. F. Tietze, *Eur. J. Org. Chem.*, 2005, 2965-2972.
8. T. Kawabata and F. Kaoru, in *Top. Stereochem.*, 2003, pp. 175-205.
9. V. Alezra and T. Kawabata, *Synthesis*, 2016, **48**, 2997-3016.
10. D. Mouysset, C. Tessonnier, A. Tintaru, F. Dumur, M. Jean, N. Vanthuyne, M. P. Bertrand, D. Siri and M. Nechab, *Chem. Eur. J.*, 2017, **23**, 8375-8379.
11. J. Clayden and N. Vassiliou, *Org. Biomol. Chem.*, 2006, **4**, 2667-2678.
12. T. Kawabata, S. Majumdar, K. Tsubaki and D. Monguchi, *Org. Biomol. Chem.*, 2005, **3**, 1609-1611.
13. D. J. Cram and K. R. Kopecky, *J. Am. Chem. Soc.*, 1959, **81**, 2748-2755.
14. X. Chen, E. R. Hortelano, E. L. Eliel and S. V. Frye, *J. Am. Chem. Soc.*, 1992, **114**, 1778-1784.
15. T. Nakata, T. Tanaka and T. Oishi, *Tetrahedron Lett.*, 1983, **24**, 2653-2656.
16. D. Morton and R. A. Stockman, *Tetrahedron*, 2006, **62**, 8869-8905.
17. H. Mei, J. Han, S. Fustero, R. Román, R. Ruzziconi and V. A. Soloshonok, *J. Fluorine Chem.*, 2018, **216**, 57-70.
18. J.-M. Garnier, C. Anstiss and F. Liu, *Adv. Synth. Catal.*, 2009, **351**, 331-338.
19. J.-M. Garnier and F. Liu, *Org. Biomol. Chem.*, 2009, **7**, 1272-1275.
20. C. Anstiss and F. Liu, *Tetrahedron*, 2010, **66**, 5486-5491.
21. F. Liu, *Chirality*, 2013, **25**, 675-683.
22. R. Kenny and F. Liu, *Chem. Rec.*, 2017, **17**, 535-553.
23. S. S. Eliseenko and F. Liu, *Tetrahedron*, 2019, **75**, 518-526.
24. C. Anstiss, J.-M. Garnier and F. Liu, *Org. Biomol. Chem.*, 2010, **8**, 4400-4407.
25. C. Chen, S. Jin, Z. Zhang, B. Wei, H. Wang, K. Zhang, H. Lv, X.-Q. Dong and X. Zhang, *J. Am. Chem. Soc.*, 2016, **138**, 9017-9020.
26. L. Ding, X. Sui and Z. Gu, *ASC Catal.*, 2018, **8**, 5630-5635.
27. Q. Wang, S. Li, C.-J. Hou, T.-T. Chu and X.-P. Hu, *Tetrahedron*, 2019, **75**, 3943-3950.
28. C. Conti, L. Proietti Monaco and N. Desideri, *Bioorg. Med. Chem.*, 2017, **25**, 2074-2083.
29. T. Jin, G. Feng, M. Yang and T. Li, *Synth. Commun.*, 2004, **34**, 1277-1283.
30. M.-J. Qi and M. Shi, *Tetrahedron*, 2007, **63**, 10415-10424.
31. N. J. Victor, J. Gana and K. M. Muraleedharan *Chem. Eur. J.*, 2015, **21**, 14742-14747.
32. A. K. Chakraborti, S. Rudrawar and A. Kondaskar, *Org. Biomol. Chem.*, 2004, **2**, 1277-1280.
33. M. Bailey, I. E. Markó, W. D. Ollis and P. R. Rasmussen, *Tetrahedron Lett.*, 1990, **31**, 4509-4512.
34. P. Knochel and R. D. Singer, *Chem. Rev.*, 1993, **93**, 2117-2188.
35. B. L. Feringa, R. Naasz, R. Imbos and L. A. Arnold, in *Modern Organocopper Chemistry*, 2002, pp. 224-258.
36. J. H. Kim, Y. O. Ko, J. Bouffard and S.-G. Lee, *Chem. Soc. Rev.*, 2015, **44**, 2489-2507.
37. C. Zhang and Z.-X. Wang, *Appl. Organomet. Chem.*, 2009, **23**, 9-18.

38. S. Ay, M. Nieger and S. Bräse, *Chem. Eur. J.*, 2008, **14**, 11539-11556.
39. L. Pu and H.-B. Yu, *Chem. Rev.*, 2001, **101**, 757-824.
40. C. K. Reddy, A. Devasagayaraj and P. Knochel, *Tetrahedron Lett.*, 1996, **37**, 4495-4498.
41. W. L. F. Armarego and C. L. L. Chai, *Purification of Laboratory Chemicals, 6th Edition*, Butterworth-Heinemann, 6 edn., 2009.
42. L. Cheng, L. Liu, H. Jia, D. Wang and Y.-J. Chen, *J. Org. Chem.*, 2009, **74**, 4650-4653.
43. H. Cai, Y. Zhou, D. Zhang, J. Xu and H. Liu, *Chem. Commun.*, 2014, **50**, 14771-14774.
44. P. C. Too, T. Noji, Y. J. Lim, X. Li and S. Chiba, *Synlett*, 2011, **2011**, 2789-2794.
45. R. Hayashi, A. Shimizu, Y. Song, Y. Ashikari, T. Nokami and J.-i. Yoshida, *Chem. Eur. J.*, 2017, **23**, 61-64.



## **CHAPTER 5**

### **Conclusions and Future Directions**

## CHAPTER 5. Conclusions and Future Directions

### 5.1 Conclusions

This thesis describes the ability of multifunctional MAP-based systems to organize the catalytic processes by H-bonding supported metal- and organocatalytic activations. A series of novel MAP-based multifunctional catalysts **2.4a-f**, bearing pyrrolyl and imidazolyl fragments were designed, synthesized, and tested in *aza*-MBH and MBH reactions providing corresponding products in excellent and synthetically useful enantioselectivity. The extended generality could be potentially attributed to the improved cooperativity by the formation of CH/ $\pi$ -interaction between the organocatalyst's pyrrole fragment and the methyl moiety of the external acid activator. Novel pyrrole-containing structures became the first representatives of pyrrolephosphine organocatalysts.

Trifunctional organocatalysts **1.46**, **1.48**, and novel indolyl-containing catalyst **2.4c** were tested as H-bonding ligands in Pd-catalysed asymmetric allylic alkylation, Cu-catalysed diethylzinc addition, and Rh-catalysed hydrogenation. All structures demonstrated ability to provide palladium and copper catalysis albeit at modest enantioselectivity. The enantiodivergency of palladium catalysis was observed for **1.46a** and **1.48a** and could be attributed to a possible synergistic influence of ligand's H-bonding and steric repulsion factors. A new donor-type "metal-ligand-substrate" H-bonding activation strategy was proposed for the trifunctional MAP-based ligands. Palladium complexes provided by **1.46a** and **1.48a** confirmed the possibility of H-bonding formation and revealed the new for MAP-core structures *P,N*-coordination mode of palladium.

The model dual catalyst **1.46a** was investigated for the ability to transfer chirality through the *in situ* generated chiral *aza*-MBH intermediate in designed *aza*-MBH / nucleophilic cyclization cascade, an *aza*-MBH / epoxidation tandem sequence, and an *aza*-MBH / diethylzinc addition sequence. The epoxidation of *in situ* generated chiral *aza*-MBH intermediates led to the two

dominant enantiomers formation due to poor diastereoselectivity of the process. The chirality translation through the *aza*-MBH / diethylzinc addition sequence afforded the single dominant enantiomer of the corresponding product. It was proposed that the *in situ* formed chiral intermediate serves as a chiral ligand for the following diethylzinc addition and out-compete the chiral catalyst **1.46a** preventing the realization of hybrid catalysis.

Finally, the dualistic nature of trifunctional MAP-based systems providing H-bonding metal- and organocatalysis has been confirmed, however, its application as a single catalyst in challenging hybrid processes requires further design and investigations.

## 5.2 Future directions

Despite significant advances achieved in MAP-based trifunctional systems in cooperative organocatalysis thus far, the development of their catalytic dualism has remained limited. The interesting enantiodivergent reactivities, as observed in Pd-catalysed AAA reactions, warrant further mechanistic investigations in order to understand cooperative drivers leading to the enantiodivergency. Tests of control and new catalysts with modifications to the phenol/aniline groups can help understanding better the role of the Brønsted acid fragment in the catalysis. NMR-based study of allyl-palladium complexes may also help characterize the allyl isomer formed in the reaction and how it may influence the final enantioselectivity. The additional investigations of MAP-based multifunctional systems in complexes with cobalt, nickel, and iron could be useful in understanding of the generality characteristic of the multifunctional ligands.

Based on the initial tests in copper catalysis, MAP-based ligands can be further investigated in diethylzinc addition. More extensive screening of conditions could be done in order to understand the catalytic profile and find a way to suppress the racemic reaction. The interesting catalytic organization of *aza*-MBH / diethylzinc addition sequence can be further explored by additional control experiments to clarify the influence of *in situ* generated chiral *aza*-MBH

intermediate on the following diethylzinc addition step. Other organozinc reagents and conditions could also be examined. Future non-linear effect (NLE) investigations could help better understand the synergy between the chiral intermediate and ligand **1.46a**.

Given the catalytic dualism exhibited by MAP-based trifunctional systems, further development of hybrid cascades could reveal new potentials of these complex catalysts. Each one of the functional motifs could be varied to introduce different coordination groups, acid-base catalytic motifs, and H-bonding donors/acceptors. New catalytic cooperativities may derive from these structures for constructing new cascade reactions. Multiple trifunctional systems could also be connected to test the possibility of spatially relayed reaction cascades.

# **APPENDICES**

## A1. Representatives of MAP-based ligands

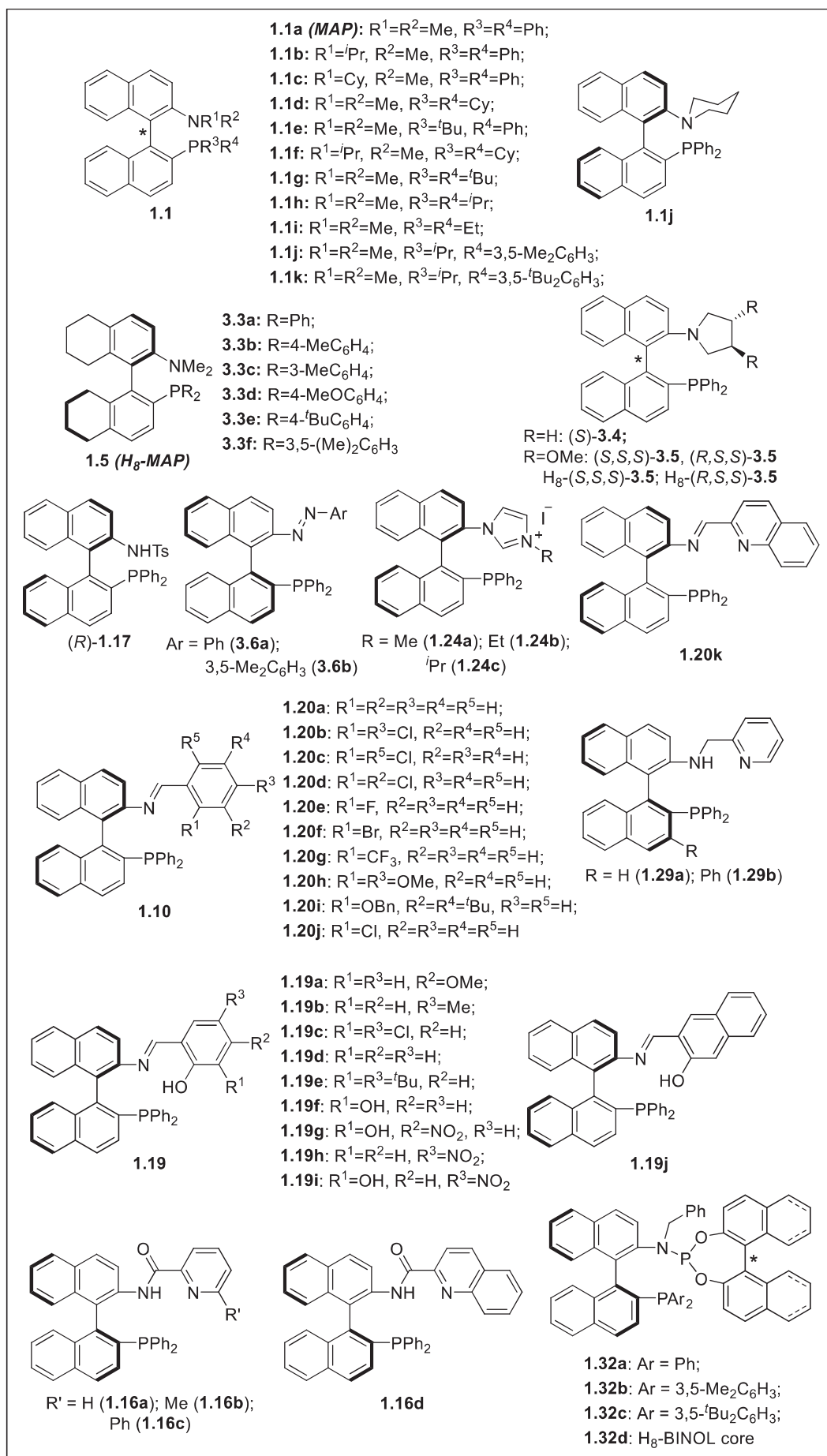


**Table A1** Application of MAP-based structures as ligands.

Reactions	Catalysts	Metal	yield, [%]	<i>ee</i> , [%] (dr)	References
Allylic substitution	<b>1.1a, 1.1b, 1.1c, 1.4j</b>	Pd	77–95	68–73	1
	<b>3.3</b>	Pd	89–99	73–84	2
	<b>3.4, 3.5</b>	Pd	81–97	27–83	3
	<b>3.6</b>	Pd	37–98	42–88	4
	<b>1.19</b>	Pd	21–99	0–76	5
Vinylation and Arylation	<b>1.1a, 1.1d, 1.1e, 1.1g</b>	Pd	<10–99	5–97	6-9
Dearomatization	<b>1.1d, 1.1e, 1.1f</b>	Pd	62–99	50–93	10, 11
Intramolecular cyclization	<b>1.1g</b>	Pd	83–95	98–99	12
Suzuki-Miyaura	<b>1.1a, 1.1d, 1.1g, 1.1h</b>	Pd	56–96	40–94	13-15
Three-component cross-coupling	<b>1.1k</b>	Pd	28–90	76–96	16
Et <sub>2</sub> Zn addition	<b>1.17</b>	Cu	44–63	84–98	17
	<b>1.16</b>	Cu	69–97	83–98	18
	<b>1.16</b>	Cu	<10–89	9–97	19
Tandem Et <sub>2</sub> Zn addition / Michael	<b>1.6a,b</b>	Cu	60–88	90–97	20
Henry	<b>1.19a-e, j</b>	Cu	28–99	7–80	21
$\alpha$ -Hydroxylation and chlorination of $\beta$ -keto esters	<b>1.19a-g, j</b>	Cu	78–99	39–82	22, 23
Vinylogous Mannich	<b>1.20</b>	Ag	51–91	38–81 (3:1–99:1)	24
Hydrogenation of ketones	<b>1.29</b>	Ru	91–98	52–98	25-27
Vinylogous Mannich	<b>1.19a, b</b>	Ag	50–53	33–35	24
Hydroformylation of alkenes	<b>1.32a-c</b>	Rh	80–98	77–96	28-30
Hydroformylation of allylic alcohols	<b>1.32c</b>	Rh	60–90	80–93	31
Interrupted Hydroaminomethylation	<b>1.32a</b>	Rh	62–99	81–95	32
Hydrocyanation of alkenes	<b>1.32a,c</b>	Rh	75–90	86–90	33

## A2. Representatives of MAP-based organocatalysts

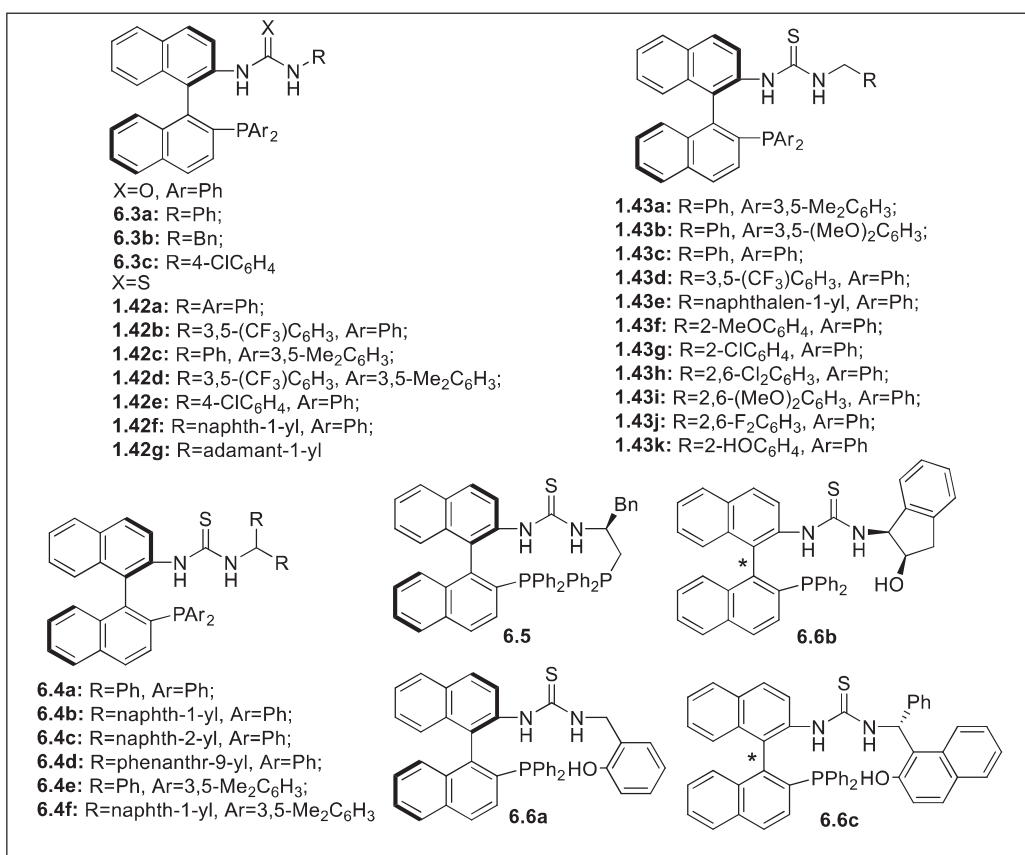
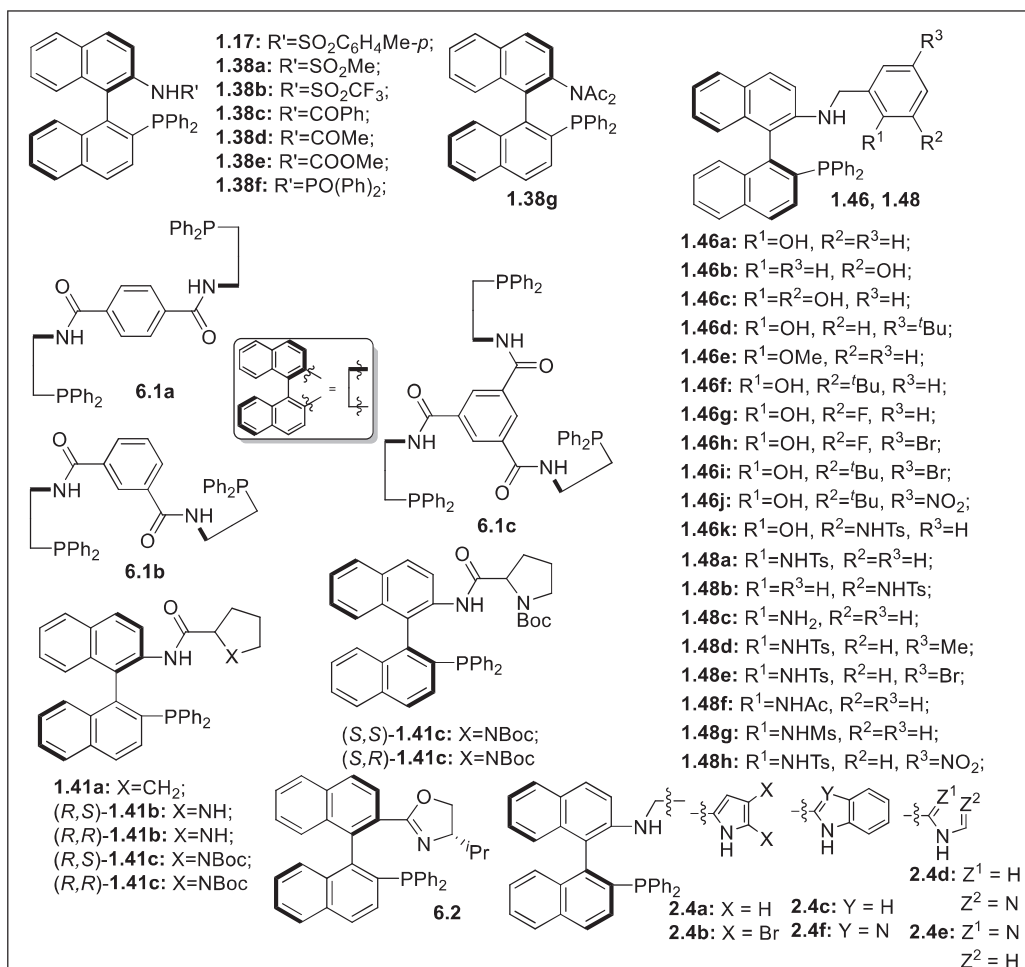


**Table A2** Application of MAP-based structures as organocatalysts.

Reactions	Catalysts	yield, [%]	<i>ee</i> , [%] ( <i>dr</i> )	References
<i>aza</i> -MBH	<b>1.17, 1.38</b>	0–99	<i>rac</i> –95	34
	<b>6.1</b>	69–98	35–91	35
	<b>6.3a, 1.42a,b</b>	50–98	64–97	36
	<b>1.46, 1.48, 2.4</b>	86–96	54–94	37-41
MBH	<b>1.46a,j, 2.4, 1.48</b>		26–77	38-40
Allylic substitution	<b>1.1a, 1.38a, d</b>	25–99	<i>rac</i> –98 (51:49 – >95:5)	42, 43
	<b>1.41</b>	47–97	85–99 (>95:5)	44
	<b>1.41b,c</b>	40–95	34–78	45
	<b>1.38d, 6.3a, 1.42c,d, 1.43a–c</b>	76–95	85–98 (2:1 – 20:1)	46
	<b>1.42a,b, 1.43c– j; 1.35a</b>	20–99	26–90	47
	<b>1.43c,f,i, 6.4a, 6.6</b>	53–99	64–97	48
[3+2] Annulation	<b>6.4a</b>	92	74 (9:1)	49
[4+1] Annulation	<b>1.42b,f, 1.43a,e,d, 6.4</b>	29–99	7–98 (1:1 – 7:1)	50, 51
[3+2] Cycloaddition	<b>6.3,c, 1.42f, 1.43c, 6.4a,c,d, 6.5</b>	42–88	36–63	52

### A3. NMR Spectra of epoxides 4.12 and product 4.14.

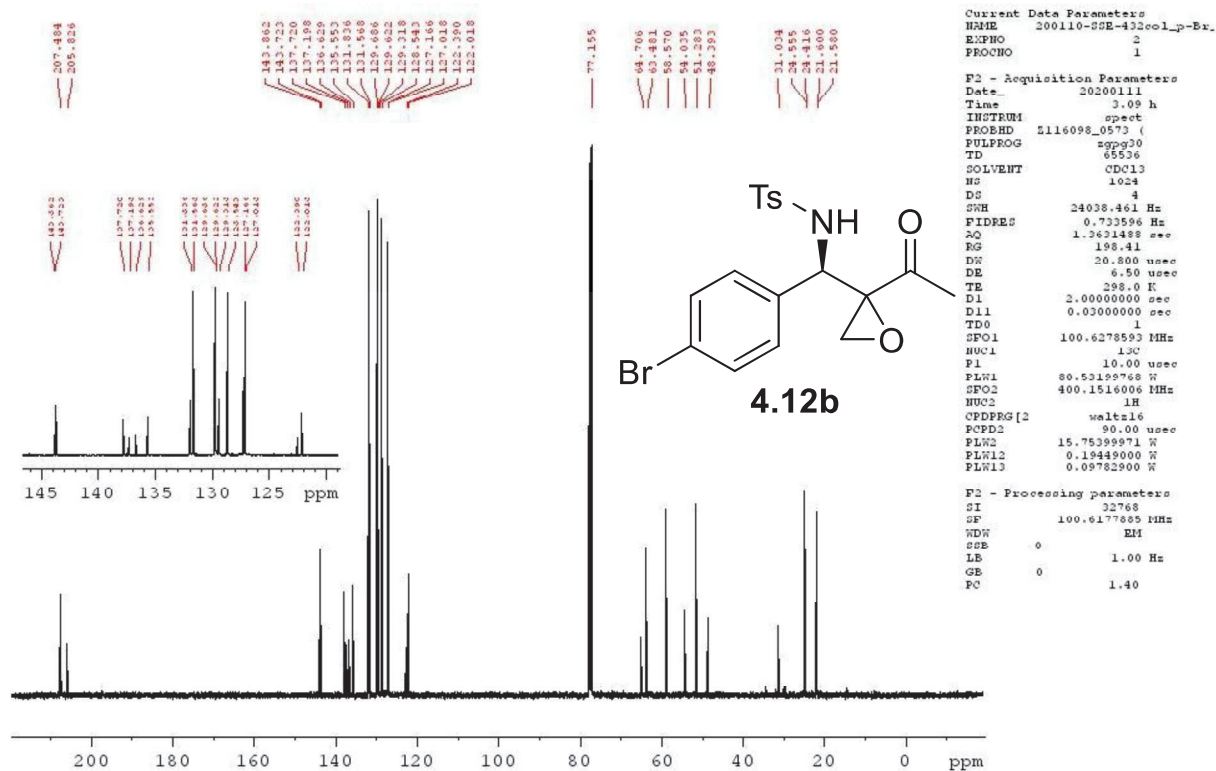
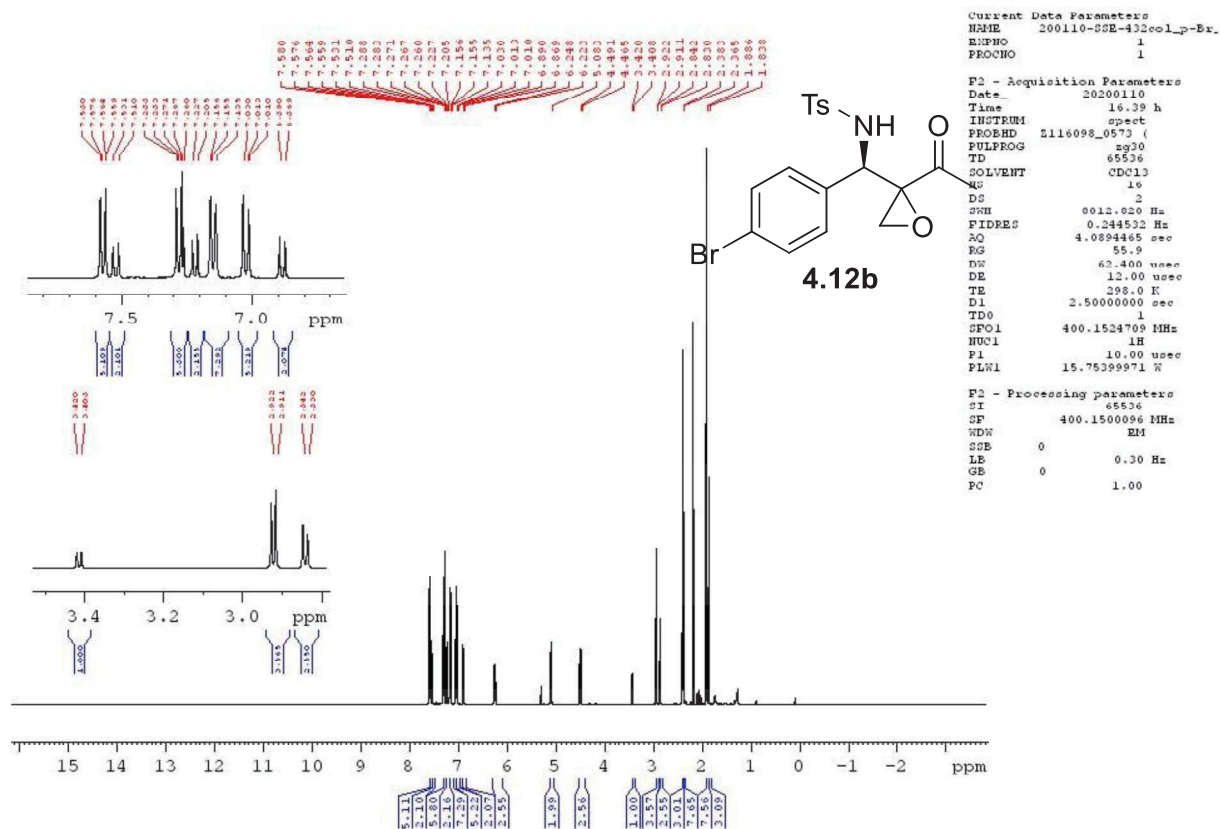


Figure A2 <sup>13</sup>C NMR spectra of 4.12b in CDCl<sub>3</sub>.

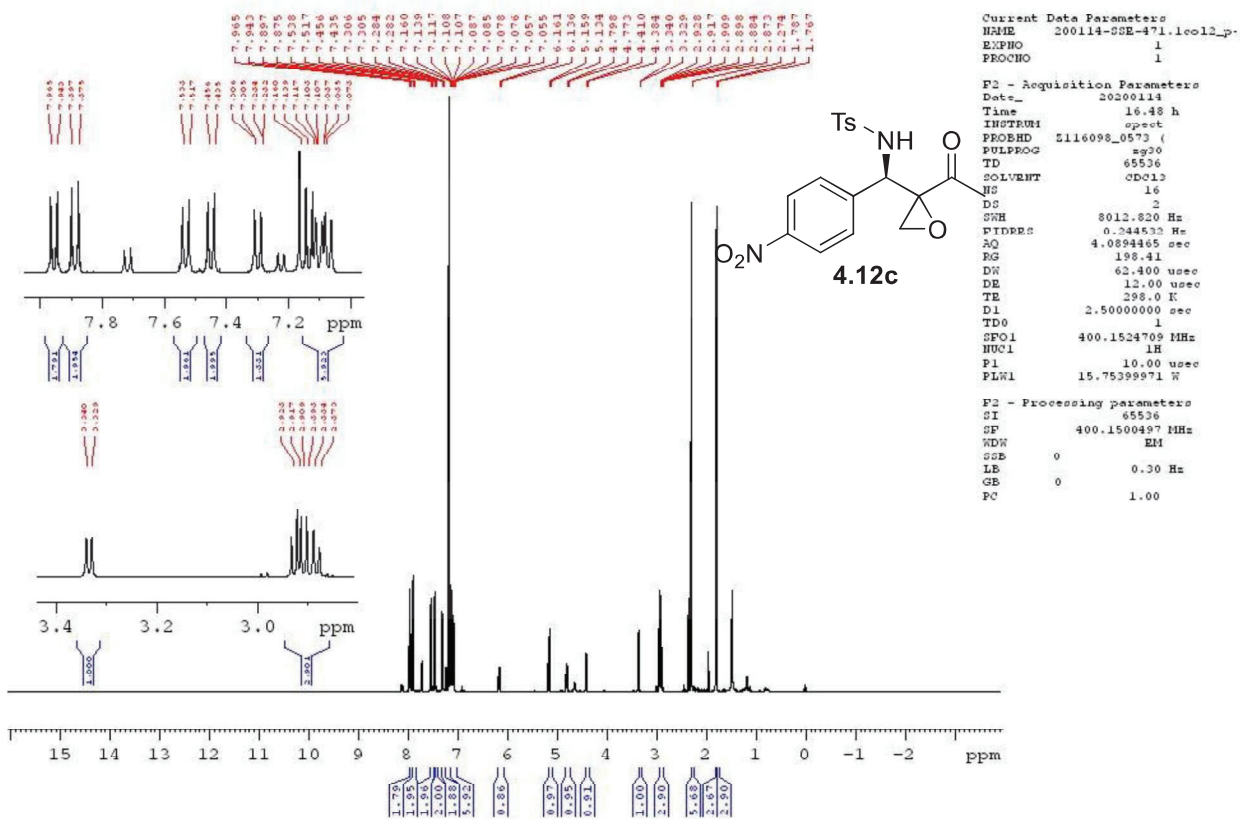


Figure A3 <sup>1</sup>H NMR spectra of 4.12c in CDCl<sub>3</sub>.

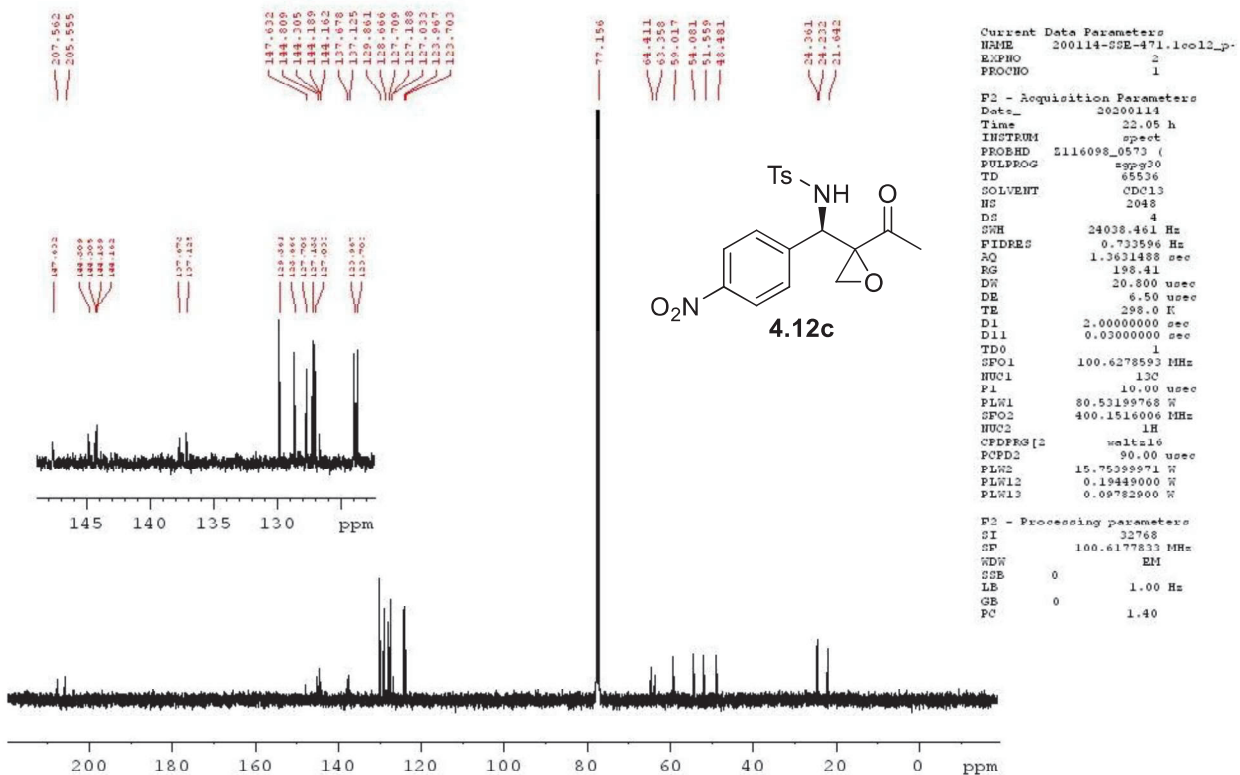


Figure A4 <sup>13</sup>C NMR spectra of 4.12c in CDCl<sub>3</sub>.

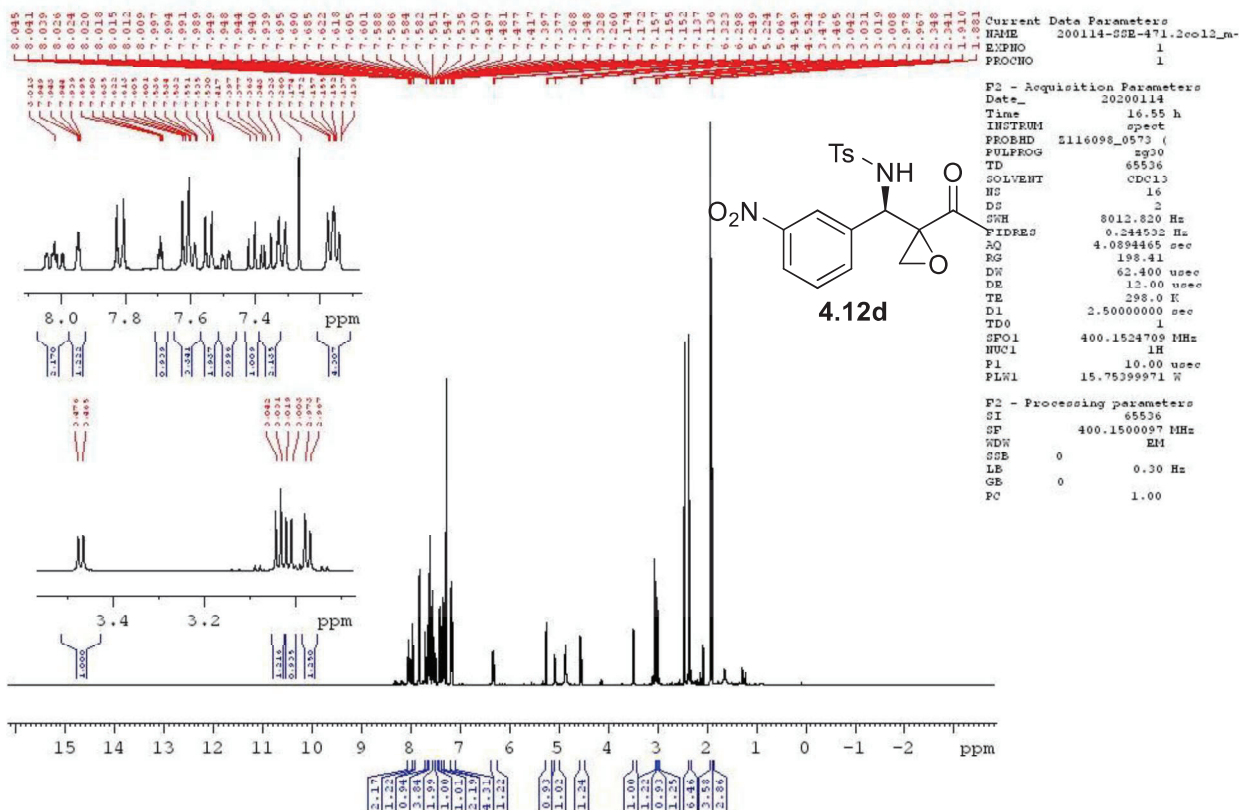


Figure A5 <sup>1</sup>H NMR spectra of **4.12d** in CDCl<sub>3</sub>.

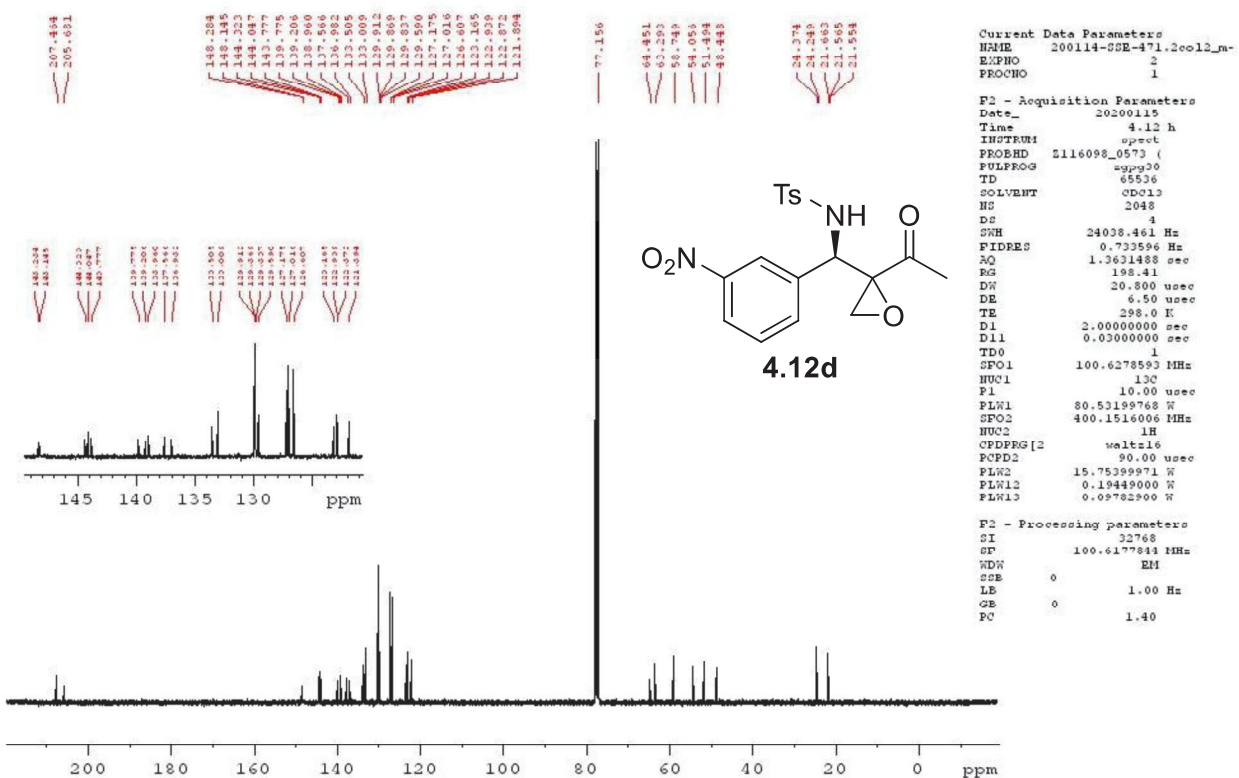


Figure A6 <sup>13</sup>C NMR spectra of **4.12d** in CDCl<sub>3</sub>.



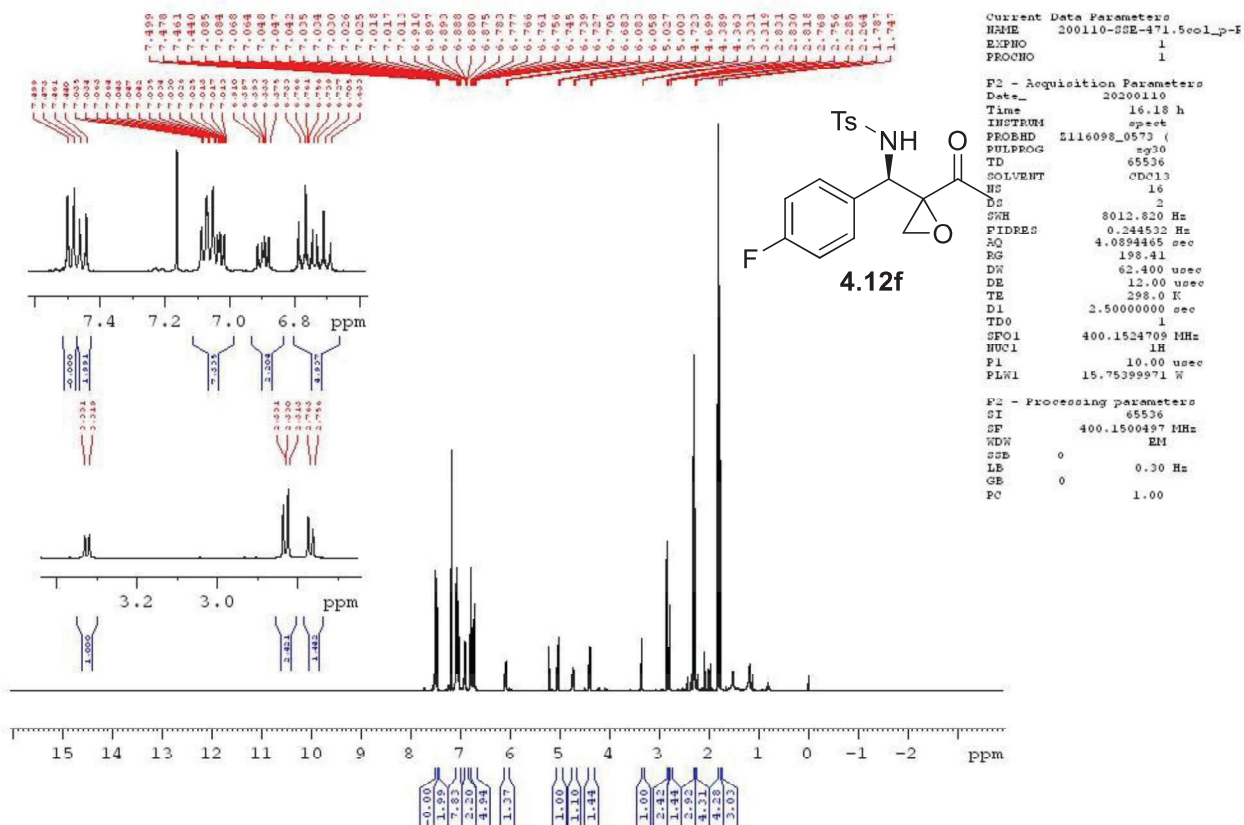


Figure A9 <sup>1</sup>H NMR spectra of **4.12f** in CDCl<sub>3</sub>.

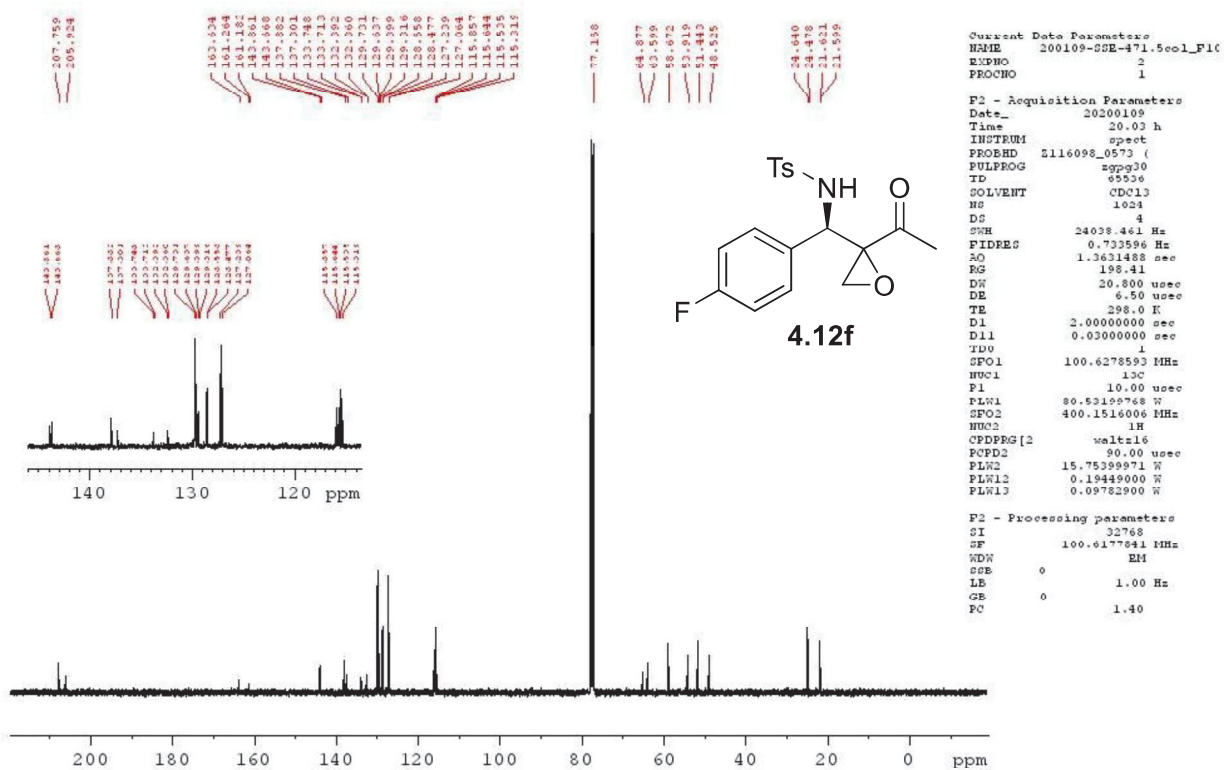


Figure A10 <sup>13</sup>C NMR spectra of **4.12f** in CDCl<sub>3</sub>.

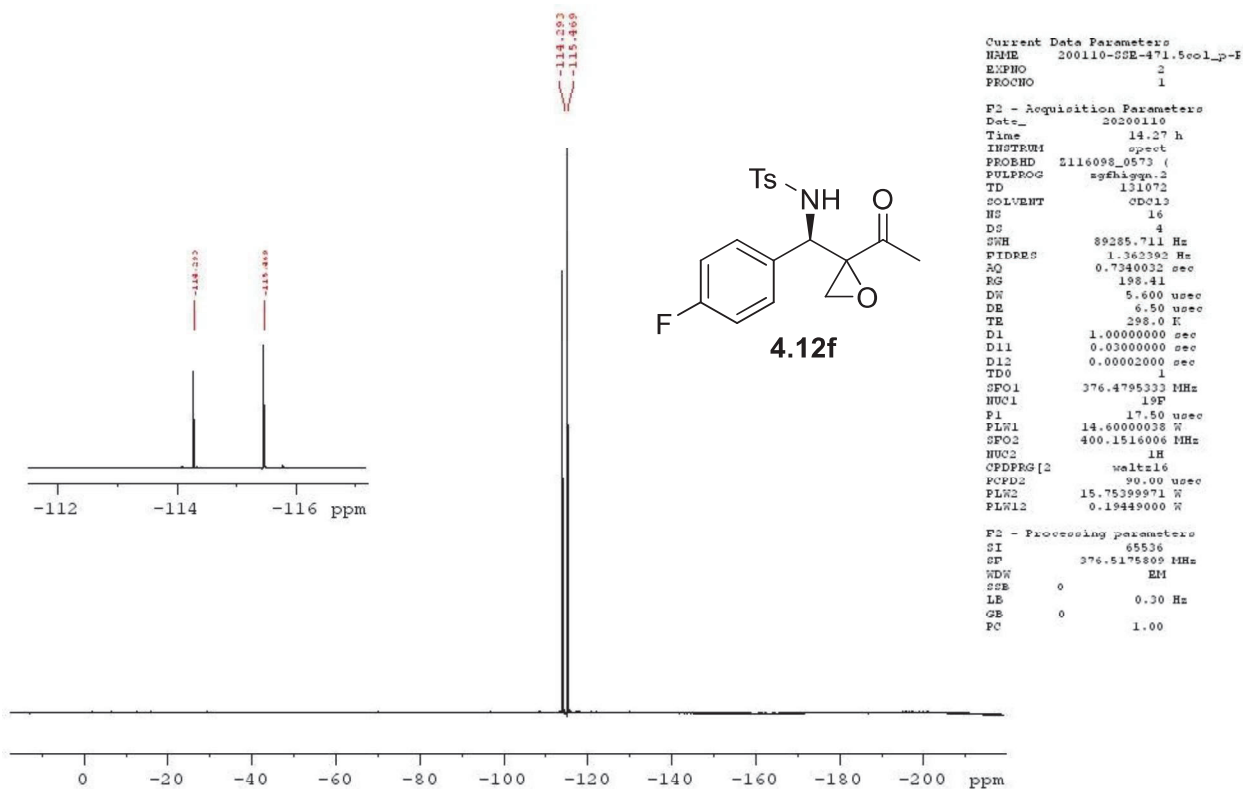


Figure A11  $^{19}\text{F}$  NMR spectra of **4.12f** in  $\text{CDCl}_3$ .

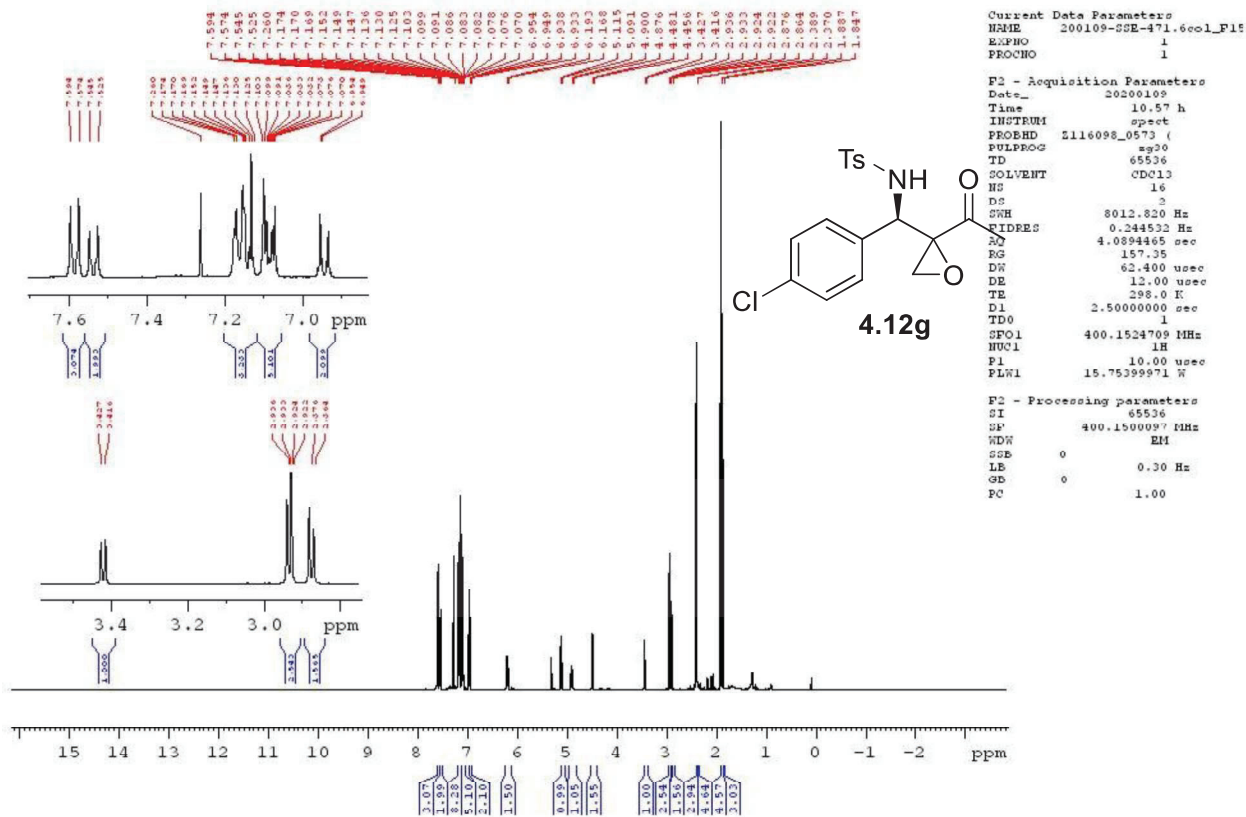


Figure A12  $^1\text{H}$  NMR spectra of **4.12g** in  $\text{CDCl}_3$ .

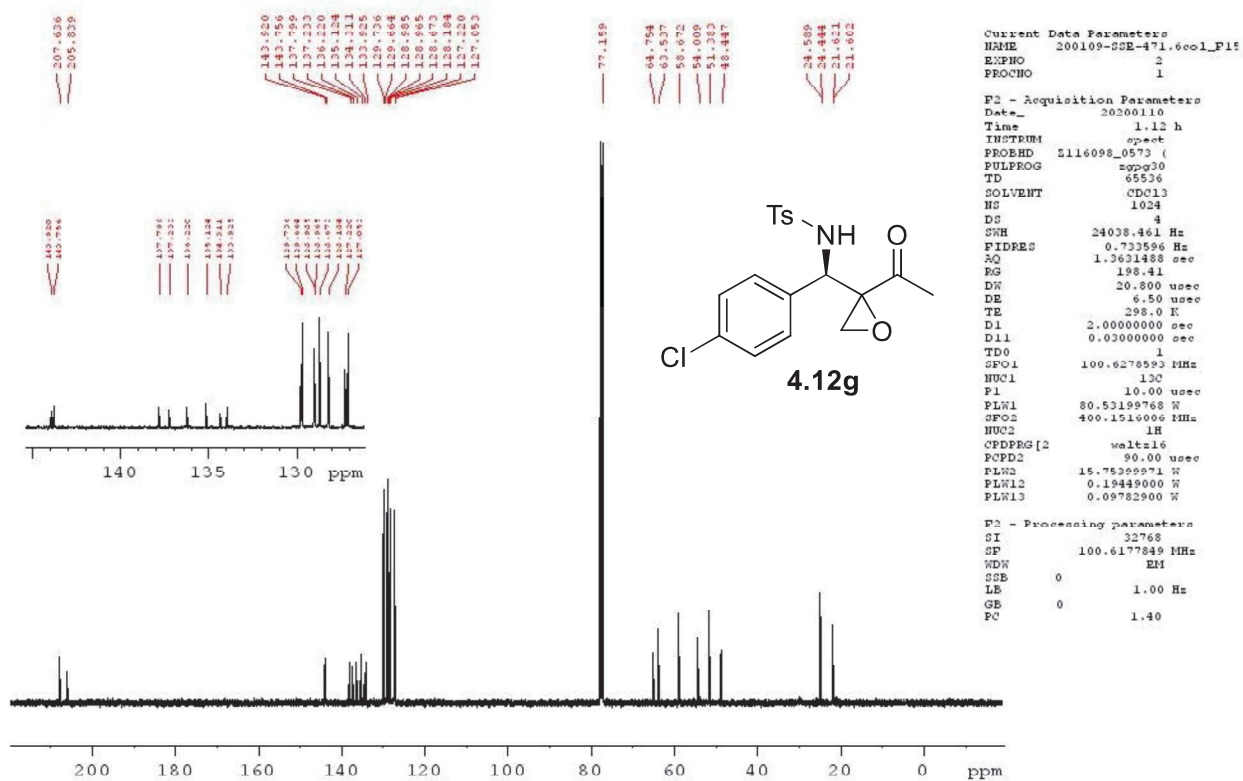


Figure A13  $^{13}\text{C}$  NMR spectra of **4.12g** in  $\text{CDCl}_3$ .

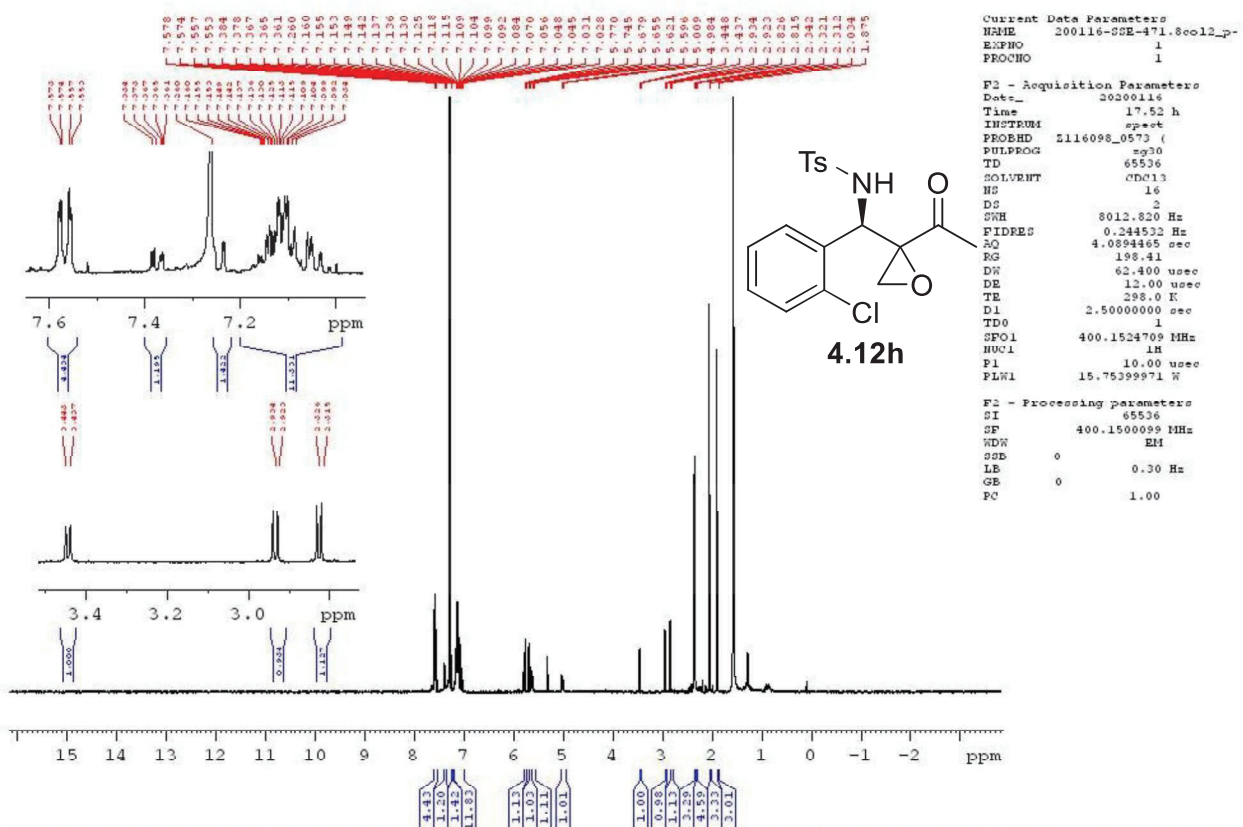


Figure A14  $^1\text{H}$  NMR spectra of **4.12h** in  $\text{CDCl}_3$ .

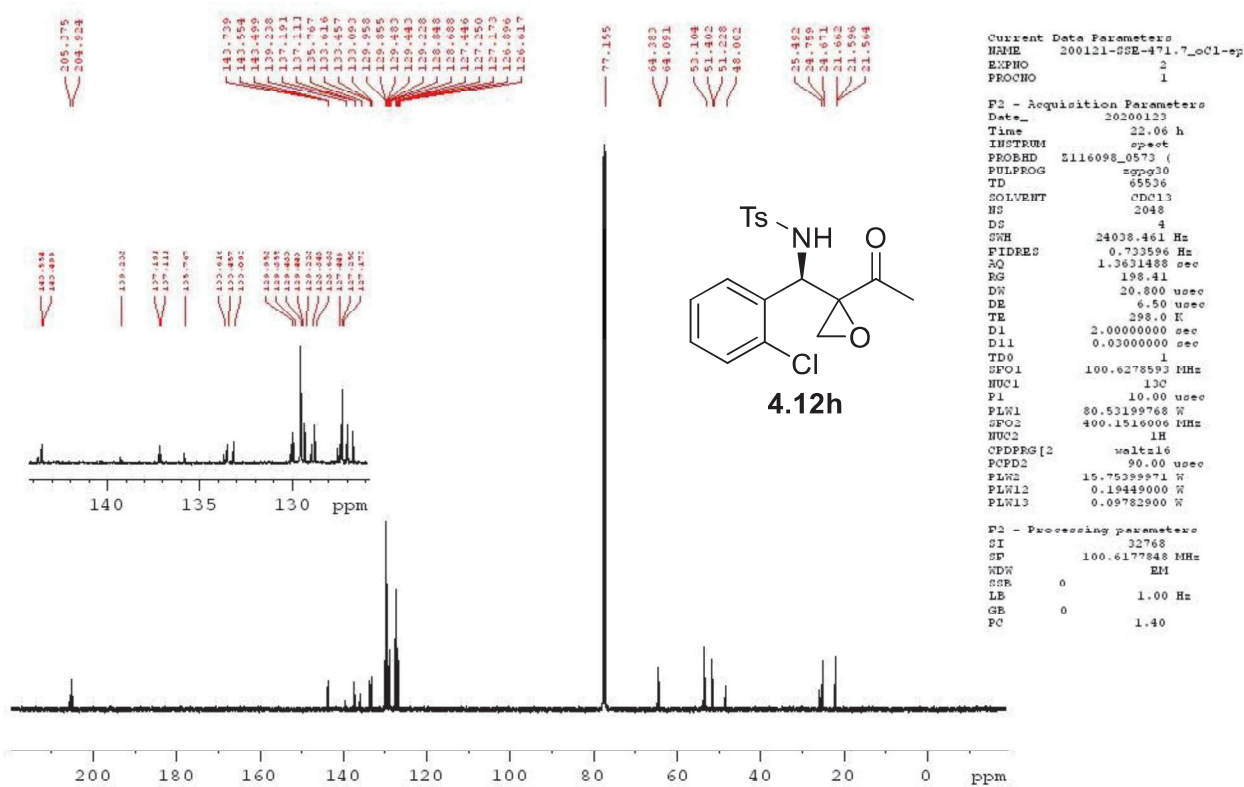


Figure A15  $^{13}\text{C}$  NMR spectra of **4.12h** in  $\text{CDCl}_3$ .

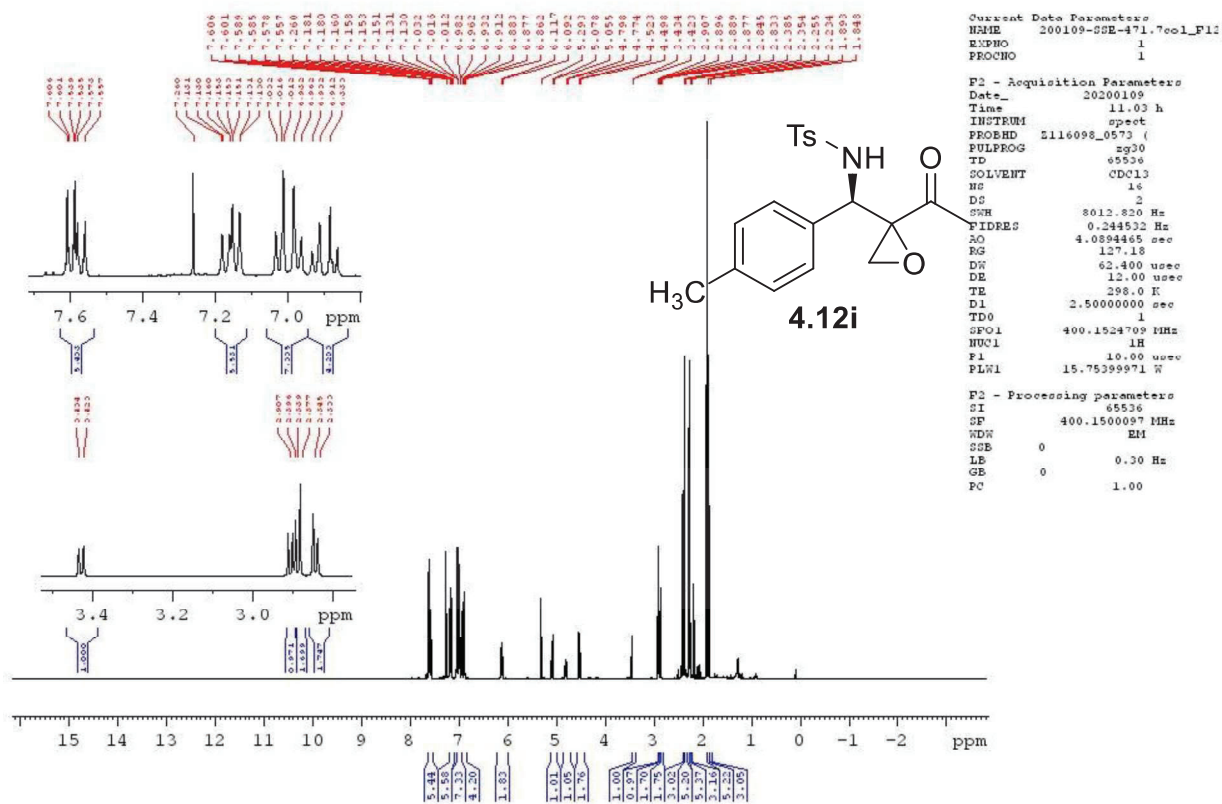


Figure A16  $^1\text{H}$  NMR spectra of **4.12i** in  $\text{CDCl}_3$ .

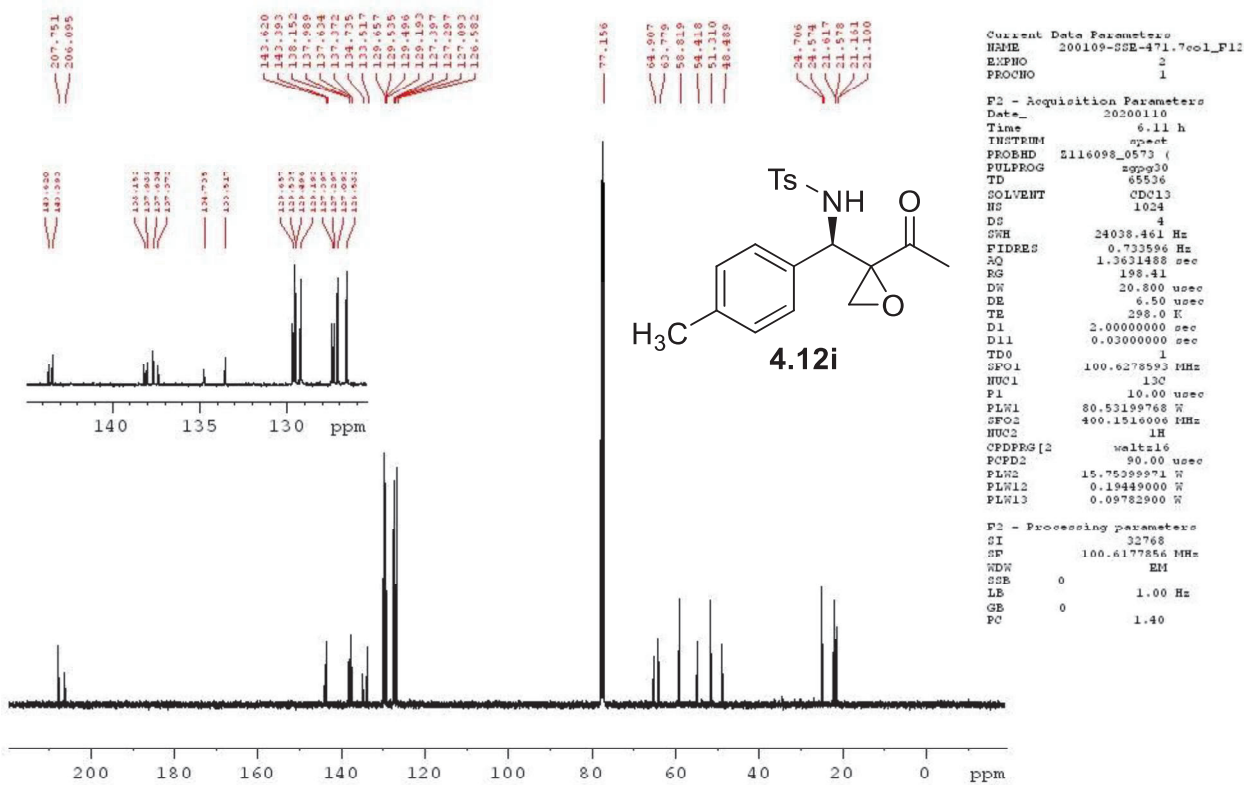


Figure A17 <sup>13</sup>C NMR spectra of **4.12i** in CDCl<sub>3</sub>.

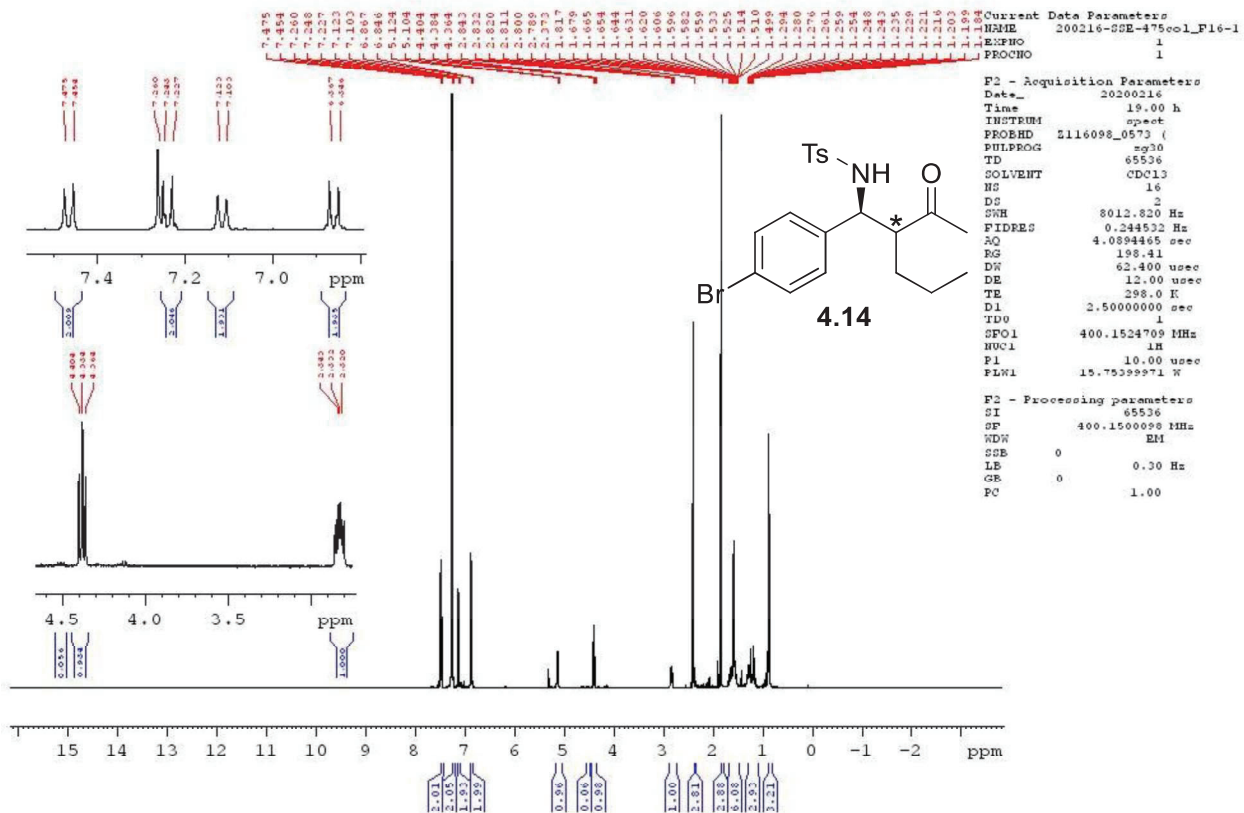


Figure A18 <sup>1</sup>H NMR spectra of **4.14** in CDCl<sub>3</sub>.

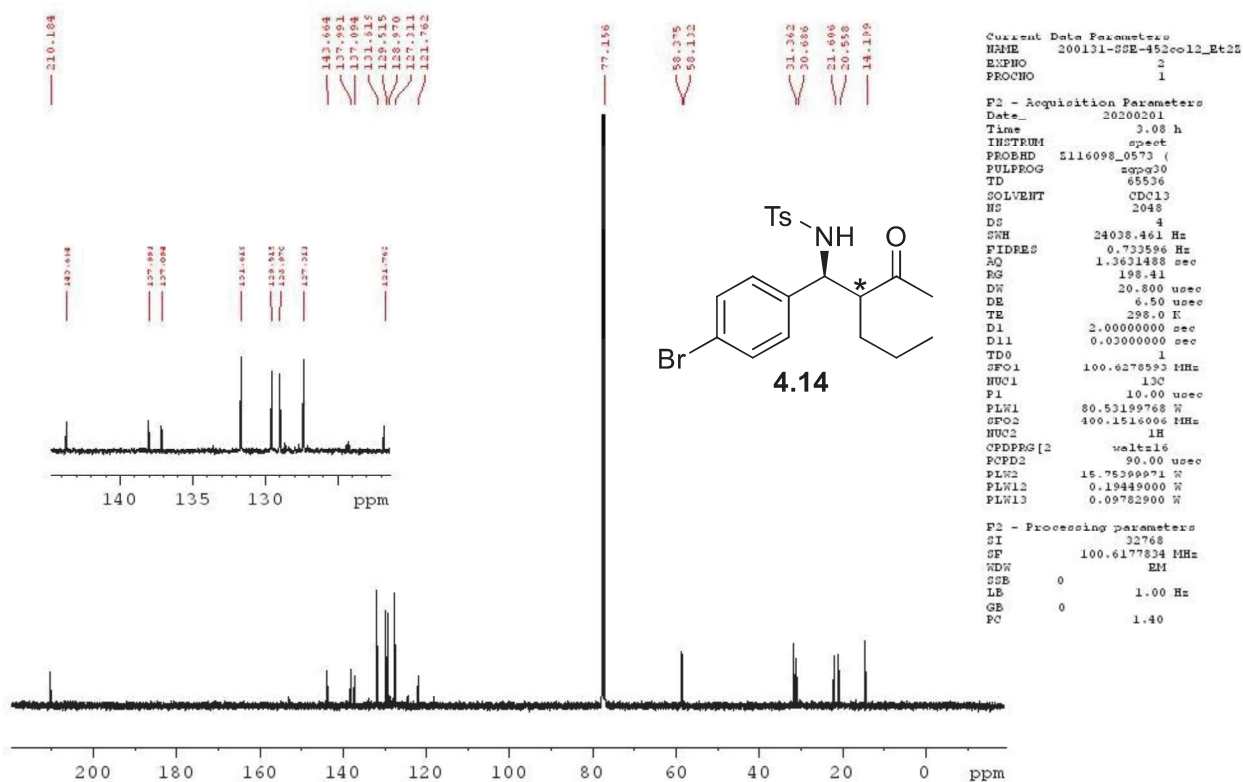


Figure A19  $^{13}\text{C}$  NMR spectra of **4.14** in  $\text{CDCl}_3$ .

#### A4. HPLC traces of selected epoxides **4.12**, product **4.14**, and product **3.11**.

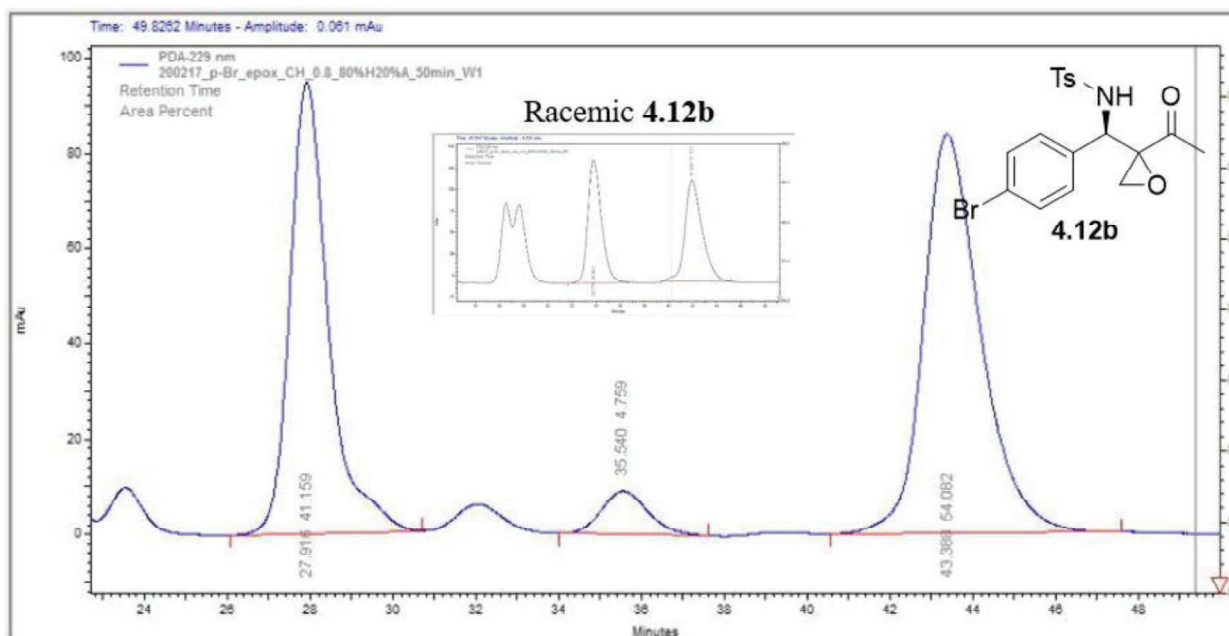


Figure A20 HPLC trace of **4.12b** and the HPLC trace of the corresponding racemic control in the extension.

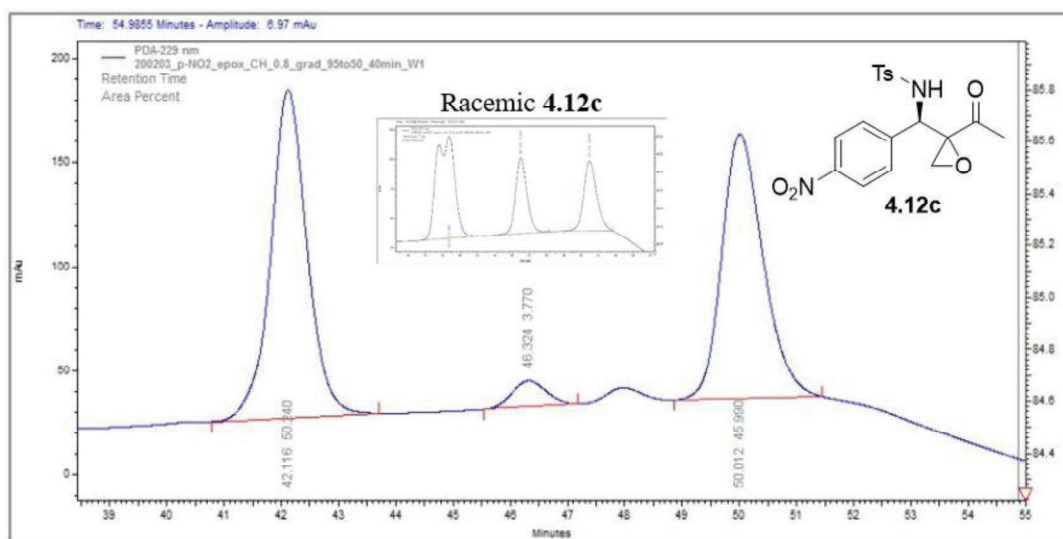


Figure A21 HPLC trace of **4.12c** and the HPLC trace of the corresponding racemic control in the extension.

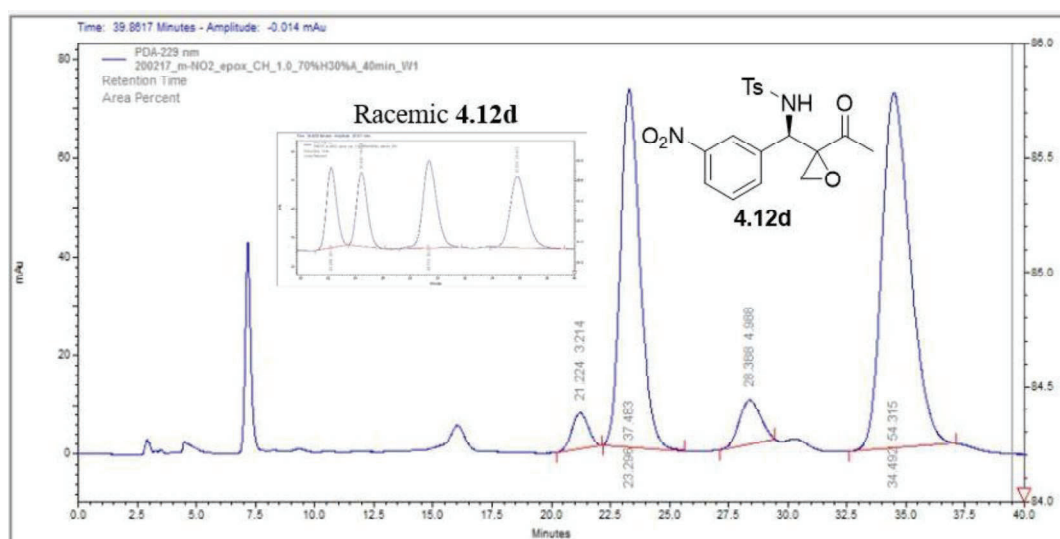


Figure A22 HPLC trace of **4.12d** and the HPLC trace of the corresponding racemic control in the extension.

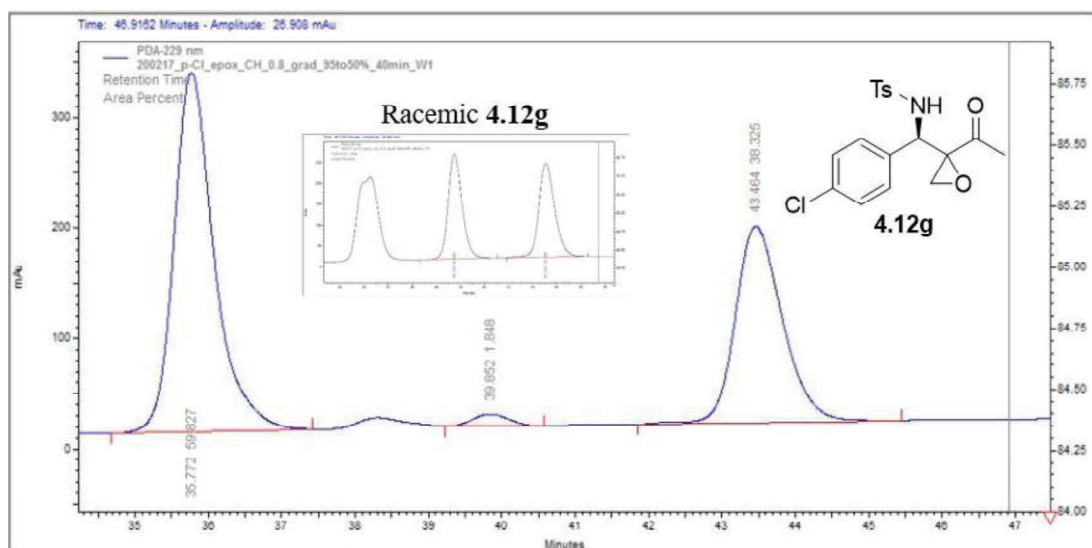


Figure A23 HPLC trace of **4.12g** and the HPLC trace of the corresponding racemic control in the extension.

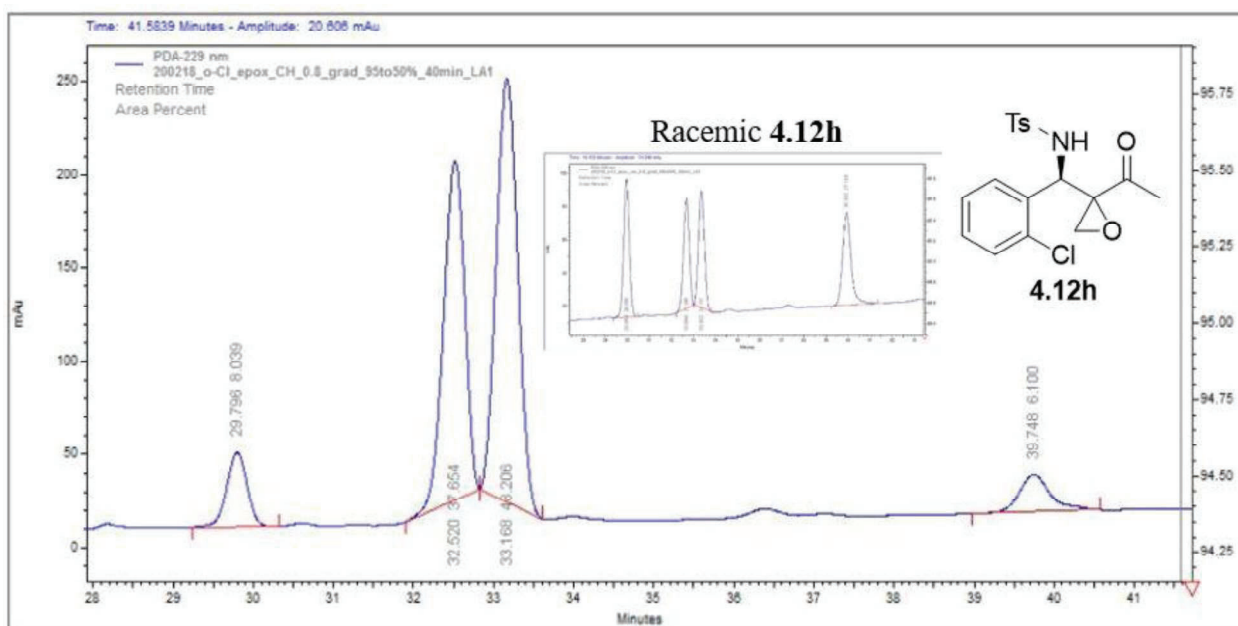


Figure A24 HPLC trace of **4.12h** and the HPLC trace of the corresponding racemic control in the extension.

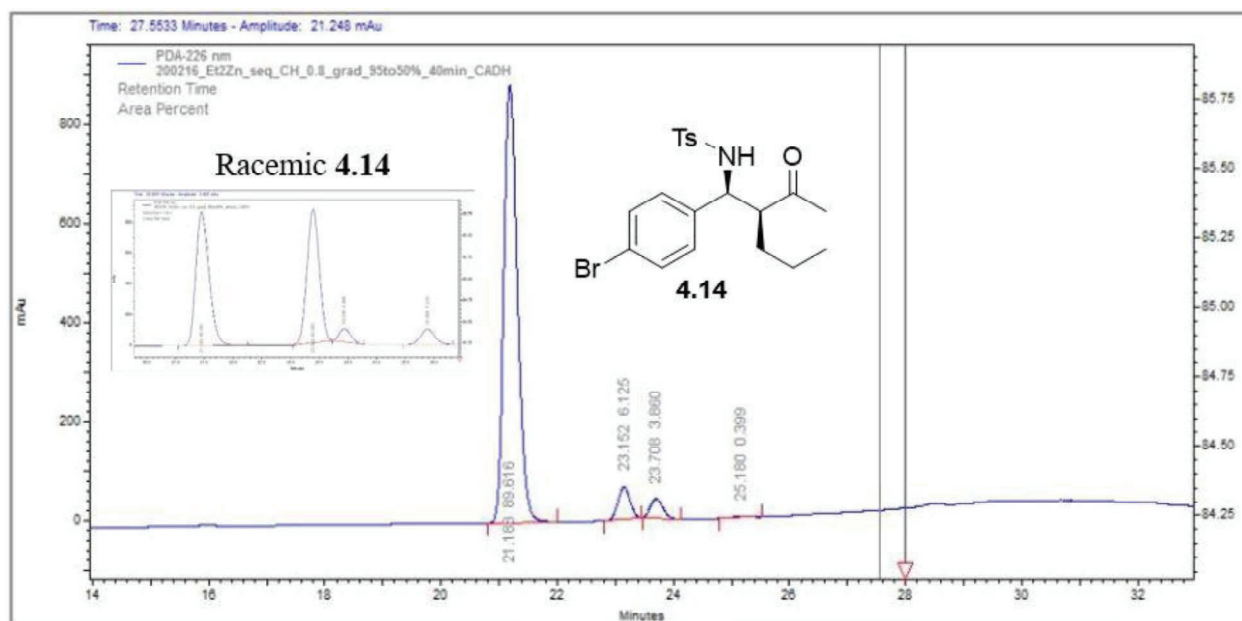


Figure A25 HPLC trace of **4.14** and the HPLC trace of the corresponding racemic control in the extension.

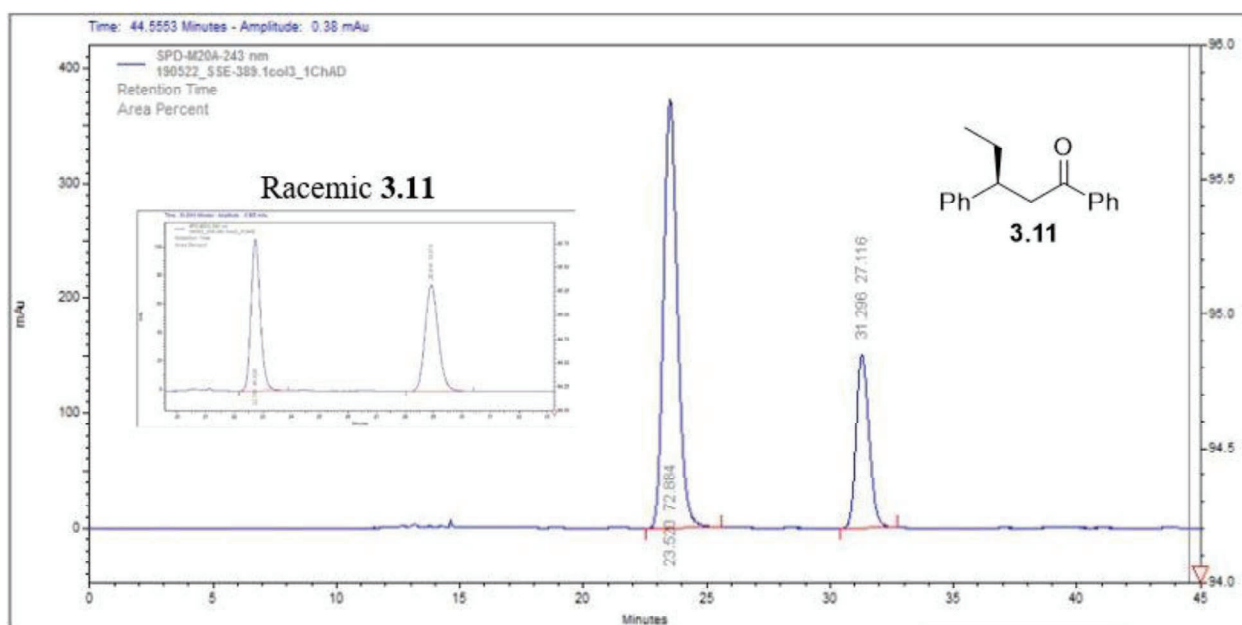


Figure A26 HPLC trace of **3.11** and the HPLC trace of the corresponding racemic control in the extension.

## A5. References

1. Š. Vyskočil, M. Smrčina and P. Kočovský, *Tetrahedron Lett.*, 1998, **39**, 9289-9292.
2. Y. Wang, H. Guo and K. Ding, *Tetrahedron: Asymmetry*, 2000, **11**, 4153-4162.
3. Y. Wang, X. Li and K. Ding, *Tetrahedron Lett.*, 2002, **43**, 159-161.
4. M. Kawamura, R. Kiyotake and K. Kudo, *Chirality*, 2002, **14**, 724-726.
5. Y.-W. Sun, J.-J. Jiang, M.-X. Zhao, F.-J. Wang and M. Shi, *J. Organomet. Chem.*, 2011, **696**, 2850-2856.
6. A. M. Taylor, R. A. Altman and S. L. Buchwald, *J. Am. Chem. Soc.*, 2009, **131**, 9900-9901.
7. T. Hamada, A. Chieffi, J. Åhman and S. L. Buchwald, *J. Am. Chem. Soc.*, 2002, **124**, 1261-1268.
8. T. Hamada and S. L. Buchwald, *Org. Lett.*, 2002, **4**, 999-1001.
9. A. Chieffi, K. Kamikawa, J. Åhman, J. M. Fox and S. L. Buchwald, *Org. Lett.*, 2001, **3**, 1897-1900.
10. S. Rousseaux, J. García-Fortanet, M. A. Del Aguila Sanchez and S. L. Buchwald, *J. Am. Chem. Soc.*, 2011, **133**, 9282-9285.
11. J. García-Fortanet, F. Kessler and S. L. Buchwald, *J. Am. Chem. Soc.*, 2009, **131**, 6676-6677.
12. S.-i. Kuwabe, K. E. Torrace and S. L. Buchwald, *J. Am. Chem. Soc.*, 2001, **123**, 12202-12206.
13. X. Shen, G. O. Jones, D. A. Watson, B. Bhayana and S. L. Buchwald, *J. Am. Chem. Soc.*, 2010, **132**, 11278-11287.
14. A. Herrbach, A. Marinetti, O. Baudoin, D. Guénard and F. Guéritte, *J. Org. Chem.*, 2003, **68**, 4897-4905.
15. J. Yin and S. L. Buchwald, *J. Am. Chem. Soc.*, 2000, **122**, 12051-12052.
16. L. Ding, X. Sui and Z. Gu, *ASC Catal.*, 2018, **8**, 5630-5635.
17. T. Morimoto, N. Mochizuki and M. Suzuki, *Tetrahedron Lett.*, 2004, **45**, 5717-5722.
18. X. Hu, H. Chen and X. Zhang, *Angew. Chem., Int. Ed.*, 1999, **38**, 3518-3521.
19. Q. Wang, S. Li, C.-J. Hou, T.-T. Chu and X.-P. Hu, *Appl. Organomet. Chem.*, 2019, **33**, e5108.
20. Q. Wang, S. Li, C.-J. Hou, T.-T. Chu and X.-P. Hu, *Tetrahedron*, 2019, **75**, 3943-3950.
21. J.-J. Jiang and M. Shi, *Tetrahedron: Asymmetry*, 2007, **18**, 1376-1382.
22. J.-J. Jiang, J. Huang, D. Wang, Z.-L. Yuan, M.-X. Zhao, F.-J. Wang and M. Shi, *Chirality*, 2011, **23**, 272-276.
23. J.-J. Jiang, J. Huang, D. Wang, M.-X. Zhao, F.-J. Wang and M. Shi, *Tetrahedron: Asymmetry*, 2010, **21**, 794-799.
24. Z.-L. Yuan, J.-J. Jiang and M. Shi, *Tetrahedron*, 2009, **65**, 6001-6007.
25. T. Yamamura, H. Nakatsuka, S. Tanaka and M. Kitamura, *Angew. Chem., Int. Ed.*, 2013, **52**, 9313-9315.
26. T. Yamamura, S. Nakane, Y. Nomura, S. Tanaka and M. Kitamura, *Tetrahedron*, 2016, **72**, 3781-3789.
27. S. Nakane, T. Yamamura, S. K. Manna, S. Tanaka and M. Kitamura, *ASC Catal.*, 2018, **8**, 11059-11075.
28. C. You, X. Li, Y. Yang, Y.-S. Yang, X. Tan, S. Li, B. Wei, H. Lv, L.-W. Chung and X. Zhang, *Nat. Commun.*, 2018, **9**, 2045.
29. C. You, S. Li, X. Li, J. Lan, Y. Yang, L. W. Chung, H. Lv and X. Zhang, *J. Am. Chem. Soc.*, 2018, **140**, 4977-4981.
30. B. Wei, C. Chen, C. You, H. Lv and X. Zhang, *Org. Chem. Front.*, 2017, **4**, 288-291.
31. C. You, S. Li, X. Li, H. Lv and X. Zhang, *ASC Catal.*, 2019, **9**, 8529-8533.
32. C. Chen, S. Jin, Z. Zhang, B. Wei, H. Wang, K. Zhang, H. Lv, X.-Q. Dong and X. Zhang, *J. Am. Chem. Soc.*, 2016, **138**, 9017-9020.

33. X. Li, C. You, J. Yang, S. Li, D. Zhang, H. Lv and X. Zhang, *Angew. Chem., Int. Ed.*, 2019, **58**, 10928-10931.
34. M.-J. Qi, T. Ai, M. Shi and G. Li, *Tetrahedron*, 2008, **64**, 1181-1186.
35. X.-Y. Guan, Y.-Q. Jiang and M. Shi, *Eur. J. Org. Chem.*, 2008, 2150-2155.
36. Y.-L. Shi and M. Shi, *Adv. Synth. Catal.*, 2007, **349**, 2129-2135.
37. J.-M. Garnier and F. Liu, *Org. Biomol. Chem.*, 2009, **7**, 1272-1275.
38. J.-M. Garnier, C. Anstiss and F. Liu, *Adv. Synth. Catal.*, 2009, **351**, 331-338.
39. S. S. Eliseenko and F. Liu, *Tetrahedron*, 2019, **75**, 518-526.
40. C. Anstiss and F. Liu, *Tetrahedron*, 2010, **66**, 5486-5491.
41. C. Anstiss, J.-M. Garnier and F. Liu, *Org. Biomol. Chem.*, 2010, **8**, 4400-4407.
42. Y.-Q. Jiang, Y.-L. Shi and M. Shi, *J. Am. Chem. Soc.*, 2008, **130**, 7202-7203.
43. D. Wang, Y.-L. Yang, J.-J. Jiang and M. Shi, *Org. Biomol. Chem.*, 2012, **10**, 7158-7166.
44. Y. Wei, G.-N. Ma and M. Shi, *Eur. J. Org. Chem.*, 2011, 5146-5155.
45. G.-N. Ma, S.-H. Cao and M. Shi, *Tetrahedron: Asymmetry*, 2009, **20**, 1086-1092.
46. Y.-L. Yang, C.-K. Pei and M. Shi, *Org. Biomol. Chem.*, 2011, **9**, 3349-3358.
47. H.-P. Deng, Y. Wei and M. Shi, *Eur. J. Org. Chem.*, 2011, 1956-1960.
48. H.-P. Deng and M. Shi, *Eur. J. Org. Chem.*, 2012, 183-187.
49. H.-P. Deng, Y. Wei and M. Shi, *Org. Lett.*, 2011, **13**, 3348-3351.
50. F.-L. Hu, Y. Wei and M. Shi, *Chem. Commun.*, 2014, **50**, 8912-8914.
51. X.-N. Zhang, H.-P. Deng, L. Huang, Y. Wei and M. Shi, *Chem. Commun.*, 2012, **48**, 8664-8666.
52. X.-N. Zhang and M. Shi, *ASC Catal.*, 2013, **3**, 507-512.